UNIVERSITÁ DEGLI STUDI DI NAPOLI FEDERICO II

DIPARTIMENTO DI AGRARIA

DOTTORATO IN FOOD SCIENCE

XXXIV CICLO

Functional genomics and bioinformatics approaches for the identification of cell fate molecular markers to implement diagnostic and monitoring devices in Food Science

Tutor:
Ch.ma Prof.ssa Maria Luisa Chiusano

Candidato:
Francesco Monticolo

Coordinatore: Ch.ma Prof.ssa Amalia Barone

2020-2021

In memory of Giulio Regeni

List of Figures, Tables and Abbreviations

Supplementary Table S1: List of differentially expressed genes (DEGs) of yeast cells treated with acetic acid.

Supplementary Table S2: Pathways enrichment of yeast cells treated with acetic acid.

Supplementary Table S3: Ribosomal protein genes details and paralog couples expression trends in acetic acid treatment.

Supplementary Table S4: Programmed cell death induced by acetic acid specific ohnologs replacement.

Supplementary Table S5: Gene ontology enrichment of WGCNA modules related to programmed cell death.

Supplementary Table S6: Pathways enrichment results of WGCNA modules related to programmed cell death.

Supplementary Table S7: List of the 149 genes and their expression trends in 9 apoptotic treatments and in 15 NutriGenomeDB experiments inducing apoptosis.

Supplementary Table S8: List of the 44 genes showing the same expression trend in bulk RNA-seq and scRNA-seq data from tissues and cells from COVID-19 infected patients.

Supplementary Table S9: List of the 13 genes showing the same expression trend in bulk RNA-seq, scRNA-seq data from tissues and cells from COVID-19 infected patients, and showing an opposite trend in nutrigenomics treatment.

Abbreviation: programmed cell death (PCD), reactive oxygen species (ROS), endoplasmic reticulum (ER), Comparative Toxicogenomics Database (CTD), Human Metabolome Database (HMDB), Chemical entities of biological interest (ChEBI), whole genome duplication (WGD), The Cancer Genome Atlas (TCGA), single-cell RNA sequencing (scRNA-seq), The adsorption, distribution, metabolism and excretion (ADME), sequence reads archive (SRA), counts per million (CPM), differentially expressed genes (DEGs), Reads Per Kilobase Million (RPKM), Gene Ontology (GO), Pan Assay Interference Compounds (PAINS), Weighted correlation network analysis (WGCNA), false discovery ratio (FDR), Kyoto encyclopedia of genes and genomes (KEGG), lymphoid neoplasm diffuse large B-cell lymphoma (DLBC), kidney renal clear cell carcinoma (KIRC), kidney renal papillary cell carcinoma (KIRP), brain lower grade glioma (LGG), liver hepatocellular carcinoma (LIHC), pancreatic adenocarcinoma (PAAD), skin cutaneous melanoma (SKCM), uterine corpus endometrial carcinoma (UCEC), interferons (IFNs), interferon-stimulated genes (ISGs), pathogen recognition receptors (PRRs), global

initiative on sharing all influenza data (GISAID), Coronavirus Disease 19 (COVID-19), RNA dependant RNA polymerase (RdRp).

Abstract

Cell fate is known to be an important aspect to consider in Food Science. Monitoring cell growth and limiting cell death are crucial for yield in industrial productions. Furthermore, the identification of molecular markers for an early detection of cellular response outcomes after exposure to treatments and substances can also be useful for the implementation of biosensors for the evaluation of food quality and healthy or toxic response. The identification of molecular markers useful for the early prediction of cell fate could also play a fundamental role in the selection of natural compounds that could be exploited in treatments for the health and well-being of *H. sapiens*.

It is crucial to consider gene expression as the earliest and fastest change in cell response. The analysis of gene expression provides direct insight into mRNA quantification. This information is fundamental for a better understanding of the early stages of cellular response.

Moreover, exploiting the methodologies and data resources available to identify natural compounds useful for influencing cellular response could be useful for applications in nutraceuticals, health, and well-being.

The project aims at the identification of early molecular markers that allow the prediction of cell fate in eukaryotic organisms: the unicellular eukaryote *Saccharomyces cerevisiae* and the multicellular organism *Homo sapiens*.

Saccharomyces cerevisiae was selected for its usefulness in detecting novel molecular processes due to its simple cell organization. Moreover, it is notoriously considered a model system of relevance in Food Science and in molecular studies of physiological processes of metazoan cells (Madeo et al., 1999). *Homo sapiens* was considered for understanding the impact of our approaches also for human healthcare and well-being.

The scope is to further investigate the molecular features that characterize gene expression during cell stress response and its outcomes to define key markers for the early detection of cell fate. The idea is to acquire knowledge for the design of sensitive molecular techniques for applications in different fields of Food Science. The results will be of use for diagnostics of cell systems exposed to bioactive substances contained in foods, for food quality, and for monitoring and predicting the cell fate (survival or cell death) in cell culture or in bioreactors.

We initially focused on the analysis of RNA-seq data related to programmed cell death both for *Saccharomyces cerevisiae* and *Homo sapiens*.

We set up a dedicated data processing pipeline to re-analyze publicly available raw datasets to obtain differentially expressed genes during programmed cell death.

With the same approach we analyzed stress response experiments for both species to compare gene expressions between programmed cell death and cell stress. Our aim was to identify genes that have a specific expression trend in programmed cell death which is opposite with the one revealed in stress response and therefore could be used to distinguish initiation of programmed cell death.

Considering gene expression data from nutrigenomics experiments, we selected food natural compounds that could influence the expression of programmed cell death related genes resulting in the induction of programmed cell death.

A bioinformatics analysis for the assessment of absorption, distribution, metabolism, and excretion of new natural compounds, was performed to select natural compounds that could play a role in human health and well-being.

The results show different interesting aspects in both biological systems.

Firstly, we identified early molecular processes that prelude to cell death in *S. cerevisiae*. These processes are associated with biogenesis of ribosomes and a reprogramming of protein translation machinery. Key genes involved in the decapping of mRNAs, translation efficiency and fidelity were identified.

In addition, a substitution of the paralogs of ribosomal proteins in the assembly of the two ribosomal subunits was highlighted. These key genes and their relative changes in expression are suitable markers of programmed cell death.

To further characterize the programmed cell death specificity of the paralog pairs expression, we compared all the 551 paralog pairs expression in programmed cell death with the paralog pairs expression in 12 different stresses. In particular, specific cell death paralog substitution was found for genes involved in sporulation, ribosome population change, mRNA decapping, and methionine biosynthesis.

These results may be useful for monitoring cell growth in bioreactors and for implementing biosensors to monitor cell response.

Subsequently, we focused on the analysis of RNA-seq datasets from *H. sapiens* cell lines undergoing programmed cell death. We identified novel genes not yet reported as involved in programmed cell death, that are co-expressed with genes known (from literature) to be associated to programmed cell death. The gene expression trend of these new genes putatively involved in programmed cell death was compared with their expression trend in 36 different cell stress RNA-seq. Our aim was to identify genes that have a specific expression trend in

programmed cell death which is opposite with the one revealed in stress response and therefore could be used to distinguish initiation of programmed cell death.

We identified 734 novel genes not yet reported as involved in programmed cell death. These genes are useful for biosensor, for selection of natural compounds that could be exploited in prevention, for diagnostics and treatments for human health and well-being.

Moreover, because one of the cancer hallmarks is the evasion to cell death (Hanahan & Weinberg, 2011) we investigated on the behaviors of these genes in nutrigenomics treatments that induce cell death. One of the roles of nutrigenomics is to help Food Science on defining the role of nutrients and bioactive compounds for the prevention and the treatment of chronic diseases, such as cancer (Sales et al., 2014).

Our aim was to implement bioinformatics strategies to select food natural compounds from nutrigenomics experiments that could influence the expression of the new programmed cell death related genes. These natural compounds could be useful in the induction of programmed cell death. This led to the identification of bioactive compounds that modulate the expression of 149 new programmed cell death related genes.

Therefore, the 149 genes were further analyzed to identify genes with opposite expression trend between apoptotic treatments and cancer, resulting in a list of 22 genes that show an opposite expression trend. Focusing on their survival role in cancer patients, 7 genes whose expression is modulated by 6 natural compounds, were highlighted.

To expand the list of natural compounds that could modulate the expression of the 7 genes, a virtual screening analysis was performed.

The resulting natural compounds were analyzed by predicting their pharmacokinetics. This led to the identification of 23 natural compounds that could be useful in cancer treatments.

Due to the great interest in the treatment of infectious diseases using natural compounds, we also tested the bioinformatics procedure implemented in this thesis to find natural compounds that could be useful for the treatment of infectious diseases, in particular for COVID-19. We collected transcriptomics data from RNA-seq and from single cell RNA-seq (scRNA-seq) of patients and cells infected with SARS-CoV-2.

Forty-four disease related candidate genes were found. The natural compounds that could modulate the 44 gene expression were again investigated in nutrigenomics experiments to search for natural food compounds useful for prevention and treatment of infectious diseases. In this case, we considered only those genes that have an opposite expression trend between SARS-CoV-2 infected patients and nutrigenomics treatments. We selected 4 bioactive

compounds that regulate the expression of 7 genes. These 4 compounds were exploited to identify, by virtual screening, new molecules with a similar structure. The resulting bioactive compounds were analyzed by predicting their pharmacokinetics. This led to the identification of 27 natural compounds that represent suitable candidates to further test their effectiveness in COVID-19 treatments modulating the expression of the 7 genes.

In conclusion the analyses here presented highlight the relevance of omics and bioinformatics application in monitoring cell growth, in the identification of molecular markers useful for the implementation of biosensors, and for the selection of natural compounds that could be exploited in the field of infectious diseases or cancer.

In addition, the analyses here performed permitted to pave the way for relevant investigations in the field of molecular biology. Indeed, novel markers, genes and processes have been detected in yeast and in human programmed cell death. All these results set the scene for deeper investigations for expansion of knowledge on the involved molecular processes.

Interestingly, of the 734 novel genes not yet reported as involved in programmed cell death identified in *H. sapiens,* 32 are orthologs with *S. cerevisiae* with the same expression trend in programmed cell death of both species. This additional outcome also represents an intriguing aspect for further investigations. These genes involved in programmed cell death may represent components of evolutionarily conserved pathways related to cell death in two phylogenetically distant species such as *H. sapiens* and *S. cerevisiae*. A subsequent analysis on the 32 identified genes allowed to better characterize their role in human pathologies.

Estratto

La morte cellulare viene considerata un aspetto importante nel Food Science. Monitorare la crescita della cellula e limitarne la morte è cruciale per la resa nella produzione industriale. Inoltre, l'identificazione di marcatori molecolari per un precoce rilevamento della risposta cellulare dopo l'esposizione a trattamenti e sostanze può risultare utile per la realizzazione di biosensori per la valutazione della qualità del cibo e della risposta cellulare.

L'identificazione di marcatori molecolari utili per una precoce predizione della morte cellulare può anche giocare un ruolo nella selezione dei composti naturali che possono venire usati nei trattamenti per la salute e il benessere dell'uomo.

È importante considerare l'espressione genica come il più veloce mutamento nella risposta cellulare. Inoltre, usare le metodologie e le risorse di dati disponibili oggigiorno per identificare composti naturali utili ad influenzare la risposta cellulare potrebbe risultare utile nelle applicazioni per la nutraceutica, la salute e il benessere umano.

Il progetto di tesi ha come scopo l'identificazione di marcatori molecolari precoci che consentono la predizione della morte cellulare negli organismi eucariotici: il lievito unicellulare *Saccharomyces cerevisiae* e l'organismo pluricellulare *Homo sapiens*. *Saccharomyces cerevisiae* è stato scelto per la sua utilità nell'individuare nuovi processi molecolari grazie alla sua semplice organizzazione. Inoltre, esso è notoriamente ritenuto un modello importante nel Food Science e negli studi molecolari dei processi fisiologici delle cellule dei metazoi. *Homo sapiens* è stato preso in considerazione per comprendere l'impatto dei nostri approcci anche sulla salute e il benessere umano.

Lo scopo è quello di indagare ulteriormente sulle caratteristiche molecolari che caratterizzano l'espressione genica e i suoi esiti per definire i marcatori chiave per una precoce individuazione della morte cellulare. L'idea è quella di acquisire conoscenze per la progettazione di tecniche molecolari per l'applicazione in diversi campi del Food Science. I risultati potranno servire per la diagnosi dei sistemi cellulari esposti a sostanze bioattive contenute nei cibi, per la qualità del cibo, e per monitorare e predire la morte cellulare nelle colture cellulari e nei bioreattori.

Inizialmente ci siamo concentrati sull'analisi dei dati di RNA-seq relativi alla morte cellulare programmata sia per *Saccharomyces cerevisiae* che per *Homo sapiens.*

Abbiamo allestito una *pipeline* per l'elaborazione dei dati grezzi da rianalizzare per ottenere geni differenzialmente espressi durante la morte cellulare programmata.

Usando lo stesso approccio abbiamo analizzato esperimenti di risposta allo stress per comparare l'espressione genica tra la morte cellulare programmata e lo stress cellulare. Il nostro scopo è

stato quello di identificare geni che hanno un *trend* di espressione nella morte cellulare programmata che si contrappone al *trend* manifestato in risposta allo stress. Questi geni pertanto potrebbero essere usati per individuare l'inizio della morte cellulare programmata.

Tenendo conto dei dati sull'espressione genica derivati dagli esperimenti di nutrigenomica, abbiamo selezionato composti alimentari naturali che potrebbero influenzare l'espressione dei geni relativi alla morte cellulare programmata.

È stata fatta un'analisi bioinformatica per la valutazione dell'assorbimento, distribuzione, metabolismo ed eliminazione dei composti naturali, al fine di selezionare quei composti che potrebbero giocare un ruolo per la salute e il benessere umano.

I risultati mostrano diversi aspetti interessanti in entrambi i sistemi biologici. Inizialmente abbiamo identificato i processi molecolari che preludono alla morte cellulare in *S. cerevisiae*. Questi processi vengono associati alla biogenesi dei ribosomi e alla riprogrammazione del meccanismo di traduzione proteico. Sono stati identificati i geni chiave implicati nel decapping dell'mRNA e nell'efficienza e fedeltà di traduzione.

Inoltre, è stata evidenziata una sostituzione dei paraloghi delle proteine ribosomali. Questi geni chiave e i loro relativi cambi nell'espressione sono marcatori idonei per la morte cellulare programmata.

Per caratterizzare ulteriormente la specificità dell'espressione delle coppie di paraloghi durante la morte cellulare programmata, abbiamo confrontato l'espressione delle 551 coppie di paraloghi con l'espressione delle coppie di paraloghi in 12 diversi stress. In particolare, è stata trovata una sostituzione tra i paraloghi specifico per la morte cellulare per i geni coinvolti nella sporulazione, nel cambiamento della popolazione dei ribosomi, nel decapping dell'mRNA e nella biosintesi della metionina. Questi risultati possono essere utili per monitorare la qualità della crescita cellulare e per controllare l'inizio della morte cellulare programmata nei bioreattori e per implementare biosensori per monitorare la risposta cellulare.

Successivamente, ci siamo concentrati sull'analisi dei dati di RNA-seq da linee cellulari di *H. sapiens* che vanno incontro a morte cellulare programmata. Abbiamo identificato nuovi geni non ancora riportati come coinvolti nella morte cellulare programmata, che sono co-espressi con geni noti (dalla letteratura) per essere coinvolti nella morte cellulare programmata. Il *trend* di espressione genica di questi nuovi geni è stato confrontato con il loro *trend* di espressione in 36 differenti RNA-seq di stress cellulare. Il nostro scopo era identificare i geni che hanno un *trend* di espressione specifico per la morte cellulare programmata che è opposto a quello

mostrato nella risposta allo stress e che quindi potrebbero essere usati per identificare l'inizio della morte cellulare programmata.

In questo modo abbiamo identificato 734 nuovi geni non ancora riportati come coinvolti nella morte cellulare programmata. Questi geni sono utili per i biosensori, per la selezione di composti naturali che potrebbero essere sfruttati nella prevenzione, nella diagnostica e nei trattamenti per la salute e il benessere umano.

Inoltre, poiché uno dei segni distintivi del cancro è l'evasione alla morte cellulare (Hanahan & Weinberg, 2011), abbiamo studiato i comportamenti di questi geni nei trattamenti di nutrigenomica che inducono la morte cellulare. Uno dei ruoli della nutrigenomica è aiutare il Food Science a definire il ruolo dei nutrienti e dei composti bioattivi per la prevenzione e il trattamento di malattie croniche come il cancro (Sales et al., 2014).

Il nostro scopo era implementare strategie bioinformatiche per selezionare composti naturali da esperimenti di nutrigenomica che potessero influenzare l'espressione dei nuovi geni correlati alla morte cellulare programmata. Ciò ha portato all'identificazione di composti bioattivi che modulano l'espressione di 149 nuovi geni correlati alla morte cellulare programmata.

Pertanto, i 149 geni sono stati ulteriormente analizzati per identificare i geni con un *trend* di espressione opposta tra trattamenti apoptotici e cancro, risultando in un elenco di 22 geni. Concentrandosi sul loro ruolo nella sopravvivenza dei pazienti oncologici, sono stati evidenziati 7 geni la cui espressione è modulata da 6 composti naturali. Per ampliare l'elenco dei composti naturali che potrebbero modulare l'espressione dei 7 geni, è stata eseguita un'analisi di *virtual screening*.

I composti naturali risultanti sono stati analizzati prevedendone la farmacocinetica. Ciò ha portato all'identificazione di 23 composti naturali che potrebbero essere utili nei trattamenti contro il cancro.

Dato il grande interesse per il trattamento delle malattie infettive utilizzando composti naturali, abbiamo testato la procedura bioinformatica implementata in questa tesi per trovare composti naturali che potrebbero essere utili per il trattamento delle malattie infettive, in particolare per il COVID-19.

Abbiamo collezionato dati di trascrittomica da RNA-seq e da single cell RNA-seq (scRNA-seq) di pazienti affetti da COVID-19. Sono stati trovati 44 geni associati alla malattia. I composti naturali che potrebbero influenzare l'espressione di questi geni sono stati nuovamente studiati in esperimenti di nutrigenomica per cercare composti alimentari naturali utili per la prevenzione e il trattamento delle malattie infettive.

In questo caso, abbiamo considerato solo quei geni che hanno una tendenza di espressione opposta tra i pazienti infetti da SARS-CoV-2 e i trattamenti di nutrigenomica. Abbiamo selezionato 4 composti bioattivi che regolano l'espressione di 7 geni. Questi 4 composti sono stati sfruttati per identificare, mediante *virtual screening*, nuove molecole chimiche con una struttura simile. I composti bioattivi risultanti sono stati analizzati prevedendone la farmacocinetica. Ciò ha portato all'identificazione di 27 composti naturali che rappresentano candidati idonei per testare ulteriormente la loro efficacia nei trattamenti COVID-19 modulando l'espressione dei 7 geni.

In conclusione, le analisi presentate in questa tesi mettono in evidenza la rilevanza delle applicazioni omiche e bioinformatiche nel monitoraggio della crescita cellulare, nell'identificazione di marcatori molecolari utili per l'implementazione di biosensori e per la selezione di composti naturali che potrebbero essere sfruttati nel campo delle malattie infettive o nel cancro. Inoltre, le analisi qui eseguite hanno permesso di aprire la strada a importanti indagini nel campo della biologia molecolare. Infatti, nuovi marcatori e nuovi processi sono stati rilevati nella morte cellulare programmata del lievito e dell'uomo. Tutti questi risultati hanno posto le basi per indagini più approfondite per ampliare le conoscenze sui processi molecolari coinvolti.

È interessante notare che dei 734 nuovi geni non ancora riportati come coinvolti nella morte cellulare programmata identificati in *H. sapiens*, 32 sono ortologhi con *S. cerevisiae* con lo stesso *trend* di espressione nella morte cellulare programmata di entrambe le specie. Questo ulteriore risultato rappresenta anche un aspetto intrigante per ulteriori indagini. Questi geni coinvolti nella morte cellulare programmata possono rappresentare componenti di percorsi evolutivamente conservati legati alla morte cellulare in due specie filogeneticamente distanti come *H. sapiens* e *S. cerevisiae*. Una successiva analisi sui 32 geni identificati ha permesso di caratterizzare meglio il loro ruolo nelle patologie umane.

Graphical abstract

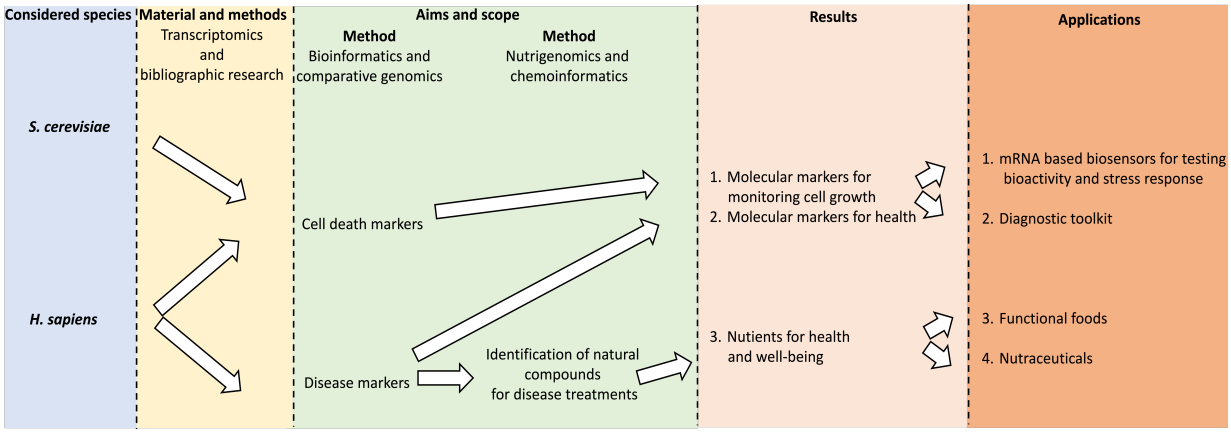

Chapter 1: Introduction

Omics and bioinformatics approaches in Food Science

Omics technologies explosion affect Food Science applications. Indeed, in 2009, Cifuentes (Cifuentes, 2009) coined the term "foodomics" referring to "omics" technologies applied to Food Science (Cifuentes, 2009). The use of "omics" approaches allows to shed light on different areas of interest in the field. Indeed, comparative genomics and bioinformatics allow the identification and the study of gene families relevant for food metabolism (Ruskovska et al., 2020), as well as in food taste (Shi & Zhang, 2006; Talevi et al., 2012), food processing (Alkema et al., 2016), and food safety (Mari et al., 2006).

In parallel, the evolution of metagenomics studies paved the way to investigations in the collective genome of uncultured microorganisms, providing information on the microbial diversity of a specific environments, including those present in foods (Ercolini, 2020) and those associated to digestive tract. These studies revealed very important results for understanding the impact of diet on microbiome not only for human (De Filippis et al., 2022; De Filippo et al., 2010; Meslier et al., 2020; Pasolli et al., 2020) but also for relevant Food Science species (Delgado et al., 2019; Ross et al., 2013; Singh et al., 2012).

Moreover, there is a growing appreciation for "omics" approaches in the areas of food safety and quality, because of the capability to fully sequence the genome of foodborne pathogens (Brul et al., 2006) or beneficial microorganisms such as *Lactobacillus acidophilus* (Altermann et al., 2005), *Lactobacillus plantarum* (Kleerebezem et al., 2003) and *Bifidobacterium longum* (Schell et al., 2002).

All these approaches reveal the relevance of omics technologies and bioinformatics in the field of Food Science and nutrition leading to the identification of novel nutrients and/or compounds with positive effects on living organisms of interest in Food Science.

Nutrigenomics

The use of "omics" technologies in nutrition offers different tools for understanding the molecular pathways affected by nutrients based on genetic, transcriptome, proteome as well as metabolome observations (Brennan & de Roos, 2021).

Nutrigenomics is the study of how nutrients and bioactive food compounds influence the expression of genes involved in metabolic pathways and homeostatic control (Martín-

Hernández et al., 2019). From a nutrigenomics perspective, nutrients are dietary signals that are detected by the cellular sensor systems that influence gene expression, protein and metabolite production (Müller & Kersten, 2003). Nutrigenomics tries to examine the nutrition effects in specific cells, tissues, and organisms, and to understand how nutrition influences homeostasis. Moreover, nutrigenomics studies aim at identifying genes that influence the risk of diet-related diseases on a genome-wide scale (Müller & Kersten, 2003). To this aim, nutrigenomics studies are based on real-time polymerase chain reaction or on next-generation sequencing approaches such as transcriptomics (Ardekani & Jabbari, 2009).

Among the many resources for investigations in the field, NutriGenomeDB (Martín-Hernández et al., 2019), is based on a set of manually curated differentially expressed genes, obtained using human cell-based assays from microarray, after treatment with nutrients or bioactive food compounds (Martín-Hernández et al., 2019).

The Monarch Initiative is a platform that integrates data across species on nutrition-related phenotypes, genotypes and diseases (Shefchek et al., 2020).

The Comparative Toxicogenomics Database (CTD) is a database that relates toxicological information for chemicals, genes and phenotypes (Davis et al., 2021). CTD includes over 2 million manually curated data from interactions of chemical–gene, chemical–phenotype, chemical–disease, gene–disease and chemical–exposure (Davis et al., 2021).

PubChem is a database that collects chemical substances and their biological activities (S. Kim et al., 2021). PubChem consists of three inter-linked databases: substance, compound, and BioAssay. The substance database contains chemical information on different chemical substances. The compound database contains unique chemical structures obtained from the substance database. BioAssay database contains biological activity data of chemical substances tested in assay experiments (S. Kim et al., 2021).

The Human Metabolome Database (HMDB) is a metabolomic database containing comprehensive information about human metabolites along with their biological roles, physiological concentrations, disease associations, chemical reactions, and metabolic pathways (Wishart et al., 2018).

ChEMBL is a drug discovery database that aims at collecting medicinal chemistry data and knowledge across the pharmaceutical research and development process. Information about small molecules and their biological activity is extracted from the full text articles of medicinal chemistry journals and integrated with data on approved drugs and clinical development candidates, such as mechanism of action and therapeutic indications. The resulting database has

a wide variety of practical applications including assessment of compound selectivity, assisting in generating drug repurposing hypotheses, and assessing target tractability (Gaulton et al., 2012).

Chemical entities of biological interest (ChEBI) is a database containing information on chemical compounds. These chemical compounds are either natural or synthetic compounds used to intercede in the processes of living organisms. It includes over than 46000 entries, classified within an ontology and with multiple annotations (chemical structure, database cross-references, synonyms and literature citations) (de Matos et al., 2010).

SwissSimilarity (Zoete et al., 2016) allows to perform a ligand-based virtual screening of libraries of small molecules. The working hypothesis of the virtual screening is that similar molecules could determine similar biological activity (Zoete et al., 2016). It could be used to identify natural bioactive compounds that could induce similar effects to those caused by compounds exploited in nutrigenomics treatments.

SwissADME (Daina et al., 2017) is a tool useful for computing the physicochemical descriptors and predicting the adsorption, the distribution, the metabolism and the excretion (ADME) parameters of small molecules to support drug discovery (Daina et al., 2017).

FooDB (http://www.foodb.ca) is a database containing information on more than 28,000 bioactive compounds found in more than 1000 unprocessed food. It allows to identify food with a particular bioactive compound.

Molecular characterization of cell response and applications in Food Science

It is well known that cell fate is an important aspect to be considered in Food Science.

Indeed, cell death is a limiting factor when employing living organisms of interest in the field. For example, monitoring cell growth and limiting cell death is fundamental for yield in massive productions, like those requiring the use of bioreactors (Grilo & Mantalaris, 2019; Krampe & Al-Rubeai, 2010). In addition, the exploitation of appropriate molecular markers that could support early detection of cell response outcomes after exposure to treatments and substances can also be useful for the implementation of molecular devices and/or biosensors in Food Science, for food quality and security, and for healthy or toxic response evaluations. For these applications biosensors can be used to monitor biosystems response (Brooks & Alper, 2021). Indeed, identify and predict cell fate induced by exposure to food components or preparations methods (such as, for example, toxicity or oxidative stress induced by carbohydrates, animal-

based proteins, and excessive consumption of fats (B. L. Tan et al., 2018)), can improve food technologies and quality assessments.

Identifying molecular markers useful for the early prediction of cell fate could play a pivotal role also in the selection of natural compounds that could be exploited in prevention, diagnostics, and treatments for human health and well-being, for example in the field of infectious diseases or cancer.

Applications of molecular investigations on cell fate prediction in Food Science are illustrated in **Figure 1.**

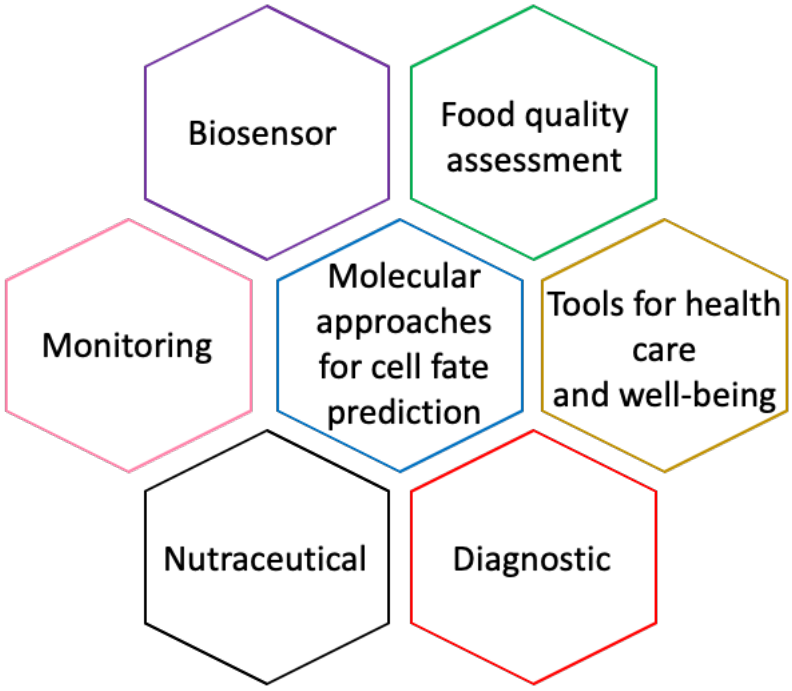

Figure 1: Molecular approaches for cell fate prediction and applications in Food Science.

Cell stress response and programmed cell death

Cell stress is defined as an abrupt change in the state of cell homeostasis (Lu et al., 2021). All organisms, from unicellular prokaryotes to multicellular eukaryotes, are constantly exposed to conditions that cause stress (Mansouri et al., 2012).

Cells can be exposed to a wide array of stimuli that can cause stress responses, falling in the category of stressors. They can be classified in biotic, including pathogen infections (Jindal & Malkovsky, 1994; Nakagawa et al., 2016; Schwarz, 1996), that lead to the development of other stressors including depletion of ATP (Corton et al., 1994), respiratory poisons (Suomalainen & Battersby, 2018), and oxidative stress (Zhou et al., 2011), or abiotic, including food components

(B. L. Tan et al., 2018), temperature variations (Hetz & Papa, 2018; Shpilka & Haynes, 2018), DNA-damaging agents (Chang et al., 2017) and nutrient deprivation (Lorenzo Galluzzi et al., 2014).

Different stressors can trigger a variety of responses. Depending on the duration and the severity of the stimuli, cells can activate different mechanisms to restore cellular homeostasis (Poljšak & Milisav, 2012) or, if the stress persists, they can activate autophagy and/or programmed cell death (PCD) (Kroemer et al., 2010).

Multiple perturbations of the intracellular or extracellular microenvironment can be successfully managed by adaptive systems that preserve cellular functions and repair macromolecular damages. For example, DNA damage is detected at cell cycle checkpoints, coupled to the recruitment of the DNA repair machinery to genetic lesions. If the DNA damage repair is unsuccessful, the same machinery triggers PCD (Lorenzo Galluzzi, Yamazaki, et al., 2018). In particular, a key role in DNA damage repair is played by Ataxia Telangiectasia Mutated (ATM) and Ataxia Telangiectasia and Rad3-related protein (ATR). Once recruited to damaged DNA, ATM and ATR phosphorylate and activate histone H2AX, Checkpoint Kinase 2 (CHEK2) and Checkpoint Kinase 1 (CHEK1), stabilizing tumor suppressor p53. Initially, p53 tries to repair DNA activating genes that enable a reversible cell cycle arrest and maintain metabolic homeostasis. If genetic lesions cannot be resolved, p53 through transcriptional and transcription-independent mechanisms activates PCD, highlighting a pivotal role of p53 in determining cell fate (Lorenzo Galluzzi, Yamazaki, et al., 2018).

Another example of repair of macromolecular damages is the unfolded protein response operating in the endoplasmic reticulum (ER). It is an adaptive response aimed at resolving the accumulation of unfolded polypeptides in the ER or eliminating cells that cannot recover proteostasis, triggering PCD (Lorenzo Galluzzi, Yamazaki, et al., 2018).

During the unfolded protein response operating in the ER there is the activation of three major effectors: Activating Transcription Factor 4 (ATF4), Activating Transcription Factor 6 (ATF6) and X-box Binding Protein 1 (XBP1). They act as transcription factors that initially control the expression of genes involved in the mechanisms of homeostatic adaptation to protein overload, including an increased capacity for protein folding and chaperoning within the ER and an increased flux of protein degradation via the proteasome and autophagy. If reticular proteostasis cannot be solved, ATF4 activates C/EBP-Homologous Protein (CHOP). Among various target genes, CHOP upregulates pro-apoptotic genes leading to programmed cell death (Lorenzo Galluzzi, Yamazaki, et al., 2018).

Lastly, autophagy is one of the central stress adaptation mechanisms in the eukaryotic kingdom. Autophagy, during stress adaptation, tries to restore homeostasis degrading potentially harmful or disposable organelles (Lorenzo Galluzzi et al., 2014).

Prolonged or severe stresses that cannot be carried on by autophagy lead to PCD of stressed cells (Lorenzo Galluzzi, Yamazaki, et al., 2018).

PCD includes a set of mechanisms for target elimination of damaged cells (Kroemer et al., 2009). PCD is genetically controlled by a dedicated molecular machinery and can be triggered by development or stress (Lorenzo Galluzzi, Vitale, et al., 2018). At the beginning, based on morphological alterations, PCD was classified in four categories: type I (apoptosis), type II (autophagy), type III (necrosis) (Schweichel & Merker, 1973) and type IV (entosis) (Martins et al., 2017). This classification is still used even if there are remarkable limitation due to the fact that numerous types of cell death show mixed morphological characteristics (Lorenzo Galluzzi, Vitale, et al., 2018).

Saccharomyces cerevisiae, that is used as a model for physiological processes in eukaryotes and metazoan cells, can undergo programmed cell death showing the canonical apoptosis hallmarks such as phosphatidylserine externalization, DNA fragmentation, chromatin condensation, cytochrome *c* release from mitochondria, and dissipation of the mitochondrial transmembrane potential (Madeo et al., 1999) (**Figure 2**). The major causes of *S. cerevisiae* apoptosis are: reactive oxygen species (ROS), drugs, aging, heat stress, UV radiation, acetic acid and heterologous expression of pro-apoptotic human genes (Falcone & Mazzoni, 2016).

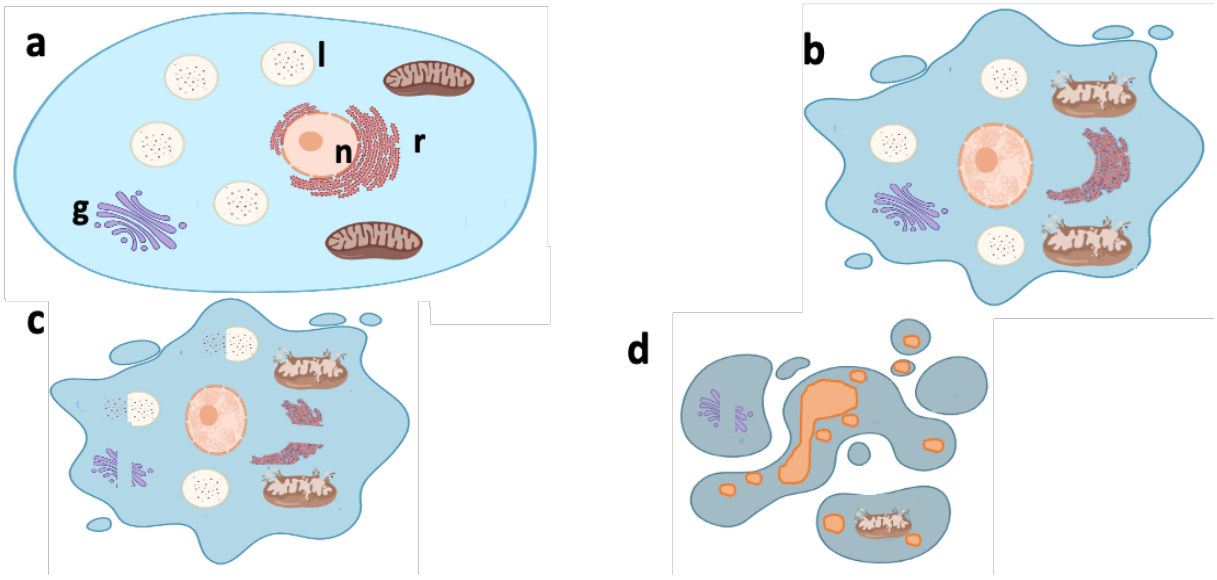

Figure 2: Schematic representation of eukaryotic apoptosis.
a) Normal cell. b) Apoptotic activation with mitochondria undergoing swelling with subsequent rupture or opening of channels in the outer membrane. c) Subsequently apoptotic activation leads to: shrinkage of the cell and the nucleus (n), condensation of nuclear chromatin into sharply delineated masses, lysosomal membrane rupture (l), endoplasmic reticulum (r) enlargement and swelling; the Golgi apparatus (g) undergoes irreversible fragmentation. d) The nucleus progressively condenses and breaks up (karyorrhexis). The plasma membrane forms a separate membrane around the detached solid cellular material (apoptotic bodies). These apoptotic bodies are full of cellular organelles and nuclear fragments.

In *Homo sapiens*, 16 different types of PCDs are currently described: apoptosis (intrinsic and extrinsic) (Ashkenazi & Dixit, 1998; Gibert & Mehlen, 2015; Kerr et al., 1972), mitotic death (Lorenzo Galluzzi, Vitale, et al., 2018), mitochondrial permeability transition driven necrosis (Izzo et al., 2016), necroptosis (Linkermann & Green, 2014), pyroptosis (Jorgensen & Miao, 2015), ferroptosis (W. S. Yang & Stockwell, 2016), lysosome-dependent cell death (Aits & Jäättelä, 2013), parthanatos (Fatokun et al., 2014), entosis (Florey et al., 2015), autophagy-related cell death (Lorenzo Galluzzi, Baehrecke, et al., 2017), autosis (Liu et al., 2013), immunogenic cell death (Lorenzo Galluzzi, Buqué, et al., 2017), NETotic cell death (Fuchs et al., 2007), apoNETosis (Azzouz & Palaniyar, 2018), oxeiptosis (Holze et al., 2018) and alkaliptosis (Song et al., 2018).

Among these, apoptosis is the best-characterized programmed cell death in *H. sapiens* and it can also contribute to physiological phenomena like tissue remodeling during embryogenesis (Renehan et al., 2001). It is induced by both intrinsic (DNA damage, replication stress, endoplasmic reticulum stress, reactive oxygen species, microtubule alterations) and extrinsic stimuli (initiated by perturbations of the extracellular microenvironment) (Lorenzo Galluzzi, Vitale, et al., 2018).

Interestingly, some forms of PCD relies on apoptotic mechanism. Indeed, mitotic death is a particular kind of PCD induced by mitotic catastrophe (Lorenzo Galluzzi, Vitale, et al., 2018). The mitotic catastrophe is accompanied by chromatin condensation, mitochondrial release of pro-apoptotic proteins, caspase activation and DNA degradation (Lorenzo Galluzzi, Vitale, et al., 2018).

Immunogenic cell death is a PCD with an apoptotic morphology, depending on the activity of apoptotic caspases and sufficient for activating an adaptive immune response specific for endogenous (cellular) or exogenous (viral) antigens expressed by dying cells (Lorenzo Galluzzi, Buqué, et al., 2017). Finally, in 2018 Azzouz and Palaniyar (Azzouz & Palaniyar, 2018), have described a particular kind of NETosis induced by high UV dose: ApoNETosis. ApoNETosis is a PCD induced by high UV dose with apoptotic and NETotic morphology (Azzouz & Palaniyar, 2018). Whereas other forms of PCD seem to repress apoptosis or to be apoptosis independent. Indeed, necroptosis initiated by the perturbations of the extracellular or intracellular microenvironment detected by pathogen recognition receptors, inhibits the activation of apoptosis (Linkermann & Green, 2014). Another type of PCD induced by pathogens is pyroptosis. Pyroptosis is a form of PCD triggered by perturbations of extracellular or intracellular homeostasis related to innate immunity (Jorgensen & Miao, 2015).

Ferroptosis is an iron- and ROS-dependent form of PCD initiated by specific perturbations of the intracellular microenvironment, notably severe lipid peroxidation, which relies on ROS generation and iron availability. Ferroptosis occurs independently of apoptosis and necroptosis components (Yang & Stockwell, 2016).

Mitochondrial permeability transition driven necrosis is due to severe oxidative stress and cytosolic Ca^{2+} overload (Izzo et al., 2016).

Lysosome-dependent cell death is a PCD initiated by perturbations of intracellular homeostasis and leads to the permeabilization of lysosomal membranes. The permeabilization of lysosomal membranes can be triggered by numerous stimuli such as: lysosomotropic detergents, viral proteins, bacterial, fungal and snake toxins, ROS, proteases and p53 (Aits & Jäättelä, 2013).

Parthanatos is a PCD initiated by severe/prolonged alkylating DNA damage, oxidative stress, reactive nitrogen species, hypoxia, hypoglycemia and inflammatory cues (Fatokun et al., 2014).

Entosis is the term used for indicating a PCD in which living cells are engulfed by other cells (Florey et al., 2015). Entosis has been observed to occur efficiently in apoptosis and autophagy incompetent cells. The internalized cells initially are alive and healthy, capable of dividing within the engulfing cell, and are sometimes released. However, the majority of the internalized

cells die by lysosomal degradation (Florey et al., 2015). Entosis is mainly triggered by the detachment of epithelial cells from the extracellular matrix and consequent loss of integrin signaling (Florey et al., 2015) and by glucose withdrawal (Florey et al., 2015).

Autosis is a PCD characterized by enhanced cell-substrate adherence, dilated and fragmented ER (early), ER disappearance (late), nuclear membrane convolution (early), focal swelling of the perinuclear space, nuclear shrinkage and a mild chromatin condensation (Liu et al., 2013). Autosis is induced by autophagy-inducing peptides, starvation and hypoxia-ischemia (Liu et al., 2013).

A ROS-dependent form of cell death, initially identified in neutrophils, is NETosis (Fuchs et al., 2007). NETosis is independent from apoptosis and necrosis and is associated with the extrusion of chromatin and histone fibers bound to cytoplasmic proteins known as neutrophil extracellular traps (Fuchs et al., 2007).

Oxeiptosis is a novel ROS-induced PCD induced by hydrogen peroxide (Holze et al., 2018).

Alkaliptosis is pH-dependent form cell death driven by intracellular alkalinization (Song et al., 2018).

The morphological and biochemical features of programmed cell death are summarized in **Table 1**.

Type	Morphological features	Biochemical features
Apoptosis	Cell rounding; nuclear condensation; membrane blebbing; apoptotic body formation	Activation of caspases; DNA fragmentation; mitochondrial membrane potential dissipation; phosphatidylserine exposure
Necroptosis	Cell swelling; rupture of plasma membrane; moderate chromatin condensation	Activation of RIPK1; RIPK3; and MLKL; cytosolic necrosome formation
Alkaliptosis	Necroptosis-like morphology	Intracellular alkalinization; activation of NF-κB; caspase-independent
ApoNETosis	Apoptotic and NETotic[1] morphology	Increased ROS production; activation of MAPK p38; caspase 3 cleavation; DNA is released in NET structures
Autosis	Autophagic vacuolization	Increased autophagic flux and lysosomal activity
Entotic cell death	Cell-in-cell structure	Activation of adhesion proteins and actomyosin; phagocytosis
Ferroptosis	Smaller mitochondria; reduced mitochondria crista; elevated mitochondrial membrane densities; increased rupture of mitochondrial membrane	Iron accumulation; lipid peroxidation; mitochondrial membrane potential dissipation; glutaminolysis; caspase-independent
Immunogenic cell death	Apoptosis-like morphology	Initiated by calreticulin (CALR), ATP, high-mobility group box 1 (HMGB1) or interferon; based on caspase activation.
Lysosome-dependent cell death	Lysosome and plasma membrane rupture	Lysosomal membrane permeabilization; release of lysosomal hydrolytic enzymes; lysosomal iron-induced oxidative injury
Mitochondrial permeability transition driven necrosis	Necroptosis-like morphology	Severe oxidative stress and cytosolic Ca2+ overload; opening of the permeability transition pore complex (PTPC) at mitochondrial membrane; based on peptidylprolyl isomerase F (CYPD), BAX, BAD, BID and BCL-xl
Mitotic cell death	Apoptosis-like morphology	Induced by mitotic catastrophe that led to chromatin condensation; mitochondrial release of proapoptotic proteins; caspase activation and DNA degradation; based on Caspase-2 and p53

Type	Morphological features	Biochemical features
[1]Netotic cell death	Plasma membrane rupture; nuclear membrane collapse; chromatin fibre release	Formation of NETs; release and translocation of granular enzymes; histone citrullination
Oxeiptosis	Apoptosis-like morphology	ROS-dependent; caspase-independent
Parthanatos	Chromatin condensation; large DNA fragmentation; lack of apoptotic body and small-scale DNA fragments; loss of membrane integrity; lack of cell swelling	Excessive activation of PARP1; mitochondrial membrane potential dissipation; caspase-independent; NAD+ and ATP depletion
Pyroptosis	Lack of cell swelling; rupture of plasma membrane; bubbling; moderate chromatin condensation	Activation of CASP1; CASP3; and GSDMD; GSDMD cleavage; GSDMD induced pore formation; IL1B release

Table 1: Summary of programmed cell death types, with morphological and biochemical features.

Interestingly, cell death and autophagy can be cross-linked. Autophagy is a lysosome-mediated degradation pathway essential for survival, differentiation, development and homeostasis (Levine & Kroemer, 2008). Autophagy is induced by different cellular stressors, including growth factor or nutrient deprivation, hypoxia, DNA damage, ROS, protein aggregates, damaged organelles and/or intracellular pathogens (Guido Kroemer et al., 2010). Among these, nutrient depletion is the most powerful known physiological inducer of autophagy (Boya et al., 2013). Three types of autophagy are currently described: chaperone-mediated, microautophagy and macroautophagy (Mizushima et al., 2010). Chaperone-mediated autophagy, that requires chaperone proteins, involves the direct translocation of cytosolic proteins into the lysosome. Microautophagy transports a small portion of cytoplasm into the lysosome through the invagination of lysosomal membrane. Macroautophagy is mediated by the autophagosome. The autophagosome is an organelle formed by a double membrane. Starting from a small vesicle, called phagophore, the elongation and the inclusion of a portion of cytoplasm lead to the formation of the autophagosome. Subsequently, the outer membrane of the autophagosome fuses with a lysosome, degrading the portion of cytoplasm included into the autophagosome. All the small molecules generated by this degradation are released to the cytoplasm contributing to recycling and/or energy production (Klionsky et al., 2016; Mizushima et al., 2010).

The biochemical pathway of mammalian autophagy involves at least five molecular components: the ATG1/UNC-5-Like Kinase (ULK) complex; the BECLIN1/class III

Phosphatidylinositol 3-Kinase (PI3K) complex; two transmembrane proteins, ATG9 and Vacuole Membrane Protein 1 (VMP1), two ubiquitin-like protein (ATG12 and ATG8) conjugation systems, proteins that mediate fusion between autophagosomes and lysosomes (Z. Yang & Klionsky, 2010). A relevant role in autophagy is played by the mammalian Target Of Rapamycin (mTOR) signaling pathway, that integrates both intracellular and extracellular signals. Furthermore, the mTOR signaling pathway acts as a regulator of cell metabolism, growth, proliferation and survival (Levine & Kroemer, 2008).

A rapid induction of autophagy can also follow the activation of apoptotic pathway in response to different signals including anticancer agents, ionizing radiation, inhibition of growth factor receptors or depletion of nutrients (H.-M. Shen & Codogno, 2011).

Interestingly, many signal transduction pathways caused by cell stress, regulate both autophagy and apoptosis explaining the sequential activation of both processes (Mariño et al., 2014). Moreover, the induction of autophagy can facilitate the activation of apoptosis (Mariño et al., 2014).

Autophagy inducers reduce the inhibitory interaction of mTOR with the ULK complex, leading to ULK complex activation (Y. C. Kim & Guan, 2015). Through the phosphorylation of Autophagy And Beclin 1 Regulator 1 (AMBRA1) protein, ULK complex activates the activity of PI3K complex. In addition to these two complexes, autophagosome formation requires ATG12 and ATG8 conjugation systems and ATG9 and VMP1. These two systems are essential for the biogenesis of the phagophore. In addition, ATG8 is required for autophagosome transport and maturation. Finally, autophagosomes fuse their external membranes with lysosomes acquiring hydrolytic activity. This hydrolytic activity allows the degradation of autophagosomes cargo and the recycle of essential biomolecules to the cytoplasm (Guido Kroemer et al., 2010).

The autophagosome formation has been implicated in the activation of caspase-8 (Young et al., 2012). Caspase-8 forms a complex with death receptor adaptor protein FAS-Associated Death Domain (FADD) and ATG5, becoming activated in an ATG5- and FADD-dependent manner (Young et al., 2012). Moreover, inhibition of the early steps of autophagy reduces the activation of apoptosis, whereas inhibition of the late steps of autophagy increases apoptosis, indicating that autophagosome formation plays a key role in activating apoptosis (Young et al., 2012).

Autophagy could induce apoptosis through the depletion of endogenous inhibitors of apoptosis. This was demonstrated in *Drosophila melanogaster*, where apoptosis is mostly regulated by the interplay between caspases and inhibitor of apoptosis proteins (IAPs). One of these IAPs,

BRUCE (BIR-Containing Ubiquitin-Conjugating Enzyme), is degraded by autophagy, highlighting the autophagic stimulation of apoptosis (Nezis et al., 2010).
In addition, the ATG proteins, that play an essential role in autophagy (Mizushima et al., 2011; Wesselborg & Stork, 2015), may also contribute to lethal signaling independently of the activation of autophagic process (Mariño et al., 2014). ATG12 could have a role in activating caspases, as its depletion reduces caspase activation in response to various apoptotic stresses, including ceramide, etoposide, paclitaxel, staurosporine or tunicamycin (Rubinstein et al., 2011).
ATG7 facilitates the induction of apoptosis after lysosomal photodamage triggering lysosomal membrane permeabilization (Kessel et al., 2012).

Aims and overview of the thesis

The project aims at the identification of early molecular markers that allow the prediction of cell fate in eukaryotic organisms: the unicellular eukaryote *Saccharomyces cerevisiae* and the multicellular organism *Homo sapiens*.
Saccharomyces cerevisiae was selected for its usefulness in detecting novel molecular processes due to its simple cell organization. Moreover, it is notoriously considered a model system of relevance in Food Science and in molecular studies of physiological processes of metazoan cells (Madeo et al., 1999). *H. sapiens* was considered for understanding the impact of our approaches also for human healthcare and well-being.
The scope is to further investigate the molecular features that characterize gene expression during cell stress response and its outcomes to define key markers for the early detection of cell fate. The idea is to acquire knowledge for the design of sensitive molecular techniques for applications in different fields of Food Science. The results will be of use for diagnostics of cell systems exposed to bioactive substances contained in foods, for food quality, and for monitoring and predicting the cell fate (survival or cell death) in cell culture or in bioreactors.
Our approach was mainly based on bioinformatic analyses of available gene expression data, from *H. sapiens* and *S. cerevisiae* cells. Specifically we collected data from the sequence reads archive (SRA) (Leinonen et al., 2010) selecting RNA-seq dataset of non-mutant *H. sapiens* and *S. cerevisiae* cells undergoing different types of stress and programmed cell death.
We initially focused on the analysis of RNA-seq data related to programmed cell death both for *Saccharomyces cerevisiae* and *Homo sapiens*.

We set up a dedicated data processing pipeline to re-analyze publicly available raw datasets to obtain differentially expressed genes during programmed cell death.

With the same approach we analyzed stress response experiments for both species to compare gene expressions between programmed cell death and cell stress. Our aim was to identify genes that have a specific expression trend in programmed cell death which is opposite with the one revealed in stress response and therefore could be used to distinguish initiation of programmed cell death.

Considering gene expression data from nutrigenomics experiments, we selected food natural compounds that could influence the expression of programmed cell death related genes resulting in the induction of programmed cell death.

A bioinformatics pipeline for the assessment of absorption, distribution, metabolism and excretion of new natural compounds, was designed to select natural compounds that could play a role in human health and well-being.

The different objectives of our study and associated results are presented in different chapters of the thesis and are here summarized. In chapter 2, with the scope of identifying molecular markers for an early prediction of cell fate in yeast, we focused on the analysis of RNA-seq data related to yeast programmed cell death caused by acetic acid (Dong et al., 2017). Beyond confirming typical hallmarks of programmed cell death in yeast, as also highlighted by Dong et al, (Dong et al., 2017), the analysis highlighted transcriptomic changes in genes associated with ribosome biogenesis, mRNA decapping, translation accuracy and paralog gene expression (ohnologs). These results, beyond highlighting a peculiar change in ohnologs gene expression, provide novel hints and markers useful for the early diagnosis of cell progress towards programmed cell death.

In chapter 3, the analysis of 9 RNA-seq related to *H. sapiens* cell death and 36 RNA-seq related to *H. sapiens* cell stress was aimed at the identification of molecular markers that could trace the post-stress processes and the progress towards programmed cell death. The analyses resulted in the identification of 734 putative candidate genes involved in *H. sapiens* programmed cell death. Furthermore, exploiting comparative computational analyses, this list of *H. sapiens* genes was compared with the gene expression trends of the corresponding ortholog genes in *S. cerevisiae*, confirming their common behavior in programmed cell death in both species and, therefore, their evolutionary conserved role.

In chapter 4, we further investigated on the 734 *H. sapiens* genes. Because one of the cancer hallmarks is the evasion to cell death (Hanahan & Weinberg, 2011), we investigated on the

behaviors of these genes in nutrigenomics treatments that induce cell death. One of the roles of nutrigenomics is to help Food Science on defining the role of nutrients and bioactive compounds for the prevention and the treatment of chronic diseases, such as cancer (Sales et al., 2014).

Our aim was to implement bioinformatics strategies to select food natural compounds from nutrigenomics experiments that could modulate the expression of the new programmed cell death related genes resulting in the induction of programmed cell death. This led to the identification of natural compounds, that modulate the expression of 149 new programmed cell death related genes.

Therefore, the 149 genes were further analyzed to identify genes with opposite expression trend between apoptotic treatments and cancer, resulting in a list of 22 genes that show an opposite expression trend. Focusing on their survival role in cancer patients, 7 genes whose expression is modulated by 6 natural compounds, were highlighted.

Lastly, starting from the 6 bioactive compounds that modulate the expression of the 7 genes, new compounds and foods useful in cancer treatments and/or prevention were identified. These results are useful for diagnostics of cell systems exposed to bioactive substances contained in foods and for human care.

Due to the great interest in the treatment of infectious diseases using natural compounds, we also tested the bioinformatics procedure implemented in this thesis to find natural compounds that could be useful for the treatment of infectious diseases, in particular for COVID-19. (chapter 5). Bulk RNA-seq and single-cell RNA-seq (scRNA-seq) from tissues and cells from COVID-19 infected patients were downloaded and used to identify natural compounds affecting genes differentially expressed in human infected tissues. We selected 44 genes that show the same expression trend between the bulk RNA-seq and the scRNA-seq experiments. Moreover, we investigated this collection with the principal aim of identifying those genes that have an opposite expression trend between SARS-CoV-2 infected patients and nutrigenomics treatments. We selected 13 genes associated to 26 different natural compound treatments. Performing the adsorption, the distribution, the metabolism, the excretion (ADME) analysis and excluding those with mutagenic, tumorigenic or irritant effects, we selected 4 natural compounds that regulate the expression of 7 genes. Further investigations based on the similarity with the 4 natural compounds led to the identification of additional 753 similar natural compounds. Excluding those with mutagenic, tumorigenic or irritant effects not respecting the

ADME parameters, we obtained a list of 27 natural compounds. We propose these 27 compounds as new candidate natural compounds that could play a role in COVID-19 care.

Chapter 2: Translational reprogramming as an early marker of programmed cell death in *Saccharomyces cerevisiae*

Abstract

In order to identify additional transcriptional molecular markers useful for the early prediction of the progress of cell stress response towards programmed cell death in yeast, we investigated RNA-seq data previously published by (Dong et al., 2017). Specifically, the authors investigated yeast response after exposure to acetic acid. It is well known that acetic acid induces programmed cell death in yeast (Carmona-Gutierrez et al., 2018; Ludovico et al., 2001). The results highlight transcriptomic changes in genes associated with ribosome biogenesis, mRNA decapping, translation accuracy and ribosomal protein paralog replacement, depicting a deep translational reprogramming preluding yeast programmed cell death.

To further investigate on the peculiar response here highlighted for the first time during yeast programmed cell death, we also considered additional transcriptome collections concerning 12 different types of stress. Interestingly, we highlight that paralog replacements are not only involving ribosomal proteins, but it is a more extensive process. Specifically, while paralogs replacements occur both in programmed cell death and in stress responses, a typical trend was shown in programmed cell death. In particular, this programmed cell death specific replacement typically acts on sporulation, changes in the ribosome population, decapping of mRNA and methionine biosynthesis.

Materials and methods

RNA-seq data of *Saccharomyces cerevisiae* exposed to acetic acid at three different time points (45, 120 and 200 minutes) (Dong et al., 2017) and 12 different stresses (heat shock, hyperosmotic shock (NaCl), glucose depletion, endoplasmic reticulum stress (tunicamycin), oxidative stress (menadione), proteotoxic stress (azetidine), target of rapamycin inhibition (rapamycin), antifungal drug exposure (fluconazole) (Mace et al., 2020), cell wall stress (puupehenone, caspofungin, puupehenone – caspofungin) (Tripathi et al., 2020) and oxidative stress (H2O2) (Blevins et al., 2019) were downloaded from SRA (Leinonen et al., 2010). Raw reads were trimmed with Trimmomatic (release 0.38) (Bolger et al., 2014) and aligned to *S. cerevisiae* strain S288c genome (version R64-1-1) using STAR (release 2.6.0) (Dobin et al., 2012) (settings: outFilterScoreMinOverLread=0, outFilterMatchNminOverLread=0,

outFilterMatchNmin=0, alignIntronMax=10000, and other parameters as default values). Reads counting was performed using FeatureCounts (release 1.6.3) (Liao et al., 2013) (settings: t="exon", g="gene_id", s="0", with the overlapping option and other parameters as default values). Read counts were normalized by count per million (CPM), filtering genes with CPM≥1 in each replicate per treatment and control. The differential expression analysis was done using edgeR (Robinson et al., 2009). Only genes with $|\log_2 \text{Fold change}| \geq 1$ and false discovery ratio (FDR)<0.05 were considered as significant differentially expressed genes (DEGs).

Gene Ontology (GO) enrichment analysis was performed using YeastMine (https://yeastmine.yeastgenome.org/yeastmine/begin.do) (Balakrishnan et al., 2012), filtering enriched GOs at p-value<$1x10^{-4}$.

Enriched biochemical pathways were obtained by ConsensusPathDB-yeast (http://cpdb.molgen.mpg.de/YCPDB) (Herwig et al., 2016), filtering enriched pathways at p-value<$1x10^{-4}$.

Paralogs genes in *Saccharomyces cerevisiae* were downloaded from the Saccharomyces Genome Database (https://www.yeastgenome.org/) (Cherry et al., 2011) and cross-confirmed by Byrne et al. (Byrne & Wolfe, 2005).

The classification of major and minor paralogs in ohnolog ribosomal protein genes was downloaded from Ghulam et al. (Ghulam et al., 2019).

Only ohnologs in which the ratio between ohnolog 1 and ohnolog 2 expression changes after acetic acid treatment and that is reported specifically in acetic acid treatment, were considered cell death specific.

Results

The processing of the RNA-seq related to cell death of *S. cerevisiae* exposed to acetic acid (Dong et al., 2017) resulted in 1118 genes at 45 minutes, 974 at 120 minutes and 1061 after 200 minutes, respectively (**Figure 3, Supplementary Table S1**).

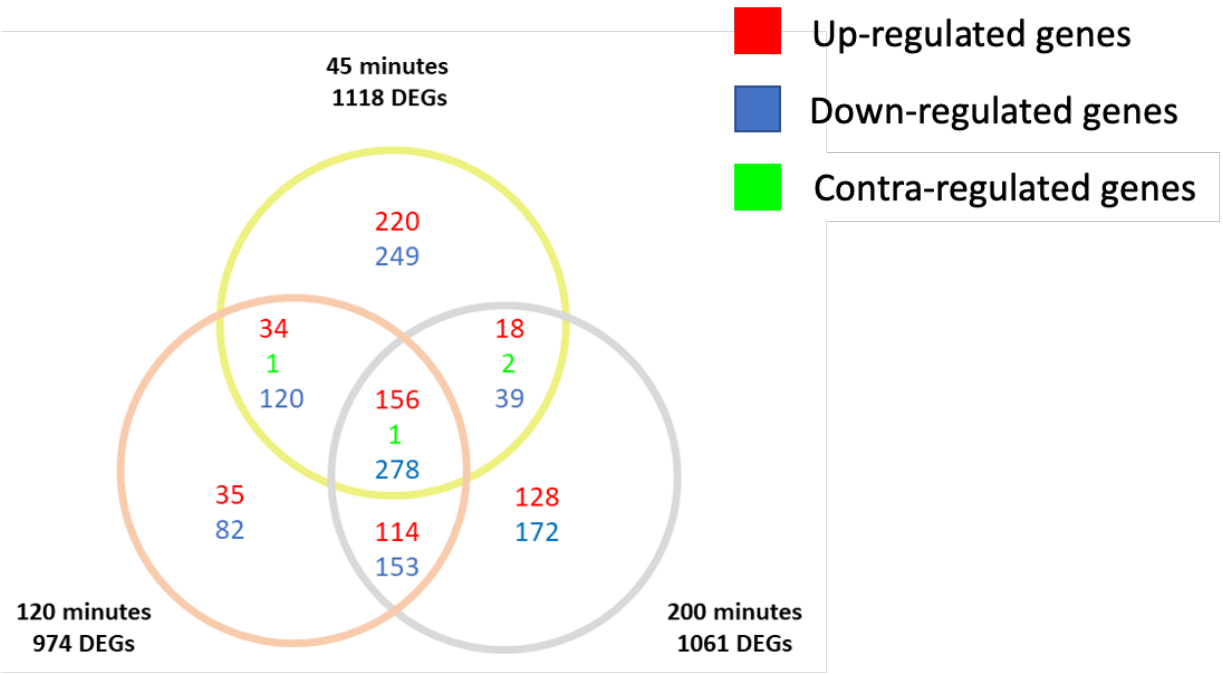

Figure 3: Number of significant differentially expressed genes per exposure time.
Total differentially expressed gene (DEGs) (in black) per time point and Venn diagram representing the up-regulated genes (red), the down-regulated genes (blue) and the contra-regulated genes (green). (Reported from (Monticolo et al., 2021)).

Interestingly 435 DEGs are in common between the three treatments (**Figure 3**). In particular, 156 resulted always up-regulated and 278 were always down-regulated in the three experimental time points, whereas one gene resulted to be up-regulated at 45 minutes, and down-regulated at 120 and 200 minutes (**Figure 3**).

The GO enrichment analysis at each time point highlights an enrichment in GOs related to ribosome organization (**Figure 4**).

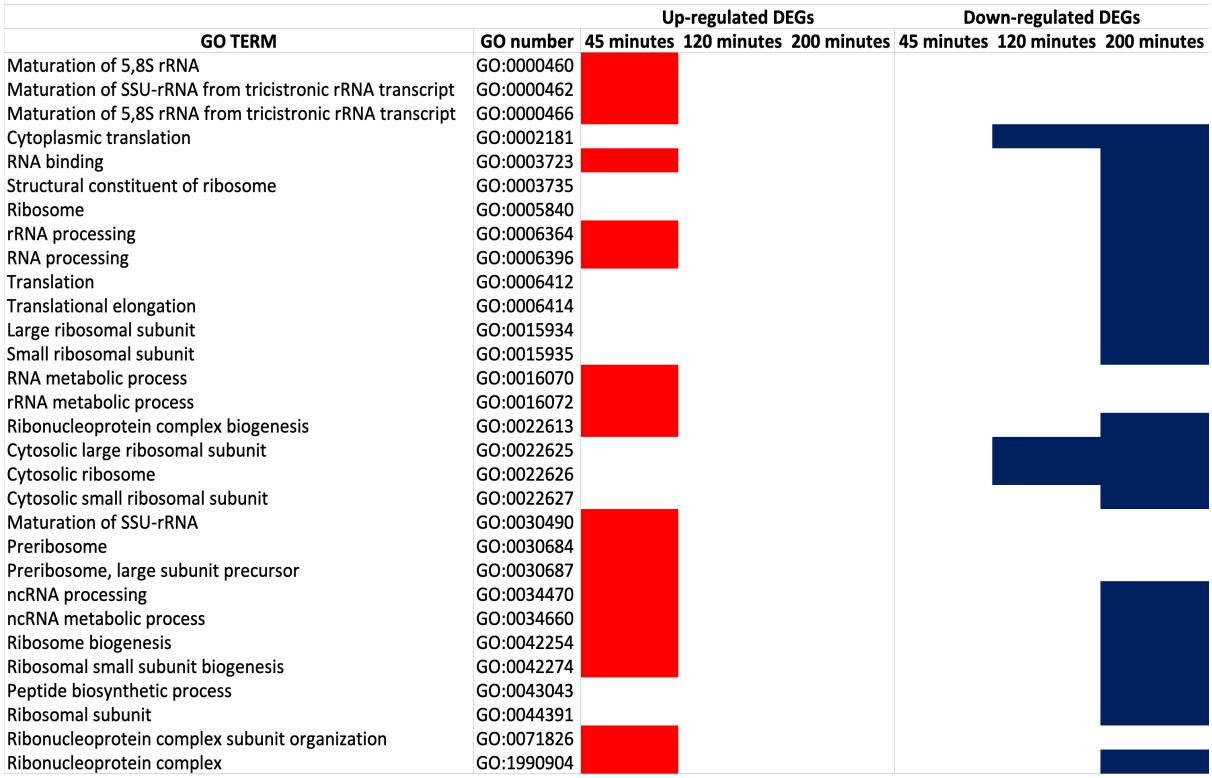

Figure 4: Gene Ontology (GO) enrichment analysis.
List of enriched GOs related to ribosome per exposure time. Colored cells per GO indicate significant enrichment (red for GOs related to up-regulated DEGs; blue for GOs related to down-regulated DEGs). (Reported from (Monticolo et al., 2021)).

Interestingly, GOs related to rRNA processing and ribosome biogenesis are enriched by up-regulated genes exclusively at 45 minutes (**Figure 4**). GOs related to cytosolic ribosome, ribosome biogenesis, rRNA processing and translation are enriched by down-regulated genes starting from 120 minutes (**Figure 4**).

The pathways enrichment with DEGs down-regulated at 120 and 200 minutes confirmed the down-regulation of processes related to ribosomal biosynthesis, ribosomal scanning and start codon recognition and cap-dependent translation initiation (**Supplementary Table S2**).

Focusing on DEGs, it is worthy to note that EDC1 (YGL222C), involved in mRNA decapping (Dunckley et al., 2001; Neef & Thiele, 2009), is up-regulated at 200 minutes (**Supplementary Table S1**). Moreover, ASC1 (YMR116C), involved in control and in fidelity of the mRNA translational activity (Wolf & Grayhack, 2015), is down-regulated at 120 and 200 minutes (**Supplementary Table S1**).

Among DEGs, 127 RPGs resulted to be DEGs in at least one stage of the treatments by acetic acid (**Supplementary Table S1**). This led to a deeper investigation on the differential expression of all the 137 RPGs annotated (**Supplementary Table S3**). Focusing on gene

expression in non-treated samples, an increment of expression is reported in 134 RPGs (**Supplementary Table S3**) whereas, in treated samples, a decrease of expression is reported in 115 RPGs (**Supplementary Table S3**).

Moreover, comparing the expression levels at 45 minutes, 56 RPGs show a higher expression in treated samples than in non-treated samples (**Supplementary Table S3**). It is worth to note that for 30 RPGs the higher expression concerns only one of the two paralogs. At 120 minutes, in 6 RPGs the expression is higher in treated samples than in non-treated ones and, in all the cases, only one of the two paralogs is involved. At 200 minutes, in 3 RPGs the expression is still higher in treated samples than in non-treated ones, and again, all the 3 RPGs involve only one of the two paralogs (**Supplementary Table S3**). In summary, among the 137 RPGs, 56 have a higher expression in the treatment compared with the relative control experiment, and in 30 out of 38 couples of genes, only one of the two paralogs shows this behavior.

In 2019, Ghulam et al. (Ghulam et al., 2019) classified major and minor paralogs in 20 couples of ohnologs (first 20 couples listed in **Supplementary Table S3**), among the 58 couples RPGs ohnologs reported in the yeast genome annotation.

Ohnologs are duplicated genes derived from whole genome duplication (WGD). They provide a pool of new genetic material from which new functions or specialization of daughter genes can evolve (Byrne & Wolfe, 2005; Zhang, 2003).

Ghulam et al. (Ghulam et al., 2019) showed that, cells exposure to stress led to decrease of ratio between major and minor paralog gene expression, because of the down-regulation of the major paralog and/or the up-regulation of the minor one (Ghulam et al., 2019).

Interestingly, a change in paralogs ratio of 3 of the annotated couples from (Ghulam et al., 2019) is highlighted during cell death (**Supplementary Table S3**). Moreover, considering the remaining not yet classified couples of paralogs, the ratio changes also in 8 additional couples (**Supplementary Table S3**). In particular, at 45 minutes the ratio is changed in 3 couples, at 120 minutes in 4 and at 200 minutes in 6 couples, respectively (**Supplementary Table S3**).

In order to investigate the behavior and the specificity of all the 551 ohnologs pairs, the processing of RNA-seq data related to 12 different stresses (heat shock, hyperosmotic shock (NaCl), glucose depletion, endoplasmic reticulum stress (tunicamycin), oxidative stress (menadione), proteotoxic stress (azetidine), target of rapamycin inhibition (rapamycin), antifungal drug exposure (fluconazole) (Mace et al., 2020), cell wall stress (puupehenone, caspofungin, puupehenone – caspofungin) (Tripathi et al., 2020) and oxidative stress (H2O2) (Blevins et al., 2019) was performed.

Only ohnologs in which the ratio between ohnolog 1 and ohnolog 2 expression changes after acetic acid treatment and that is reported only in acetic acid treatment were considered cell death specific (**Supplementary Table S4**).

This led to the identification of 54 ohnolog pairs switches specific for programmed cell death induced by acetic acid treatment at 45 minutes after treatment; 54 ohnolog pairs switches specific for programmed cell death induced by acetic acid treatment at 120 minutes after treatment and 53 ohnolog pairs switches specific for programmed cell death induced by acetic acid treatment at 200 minutes after treatment (**Supplementary Table S4**).

Focusing only on ohnolog pairs switches specific for programmed cell death induced by acetic acid, the ratio between ohnologs couple YHR033W and PRO1 (YDR300C) is changed (in favor of PRO1) at all three time points after treatments (**Supplementary Table S4**). YHR033W encodes for putative protein of unknown function whereas PRO1 encodes for a gamma-glutamyl kinase involved in the selective autophagy of ribomosome (ribophagy) (Tatehashi et al., 2016). Furthermore, YHR033W is down-regulated 45 minutes after acetic acid treatment whereas PRO1 is up-regulated after 45 minutes (**Supplementary Table S4**).

The ratio between GLK1 (YCL040W) and EMI2 (YDR516C) is changed (in favor of EMI2) from 45 minutes after treatment to 200 minutes after treatment and GLK1 results to be down-regulated whereas EMI2 results to be up-regulated at all three time points after acetic acid treatment (**Supplementary Table S4**). EMI2 encodes for a glucokinase not involved in glucose phosphorylation but required for transcriptional induction of the master regulator of sporulation IME1 (YJR094C) (Enyenihi & Saunders, 2003), whereas GLK1 encodes a glucokinase active in phosphorylating glucose (Legrand et al., 2016).

The ratio between MHT1 (YLL062C) and SAM4 (YPL273W) is changed in favor of SAM4 at all three time points after acetic acid treatment (**Supplementary Table S4**). Interestingly, at 45 minutes SAM4 results to be up-regulated whereas MHT1 is down-regulated (**Supplementary Table S4**). SAM4 is a S-adenosylmethionine(AdoMet)-homocysteine methyltransferase whereas MHT1 is a S-methylmethionine-homocysteine methyltransferase involved in the methyonine biosynthetic pathway (Thomas et al., 2000).

The ratio between GSY1 (YFR015C) and GSY2 (YLR258W) is changed in favor of GSY1 at 200 minutes after acetic acid treatment. Interestingly GSY1 resulted up-regulated at 45, 120 and 200 minutes after acetic acid treatment (**Supplementary Table S4**). These genes encode for glycogen synthase of which Gsy2p is predominant (80% of the glycogen synthase activity) (Wang et al., 2001).

The ratio between ohnologs couple TDA6 (YPR157W) and VPS62 (YGR141W) is changed (in favor of TDA6) from 45 minutes after acetic acid treatment up to 200 minutes after treatment (**Supplementary Table S4**) and TDA6 results up-regulated from 45 minutes after acetic acid treatment up to 200 minutes whereas VPS62 results down-regulated at all three time points. Interestingly, TDA6 encodes for a putative protein of unknown function that is up-regulated by the transcriptional factor HAA1p (Carvalho-Netto et al., 2015; Mira et al., 2011). HAA1 (YPR008W) is a gene required for a more rapid adaptation of a yeast cell population to several weak acid treatment (Fernandes et al., 2005).

Finally, the ratio between ohnologs couple EDC1 (YKL043W) and EDC2 (YMR016C) is changed (in favor of EDC1) from 45 minutes after acetic acid treatment up to 200 minutes after treatment (**Supplementary Table S4**) and EDC1 results up-regulated at 200 minutes after acetic acid treatment. These two genes encode for RNA-binding proteins involved in mRNA decapping (Schwartz et al., 2003) and, in particular, Edc1p is required for decapping during carbon-source switch (Schwartz et al., 2003).

Discussion

It is well-known that acetic acid induces transcriptomic changes (Dong et al., 2017) and programmed cell death in yeast (Carmona-Gutierrez et al., 2018; Ludovico et al., 2001). Transcriptomic changes involve genes associated with ribosome biogenesis and inducing mRNA decapping and affecting translation accuracy, indicating a reprogramming of the cell translational apparatus during the exposure. Indeed, the up-regulation of EDC1 (YGL222C), involved in mRNA decapping, highlights the possible role of this mechanism in response to exposure to acetic acid, a phenomena associated also to the yeast response to heat stress (Dunckley et al., 2001; Neef & Thiele, 2009). In addition, the down-regulation of ASC1 (YMR116C) causes higher translational activity (Gerbasi et al., 2004). Moreover, its down-regulation favors frameshifting (Wolf & Grayhack, 2015) and affects the rate and the products of protein translation during the stress response.

Moreover, a change in ohnologs of RPGs expression is highlighted.

Ohnologs are duplicated genes derived from WGD. In 1970, Ohno (Ohno, 1970) proposed that WGD is an advantageous evolutionary mechanism (Ohno, 1970). Since WGD produces duplicated genes, it can provide new genetic material for natural selection, drift and mutation (Zhang, 2003). After WGD, many duplicate genes will be eliminated (Ehrenreich, 2020; Kellis et al., 2004). Wolf et al. (Wolfe, 2000) have suggested to call duplicated genes, that did not

return to single copy, as ohnologs, in honor of Susumu Ohno (Wolfe, 2000). Ohnologs form a pool of new genetic material from which new functions (neo-functionalization) or specialization of daughter genes (sub-functionalization) can evolve through natural selection, drift and mutation (Byrne & Wolfe, 2005; Zhang, 2003).

Focusing on ohnologs of RPGs, the exposure to acetic acid induces the differential expression of 127 over 137 RPGs. Moreover, the relative ratio of 11 couples of ribosomal protein ohnologs is changed during acetic acid treatment. This is in agreement with the results of Ghulam et al. (Ghulam et al., 2019), that demonstrated that RPGs paralogs relative content changes in cells exposed to stress. They also show that the repression of the major paralogs and/or the up-regulation of the minor paralogs reduce the ratio of the major versus the corresponding minor paralog in the cells, increasing the frequency of the minor paralogs in the overall ribosome population. The over-expression of 3 minor paralogs described in (Ghulam et al., 2019) is highlighted, confirming the changes of the ratios in favor of the minor paralogs during programmed cell death. Among these, also the two paralogs RPL1A and RPL1B have an opposite trend in gene expression at 45 minutes, with the down-regulation of RPL1B and the up-regulation of RPL1A, respectively. It is known that RPL1B is involved in proper mitochondrial function and morphology, roles that cannot be compensated by the paralog RPL1A when RPL1B is not present in the cell (Segev & Gerst, 2017).

In order to identify a possible programmed cell death specific behavior for all ohnologs pairs expression, 12 different stresses were analyzed and compared with acetic acid treatment.

This led to the identification of 54 ohnolog pairs switches specific for programmed cell death induced by acetic acid treatment at 45 minutes after treatment; 54 ohnolog pairs switches specific for programmed cell death induced by acetic acid treatment at 120 minutes after treatment and 53 ohnolog pairs switches specific for programmed cell death induced by acetic acid treatment at 200 minutes after treatment.

Among these, the ratio between MHT1 (YLL062C) and SAM4 (YPL273W) is changed in favor of SAM4 at all three time points after acetic acid treatment. Interestingly, at 45 minutes SAM4 results to be up-regulated whereas MHT1 is down-regulated. Sam4p appears to function exclusively with AdoMet as a substrate whereas Mht1p is less specific, capable of transferring to homocysteine the methyl group of either AdoMet or S-methylmethionine (SMM) (Thomas et al., 2000). The induction of SAM4 expression in response to high extracellular methionine indicates that the Sam4p AdoMet-homocysteine methyltransferase plays a major role in the control of the equilibrium between methionine and AdoMet in yeast cells (Thomas et al., 2000).

Interestingly, in the presence of high extracellular methionine, yeast cells repress SMM (that through remethylation of homocysteine by SMM releases two methionine molecules) but not AdoMet utilization (that releases only one methionine molecule). It is worthy to note that homocysteine is only needed at a catalytic level for AdoMet-dependent methylation. Indeed the reaction also produces S-adenosylhomocysteine, which in turn is converted into homocysteine by the S-adenosylhomocysteine hydrolase (Thomas et al., 2000). Interestingly, the S-adenosylhomocysteine hydrolase SAH1 (YER043C) is down-regulated at 120 and 200 minutes after acetic acid treatment (**Supplementary Table S1**) indicating a possible S-adenosylhomocysteine accumulation. In 2005, Kharbanda et al. report that the accumulation of hihg S-adenosylhomocysteine levels in liver is the major factor that increase cell death of cells treated with ethanol (Kharbanda et al., 2005).

Moreover, the ratio between ohnologs couple YHR033W and PRO1 (YDR300C) is changed (in favor of PRO1) at all three time points after acetic acid treatment. Furthermore, YHR033W is down-regulated at all the three time points after acetic acid treatment whereas PRO1 is up-regulated only 45 minutes after treatment. PRO1 encodes for a gamma-glutamyl kinase involved in the selective autophagy of ribomosome (ribophagy) (Tatehashi et al., 2016). Ribophagy pathway could target defective ribosomes and eliminates nonfunctional, incorrectly assembled, and/or damaged ribosomes (Cebollero et al., 2012).

Furthermore, the ratio between GLK1 (YCL040W) and EMI2 (YDR516C) is changed (in favor of EMI2) from 45 minutes after acetic acid treatment to 200 minutes. Interestingly, GLK1 results to be down-regulated whereas EMI2 up-regulated at all the three time points after acetic acid treatment. EMI2 encodes for a glucokinase not involved in glucose phosphorylation but required for sporulation (Enyenihi & Saunders, 2003), whereas GLK1 encodes a glucokinase active in phosphorylating glucose (Legrand et al., 2016). The presence of at least some non-fermentable carbon, such as acetate (Fast, 1973), is crucial for the initiation of sporulation (Eastwood & Meneghini, 2015). Sporulation in yeast is characterized by sequential transcription of at least four sets of genes: early, middle, mid-late and late. Most of the known early genes are involved in meiotic prophase (Chu et al., 1998). This process is triggered by the expression of the IME1 transcription factor. Ime1p acts as a master regulator of the sporulation process, in fact ectopic expression of IME1 is sufficient to induce sporulation of vegetative diploid cells (Eastwood & Meneghini, 2015). Thus, the expression of IME1 defines cell fate inducing the transcription of early meiotic genes required for entry into pre-meiotic S phase, for the chromosome recombination and pairing events of meiotic prophase (Primig et al., 2000).

Subsequently, the expression of NDT80 (YHR124W) initiates entry of the cells into the meiotic divisions (Eastwood & Meneghini, 2015). Ndt80p, a meiosis-specific transcription factor, has been shown to be important in inducing transcription of middle genes at the end of meiotic prophase, binding to the middle gene sporulation element motif found upstream of many of these genes (Chu et al., 1998). Interestingly, IME1 is up-regulated 45 minutes after acetic acid treatment, indicating a possible activation of sporulation process but NDT80 is down-regulated 45 minutes after treatment (**Supplementary Table S1**). These data could highlight that spore formation is repressed in response to acetic acid stress but a first tentative of activation of meiotic process is stopped in the middle phase. This could led to programmed cell death by vacuolar rupture (Eastwood et al., 2012; Eastwood & Meneghini, 2015).

Moreover, the ratio between GSY1 (YFR015C) and GSY2 (YLR258W) is changed in favor of GSY1 at 200 minutes after acetic acid treatment. GSY1 resulted up-regulated at 45, 120 and 200 minutes after acetic acid treatment. GSY2 is induced by different stress such as heat shock or nitrogen starvation (Ni & LaPorte, 1995). Interestingly, during programmed cell death induced by acetic acid only GSY1 is up-regulated, indicating a possible role of this gene in response to acetic acid stress.

The ratio between ohnologs couple TDA6 (YPR157W) and VPS62 (YGR141W) is changed (in favor of TDA6) from 45 minutes after acetic acid treatment up to 200 minutes after treatment and TDA6 results up-regulated from 45 minutes after acetic acid treatment up to 200 minutes after treatment whereas VPS62 results down-regulated at all three time points. Tda6p is a putative protein of unknown function up-regulated by the transcriptional factor HAA1p (Carvalho-Netto et al., 2015; Mira et al., 2011). HAA1 (YPR008W) is a gene required for a more rapid adaptation of a yeast cell population to several weak acid treatment (Fernandes et al., 2005). Maximal protection is exerted against the short-chain length acetic or propionic acids (Fernandes et al., 2005). These data could highlight a specific role of TDA6 in response to acetic acid.

Finally, the ratio between ohnologs couple EDC1 (YKL043W) and EDC2 (YMR016C) is changed (in favor of EDC1) from 45 minutes after acetic acid treatment to 200 minutes after treatment and EDC1 results up-regulated at 200 minutes. These two genes encode for RNA-binding proteins that enhances decapping (Schwartz et al., 2003). Interestingly, Edc1p is required not only for decapping but also during carbon-source switch (Schwartz et al., 2003).

In 2017 Dong et al. performed metabolomic analysis on yeast cell treated with acetic acid at three time points (45 minutes, 120 minutes and 200 minutes) (Dong et al., 2017). Interestingly,

they found an up-regulation in change of intracellular glucose. In particular, they found an accumulation of glucose at 45 minutes treatments but a reduction at 120 and 200 minutes after treatment (Dong et al., 2017). The up-regulation of EDC1 could indicate a possible carbon source change due to acetate accumulation into the cells. Acetate might be consumed by the tricarboxylic acid cycle and fatty acid metabolism after conversion into acetyl Co-A (Shi & Tu, 2015; Vilela-Moura et al., 2011). In fact, citric acid is accumulated in the acetic acid-treated cells under the given conditions, but the subsequent metabolic process in tricarboxylic acid cycle was suppressed (Dong et al., 2017). The dissociated acetate could not be metabolized via tricarboxylic acid cycle, thus intracellular acetylation was largely intensified (Dong et al., 2017).

In conclusion, these results, beyond highlighting a peculiar change in ohnologs gene expression, provide novel hints and markers useful for the rapid diagnosis of cell progress towards programmed cell death.

Chapter 3: Identification of *Homo sapiens* candidate genes involved in programmed cell death by integrated comparative analyses

Abstract

A collection of 9 *Homo sapiens* transcriptome data based on RNA-seq experiments associated to programmed cell death was analyzed. Moreover, 36 different RNA-seq human cell stress response were considered and aimed at identifying key genes associated with exclusive expression trend in cell death response.

Through the identification of dysregulated pathways across the experiments and determining co-expressed genes, the list of potential novel human genes involved in programmed cell death was expanded. The resulting list of co-expressed genes was then crosschecked with transcriptome expression levels from cell stress identifying key genes associated with exclusive expression trend in cell death response.

Finally, using the power of comparative functional genomics, the list of new *H. sapiens* candidate genes was compared with the corresponding cell death related ortholog genes in *S. cerevisiae*, to identify potential novel genes involved in programmed cell death.

Materials and methods

RNA-seq data from 9 experiments from *H. sapiens* apoptosis (Eriksson et al., 2017; Oh et al., 2017; Pulikkan et al., 2018; Rouhimoghadam et al., 2018; Sant et al., 2018; Sareddy et al., 2017; Sun et al., 2017) and 36 from stress conditions (Iglesias-Bartolome et al., 2018; Landeras-Bueno et al., 2016; Marais et al., 2017; Quirós et al., 2017; Rendleman et al., 2018; Tajan et al., 2018), together with one experiment (SRP075510) of expression profiling at three different time points from *Saccharomyces cerevisiae* induced cell death by exposure to acetic acid (Dong et al., 2017) were downloaded from SRA (Leinonen et al., 2010).

Raw reads were trimmed with Trimmomatic (release 0.38) (Bolger et al., 2014) and mapped to the *H. sapiens* genome sequence (version GRCh38.96) using STAR (release 2.6.0) (Dobin et al., 2012) (settings: outFilterScoreMinOverLread=0, outFilterMatchNminOverLread=0, outFilterMatchNmin=0, alignIntronMax=10000, and other parameters as default values). Reads counting was performed using FeatureCounts (release 1.6.3) (Liao et al., 2013) (settings: t="exon", g="gene_id", s="0", with the overlapping option and other parameters as default values). Read counts were normalized by CPM, filtering protein coding genes with CPM≥1 in each replicate per treatment and control. The differential expression analysis was done using

edgeR (Robinson et al., 2009). Only genes with $|\log_2\text{Fold change}| \geq 1$ and FDR<0.05 were considered as significant DEGs.

Dysregulated pathways were obtained using gep2pep (v 1.8.0) (Napolitano et al., 2019) using as pathway database MSigDB (v 7.1) (Liberzon et al., 2011). Only pathways with p-value <0.01 were considered as significant.

Co-expression analysis to identify different modules in *H. sapiens* apoptosis was performed with the R package WGCNA (Langfelder & Horvath, 2008), using as input the log2(Reads Per Kilobase Million (RPKM) +1) of protein coding genes with at least 10 raw reads mapped in at least 80% of replicates.

To test whether the identified modules are stable, the modulePreservation function of Weighted correlation network analysis (WGCNA) R package (Langfelder & Horvath, 2008) (with nPermutations = 200) was used. The preservation statistic Zsummary > 10 was used to quantify the preservation of gene modules among the datasets.

H. sapiens GO enrichment analysis was performed using the anRichment R package (Langfelder, 2018), filtering enriched GOs at FDR<0.01.

Enriched biochemical pathways were obtained by the ConsensusPathDB (http://cpdb.molgen.mpg.de/CPDB) (Herwig et al., 2016), filtering enriched pathways at q-value <0.01.

Genes involved in autophagy were obtained from the Human autophagy database (http://autophagy.lu/clustering/).

GO annotation and Orthologs between *Homo sapiens* and *Saccharomyces cerevisiae* were obtained from Biomart (Ensembl release 101) (Smedley et al., 2009).

Results

The number of DEGs resulting from the 9 RNA-seq experiments on *H. sapiens* cells exposed to apoptotic stimuli is reported in **Figure 5**.

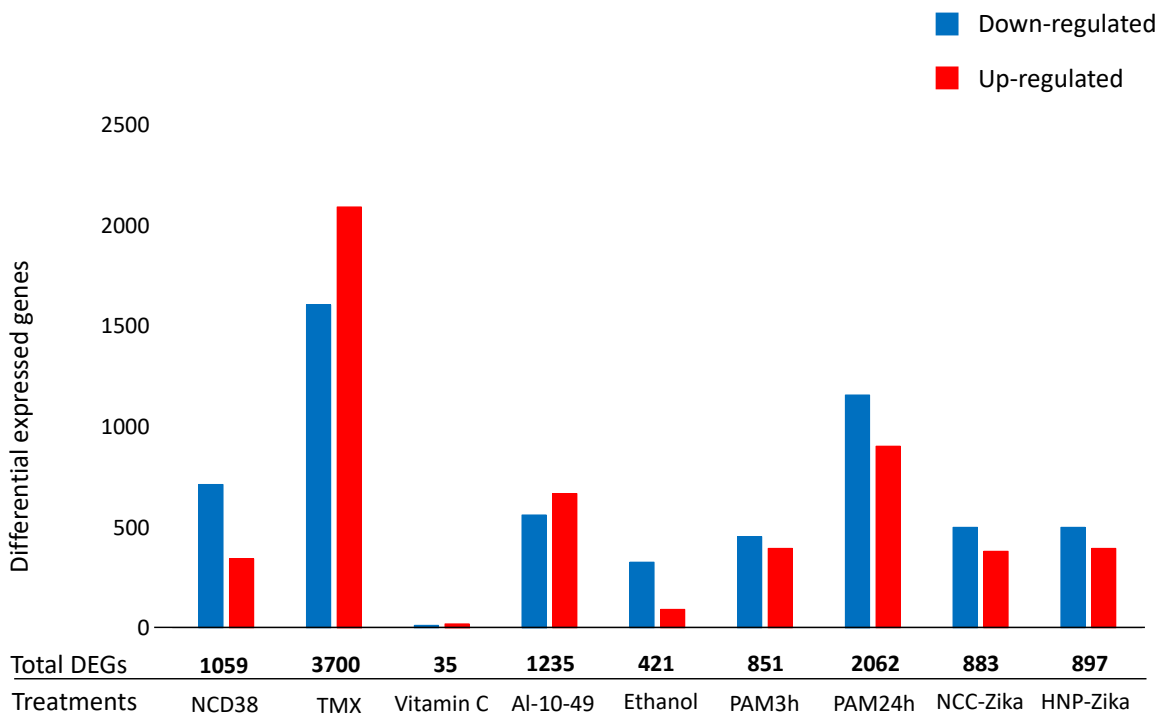

Figure 5: Number of differentially expressed genes in *H. sapiens* cell death related RNA-seq experiments. The histogram represents the number of up-regulated (red) and down-regulated (blue) DEGs for each experiment. Number in bold represents the total number of DEGs per experiments. (Reported from (Monticolo et al., 2020)).

To identify GO enrichment between treatments, DEGs were analyzed by gep2pep package (Napolitano et al., 2019) highlighting 31 significantly dysregulated pathways, among which 2 pathways are strictly associated to apoptosis or to autophagy, both enriched by up-regulated genes (**Table 2**).

Dysregulated Pathways	ES	PV
Defense response to other organism	1	0,001
Innate immune response	1	0,001
Cellular response to topologically incorrect protein	1	0,002
Regulation of response to biotic stimulus	1	0,002
Response to topologically incorrect protein	1	0,002
FC epsilon receptor signaling pathway	1	0,003
Natural killer cell mediated immunity	1	0,003
Golgi organization	1	0,003
Autophagy of mitochondrion	1	0,003
Negative regulation of innate immune response	1	0,004
Protein k48 linked ubiquitination	1	0,004
Response to cytokine	0,889	0,006
Tumor necrosis factor mediated signaling pathway	0,875	0,009
Intrinsic apoptotic signaling pathway	0,875	0,009
Positive regulation of response to biotic stimulus	0,875	0,009
Organelle disassembly	0,875	0,009
Endoplasmic reticulum unfolded protein response	0,875	0,009
Forebrain development	-0,875	0,009
Embryonic morphogenesis	-0,875	0,009
Head development	-0,875	0,009
Tube formation	-0,875	0,009
Urogenital system development	-0,875	0,009
Homophilic cell adhesion via plasma membrane adhesion molecules	-0,875	0,009
Reactive oxygen species metabolic process	-0,875	0,009
Male sex differentiation	-0,875	0,009
Development of primary sexual characteristics	-0,875	0,009
Regulation of neurotransmitter levels	-0,889	0,006
Osteoclast differentiation	-1	0,002
Spindle organization	-1	0,003
Regulation of membrane lipid distribution	-1	0,008
Phospholipid transport	-1	0,008

Table 2: List of dysregulated pathways of *H. sapiens* resulting from the differential expression analysis of the cell death related treatments.
Significant Dysregulated Pathways, relative Enrichment Score (ES) and corresponding p-value (PV) in cell death treatments. Dysregulated Pathways associated to cell death are highlighted in bold. (Reported from (Monticolo et al., 2020)).

In order to identify new genes involved in programmed cell death, we performed a co-expression network analysis by WGCNA (Langfelder & Horvath, 2008), that resulted in 20 clusters of co-expressed genes in the apoptotic treatments (**Figure 6**), and 18 clusters in the controls (**Figure 7**). Permutating the 20 modules concerning the apoptotic treatments, high preservation was highlighted (**Figure 8**).

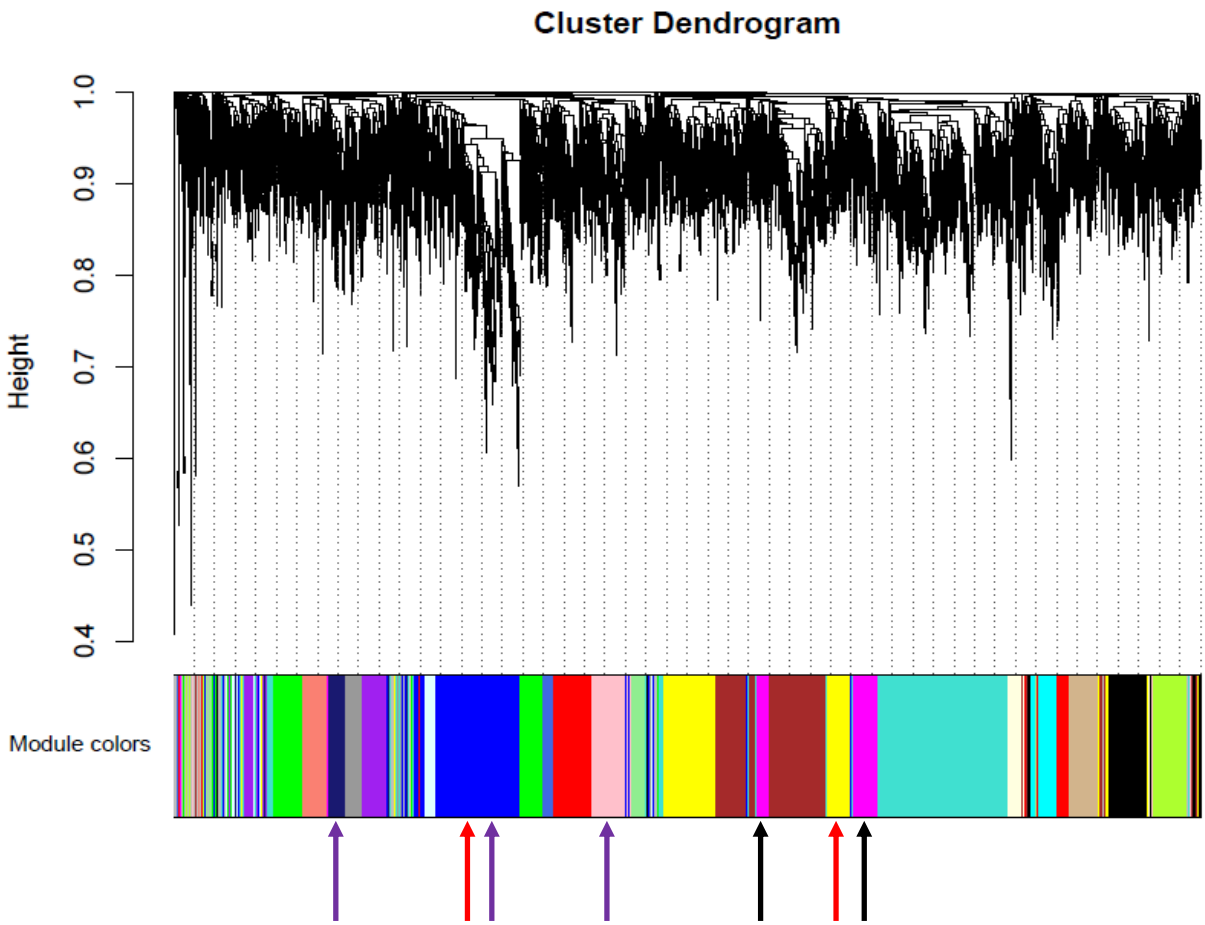

Figure 6: Dendrogram of WGCNA modules of cell death related treatments.
Modules of co-expressed genes obtained using cell death related treatments. The WGCNA modules enriched with GO related to cell death processes are highlighted with a red arrow, WGCNA modules enriched with pathway related to cell death processes are highlighted with a purple arrow and WGCNA modules enriched with pathway related to autophagy processes are highlighted with a black arrow. (Reported from (Monticolo et al., 2020)).

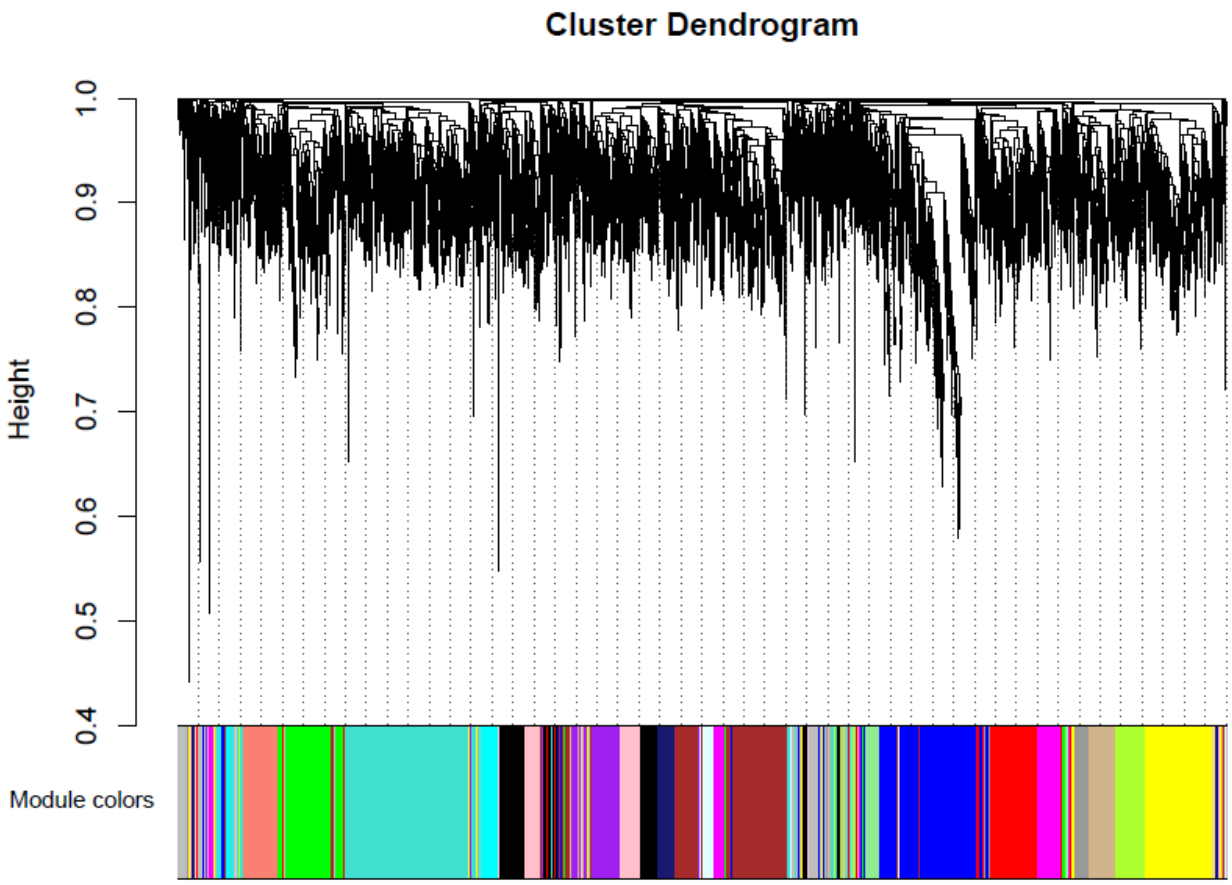

Figure 7: Dendrogram of WGCNA modules of control experiments.
Modules of co-expressed genes obtained using the control experiments results. (Reported from (Monticolo et al., 2020)).

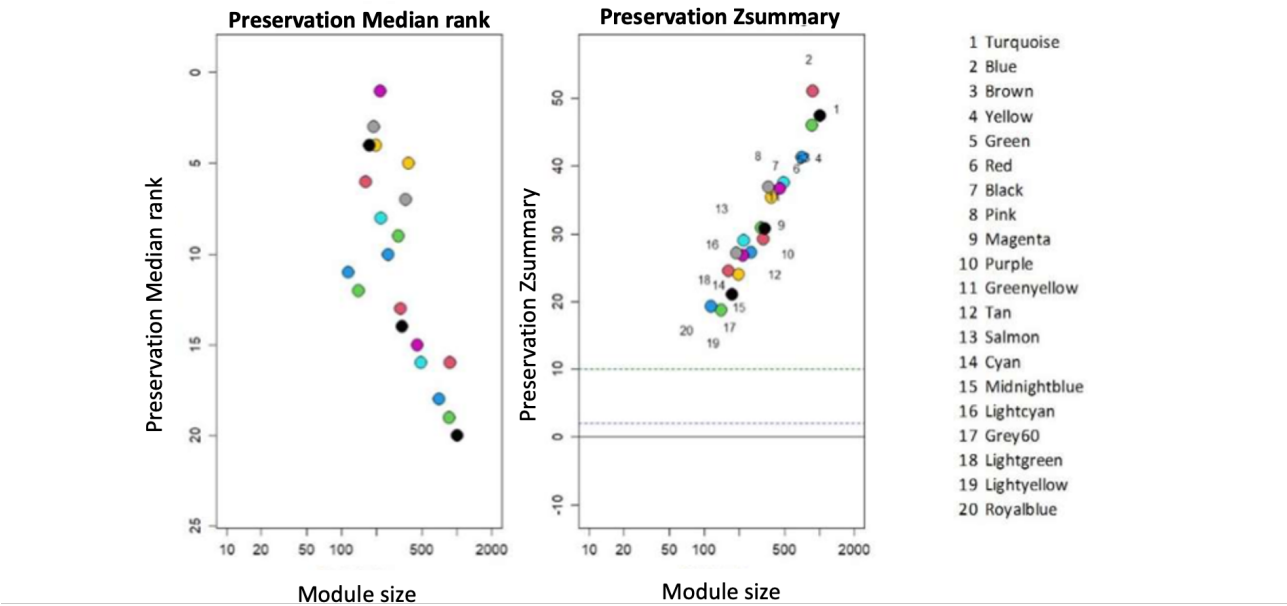

Figure 8: MedianRank and Z-summary statistics in module preservation. In the preservation medianRank graph (left), a medianRank value close to zero indicates a high degree of module preservation. In the preservation Z-summary graph (right), the dashed lines indicate the thresholds $Z = 2, 10$. These horizontal lines indicate the Z-summary thresholds for a strong conservation (above 10) and for a low to moderate conservation (above 2). (Reported from (Monticolo et al., 2020)).

The GO and the functional enrichment analysis on the modules in both treatments and controls resulted in 4 modules (blue, lightyellow, pink, and midnightblue modules) that are enriched with genes related to cell death or apoptotic processes only in treatments modules (**Supplementary Table S5**). Moreover, 2 modules (magenta and turquoise modules) are enriched with genes related to autophagy only in treatments modules (**Supplementary Table S6**).

The 6 modules of co-expressed genes in the apoptotic treatments contain 3180 genes. Interestingly, 2451 out of the 3180 genes are not reported as associated to autophagy or apoptosis processes by both GO and/or Kyoto encyclopedia of genes and genomes (KEGG) pathways. Moreover, 1051 out of the 2451 genes are DEGs in at least one of the experiments related to cell death, and 368 are DEGs in more than one experiment (**Figure 9**).

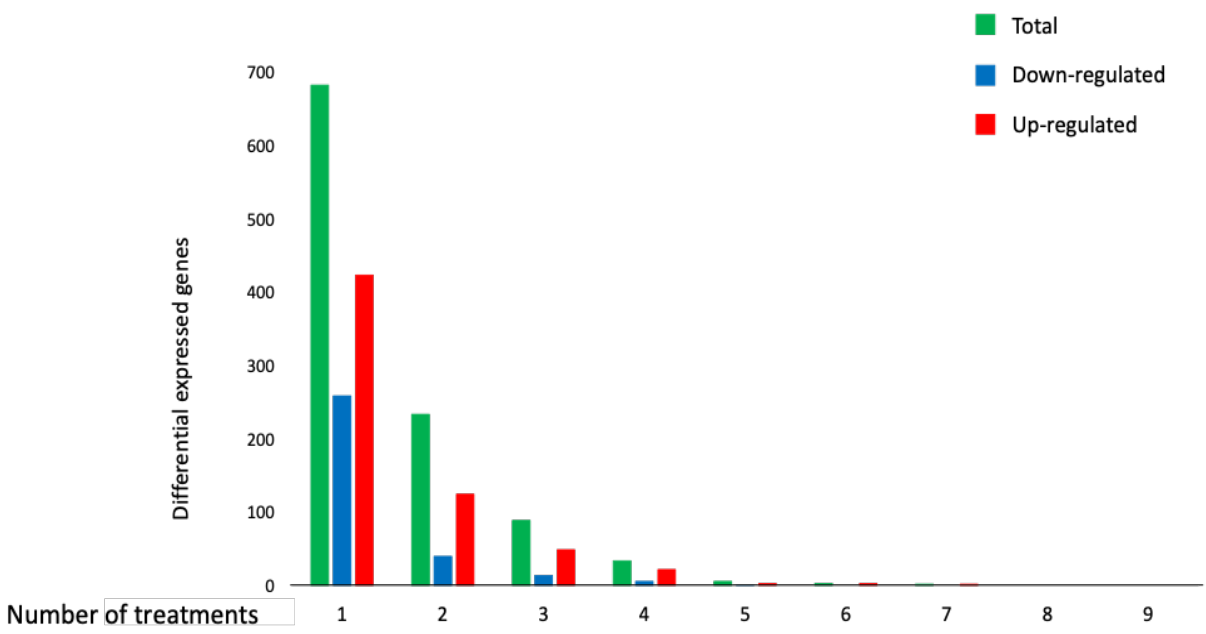

Figure 9: Distributions of the number of differentially expressed genes (DEGs) in common per number of *H. sapiens* cell death related experiments.
The histogram represents the total number of DEGs (green) for cell death treatments. The number of up-regulated (red) and down-regulated (blue) DEGs with the same expression trend are also reported. (Reported from (Monticolo et al., 2020)).

Interestingly, 948 out of 1051 genes have the same expression trend in cell death treatments (always up or down regulated in the different experiments).

The comparison of these 948 DEGs expression trend with their expression in stress related experiments leads to the identification of 734 genes that are DEGs only in cell death related experiments or with an opposite expression trend in comparison with stress experiments. Interestingly, of these 734 human DEGs, 278 genes have orthologs in *S. cerevisiae*. Comparing their expression profiles with the corresponding best ortholog in *S. cerevisiae* programmed cell death (Dong et al., 2017), 32 *H. sapiens* DEGs had an ortholog that resulted to be a DEG with the same expression trend in *S. cerevisiae* (**Table 3**).

Occurrence in cell death treatments	Cell death DEGs	Concordant cell death DEGs	Concordant DEGs specific to cell death vs stress	Orthologs with *S. cerevisiae*	Concordant in *S. cerevisiae* cell death	Confirmed in *S. cerevisiae* by GOs
1	683	683	561	155	27	2
>1	368	265	173	61	5	0
Total	1051	948	734	216	32	2

Table 3: Number of *H. sapiens* candidate genes involved in programmed cell death and orthologs with *S. cerevisiae*.
The number of differentially expressed genes in *H. sapiens* in cell death treatments (Cell death DEGs), together with the number of differentially expressed genes with the same trend of expression in *H. sapiens* cell death experiments (Concordant cell death DEGs), the concordant differentially expressed genes with expression trends specific of cell death when compared with stress experiments (Concordant DEGs specific to cell death vs stress), the number of Orthologs with *S. cerevisiae* are reported. The number of *S. cerevisiae* DEGs having the same expression trends in cell death experiments revealed in *H. sapiens* is also indicated (Concordant in *S. cerevisiae* cell death). S. cerevisiae DEGs with confirmed GOs related to cell death or autophagy (Confirmed in *S. cerevisiae* by GOs) are shown.

Discussion

The analysis of *H. sapiens* cell death-related RNA-seq highlights changes in pathways related to the intrinsic apoptotic pathway and to mitophagy (the autophagy of mitochondrion). Mitophagy has a double role: it could act favoring stress adaptation removing damaged mitochondria (Green et al., 2011) or it could activate programmed cell death (Kubli & Gustafsson, 2012).

Moreover, 6 modules of co-expressed genes enriched in GO terms related to apoptosis or autophagy were identified. These 6 modules of co-expressed genes contain a total of 3180 genes. Interestingly, 2451 out of 3180 genes are not associated with a GO (Smedley et al., 2009) or pathways (Kanehisa et al., 2016) related to cell death or autophagy processes. Moreover, 1051 out of 2451 genes are DEGs in at least one experiment related to cell death.

Interestingly, 948 out of 1051 genes have the same expression trend in cell death treatments (always up or down regulated in the different experiments).

When comparing the expression trend of the 948 genes with their expression trend in 36 RNA-seq experiments of human cell stress, 734 out of 948 genes are DEGs with typical expression trends exclusive to cell death. The identification of these molecular markers could trace the post-stress processes for an early characterization of cell fate providing an innovative molecular tool in the frame of Food Science.

Exploiting comparative computational analyses, this list of *H. sapiens* genes was compared with the gene expression trends of the corresponding ortholog genes in *S. cerevisiae*, to confirm

their common behavior in programmed cell death in both species and, therefore, their evolutionary conserved role.

The 734 *H. sapiens* candidate cell death specific DEGs with their ortholog DEGs in *S. cerevisiae* exposed to acetic acid (Dong et al., 2017) were compared. Thirty-two DEGs showed the same expression trend. These genes can be considered as conserved candidate genes involved in programmed cell death in both species.

Among these 32 genes, *SURF1* in *H. sapiens* and its yeast ortholog, SHY1, are up-regulated. *SURF1*, encodes for factor involved in the biogenesis of cytochrome c oxidase. In 2007, D'Agnello et al. (Dell'Agnello et al., 2007) showed that adult Surf1−/− mice were protected from neurodegeneration at any age, showing prolonged lifespan (Dell'Agnello et al., 2007). The human gene *ABDH11* and its yeast ortholog (IMO32), are both down-regulated. In 2020, Bayley et al, (Bailey et al., 2020) demonstrated that inhibition of ABHD11 leads to a rapid increase in 2-oxoglutarate levels (Bailey et al., 2020). High levels of 2-oxoglutarate lead to reduced tumor growth, confirming a possible role in programmed cell death (Abla et al., 2020). The human gene *LTV1* and its yeast ortholog LTV1 are both up-regulated. In yeast, the ribosome assembly factor Ltv1p facilitates the incorporation of Rps3p, Rps10p, and Asc1p/RACK1 into the small ribosomal subunit. Ribosomes from Ltv1-deficient yeasts have reduced amounts of Rps10p and Asc1p and show defects in translational fidelity and ribosome-mediated RNA quality control. These defects provide a growth advantage but sensitize the cells to oxidative stress. Interestingly, glioma cancer cells have reduced levels of LTV1 and produce ribosomes lacking RPS3, RPS10, and RACK1 (Collins et al., 2018).

These genes reveal the presence of a conserved, still under investigated, pathways in the two species programmed cell death.

Furthermore, these expression markers can be exploited for the implementation of sensitive molecular devices useful for diagnostics and monitoring. In addition, they can also be exploited as key molecular targets to be controlled or influenced by specific treatments.

Chapter 4: From gene expression to functional foods: opportunities for cancer-fighting

Abstract

Previously, we identified 734 novel genes not yet reported as involved in programmed cell death. Because one of the cancer hallmarks is the evasion to cell death (Hanahan & Weinberg, 2011), we investigated on the behaviors of these genes in nutrigenomics treatments that induce cell death. One of the roles of nutrigenomics is to help Food Science on defining the role of nutrients and bioactive compounds for the prevention and the treatment of chronic diseases, such as cancer (Sales et al., 2014).

Our aim was to implement bioinformatics strategies to select food natural compounds from nutrigenomics experiments that could influence the expression of the new programmed cell death related genes resulting in the induction of programmed cell death. This led to the identification of bioactive compounds that modulate the expression of 149 new programmed cell death related genes.

Therefore, the 149 genes were further analyzed to identify genes with opposite expression trend between apoptotic treatments and cancer, resulting in a list of 22 genes that show an opposite expression trend. Focusing on their survival role in cancer patients, 7 genes whose expression is modulated by 6 natural compounds, were highlighted.

These 6 compounds were exploited to identify, by ligand based virtual screening, additional molecules with similar structure. The resulting bioactive compounds were also analyzed for their pharmacokinetics, drug-likeness and medicinal chemistry friendliness using SwissADME (Daina et al., 2017), to compute the physicochemical descriptors and predict the ADME parameters of small molecules to support drug discovery. Twenty-three natural compounds representing suitable candidates for further testing their efficacy in apoptosis induction were selected.

Materials and methods

Cell death co-expressed genes were obtained from (Monticolo et al., 2020).

Gene expression data of nutrigenomics treatments were obtained from NutriGenomeDB (Martín-Hernández et al., 2019). Among these, only the nutrigenomics treatments that are known to induce apoptosis (Agyeman et al., 2012; Batova et al., 2017; Caruso et al., 2014;

Dumont et al., 2007; Mazzio & Soliman, 2018; Moore et al., 2016; Naciff et al., 2016; Szarc vel Szic et al., 2014) and only those genes with a FDR < 0.05 and a |log2 Fold Change| > 1.5 were considered. Only genes with the same expression trend between apoptotic treatments and nutrigenomics apoptotic treatments were considered.

The comparison of the gene expression trends in apoptosis and cancer was done using GEPIA2 (Tang et al., 2019). GEPIA2 is web resource for gene expression analysis based on tumor and normal samples from the Cancer Genome Atlas (TCGA) (Network, 2013).

TCGA project provides large-scale multi-dimensional analyses of multiple chromosomal aberrations, nucleotide substitutions and epigenetic modifications that drive malignant transformations (Network, 2013). In 2014, the TCGA Research Network reported on 3,527 tumors from 12 different cancer types, integrating different -omics platforms to assay tumor DNA, RNA and a cancer-relevant set of proteins and phosphoproteins (Hoadley et al., 2014). Currently, TCGA provides data from 33 different tumor types (the PanCancer Atlas), ranging from epigenomics and genomics to transcriptomics and proteomics (Hoadley et al., 2018).

The differential expression analysis in each cancer type was determined using LIMMA option and filtering an FDR < 0.01 and a |log2 Fold Change| > 1. Only genes differentially expressed in at least one cancer type, that had a uniform behavior (up or down-regulation) in different cancer types, and with an opposite expression trend when compared with those from apoptotic treatments were considered.

The survival analysis was performed using UALCAN (Chandrashekar et al., 2017). Only genes that showed an enhanced survival plot (p-value < 0.05) when the expression trend was similar to the one shown in apoptotic induced treatments, and opposite to cancer were considered.

Protein-protein interaction analysis was performed using STRING (Szklarczyk et al., 2019). Only interactions with 0.500 “minimum required interaction score” and 25 “max number of interactors to show” were considered.

SwissSimilarity (Zoete et al., 2016) was used to identify additional bioactive natural compounds that could induce similar effects to those caused by the compounds already exploited in the nutrigenomics treatments. The SMILE format of the initial compounds was obtained using PubChem (S. Kim et al., 2021). The screening was performed using the combined score considering bioactive compounds from all libraries: PDB (Berman et al., 2000), ChEMBL (activity<10μM) (Gaulton et al., 2012), ChEBI (de Matos et al., 2010), Kinase inhibitors (ChEMBL) (Gaulton et al., 2012), GPCR Ligands (ChEMBL) (Gaulton et al., 2012), GPCR Ligands (GLASS) (Chan et al., 2015) and Human metabolomic database (HMDB)

(Wishart et al., 2018). Only compounds showing a similarity score > 0.6 with the reference compounds were considered.

SwissADME (Daina et al., 2017) was used to compute the physicochemical descriptors and predict ADME parameters. Only bioactive compounds with 0 violation of the Lipinski (Lipinski et al., 2001), Ghose (Ghose et al., 1999), Veber (Veber et al., 2002), Egan (Egan et al., 2000) and Muegge (Muegge et al., 2001) methods and ≤ 1 violation in Pan Assay Interference Compounds (PAINS) (Baell & Holloway, 2010), Brenk (Brenk et al., 2008), leadlikeness (Teague et al., 1999) and high gastrointestinal absorption were considered.

Possible unprocessed foods possibly containing one of the bioactive compounds were investigated with FooDB (http://www.foodb.ca).

Results

The previously identified 734 putative candidate genes involved in *H. sapiens* programmed cell death (Monticolo et al., 2020) were investigated exploiting NutriGenomeDB (Martín-Hernández et al., 2019), in order to identify nutrigenomics treatments that induce cell death. This analysis highlighted 149 genes that showed the same expression trend in 15 nutrigenomics experiments that induce apoptosis (**Supplementary Table S7**).

The cross comparison between the gene expression of the 149 genes responsive to apoptosis and their behavior in 33 different tumor types, permitted to select 22 genes that showed an opposite expression trend between the apoptotic/nutrigenomics treatments and cancer. The checking of the survival role of these 22 genes in the cancer types confirmed that 7 genes in 8 different cancer types had an enhanced survival role (**Table 4**, **Figure 10**).

	Treatments										Cancers							
	Apoptotic		Nutrigenomic															
	TMX	Al-10-49	Rosemary	Withaferin A	BruceineD	Japonicone A	Indole3carbinol	Indole3carbinol	Indole3carbinol	Eusynstyelamide B	DLBC	KIRC	KIRP	LGG	LIHC	PAAD	SKCM	UCEC
Cell line	**MCF7**	**ME1**	**SW620**	**MDA**	**MCF7**	**MCF7**	**MCF7**	**T47D**	**ZR75**	**LNCaP**								
Gene Symbol																		
CENPB	-	-1,3	-	-1,5	-	-	-1,5	-	-	-	Up	-	-	Up/*	-	Up	-	-
ERGIC1	-1,2	-	-	-	-	-	-	-1,7	-	-	-	Up	-	Up/*	-	Up	-	-
CD47	-1,3	-	-	-2,1	-	-	-1,6	-1,8	-1,9	-	Up	-	-	-	-	Up	-	Up/*
PAQR4	-1,5	-2,3	-3,1	-1,8	-	-	-	-	-	-1,9	Up	Up/*	Up/*	-	Up/*	Up	Up	Up
POMGNT1	-	-1,1	-	-	-1,6	-	-	-	-	-	Up/*	-	-	-	-	Up	Up/*	-
PPRC1	-	-1,9	-	-	-	-1,5	-2,1	-	-	-	Up	-	-	-	-	Up/*	-	-
SLC44A1	-1,1	-	-	-1,8	-	-	-	-1,9	-	-	Up	-	-	Up	-	Up/*	-	-

Table 4: List of the 7 genes with confirmation of enhanced survival rate in cancer types and expression trends in Apoptotic, Nutrigenomic and Cancer.
Gene identifier (Gene Symbol), expression trend (log2 fold change) in Apoptotic (TMX and Al-10-49) and Nutrigenomic treatments (Rosemary, Withaferin A, Bruceine D, Japonicone A, Indole3carbinol and Eusynstyelamide B), as well as treated Cell lines are shown. For TCGA cancer types gene regulation is reported too (UP and DOWN). Cells with asterisks indicate TCGA cancer types in which the gene expression trend in the apoptotic conditions is associated to a favorable survival outcome (Figure 1).
Note: DLBC: lymphoid neoplasm diffuse large B-cell lymphoma, KIRC: kidney renal clear cell carcinoma, KIRP: kidney renal papillary cell carcinoma, LGG: brain lower grade glioma, LIHC: liver hepatocellular carcinoma, PAAD: pancreatic adenocarcinoma, SKCM: skin cutaneous melanoma, UCEC: uterine corpus endometrial carcinoma. (Reported from (Monticolo & Chiusano, 2021)).

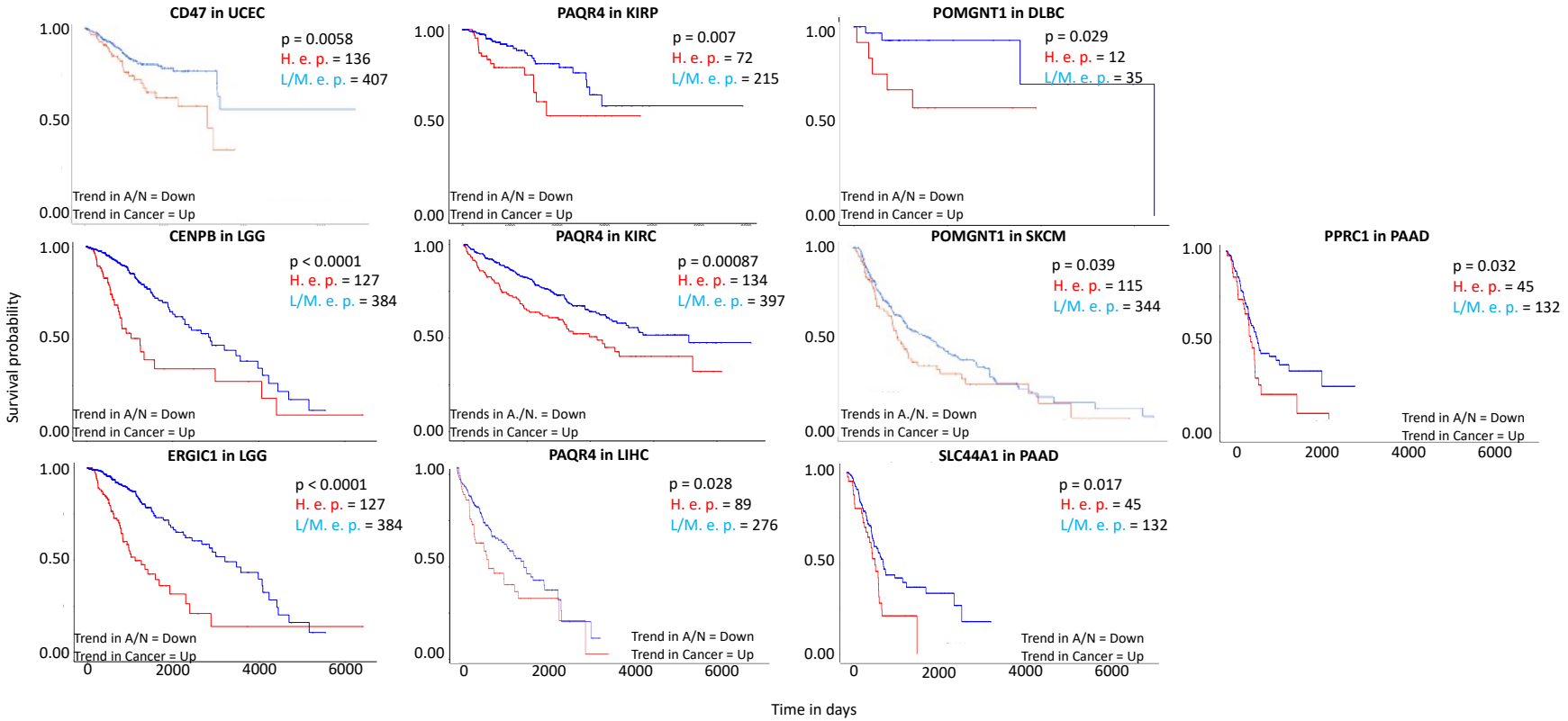

Figure 10: Survival plots **(**Kaplan-Meier curves) displaying effects of the 7 candidate genes from clinical studies.
On the y-axis the survival probability and on the x-axis the time (in days) are reported for each considered gene. H. e. p. (High expression patients) and L/M. e. p. (Low/Medium expression patients) indicate the number of patients showing a gene expression value > 3rd quartile and ≤ 3rd quartile, respectively, for each candidate gene. The statistical significance of the difference between the survival curves of H. e. p and L/M. e. p is p (p-value by the log-rank test). Trends in Apoptotic, Nutrigenomic treatments (Trend in A/N) and in cancer (Trend in Cancer) of gene expression (Up or Down regulated) are also reported. The plots suggest more favorable outcomes in patients showing the expression trends corresponding to those reported for Apoptotic and Nutrigenomic treatments.
Note: DLBC: lymphoid neoplasm diffuse large B-cell lymphoma, KIRC: kidney renal clear cell carcinoma, KIRP: kidney renal papillary cell carcinoma, LGG: brain lower grade glioma, LIHC: liver hepatocellular carcinoma, PAAD: pancreatic adenocarcinoma, SKCM: skin cutaneous melanoma, UCEC: uterine corpus endometrial carcinoma. (Reported from (Monticolo & Chiusano, 2021))

In order to investigate the protein-protein interactions of the 7 genes, STRING database was used (Szklarczyk et al., 2019) (**Figure 11**).

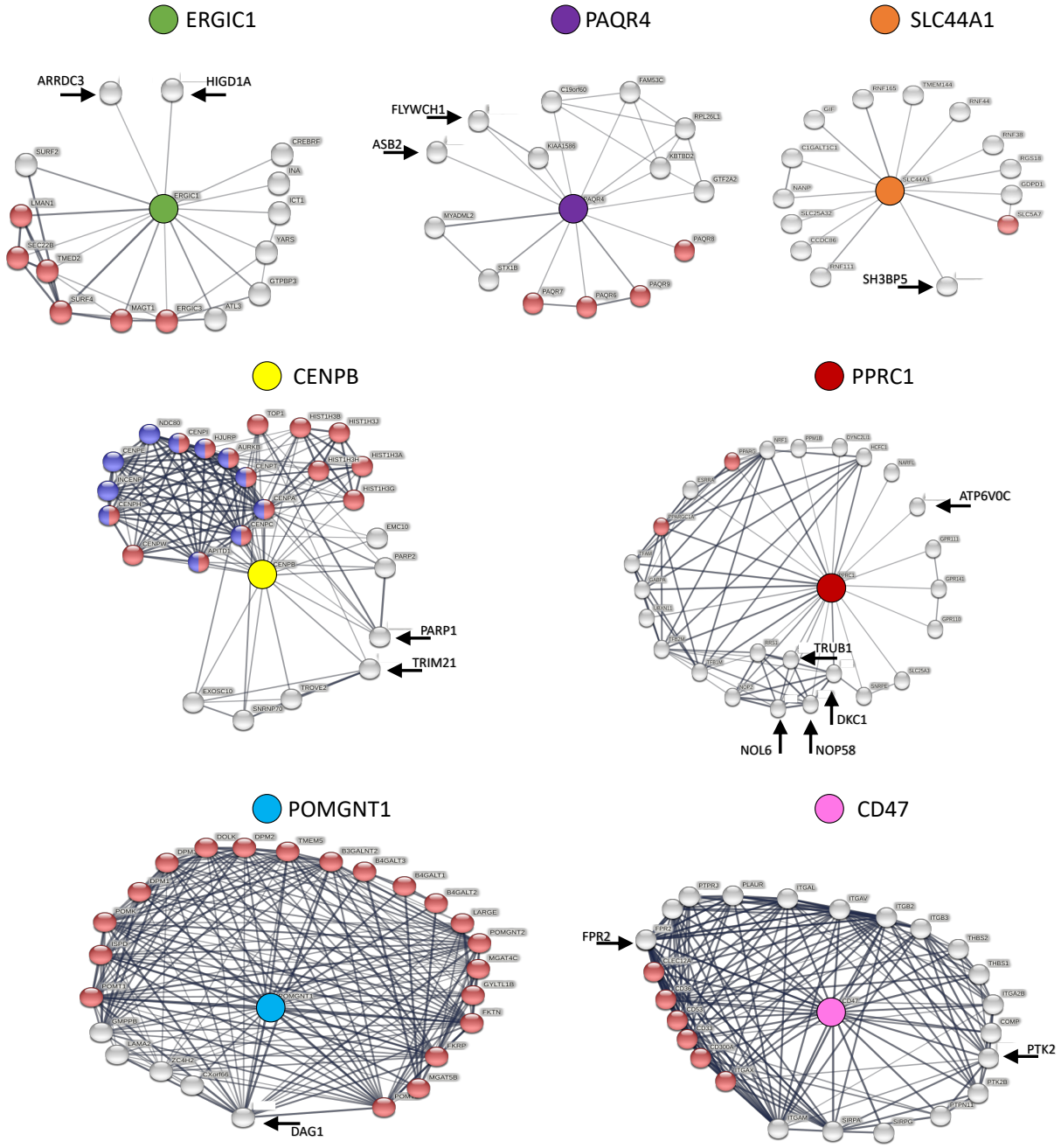

Figure 11: Functional interactions of the 7 candidate genes revealed by the STRING analysis.
CENPB (yellow ball) mainly interacts with proteins involved in chromatin organization (red balls) and proteins involved in centromere formation (blue balls). ERGIC1 (green ball) mainly interacts with proteins involved in vesicle-mediated transport (red balls). PAQR4 (purple ball) mainly interacts with other adipoQ receptor (red balls). POMGNT1 (light-blue ball) mainly interacts with proteins involved in glycosylation (red balls). PPRC1 (brown ball) interacts mainly with other peroxisome proliferator-activated receptor (red balls). SCL44A1 (orange ball) interacts mainly with other choline transporter (red balls). CD47 (pink ball) interacts mainly with other CD proteins (red balls). Black arrows and conventional gene names indicate other functional interactors with documented involvement in cancer or programmed cell death. (Reported from (Monticolo & Chiusano, 2021)).

The gene *CD47* encodes for a membrane receptor that belongs to the cluster of differentiation proteins of the immunoglobulin superfamily (Sick et al., 2012). It results associated with a tyrosine kinase (PTK2) and a G-protein coupled receptor (FPR2) (**Figure 11**).

CENPB encodes for the major centromere autoantigen B, that facilitates centromere formation (Earnshaw et al., 1987). It interacts with PARP1and TRIM21 (**Figure 11**).

ERGIC1 encodes for a protein that is involved in the transport from the endoplasmic reticulum to the Golgi apparatus (Breuza et al., 2004). It results associated with a member of the arrestin protein family (ARRDC3) and with HIGD1A (**Figure 11**).

The gene *PAQR4* encodes for a progestin and adipoQ receptor (Tang et al., 2005). It interacts with ASB2, an ankyrin repeat protein, and with FLYWCH1, a suppressor of the nuclear β-catenin (**Figure 11**).

The gene *POMGNT1* encodes for a O-mannose beta-1,2-N-acetylglucosaminyltransferase, that participates in O-mannosyl glycan synthesis (Kuwabara et al., 2016; Yoshida et al., 2001). It results associated with the dystroglycan (DAG1) protein (**Figure 11**).

PPRC1 encodes for a peroxisome proliferator-activated receptor γ coactivator 1, that is linked to mitochondrial biogenesis (Andersson & Scarpulla, 2001). It interacts with proteins involved in ribosome biogenesis (DKC1, NOL6 and NOP56), a protein involved in mRNA pseudouridylation (TRUB1) and a vacuolar ATPase (ATP6V0C).

The gene *SLC44A1* encodes for a mediator of the choline transport across both the plasma and the mitochondrial membranes (Michel & Bakovic, 2009). It results associated with a guanine nucleotide exchange factor (SH3BP5) (**Figure 11**).

Focusing on the natural compounds that induce the expression of the 7 genes, the 5 reference natural compounds (except for the rosemary extract that has not a defined molecular organization) were used to identify similar chemical compounds. Two-hundred-and-thirty-one compounds with similarity to at least one of the reference compounds were identified. The prediction of the ADME of the natural compounds, results in 23 bioactive compounds (**Figure 12**).

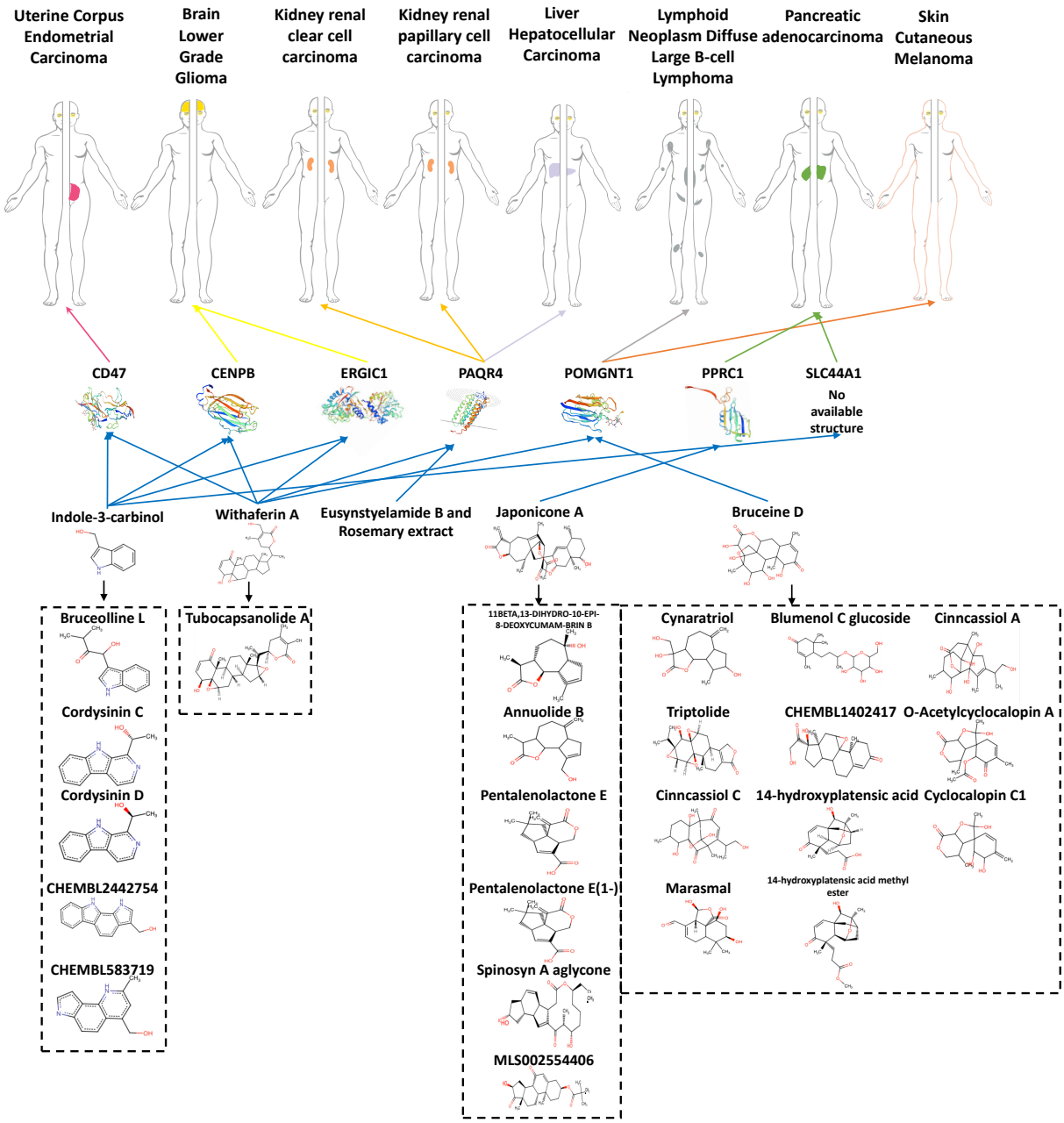

Figure 12: Natural compounds proposed for treatments in specific cancers.
The 5 reference compounds (Bruceine D, Eusynstyelamide B, Japonicone A, Withaferin A and Indole-3-carbinol) associated to the specific cancer types where they can have potential efficacy, and the corresponding similar ones detected by SwissSimilarity and SwissADME (23 in total) are shown.
Five compounds are analogous to Indole-3-Carbinol, that triggers the regulation of 5 different genes. In particular, the down-regulation of *CD47* enhances the survival in uterine corpus endometrial carcinoma; the down-regulation of *CENPB* and *ERGIC1* enhances the survival in brain lower grade glioma; the down-regulation of *PPRC1* and *SLC44A1* enhances the survival in pancreatic adenocarcinoma.
Eleven compounds are similar to Bruceine D, that triggers the down-regulation of *POMGNT1* that enhances the survival in lymphoid neoplasm diffuse large B-cell lymphoma and skin cutaneous melanoma.
One compound, that is analogous to Withaferin A, triggers the regulation of 4 different genes. In particular, the down-regulation of *CD47* enhances the survival in uterine corpus endometrial carcinoma, the down-regulation of *CENPB* enhances the survival in brain lower grade glioma; the down-regulation of *PAQR4* enhances the survival in kidney renal clear cell carcinoma, in kidney renal papillary cell carcinoma and in liver hepatocellular carcinoma; and the down-regulation of *SLC44A1* enhances the survival in pancreatic adenocarcinoma.
Six compounds are analogous to Japonicone A, that triggers the down-regulation of *PPRC1,* that enhances the survival in pancreatic adenocarcinoma. (Reported from (Monticolo & Chiusano, 2021)).

Summarizing, 5 compounds are analogous to Indole-3-Carbinol, that could down-regulate 5 different genes (*CD47, CENPB, ERGIC1, PPRC1, SLC44A1*). Eleven compounds are analogous to Bruceine D, that could down-regulate *POMGNT1*. One compound is analogous to Withaferin A, that could down-regulate 4 different genes (*CD47, CENPB, PAQR4, SLC44A1*). Six compounds are analogous to Japonicone A, that could down-regulate *PPRC1* (**Figure 12**).

The presence of the 23 bioactive compounds was searched in food, using FooDB (http://www.foodb.ca), to identify possible foods useful in cancer prevention or treatment. This analysis confirmed the presence in 4 foods for 4 compounds, all similar to Bruceine D (**Figure 13**).

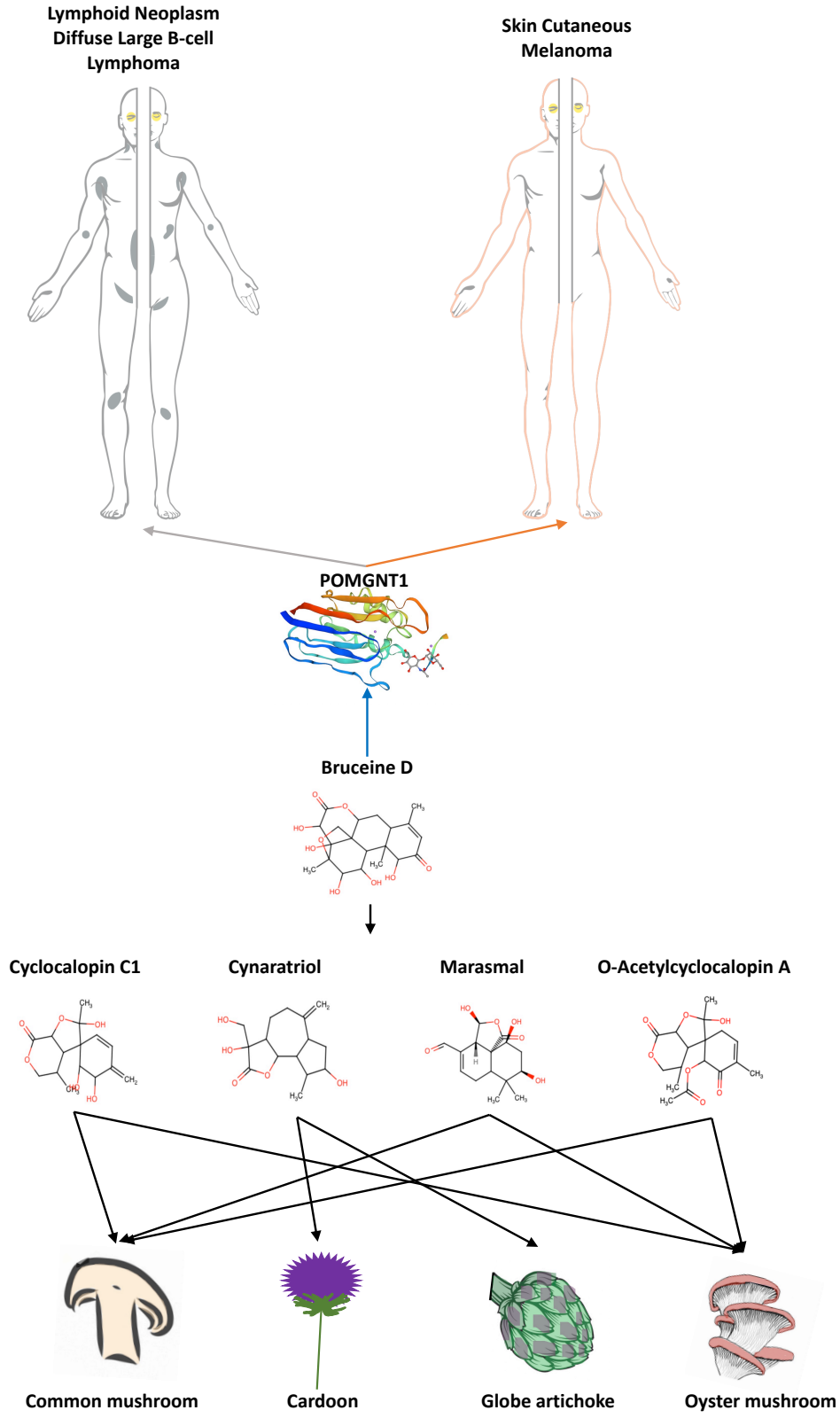

Figure 13: Potential novel foods useful in cancer treatments and/or prevention.
Four new identified compounds analogous to Bruceine D and that could play a role in the regulation of genes that enhance the survival in lymphoid neoplasm diffuse large B-cell lymphoma and in skin cutaneous melanoma. O-Acetylcyclocalopin A, Marasmal and Cyclocalopin C1 are predicted in Oyster mushroom and in common mushroom. Cynaratriol is expected in cardoon and globe artichoke. (Reported from (Monticolo & Chiusano, 2021)).

Discussion

The expression of the 734 putative candidate genes involved in *H. sapiens* programmed cell death (Monticolo et al., 2020), were compared with nutrigenomics treatments inducing apoptosis. One-hundred-forty-nine out of 734 genes showed the same expression trend in the apoptotic experiments and in 15 nutrigenomics treatments inducing apoptosis. Among these 149 genes, 22 were found to respect the conditions of having an opposite trend in at least one cancer type from TCGA (Ding et al., 2018). Then, the TCGA data were exploited in order to compare survival plots from patients with different expression trends. A favorable outcome considering the apoptotic trends in gene expression of 7 genes in 8 cancer types was confirmed. The down-regulation of these 7 genes in apoptotic inducing experiments and the up-regulation in cancer types may suggest their active role in the respective cancer types.

Among these 7 genes, *CD47,* up-regulated endometrial carcinoma, encodes for a membrane receptor that belongs to the cluster of differentiation of the immunoglobulin superfamily (Sick et al., 2012). Interestingly, in 2020, Liu et al., (Liu et al., 2020) already described the up-regulation of *CD47* in endometrial carcinoma tissues that lead to enhanced cell viability, suppression of apoptosis and inhibition of cell cycle arrest (Liu et al., 2020).

Moreover, CD47 interacts with PTK2 and FPR2. *PTK2* encodes for the focal adhesion kinase, critical for the regulation of adhesion and motility. Its overexpression is associated with increased metastatic potential (Anaganti et al., 2011). In fact, the overexpression of *PTK2* allows epithelial cell to survive in absence of contact with the extracellular matrix contributing to metastasis formation (Anaganti et al., 2011).

FPR2 is a transmembrane G-protein–coupled formyl peptide receptors family, that plays a role in inflammation (Ye et al., 2009). Furthermore, it is associated with different cancers types, such as colon cancer, melanoma and ovarian cancer (Chakravarti et al., 2013; Coffelt et al., 2009; Xiang et al., 2016).

CENPB, up-regulated in brain lower grade glioma, is a gene that encodes a protein that facilitates centromere formation (Earnshaw et al., 1987). Interestingly, in 2005, Atalay et al. (Atalay et al., 2005) revealed that, in breast cancer patients, the anti-CENP-B antibody had higher positivity compared to the control group, indicating a possible role of *CENPB* in breast cancer (Atalay et al., 2005).

Furthermore, CENPB interacts with TRIM21, that is involved in both cancer proliferation and in innate immunity (Alomari, 2021). TRIM21 plays a dual role in cancer, in fact it enhances

cancer proliferation, or it allows the proteasomal degradation of cancer-triggering proteins increasing their ubiquitination (Alomari, 2021).

Finally, CENPB interacts with PARP1, that is part of the poly(ADP-ribose) polymerase family (Gibson & Kraus, 2012; Rajman et al., 2018). PARP1 is implicated in the cellular response to DNA damage (Pascal, 2018), in programmed cell deaths (Chaitanya et al., 2010; D'Amours et al., 2001; Fatokun et al., 2014), and in cancer (Engbrecht & Mangerich, 2020). PARP1 is already used as target in clinical oncology. In fact, PARP1 inhibitors are used to treat ovarian or pancreatic cancers (Engbrecht & Mangerich, 2020).

ERGIC1, up-regulated in brain lower grade glioma, encodes for a protein involved in the transport between endoplasmic reticulum and the Golgi apparatus (Breuza et al., 2004).

ERGIC1 interacts with ARRDC3, an arrestin-related domain-containing protein that promotes lysosome-mediated protein degradation (X. Shen et al., 2018). Interestingly, ARRDC3 has been reported to act as tumor suppressor in different type of cancers, like in breast, colorectal and prostate cancer (Arakaki et al., 2018; X. Shen et al., 2018; Soung et al., 2014; Xiao et al., 2018; Zheng et al., 2017). Furthermore, ERGIC1 interacts with HIGD1A, that is essential for mitochondrial homeostasis. In fact, *HIGD1A* knockdown leads to mitochondrial fission, loss of mitochondrial DNA, and cell growth retardation (An et al., 2013).

The gene *PAQR4,* up-regulated in kidney renal clear, kidney renal papillary cells cancers and liver hepatocellular carcinoma, encodes for a progestin and adipoQ receptor (Tang et al., 2005).

PARQ4 interacts with FLYWCH1, a transcription modulator with an FLYWCH/Zn-finger DNA-binding domain (Muhammad et al., 2018). FLYWCH1 binds the β-catenin, suppressing its transcriptional activity and blocking the expression of specific downstream genes associated with cell migration and morphology (Muhammad et al., 2018). Moreover, PAQR4 interacts with ASB2, an ankyrin repeat-containing protein with a suppressor of cytokine signaling box-2 (Guibal et al., 2002). Upon treatment with retinoic acid that induces differentiation in leukemia cells, *ASB2* is overexpressed and induces growth inhibition and chromatin condensation (Guibal et al., 2002).

The gene *POMGNT1,* up-regulated in lymphoid neoplasm diffuse large B-cell lymphoma and in skin cutaneous melanoma, encodes for a O-mannose beta-1,2-N-acetylglucosaminyltransferase (Kuwabara et al., 2016; Yoshida et al., 2001).

POMGNT1 interacts with DAG1. *DAG1* encodes for the dystroglycan complex implied in muscular dystrophy (Côté et al., 1999). The dystroglycan links the extracellular matrix to the intracellular actin cytoskeleton, providing structural integrity. Loss of the dystroglycan

expression could lead to the loss of interaction with basement membrane and with the extracellular matrix. This is frequently observed in the development and progression of cancer (Sgambato & Brancaccio, 2005).

The gene *PPRC1,* up-regulated in pancreatic adenocarcinoma, encodes for a peroxisome proliferator-activated receptor γ coactivator 1, linked to mitochondrial biogenesis (Andersson & Scarpulla, 2001).

PPRC1 interacts with TRUB1, a synthase that catalyzes the pseudouridylation of mRNAs (Safra et al., 2017). In 2020, Kurimoto et al. (Kurimoto et al., 2020) described the role of TRUB1 in the maturation of the miRNA let-7, that regulates cell development and differentiation, proposing TRUB1 as a suppressor of cell proliferation (Kurimoto et al., 2020). Moreover, PPRC1 interacts with NOP56 and DKC1. NOP56 is involved in the 2'-O-methylation of target RNAs (Spacková et al., 2010), whereas DKC1 is a pseudouridine synthase that guides the pseudouridylation of target RNAs (Kiss et al., 2010). *NOP56* and *DKC1* were overexpressed in more than five different cancer types (Gong et al., 2017). In 2017, Gong et al. (Gong et al., 2017) highlighted that the *NOP56* and *DKC1* up-regulation was associated with poor survival prognosis (Gong et al., 2017). PPRC1 interacts also with NOL6. NOL6 is a nucleolar RNA involved in pre-rRNA processing and in ribosome biogenesis (Utama et al., 2002). In 2020, Dong et al. (Dong et al., 2020) proposed NOL6 as a human prostate cancer oncogene (Dong et al., 2020). PPRC1 interacts also with ATP6V0C that encodes for a vacuolar ATPase that, when silenced, determines the suppression of the migration of prostate carcinoma cells (P. Zou et al., 2018).

SLC44A1, up-regulated in pancreatic adenocarcinoma, encodes for a mediator of the choline transport across both the plasma membrane and the mitochondrial membrane (Michel & Bakovic, 2009). Interestingly, in 2015 Panett et al. (Penet et al., 2015), already reported the role of *SLC44A1* in pancreatic ductal adenocarcinoma (Penet et al., 2015).

SLC44A1 interacts with SH3BP5, a kinase involved in B cell differentiation and proliferation (Kobayashi et al., 2016). In 2019, Li et al. (M. Li et al., 2019) highlighted that overexpression of *SH3BP5* correlates with poor outcomes in acute myeloid leukemia patients (M. Li et al., 2019).

Natural compounds play an important role in pharmacotherapy, especially for cancer, bringing great interest in natural compounds as drug leads (Atanasov et al., 2021).

Interestingly, the 5 compounds (with the exclusion of the rosemary extract) that modulate the expression of the 7 genes are known and tested for their role in inducing cell death.

Withaferin A is a lactone found in plant *Withania somnifera*. It has been shown to exert cytotoxic activity in a variety of tumor cell lines (Choi et al., 2011; Lee et al., 2016; Malik et al., 2007; Nishikawa et al., 2015; Sari et al., 2020; Stan et al., 2008; Suman et al., 2016; Sundar et al., 2019; Widodo et al., 2010; Yu et al., 2017). Withaferin A anticancer activity includes the induction of oxidative stress, through ROS production, the inhibition of NF-kappa B signaling, the activation of protein kinase B (involved in autophagy) signaling, the degradation of a protein (vimentin) involved in adhesion, migration, survival, and epithelial-mesenchymal transition, the downregulation of human papilloma virus oncoproteins, and the induction of proteins involved in apoptosis (Bhargava et al., 2019; Choi et al., 2011; Grin et al., 2012; Lee et al., 2016; Malik et al., 2007; Mohan & Bargagna-Mohan, 2016; Munagala et al., 2011; Nishikawa et al., 2015; Sari et al., 2020; Stan et al., 2008; Suman et al., 2016; Sundar et al., 2019; Thaiparambil et al., 2011; Widodo et al., 2010).

Indole-3-Carbinol is a glucosinolate found in cruciferous vegetables (Agerbirk et al., 2008).

Indole-3-Carbinol has been shown to induce programmed cell death and to suppress the cell proliferation of various cancer cell lines, including colon, breast, endometrial and prostate cancer cell lines (Aggarwal & Ichikawa, 2005; Fujioka et al., 2016; Katz et al., 2018). Furthermore, Indole-3-Carbinol could induce autophagy in different cancer cell lines (Luca Galluzzi et al., 2012). Noticeable, it seems to induce programmed cell death specifically in cancer cells. Indeed, in 2003, Rahman et al. (Rahman et al., 2003) treated non-tumorigenic and tumorigenic breast epithelial cells with Indole-3-Carbinol, showing that Indole-3-Carbinol induces programmed cell death only in breast cancer cells (Rahman et al., 2003).

The Indole-3-Carbinol anticancer activity is not yet well characterized (Katz et al., 2018). Indole-3-Carbinol induces G1 cell cycle arrest and induces the activation of proteins involved in apoptosis (Aggarwal & Ichikawa, 2005; Brandi et al., 2003; Z. Chen et al., 2013; Cover et al., 1998, 1999; Ge et al., 1999; Safa et al., 2017; Joann Zhang et al., 2003). These preclinical results highlight the role of Indole-3-Carbinol in cancer prevention and therapy (Weng et al., 2008), leading to human clinical trials in cervical dysplasia (Bell et al., 2000), in vulvar intraepithelial neoplasia (Naik et al., 2006), and in breast cancer (Reed et al., 2005, 2006).

Japonicone A is a sesquiterpenoid found in plant *Inula japonica* (Haque et al., 2021). Japonicone A has been showed to induce programmed cell death and to suppress the cell proliferation in lymphoma, breast and lung cancer cells (Du et al., 2015; X. Li et al., 2013; Qin et al., 2015). Japonicone A anticancer activity includes the G2/M cell cycle arrest and induction

of apoptosis through the down-regulation of MDM2, that triggers p53 apoptotic activity (Qin et al., 2015).

Bruceine D is a quassinoid found in plant *Brucea javanica* (S.-H. Dong et al., 2013). Bruceine D has been showed to induce programmed cell death and to suppress the cell proliferation of various cancer cell lines, including pancreatic (Lau et al., 2010), lung (Fan et al., 2020; B. Tan et al., 2019), chronic myeloid leukemia (J.-Y. Zhang et al., 2016), breast (Luo et al., 2020), hepatocellular (Cheng et al., 2017), and osteosarcoma cancer cell lines (S. Wang et al., 2019). Bruceine D anticancer activity includes the up-regulation of pro-apoptotic proteins and the down-regulation of anti-apoptotic proteins (Sin et al., 2020).

Interestingly, no significant toxicity of Bruceine D was observed against non-tumorigenic cell lines (Sin et al., 2020).

Eusynstyelamide B is an indole alkaloid found in the ascidian *Eusynstyela latericius* (Tapiolas et al., 2009). Interestingly, Eusynstyelamide B was shown to cause cell cycle arrest in G2/M phase and induced apoptosis after 72 h treatment in breast cancer cells acting as topoisomerase II poison (Liberio et al., 2014, 2015).

Starting from these 5 compounds identified (with the exclusion of the rosemary extract), 231 similar compounds were identified. Predicting their ADME (Daina et al., 2017), 23 bioactive compounds were selected. All these compounds are to be considered suitable candidates for further tests in the cancer types here described.

Among the 23 additional bioactive compounds, Triptolide, a terpene (S. Kim et al., 2021), is already known to induce apoptosis in promyelocytic leukemia, in T cell lymphoma (Chan et al., 2001) and in melanoma (Tao et al., 2012).

Tubocapsanolide A, an alcohol (S. Kim et al., 2021), is reported to inhibit proliferation of human lung cancer (Chang et al., 2007).

Lastly, Cordysinin C and D are already known to have anti-inflammatory properties (Chen et al., 2013).

Subsequently, a preliminary investigation on foods that contain or that are predicted to contain some of the 23 compounds here selected were performed. Four out the 23 bioactive compounds were identified in 4 different foods. All these compounds are analogous to Bruceine D, indicating a possible role, of these foods, for treatments or prevention in lymphoid neoplasm diffuse large B-cell lymphoma and in skin cutaneous melanoma.

Among these 4 compounds, Marasmal, O-Acetylcyclocalopin A and Cyclocalopin C1 are predicted to be found in *Agaricus bisporus* (common mushroom) and in *Pleurotus ostreatus*

(Oyster mushroom). Interestingly, Oyster mushroom is known to have anti-cancer activity against lymphoma and melanoma (Maiti et al., 2011; Meerovich et al., 2005), whereas the common mushroom shows an anti-cancer activity against melanoma (Mohammed, 2020). Cynaratriol is expected but not yet quantified in *Cynara cardunculus* (cardoon) and *Cynara scolymus* (globe artichoke). This is the first time that cardoon and globe artichoke are suggested to play an anti-cancer role in lymphoma and/or melanoma.

Validation of candidate marker genes and the bioactivity of the selected compounds in modulating gene expression is mandatory to translate these results into practice. However, our results highlight the relevance of public data resources as they can have a major impact on Food Science.

Chapter 5: Natural compounds against COVID-19

Abstract

Due to the great interest in the treatment of infectious diseases using natural compounds, we also tested the bioinformatics procedure implemented in this thesis to find natural compounds that could be useful for the treatment of infectious diseases, in particular for COVID-19. A proper diet can play an active role in fighting viral infections (Aman & Masood, 2020). Indeed, professional dietary guidelines to withstand COVID-19 recommend: fruits (guava, apple, banana, strawberry, cantaloupe melon, grapefruit, pineapple, papaya, orange, Longman fruit, blackcurrant, pummelo) and fresh vegetables (green bell peppers, garlic, ginger, kale, lime, dried coriander, broccoli, green chili pepper) daily; whole grains (unprocessed maize, oats, wheat, millet, brown rice or roots such as yam, potato, taro or cassava) and nuts (almonds, coconut and pistachio); foods from animal sources (fish, eggs, and milk); consumption of unsaturated fats (found in avocado, fish, nuts, soy, olive oil, canola, corn oil, and sunflower); limited salt intake to 5 g a day and avoid all fizzy, carbonated, concentrated juices, and all drinks which contain sugar (Aman & Masood, 2020).

Here, starting from the analysis of bulk RNA-seq and single-cell RNA-seq (scRNA-seq) databases of patients infected by SARS-CoV-2, we looked for new potential genes that could play a relevant role in COVID-19 infection and possible natural compounds useful for COVID-19 prevention, treatments, and therapies. Forty-four genes that show the same expression trend between the bulk RNA-seq and the scRNA-seq experiments were identified and selected. Moreover, this gene collection was investigated with the additional aim to identify those genes that have an opposite expression trend between SARS-CoV-2 infected patients and nutrigenomics treatments, with the aim of searching for nutrient contrasting their expression during the infection. Thirteen genes from 26 different bioactive compound treatments were selected. Performing the ADME analysis and excluding those compounds with mutagenic, tumorigenic or irritant effects, 4 different compounds that regulate the expression of 7 genes were identified. Further investigations to look for compounds similar to the 4 here identified, permitted to identify 753 novel compounds. Excluding those with mutagenic, tumorigenic or irritant effects and that do not respect the ADME parameters, a final list of 27 natural compounds was obtained. These 27 natural compounds could represent idoneous candidate to test for their role in COVID-19 treatments.

SARS-CoV-2 genomic features and omics and bioinformatics resources

Coronaviruses are enveloped viruses with a positive single-strand RNA genome of 26-32 kilobases (Schoeman & Fielding, 2019), belonging to the Coronaviridae family. Based on genetic criteria, coronaviruses have been divided into three groups: alfa, beta and gamma coronaviruses. Alpha and beta coronaviruses are of particular interest because these strains can infect mammals and occasionally *H. sapiens* (Schoeman & Fielding, 2019).

SARS-CoV-2, a betacoronavirus, is responsible for COVID-19, the pandemic that is causing the serious emergency threating public health and causing 5,600,434 deaths worldwide (https://covid19.who.int January 2022).

The genomic features of SARS-CoV-2 consists of 6 open-reading frames (ORFs) and other accessory genes (Chan et al., 2020; Zumla et al., 2016). The 5' end main ORFs of the genomic RNA, ORF1a and ORF1ab, are used as templates to produce the polyproteins 1a/1ab, respectively, which encode non-structural proteins that form the replication-transcription complex (Chen et al., 2020; Zumla et al., 2016). The two replicases are cleaved by two different proteases, the 3CLPro, and the papain-like protease (PLPro) (Zhang et al., 2020). The 3CLPro can cleave at least 11 sites on the replicase 1ab, whereas, PLPro acts on secondary cleavage sites on PP1a and PP1ab (L. Zhang et al., 2020). These events produce the two replicases and other enzymes involved in viral transcription and replication, including an RNA dependant RNA polymerase (RdRp) and an helicase (Zumla et al., 2016). At the 3' end of the genome there are ORFs that encode for viral essential structural components: the spike glycoprotein (S), the envelope protein, the membrane protein and the nucleocapsid protein (Su et al., 2016; Zumla et al., 2016).

SARS-CoV-2 initiates its lifecycle binding the cellular receptor angiotensin-converting enzyme 2 (ACE2), via the S protein, to enter and infect host cells (Hoffmann et al., 2020). Virus entry is based on ACE2, furin proteases and on the transmembrane serine protease 2 that cleave and activate the SARS-CoV-2 S protein (Hoffmann et al., 2020). The translation of the positive-strand RNA genome is initiated following the release of the viral genome into the cytosol, and viral proteins induce the formation of cellular membrane-derived compartments for virus replication and *de novo* assembly of virus particles (Cortese et al., 2020). The host cells execute several strategies to counteract viral replication. Cellular pathogen recognition receptors (PRRs) sense viral molecular signatures or pathogen-associated molecular patterns and induce a signaling cascade leading to the induction of interferons (IFNs) and pro-inflammatory molecules (Schoggins & Rice, 2011). IFNs is the first line of viral infection defense leading to

the production of hundreds of interferon-stimulated genes (ISGs) known to exert broad antiviral functions (Schoggins & Rice, 2011).

Omics and bioinformatics technologies are being widely used to investigate the pathogenesis of COVID-19, new potential drugs, and drug targets. Indeed, omics analysis has been applied to identify the mutations of SARS-CoV-2, changes in SARS-CoV-2 gene expression in different biological samples, detection and quantification of proteins and metabolites (J. Yang et al., 2021).

Among these, global initiative on sharing all influenza data (GISAID) (Shu & McCauley, 2017), collects the largest number of SARS-CoV-2 genome sequences, playing an important role in sequence archive, homology searching, and variation discovery (Shu & McCauley, 2017).

WikiPathways provides a curated database collecting knowledge on biological pathways (Slenter et al., 2018). Interestingly, WikiPathways contributed to the COVID-19 Disease Map project aims to understand biological processes relevant to the COVID-19 pandemic (Ostaszewski et al., 2020). The WikiPathways COVID-19 portal (http://covid.wikipathways.org) contains a collection of eleven molecular pathways on SARS-CoV-2 itself and nine on other coronaviruses from earlier outbreaks.

SCovid is a single-cell atlas collecting scRNA-seq data from tissues and cells from COVID-19 infected patients across 10 human tissues (Qi et al., 2021). SCovid records 1,042,227 single cells of 21 single-cell datasets across 10 human tissues, 11,713 stably expressed genes and 3,778 significant DEGs (Qi et al., 2021).

STRING-covid (https://string-db.org/cgi/covid.pl) is the graphical representation of the SARS-CoV-2 protein interaction map useful for drug repurposing, obtained by Gordon et al. (Gordon et al., 2020).

The COVID-19 Drug and Gene Set Library (Kuleshov et al., 2020) is a collection of drug and gene sets related to COVID-19 research from multiple sources. The platform enables users to view, download, analyze, visualize, and contribute drug and gene sets related to COVID-19 research (Kuleshov et al., 2020).

Material and methods

Bulk RNA-seq data from tissues and cells from COVID-19 infected patients were downloaded from (Kuleshov et al., 2020) (accessed on 10 July 2021). Only human and wild type SARS-CoV-2 virus datasets were considered. Moreover, only datasets that were downloadable from

BioJupies (Torre et al., 2018) were considered. Only genes with FDR < 0.05, |log2 Fold Change| > 2.5 in at least 10% of experiments and the same expression trend were considered.

Single-cell RNA-seq datasets were downloaded from (Qi et al., 2021) (accessed on 10 November 2021). Briefly, scRNA-seq consists of four steps: isolation of single cells; reverse transcription; cDNA amplification; sequencing library construction (Y. Zhang et al., 2021). Only genes with p-value < 0.01, a |log2 Fold Change| > 0.5 were considered. Only genes with the same expression trend between scRNA-seq and bulk RNA-seq data were considered.

Nutrigenomic treatments were downloaded from NutriGenomeDB (Martín-Hernández et al., 2019) (accessed on 10 November 2021). Only genes with FDR < 0.05 and a |log2 Fold Change| > 2.5 were considered. Only genes with opposite expression trend between nutrigenomics treatments and SARS-CoV-2 infected patients were considered.

SwissADME (Daina et al., 2017) was used to compute the physicochemical descriptors and predict ADME parameters. Only bioactive compounds with 0 violation of the Lipinski (Lipinski et al., 2001), Ghose (Ghose et al., 1999), Veber (Veber et al., 2002), Egan (Egan et al., 2000) and Muegge (Muegge et al., 2001) methods and ≤ 1 violation in PAINS (Baell & Holloway, 2010), Brenk (Brenk et al., 2008), leadlikeness (Teague et al., 1999) and high gastrointestinal absorption were considered.

The possible mutagenic, tumorigenic and irritant effects were predicted with OSIRIS property explorer (https://www.organic-chemistry.org/prog/peo/) (accessed on 10 November 2021). Only bioactive compounds with no mutagenic, tumorigenic and irritant effects were selected.

The resulting bioactive compounds were analyzed with SwissADME (Daina et al., 2017) and OSIRIS property explorer (https://www.organic-chemistry.org/prog/peo/) (accessed on 10 November 2021) with the same previous parameters.

SwissSimilarity (Zoete et al., 2016) was used to identify additional bioactive natural compounds that could induce similar effects to those caused by the compounds already exploited in the nutrigenomics treatments. The SMILE format of the initial compounds was obtained using PubChem (S. Kim et al., 2021). The screening was performed using the combined score considering bioactive compounds from all libraries: PDB (Berman et al., 2000), ChEMBL (activity<10μM) (Gaulton et al., 2012), ChEBI (de Matos et al., 2010), Kinase inhibitors (ChEMBL) (Gaulton et al., 2012), GPCR Ligands (ChEMBL) (Gaulton et al., 2012), GPCR Ligands (GLASS) (Chan et al., 2015) and HMDB (Wishart et al., 2018). Only compounds showing a similarity score > 0.85 with the reference compounds were considered.

The GO enrichment analysis was performed using g:profiler (Raudvere et al., 2019), with Ensembl v104 (Howe et al., 2021) as annotation, and Benjamini-Hochberg FDR as significant threshold. Only enriched GOs with FDR < 1×10^{-5} were considered.

Results

Thirty-three bulk RNA-seq data from tissues and cells from COVID-19 infected patients were downloaded from (Kuleshov et al., 2020). Focusing on genes that show the same expression trend in at least 10% of experiments, a list of 110 genes was obtained.

Twenty-one scRNA-seq data of tissues from COVID-19 infected patients were downloaded from (Qi et al., 2021). Focusing on genes that show the same expression trend between the 110 genes obtained from bulk RNA-seq and scRNA-seq, a list of 44 genes was obtained (**Supplementary Table S8**).

These 44 genes were used as a reference to select bioactive compounds from nutrigenomic treatments under the condition that these compounds determined an opposite expression when considering the expression trend from SARS-CoV-2 infected patients experiments. This results in a list of 13 genes (all up-regulated in SARS-CoV-2 infected patients) and 26 natural compounds (in which the 13 genes are down-regulated) (**Supplementary Table S9**).

Focusing on the 26 natural compounds mutagenic, tumorigenic, irritant compounds and those that do not respect the ADME parameters were excluded. This results in 7 genes down-regulated by 4 natural compounds (**Figure 14A-B**).

Focusing on the 7 genes, a GO enrichment analysis highlights the involvement of these 7 genes in the type I interferons response (**Figure 14C**).

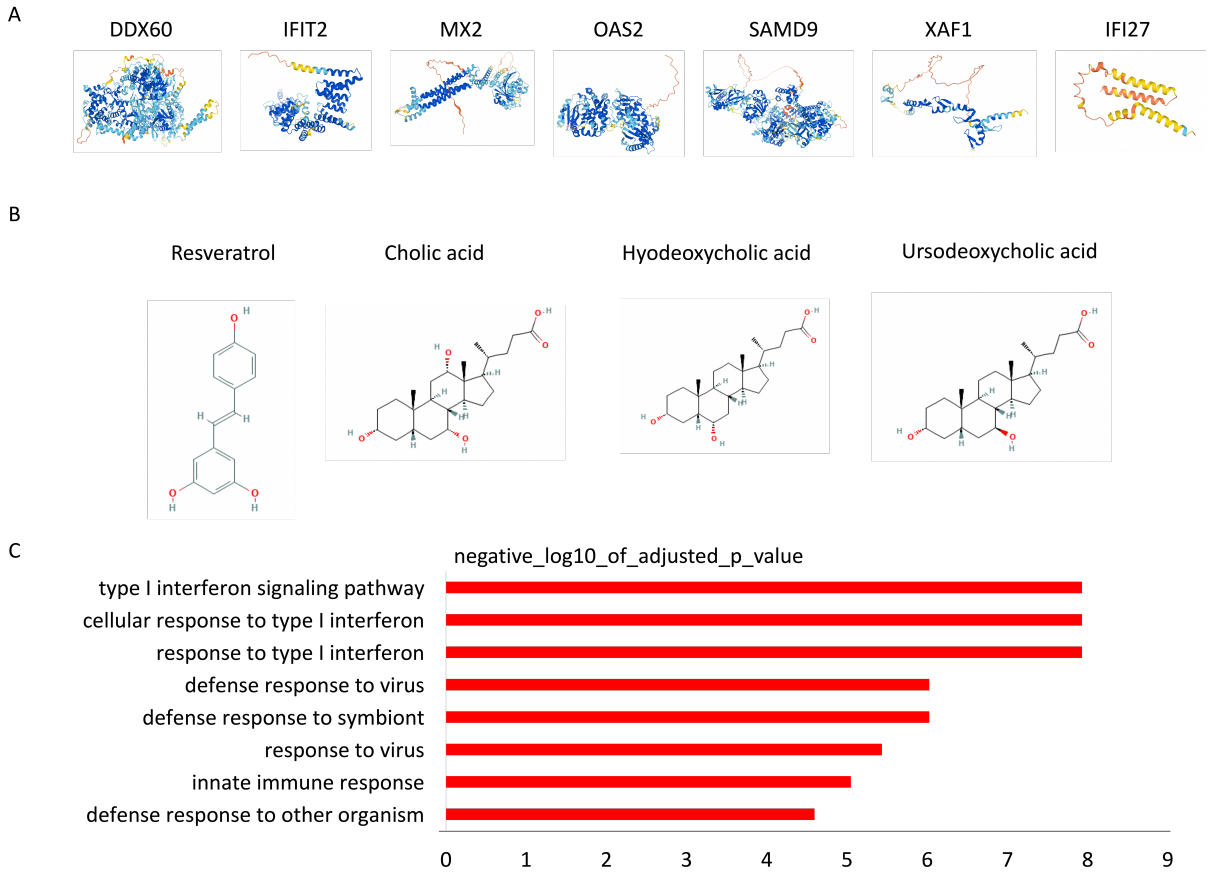

Figure 14: A) Protein structures of the 7 genes down-regulated by nutrigenomic treatments. **B**) Chemical structure of the 4 compounds that down-regulate the 7 genes are shown. **C**) Results of Gene Ontology (GO) enrichment analysis performed on the 7 genes (false discovery rate (FDR) $< 1 \times 10^{-5}$).

Dysregulation of type I IFNs responses is indicative of coronavirus infections (Acharya et al., 2020). Although the low amounts of type I IFNs, SARS-CoV-2 triggers the expression of numerous ISGs that could exhibit immunopathogenic potential (Zhou et al., 2020).

Pointing attention on ISGs, DExD/H-box helicase 60 (*DDX60*) (Karami et al., 2022), XIAP-Associated Factor 1 (*XAF1*), Interferon alpha Inducible protein 27 (*IFI27*) (Xin Gao et al., 2021), 2'-5'-Oligoadenylate Synthetase 2 (*OAS2*) (Prasad et al., 2020) are proposed as new putative candidates genes with a role in SARS-CoV-2 infection. Moreover, Interferon Induced protein with Tetratricopeptide repeats 2 (*IFIT2*) and *XAF1* are up-regulated in highly infected cell types (**Supplementary Table S8**) (Ravindra et al., 2021; Triana et al., 2021; Zhu et al., 2020).

The 4 natural compounds that down-regulate the 7 gene expression (**Figure 14B**) are already known for their anti-COVID-19 activity (Subramanian et al., 2020; Wahedi et al., 2021; Cheng, 2020).

In order to identify new natural compounds with similar propriety, a virtual screening was performed. A list of 753 bioactive compounds was obtained. Predicting their ADME, mutagenicity, tumorigenicity and ability to produce physical irritation, a list of 27 bioactive compounds that could exhibits anti-COVID-19 activity was obtained (**Figure 15**). Interestingly, chenodeoxycholate is already known for its anti-COVID-19 activity (Yadav et al., 2020).

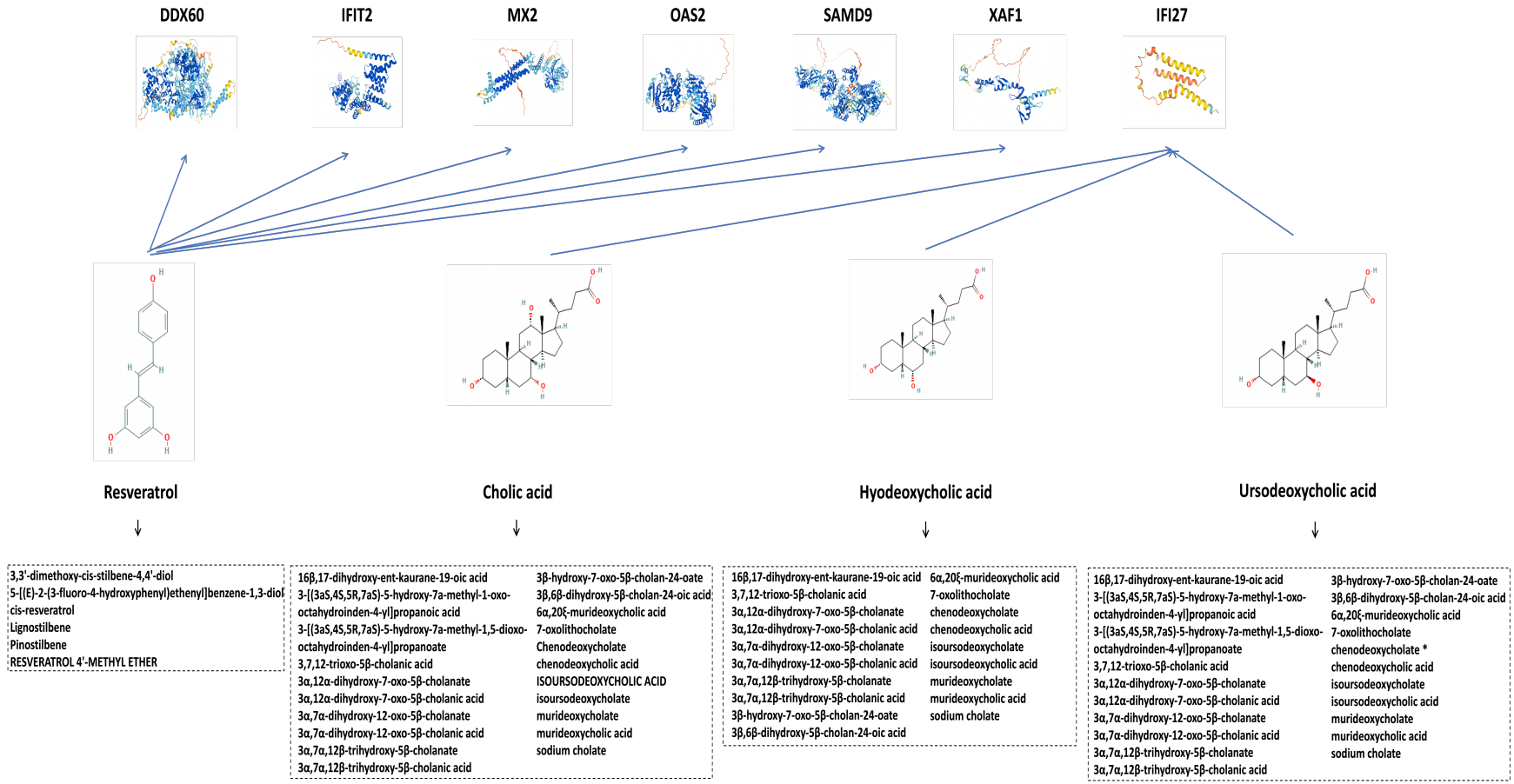

Figure 15: Natural compounds effective on the 7 genes and therefore proposed for COVID-19 treatments.
The 4 reference compounds (Resveratrol, Cholic acid, Hyodeoxycholic acid and Ursodeoxycholic acid) and their association to each gene is shown by blue arrows. The corresponding similar compounds (enclosed in dashed rectangles) detected by Swiss-Similarity, SwissADME and OSIRIS are also indicated. Six compounds are similar to Resveratrol, which triggers the down-regulation of 6 different genes. Twenty-two compounds are similar to Cholic acid, that triggers the down-regulation of IFI27. Twenty compounds are similar to Hyodeoxycholic acid that triggers the down-regulation of IFI27. Twenty-two compounds are similar to Ursodeoxycholic acid, that triggers the down-regulation of IFI27.

Discussion

Using data publicly available of bulk and single-cell RNA-seq from tissues and cells from COVID-19 infected patients, 44 genes that show the same expression trend in all experiments were identified. These 44 genes were used as a reference to select bioactive compounds from nutrigenomic treatments under the condition that these compounds determined an opposite expression when considering the expression trend from SARS-CoV-2 infected patients experiments. This resulted in a list of 13 genes (all up-regulated in SARS-CoV-2 infections) and 26 natural compounds that determined the down-regulation of the 13 genes. Removing mutagenic, tumorigenic, irritant compounds using OSIRIS (https://www.organic-chemistry.org/prog/peo/) and those that do not respect the ADME parameters, 7 genes down-regulated by 4 bioactive compounds were obtained.

Interestingly, the GO enrichment analysis revealed that these 7 genes are all involved in type I IFNs responses. A minimal amount of type I IFNs has been detected in the peripheral blood or lungs of patients with severe COVID-19 (Acharya et al., 2020). Dysregulation of type I IFNs responses is typical of coronaviruses infections. In fact, during the incubation phase, SARS-CoV-2 replicates in host cells without detectable IFN activation because it induces the formation of membranous compartments dedicated to the synthesis of viral RNA, thus hiding the molecular patterns associated with viral pathogens from detection by host PRRs. Furthermore, several conserved betacoronavirus proteins are known to exert direct IFN antagonistic activities, modifying specific characteristics of viral RNA to avoid recognition by specific PRRs or inhibiting PRR-mediated signal transduction (Acharya et al., 2020). This reduced IFNs production could lead to disparity in the pro-inflammatory versus pro-repair functions of macrophages (Acharya et al., 2020). Although the low amount of type I IFNs, SARS-CoV-2 triggers a robust expression of numerous ISGs that could exhibit immunopathogenic potential (Zhou et al., 2020). Nienhold et al. (Nienhold et al., 2020) pointed out that patients that show high expression of ISGs have a higher susceptibility to death, that often occurred earlier after hospitalization than patients that show lower ISGs expression (Nienhold et al., 2020). This highlights the controversial role of ISGs in COVID-19.

Among the 7 ISGs here detected, DExD/H-box helicase 60 (*DDX60*) (Karami et al., 2022), XIAP-associated factor 1 (*XAF1*), interferon alpha inducible protein 27 (*IFI27*) (Xin Gao et al., 2021), 2'-5'-oligoadenylate synthetase 2 (*OAS2*) (Prasad et al., 2020) are proposed as new putative candidates genes with a role in SARS-CoV-2 infection in other studies.

Interestingly, interferon induced protein with tetratricopeptide repeats 2 (IFIT2) is known to inhibit the translation of viral messenger RNAs that lack the 2'-O-methylation of the ribose at the 5' cap. The ribose 2'-O-methylation would provide a molecular signature to let the host cells distinguish between self and non-self mRNAs during the viral infection. Moreover, IFIT2 can promote apoptosis (Stawowczyk et al., 2011) and can bind directly to cellular mRNAs in AU-rich regions preventing ribosome pausing along mRNAs during translation, increasing the translation of cellular mRNAs to support antiviral responses. Interestingly, it was recently demonstrated that *IFIT2* is repurposed during the infection by the influenza virus to promote viral protein synthesis too (Tran et al., 2020), redirecting a classically antiviral protein into a pro-viral effector (Tran et al., 2020).

Another important ISG, although already proposed as involved in COVID-19, is *XAF1*. XAF1 can bind and inhibit XIAP, inducing apoptosis. XIAP is a member of the IAP family that has the ability to inhibits apoptosis through the inhibition of the caspase cascade (Liston et al., 2001). Overexpression of *XAF1* is reported to induce G2/M cell cycle arrest and mitotic catastrophe (Wang et al., 2009). Interestingly, Bouhaddou et al. (Bouhaddou et al., 2020) treated Vero E6 cells with SARS-CoV-2 for 24 hours and found a significant increase in the fraction of cells in S phase and at the G2/M transition, confirming that SARS-CoV-2 infection affects cell cycle progression.

Interestingly, *XAF1* and *IFIT2* are both up-regulated in ciliated cells (Ravindra et al., 2021), in transient amplifying cells and in enterocyte cells (Triana et al., 2021), that are reported as the main virus-targeted cell types, the highly infected cells and the major target at the onset of infection (Ravindra et al., 2021; Triana et al., 2021).

Moreover, *XAF1* is up-regulated in CD4+ and CD8+ T cells (Arunachalam et al., 2020) and could lead to the increased T cell apoptosis in COVID-19 patients (Zhu et al., 2020).

These data confirm the crucial roles of these ISGs and their interest as potential targets for anti-COVID-19 therapies.

Focusing on the 4 natural compounds that modulate the expression of the 7 genes during the infection, they are already known for their anti-COVID-19 activity (Subramanian et al., 2020; Wahedi et al., 2021; Cheng, 2020). Among these 4 natural compounds, Resveratrol is the most effective being able to affect the expression of 6 out of 7 genes here identified. Resveratrol is a polyphenol initially isolated from the plant *Veratrum grandiflorum* in 1940 (Siemann & Creasy, 1992). Resveratrol was postulated to explain the cardioprotective effects of red wine (Siemann & Creasy, 1992). Subsequently, different studies highlighted the role of Resveratrol in

prevention or treatments of cancer (Jang et al., 1997), cardiovascular diseases (Bradamante et al., 2004) and ischemic injuries (Q. Wang et al., 2002). Moreover, Resveratrol could have beneficial effects on male (Mongioì et al., 2021) and female (Sirotkin, 2021) fertility, and in cognitive disturbances reducing metabolic stress (Palomera-Ávalos et al., 2017). Furthermore, Resveratrol plays an important role in inflammation and immunity (Baur & Sinclair, 2006). Moreover, it was shown that Resveratrol decreases viral replication with the suppression of the production of cytokines interleukin (IL)-1α, IL-2, IL-6, IL-8, IL-17, and TNF-α (X Gao et al., 2001; Vidoni et al., 2021; M. Zou et al., 2020).

Moreover, Resveratrol plays a role in contrasting human coronaviruses infection (Filardo et al., 2020; G. Li & De Clercq, 2020; Lin et al., 2017; Pasquereau et al., 2021; M. Yang et al., 2021). In silico analyses also suggested the role of Resveratrol in blocking the activity of SARS-CoV-2 proteins PLPro, RdRp, and S protein (Ranjbar et al., 2020; Wahedi et al., 2021). These effects make resveratrol an interesting candidate for investigations on treatments of SARS-CoV-2 infection (Vidoni et al., 2021).

Starting from these 4 compounds, an investigation on additional similar compounds that could exert the same effects was here performed. A list of 753 compounds was obtained. Predicting their ADME, 27 bioactive compounds were selected. All these compounds are suitable candidates for further tests their role in anti-COVID-19 treatments. Among the 27 additional bioactive compounds, it is interesting to mention that in 2020, Yadav et al. (Yadav et al., 2020) proposed that chenodeoxycholate could stably bind to SARS-CoV-2 envelope protein through H-bonds, water-bridges and hydrophobic contacts, disrupting the structure of SARS-CoV-2 envelope proteins and facilitating the entry of solvents/polar inhibitors inside the viral cell (Yadav et al., 2020).

Many efforts for the prediction and assessment of bioactive compounds that could act against COVID-19 are taking place because of the pandemic emergency. Here new natural compounds that could exhibits anti-COVID-19 activity based on gene expression of bulk and scRNA-seq of SARS-CoV-2 infected patients and nutrigenomic treatments are proposed. These approaches appear promising since they permitted to highlight possible novel target genes involved in the infection. In addition, using nutrigenomic studies, we could propose new bioactive compounds that could be useful for testing against COVID-19, offering novel opportunities for testing and drug discovery.

Chapter 6: Conclusions

The aim of this thesis is the identification of early molecular markers that allow the prediction of cell fate in eukaryotic organisms: the unicellular eukaryote *Saccharomyces cerevisiae* and the multicellular organism *Homo sapiens*.

Saccharomyces cerevisiae was selected for its usefulness in detecting novel molecular processes due to its simple cell organization. Moreover, it is notoriously considered a model system of relevance in Food Science and in molecular studies of physiological processes of metazoan cells (Madeo et al., 1999). *Homo sapiens* was considered for understanding the impact of our approaches also for human healthcare and well-being.

The scope is to further investigate the molecular features that characterize gene expression during cell stress response and its outcomes to define key markers for the early detection of cell fate. The idea is to acquire knowledge for the design of sensitive molecular techniques for applications in different fields of Food Science.

We exploited omics resources for solving Food Science hot questions, such as the selection of bioactive nutrients and chemical compounds useful for health and well-being.

In chapter 2, collecting RNA-seq from *S. cerevisiae* related to programmed cell death induced by acetic acid we revealed transcriptomic changes in genes associated with ribosome biogenesis, mRNA decapping, translation accuracy and ohnologs expression. Ohnologs are duplicated genes derived from whole genome duplication providing new genetic material for natural selection, drift and mutation (Zhang, 2003).

This highlighted a typical translational reprogramming preceding programmed cell death. To further investigate on this phenomenon and on its possible specificity in programmed cell death, 12 additional experiments related to different types of stress were considered. Comparing the changes in ohnologs expression between programmed cell death induced by acetic acid and the 12 different types of stress, a programmed cell death specific ohnologs replacement was identified. This cell death specific replacement acts on sporulation, changing the ribosome population, decapping mRNA and methionine biosynthesis. These results may be useful for monitoring cell growth and for controlling the initiation of programmed cell death in bioreactors and for implementing biosensors to monitor cell response.

In chapter 3, nine *Homo sapiens* transcriptome data based on RNA-seq experiments associated to programmed cell death were analyzed. Furthermore, 36 transcriptome data based on RNA-seq experiments of human cell stress response were considered, in order to identify key genes associated with exclusive expression trend in programmed cell death response.

Through the identification of dysregulated pathways across the experiments and determining co-expressed genes, the list of potential novel human genes involved in programmed cell death was expanded. The resulting list of co-expressed genes was then crosschecked with transcriptome expression levels from cell stress. This led to the identification of key genes associated with exclusive expression trend in cell death. The result was a list of 734 putative candidate genes involved in *H. sapiens* programmed cell death. Finally, the list of 734 *H. sapiens* genes was compared with the corresponding cell death related ortholog genes in *S. cerevisiae*. We identified potential genes involved in programmed cell death in both species, revealing the presence of under investigated conserved pathways in the two species programmed cell death. This opens the way to future analysis for a better understanding of the molecular mechanisms involved.

In this thesis we further focused on the aspects of nutrigenomics to investigate potential beneficial foods for the health and well-being of *H. sapiens*. Indeed, in chapter 4, we deeply investigated on the 734 *H. sapiens* genes.

One of the cancer hallmarks is the evasion to cell death (Hanahan & Weinberg, 2011), therefore, we investigated on the behaviors of these genes in nutrigenomics treatments that induce cell death. One of the roles of nutrigenomics is to help Food Science on defining the role of nutrients and bioactive compounds for the prevention and the treatment of chronic diseases, such as cancer (Sales et al., 2014).

Our aim was to implement bioinformatics strategies to select food natural compounds from nutrigenomics experiments that could influence the expression of the new programmed cell death related genes. These natural compounds could be useful in the induction of programmed cell death. This led to the identification of bioactive compounds that modulate the expression of 149 new programmed cell death related genes. These 149 genes were further analyzed to identify genes with opposite expression trend between apoptotic treatments and cancer. The comparison of gene expression trend of these 149 genes with their gene expression in 33 different cancer types led to the identification of 22 genes that show an opposite expression trend. Focusing on their survival role in cancer patients, 7 genes, modulated by 6 natural compounds, that could have a prognostic role in 8 cancer types, were highlighted. Starting from 5 out of 6 natural compounds that modulate the expression of the 7 genes, new compounds, and foods useful in cancer treatments and/or prevention were identified. These results are useful for diagnostics of cell systems exposed to bioactive substances contained in foods, food quality, and human care.

Lastly, due to the great interest in the treatment of infectious diseases using natural compounds, we also tested the bioinformatics procedure implemented in this thesis to find natural compounds that could be useful for the treatment of infectious diseases, in particular for COVID-19. In chapter 5, starting from the analysis of bulk RNA-seq and single-cell RNA-seq (scRNA-seq) databases of tissues from patients infected by SARS-CoV-2, new potential genes involved in COVID-19 infection and new natural compounds useful for COVID-19 therapies were identified. Forty-four genes that show the same expression trend between the bulk RNA-seq and the scRNA-seq experiments were selected. Moreover, this collection was investigated with the main aim to identify those genes that have an opposite expression trend between SARS-CoV-2 infected patients and nutrigenomics treatments. Thirteen genes influenced in their expression by 26 different natural compounds treatments were selected. Performing the ADME analysis on these compounds and excluding those with mutagenic, tumorigenic or irritant effects, 4 different compounds that regulate the expression of 7 genes were identified. Interestingly, the 7 genes were found to be ISGs. Based on the similarity with the 4 natural compounds we identified 753 similar compounds. Performing the ADME analysis on these compounds and excluding those with mutagenic, tumorigenic or irritant effects, a list of 27 bioactive compounds was obtained. These 27 natural compounds are here proposed as new candidate compounds that could play a role in COVID-19 care and drug discovery.

Perspectives

In this thesis, bioinformatics was the main technology exploited. Data resources, databases and pipelines were tested and implemented to identify molecular markers useful for the prediction of cell fate.

The selection of novel possible genes and pathways associated to programmed cell death is crucial for monitoring and for predicting the cell fate in cell culture or in bioreactors, and for the identification of natural compounds useful for health and well-being.

The association between nutrients and natural compounds exploits the power of nutrigenomics resources. The selection of potential drugs permitted good results in nutraceutical and well-being. In addition, this paves the way to knowledge also in molecular biology.

Some of the natural compounds here identified are already known for their role in COVID-19 treatments or in the induction of programmed cell death in cancer cells. Indeed, literature analysis confirmed the application of some of these natural compounds in clinical trials, highlighting their importance in cancer and COVID-19 treatments.

Our results need to be experimentally validated. Indeed, treating cell lines with the new identified bioactive compounds could confirm their anti-cancer and anti-COVID-19 activities and shed lights on the molecular mechanisms of action of these compounds.

Moreover, our results need to be experimentally validated because virtual screening has the limitation that a high similarity coefficient value does not always imply that two compounds will have the same activity (Gimeno et al., 2019). Furthermore, similarity coefficients could select an inactive compound that does not have the features essential for the bioactivity present in the reference compounds but with a good structural similarity. On the other hand, similarity coefficients could exclude bioactive compounds that only match the features essential for the bioactivity of the reference compound but with a low structural similarity (Gimeno et al., 2019). The prediction of ADME parameters also could have limitations due to a too simplistic prediction of drug behavior in a whole organism.

For application in nutraceutical industry of the natural compounds here identified some other steps are required. A technological effort must be done to deliver health benefits through food. The natural compounds here identified could be added in foods, obtaining enriched or fortified foods. During the food addition of natural compounds, it is important to consider the interactions among food components. Indeed, it is important to consider that a natural compound could be effective when assessed alone but it could be ineffective when used within a food formulation, due to antagonist, additive, or synergistic effects among food components. Finally, the consumer response plays a key role in nutraceutical industry. The successful delivery of a newly developed functional food on the market is affected not only by the health benefit but also by other factors, such as taste, convenience, and price (Alongi & Anese, 2021). Nevertheless, the results obtained in this thesis could be useful in many fields of Food Science. The translational reprogramming and ohnologs replacement highlighted in *S. cerevisiae* programmed cell death induced by acetic acid (chapter 2), could be useful for the development of biosensors that allow an early prediction of programmed cell death measuring the mRNA level changes. These methodologies are already used to detect the presence of *Escherichia coli* in drinking water (Baeumner et al., 2003), to identify toxic algae in Mediterranean sea (Orozco et al., 2016), and to detect the level of anti-apoptotic mRNA surviving in cancer patients (Stobiecka et al., 2019).

Lastly, the bioactive compounds identified in Chapter 4 and in Chapter 5 could be useful in nutraceutical industry, playing a significant role in cancer and COVID-19 treatments.

Reference

Abla, H., Sollazzo, M., Gasparre, G., Iommarini, L., & Porcelli, A. M. (2020). The multifaceted contribution of α-ketoglutarate to tumor progression: An opportunity to exploit? *Seminars in Cell & Developmental Biology*, *98*, 26–33. https://doi.org/https://doi.org/10.1016/j.semcdb.2019.05.031

Acharya, D., Liu, G., & Gack, M. U. (2020). Dysregulation of type I interferon responses in COVID-19. *Nature Reviews. Immunology*, *20*(7), 397–398. https://doi.org/10.1038/s41577-020-0346-x

Agerbirk, N., De Vos, M., Kim, J. H., & Jander, G. (2008). Indole glucosinolate breakdown and its biological effects. *Phytochemistry Reviews*, *8*(1), 101. https://doi.org/10.1007/s11101-008-9098-0

Aggarwal, B. B., & Ichikawa, H. (2005). Molecular targets and anticancer potential of indole-3-carbinol and its derivatives. *Cell Cycle (Georgetown, Tex.)*, *4*(9), 1201–1215. https://doi.org/10.4161/cc.4.9.1993

Agyeman, A. S., Chaerkady, R., Shaw, P. G., Davidson, N. E., Visvanathan, K., Pandey, A., & Kensler, T. W. (2012). Transcriptomic and proteomic profiling of KEAP1 disrupted and sulforaphane-treated human breast epithelial cells reveals common expression profiles. *Breast Cancer Research and Treatment*, *132*(1), 175–187. https://doi.org/10.1007/s10549-011-1536-9

Aits, S., & Jäättelä, M. (2013). Lysosomal cell death at a glance. *Journal of Cell Science*, *126*(9), 1905 LP – 1912. https://doi.org/10.1242/jcs.091181

Alkema, W., Boekhorst, J., Wels, M., & van Hijum, S. A. F. T. (2016). Microbial bioinformatics for food safety and production. *Briefings in Bioinformatics*, *17*(2), 283–292. https://doi.org/10.1093/bib/bbv034

Alomari, M. (2021). TRIM21 - A potential novel therapeutic target in cancer. *Pharmacological Research*, 105443. https://doi.org/10.1016/j.phrs.2021.105443

Alongi, M., & Anese, M. (2021). Re-thinking functional food development through a holistic approach. *Journal of Functional Foods*, *81*, 104466. https://doi.org/https://doi.org/10.1016/j.jff.2021.104466

Altermann, E., Russell, W. M., Azcarate-Peril, M. A., Barrangou, R., Buck, B. L., McAuliffe, O., Souther, N., Dobson, A., Duong, T., Callanan, M., Lick, S., Hamrick, A., Cano, R., & Klaenhammer, T. R. (2005). Complete genome sequence of the probiotic lactic acid bacterium Lactobacillus acidophilus NCFM. *Proceedings of the National Academy of Sciences of the United States of America*, *102*(11), 3906–3912. https://doi.org/10.1073/pnas.0409188102

Aman, F., & Masood, S. (2020). How Nutrition can help to fight against COVID-19 Pandemic. *Pakistan Journal of Medical Sciences*, *36*(COVID19-S4), S121–S123. https://doi.org/10.12669/pjms.36.COVID19-S4.2776

An, H.-J., Cho, G., Lee, J.-O., Paik, S.-G., Kim, Y. S., & Lee, H. (2013). Higd-1a interacts with Opa1 and is required for the morphological and functional integrity of mitochondria. *Proceedings of the National Academy of Sciences of the United States of America*, *110*(32), 13014–13019. https://doi.org/10.1073/pnas.1307170110

Anaganti, S., Fernández-Cuesta, L., Langerød, A., Hainaut, P., & Olivier, M. (2011). p53-Dependent repression of focal adhesion kinase in response to estradiol in breast cancer cell-lines. *Cancer Letters*, *300*(2), 215–224. https://doi.org/10.1016/j.canlet.2010.10.008

Andersson, U., & Scarpulla, R. C. (2001). Pgc-1-related coactivator, a novel, serum-inducible coactivator of nuclear respiratory factor 1-dependent transcription in mammalian cells. *Molecular and Cellular Biology*, *21*(11), 3738–3749. https://doi.org/10.1128/MCB.21.11.3738-3749.2001

Arakaki, A. K. S., Pan, W.-A., Lin, H., & Trejo, J. (2018). The α-arrestin ARRDC3 suppresses breast carcinoma invasion by regulating G protein-coupled receptor lysosomal sorting and signaling. *The Journal of Biological Chemistry*, *293*(9), 3350–3362. https://doi.org/10.1074/jbc.RA117.001516

Ardekani, A. M., & Jabbari, S. (2009). Nutrigenomics and cancer. *Avicenna Journal of Medical Biotechnology*, *1*(1), 9–17.

Arunachalam, P. S., Wimmers, F., Mok, C. K. P., Perera, R. A. P. M., Scott, M., Hagan, T., Sigal, N., Feng, Y., Bristow, L., Tak-Yin Tsang, O., Wagh, D., Coller, J., Pellegrini, K. L., Kazmin, D., Alaaeddine, G., Leung, W. S., Chan, J. M. C., Chik, T. S. H., Choi, C. Y. C., … Pulendran, B. (2020). Systems biological assessment of immunity to mild versus severe COVID-19 infection in humans. *Science (New York, N.Y.)*, *369*(6508), 1210–1220. https://doi.org/10.1126/science.abc6261

Ashkenazi, A., & Dixit, V. M. (1998). Death receptors: signaling and modulation. *Science (New York, N.Y.)*, *281*(5381), 1305–1308. https://doi.org/10.1126/science.281.5381.1305

Atalay, C., Atalay, G., Yilmaz, K. B., & Altinok, M. (2005). The role of anti-CENP-B and anti-SS-B antibodies in breast cancer. *Neoplasma*, *52*(1), 32–35.

Atanasov, A. G., Zotchev, S. B., Dirsch, V. M., & Supuran, C. T. (2021). Natural products in drug discovery: advances and opportunities. *Nature Reviews. Drug Discovery*, *20*(3), 200–216. https://doi.org/10.1038/s41573-020-00114-z

Azzouz, D., & Palaniyar, N. (2018). ApoNETosis: discovery of a novel form of neutrophil death with concomitant apoptosis and NETosis. *Cell Death & Disease*, *9*(8), 839. https://doi.org/10.1038/s41419-018-0846-9

Baell, J. B., & Holloway, G. A. (2010). New substructure filters for removal of pan assay interference compounds (PAINS) from screening libraries and for their exclusion in bioassays. *Journal of Medicinal Chemistry*, *53*(7), 2719–2740. https://doi.org/10.1021/jm901137j

Baeumner, A. J., Cohen, R. N., Miksic, V., & Min, J. (2003). RNA biosensor for the rapid detection of viable Escherichia coli in drinking water. *Biosensors & Bioelectronics*, *18*(4), 405–413. https://doi.org/10.1016/s0956-5663(02)00162-8

Bailey, P. S. J., Ortmann, B. M., Martinelli, A. W., Houghton, J. W., Costa, A. S. H., Burr, S. P., Antrobus, R., Frezza, C., & Nathan, J. A. (2020). ABHD11 maintains 2-oxoglutarate metabolism by preserving functional lipoylation of the 2-oxoglutarate dehydrogenase complex. *Nature Communications*, *11*(1), 4046. https://doi.org/10.1038/s41467-020-17862-6

Balakrishnan, R., Park, J., Karra, K., Hitz, B. C., Binkley, G., Hong, E. L., Sullivan, J., Micklem, G., & Cherry, J. M. (2012). YeastMine--an integrated data warehouse for Saccharomyces cerevisiae data as a multipurpose tool-kit. *Database : The Journal of Biological Databases and Curation*, *2012*, bar062–bar062. https://doi.org/10.1093/database/bar062

Batova, A., Altomare, D., Creek, K. E., Naviaux, R. K., Wang, L., Li, K., Green, E., Williams, R., Naviaux, J. C., Diccianni, M., & Yu, A. L. (2017). Englerin A induces an acute inflammatory response and reveals lipid metabolism and ER stress as targetable vulnerabilities in renal cell carcinoma. *PloS One*, *12*(3), e0172632. https://doi.org/10.1371/journal.pone.0172632

Baur, J. A., & Sinclair, D. A. (2006). Therapeutic potential of resveratrol: the in vivo evidence. *Nature Reviews. Drug Discovery*, *5*(6), 493–506. https://doi.org/10.1038/nrd2060

Bell, M. C., Crowley-Nowick, P., Bradlow, H. L., Sepkovic, D. W., Schmidt-Grimminger, D., Howell, P., Mayeaux, E. J., Tucker, A., Turbat-Herrera, E. A., & Mathis, J. M. (2000). Placebo-controlled trial of indole-3-carbinol in the treatment of CIN. *Gynecologic*

Oncology, *78*(2), 123–129. https://doi.org/10.1006/gyno.2000.5847
Berman, H. M., Westbrook, J., Feng, Z., Gilliland, G., Bhat, T. N., Weissig, H., Shindyalov, I. N., & Bourne, P. E. (2000). The Protein Data Bank. *Nucleic Acids Research*, *28*(1), 235–242. https://doi.org/10.1093/nar/28.1.235
Bhargava, P., Malik, V., Liu, Y., Ryu, J., Kaul, S. C., Sundar, D., & Wadhwa, R. (2019). Molecular Insights Into Withaferin-A-Induced Senescence: Bioinformatics and Experimental Evidence to the Role of NFκB and CARF. *The Journals of Gerontology. Series A, Biological Sciences and Medical Sciences*, *74*(2), 183–191. https://doi.org/10.1093/gerona/gly107
Blevins, W. R., Tavella, T., Moro, S. G., Blasco-Moreno, B., Closa-Mosquera, A., Díez, J., Carey, L. B., & Albà, M. M. (2019). Extensive post-transcriptional buffering of gene expression in the response to severe oxidative stress in baker's yeast. *Scientific Reports*, *9*(1), 11005. https://doi.org/10.1038/s41598-019-47424-w
Bolger, A. M., Lohse, M., & Usadel, B. (2014). Trimmomatic: a flexible trimmer for Illumina sequence data. *Bioinformatics*, *30*(15), 2114–2120. https://doi.org/10.1093/bioinformatics/btu170
Bouhaddou, M., Memon, D., Meyer, B., White, K. M., Rezelj, V. V, Correa Marrero, M., Polacco, B. J., Melnyk, J. E., Ulferts, S., Kaake, R. M., Batra, J., Richards, A. L., Stevenson, E., Gordon, D. E., Rojc, A., Obernier, K., Fabius, J. M., Soucheray, M., Miorin, L., … Krogan, N. J. (2020). The Global Phosphorylation Landscape of SARS-CoV-2 Infection. *Cell*, *182*(3), 685-712.e19. https://doi.org/10.1016/j.cell.2020.06.034
Boya, P., Reggiori, F., & Codogno, P. (2013). Emerging regulation and functions of autophagy. *Nature Cell Biology*, *15*(7), 713–720. https://doi.org/10.1038/ncb2788
Bradamante, S., Barenghi, L., & Villa, A. (2004). Cardiovascular protective effects of resveratrol. *Cardiovascular Drug Reviews*, *22*(3), 169–188. https://doi.org/10.1111/j.1527-3466.2004.tb00139.x
Brandi, G., Paiardini, M., Cervasi, B., Fiorucci, C., Filippone, P., De Marco, C., Zaffaroni, N., & Magnani, M. (2003). A new indole-3-carbinol tetrameric derivative inhibits cyclin-dependent kinase 6 expression, and induces G1 cell cycle arrest in both estrogen-dependent and estrogen-independent breast cancer cell lines. *Cancer Research*, *63*(14), 4028–4036.
Brenk, R., Schipani, A., James, D., Krasowski, A., Gilbert, I. H., Frearson, J., & Wyatt, P. G. (2008). Lessons learnt from assembling screening libraries for drug discovery for neglected diseases. *ChemMedChem*, *3*(3), 435–444. https://doi.org/10.1002/cmdc.200700139
Brennan, L., & de Roos, B. (2021). Nutrigenomics: lessons learned and future perspectives. *The American Journal of Clinical Nutrition*, *113*(3), 503–516. https://doi.org/10.1093/ajcn/nqaa366
Breuza, L., Halbeisen, R., Jenö, P., Otte, S., Barlowe, C., Hong, W., & Hauri, H.-P. (2004). Proteomics of endoplasmic reticulum-Golgi intermediate compartment (ERGIC) membranes from brefeldin A-treated HepG2 cells identifies ERGIC-32, a new cycling protein that interacts with human Erv46. *The Journal of Biological Chemistry*, *279*(45), 47242–47253. https://doi.org/10.1074/jbc.M406644200
Brooks, S. M., & Alper, H. S. (2021). Applications, challenges, and needs for employing synthetic biology beyond the lab. *Nature Communications*, *12*(1), 1390. https://doi.org/10.1038/s41467-021-21740-0
Brul, S., Schuren, F., Montijn, R., Keijser, B. J. F., van der Spek, H., & Oomes, S. J. C. M. (2006). The impact of functional genomics on microbiological food quality and safety. *International Journal of Food Microbiology*, *112*(3), 195–199. https://doi.org/10.1016/j.ijfoodmicro.2006.04.014

Byrne, K. P., & Wolfe, K. H. (2005). The Yeast Gene Order Browser: combining curated homology and syntenic context reveals gene fate in polyploid species. *Genome Research*, *15*(10), 1456–1461. https://doi.org/10.1101/gr.3672305

Carmona-Gutierrez, D., Bauer, M. A., Zimmermann, A., Aguilera, A., Austriaco, N., Ayscough, K., Balzan, R., Bar-Nun, S., Barrientos, A., Belenky, P., Blondel, M., Braun, R. J., Breitenbach, M., Burhans, W. C., Büttner, S., Cavalieri, D., Chang, M., Cooper, K. F., Côrte-Real, M., … Madeo, F. (2018). Guidelines and recommendations on yeast cell death nomenclature. *Microbial Cell (Graz, Austria)*, *5*(1), 4–31. https://doi.org/10.15698/mic2018.01.607

Caruso, J. A., Campana, R., Wei, C., Su, C.-H., Hanks, A. M., Bornmann, W. G., & Keyomarsi, K. (2014). Indole-3-carbinol and its N-alkoxy derivatives preferentially target ERα-positive breast cancer cells. *Cell Cycle (Georgetown, Tex.)*, *13*(16), 2587–2599. https://doi.org/10.4161/15384101.2015.942210

Carvalho-Netto, O. V, Carazzolle, M. F., Mofatto, L. S., Teixeira, P. J. P. L., Noronha, M. F., Calderón, L. A. L., Mieczkowski, P. A., Argueso, J. L., & Pereira, G. A. G. (2015). Saccharomyces cerevisiae transcriptional reprograming due to bacterial contamination during industrial scale bioethanol production. *Microbial Cell Factories*, *14*, 13. https://doi.org/10.1186/s12934-015-0196-6

Cebollero, E., Reggiori, F., & Kraft, C. (2012). Reticulophagy and Ribophagy: Regulated Degradation of Protein Production Factories. *International Journal of Cell Biology*, *2012*, 182834. https://doi.org/10.1155/2012/182834

Chaitanya, G. V., Steven, A. J., & Babu, P. P. (2010). PARP-1 cleavage fragments: signatures of cell-death proteases in neurodegeneration. *Cell Communication and Signaling : CCS*, *8*, 31. https://doi.org/10.1186/1478-811X-8-31

Chakravarti, N., Peddareddigari, V. G. R., Warneke, C. L., Johnson, M. M., Overwijk, W. W., Hwu, P., & Prieto, V. G. (2013). Differential expression of the G-protein-coupled formyl Peptide receptor in melanoma associates with aggressive phenotype. *The American Journal of Dermatopathology*, *35*(2), 184–190. https://doi.org/10.1097/DAD.0b013e31825b2506

Chan, E. W., Cheng, S. C., Sin, F. W., & Xie, Y. (2001). Triptolide induced cytotoxic effects on human promyelocytic leukemia, T cell lymphoma and human hepatocellular carcinoma cell lines. *Toxicology Letters*, *122*(1), 81–87. https://doi.org/10.1016/s0378-4274(01)00353-8

Chan, J. F.-W., Kok, K.-H., Zhu, Z., Chu, H., To, K. K.-W., Yuan, S., & Yuen, K.-Y. (2020). Genomic characterization of the 2019 novel human-pathogenic coronavirus isolated from a patient with atypical pneumonia after visiting Wuhan. *Emerging Microbes & Infections*, *9*(1), 221–236. https://doi.org/10.1080/22221751.2020.1719902

Chan, W. K. B., Zhang, H., Yang, J., Brender, J. R., Hur, J., Özgür, A., & Zhang, Y. (2015). GLASS: a comprehensive database for experimentally validated GPCR-ligand associations. *Bioinformatics (Oxford, England)*, *31*(18), 3035–3042. https://doi.org/10.1093/bioinformatics/btv302

Chandrashekar, D. S., Bashel, B., Balasubramanya, S. A. H., Creighton, C. J., Ponce-Rodriguez, I., Chakravarthi, B. V. S. K., & Varambally, S. (2017). UALCAN: A Portal for Facilitating Tumor Subgroup Gene Expression and Survival Analyses. *Neoplasia (New York, N.Y.)*, *19*(8), 649–658. https://doi.org/10.1016/j.neo.2017.05.002

Chang, H.-C., Chang, F.-R., Wang, Y.-C., Pan, M.-R., Hung, W.-C., & Wu, Y.-C. (2007). A bioactive withanolide Tubocapsanolide A inhibits proliferation of human lung cancer cells via repressing Skp2 expression. *Molecular Cancer Therapeutics*, *6*(5), 1572–1578. https://doi.org/10.1158/1535-7163.MCT-06-0812

Chang, H. H. Y., Pannunzio, N. R., Adachi, N., & Lieber, M. R. (2017). Non-homologous

DNA end joining and alternative pathways to double-strand break repair. *Nature Reviews Molecular Cell Biology*, *18*(8), 495–506. https://doi.org/10.1038/nrm.2017.48

Chen, P. X., Wang, S., Nie, S., & Marcone, M. (2013). Properties of Cordyceps Sinensis: A review. *Journal of Functional Foods*, *5*(2), 550–569. https://doi.org/10.1016/j.jff.2013.01.034

Chen, Y., Liu, Q., & Guo, D. (2020). Emerging coronaviruses: Genome structure, replication, and pathogenesis. *Journal of Medical Virology*, *92*(4), 418–423. https://doi.org/10.1002/jmv.25681

Chen, Z., Tao, Z.-Z., Chen, S.-M., Chen, C., Li, F., & Xiao, B. (2013). Indole-3-carbinol inhibits nasopharyngeal carcinoma growth through cell cycle arrest in vivo and in vitro. *PloS One*, *8*(12), e82288. https://doi.org/10.1371/journal.pone.0082288

Cheng, Z., Yuan, X., Qu, Y., Li, X., Wu, G., Li, C., Zu, X., Yang, N., Ke, X., Zhou, J., Xie, N., Xu, X., Liu, S., Shen, Y., Li, H., & Zhang, W. (2017). Bruceine D inhibits hepatocellular carcinoma growth by targeting β-catenin/jagged1 pathways. *Cancer Letters*, *403*, 195–205. https://doi.org/10.1016/j.canlet.2017.06.014

Cherry, J. M., Hong, E. L., Amundsen, C., Balakrishnan, R., Binkley, G., Chan, E. T., Christie, K. R., Costanzo, M. C., Dwight, S. S., Engel, S. R., Fisk, D. G., Hirschman, J. E., Hitz, B. C., Karra, K., Krieger, C. J., Miyasato, S. R., Nash, R. S., Park, J., Skrzypek, M. S., … Wong, E. D. (2011). Saccharomyces Genome Database: the genomics resource of budding yeast. *Nucleic Acids Research*, *40*(D1), D700–D705. https://doi.org/10.1093/nar/gkr1029

Choi, M. J., Park, E. J., Min, K. J., Park, J.-W., & Kwon, T. K. (2011). Endoplasmic reticulum stress mediates withaferin A-induced apoptosis in human renal carcinoma cells. *Toxicology in Vitro : An International Journal Published in Association with BIBRA*, *25*(3), 692–698. https://doi.org/10.1016/j.tiv.2011.01.010

Chu, S., DeRisi, J., Eisen, M., Mulholland, J., Botstein, D., Brown, P. O., & Herskowitz, I. (1998). The transcriptional program of sporulation in budding yeast. *Science (New York, N.Y.)*, *282*(5389), 699–705. https://doi.org/10.1126/science.282.5389.699

Cifuentes, A. (2009). Food analysis and foodomics. In *Journal of chromatography. A* (Vol. 1216, Issue 43, p. 7109). https://doi.org/10.1016/j.chroma.2009.09.018

Coffelt, S. B., Tomchuck, S. L., Zwezdaryk, K. J., Danka, E. S., & Scandurro, A. B. (2009). Leucine leucine-37 uses formyl peptide receptor-like 1 to activate signal transduction pathways, stimulate oncogenic gene expression, and enhance the invasiveness of ovarian cancer cells. *Molecular Cancer Research : MCR*, *7*(6), 907–915. https://doi.org/10.1158/1541-7786.MCR-08-0326

Collins, J. C., Ghalei, H., Doherty, J. R., Huang, H., Culver, R. N., & Karbstein, K. (2018). Ribosome biogenesis factor Ltv1 chaperones the assembly of the small subunit head. *The Journal of Cell Biology*, *217*(12), 4141–4154. https://doi.org/10.1083/jcb.201804163

Cortese, M., Lee, J.-Y., Cerikan, B., Neufeldt, C. J., Oorschot, V. M. J., Köhrer, S., Hennies, J., Schieber, N. L., Ronchi, P., Mizzon, G., Romero-Brey, I., Santarella-Mellwig, R., Schorb, M., Boermel, M., Mocaer, K., Beckwith, M. S., Templin, R. M., Gross, V., Pape, C., … Bartenschlager, R. (2020). Integrative Imaging Reveals SARS-CoV-2-Induced Reshaping of Subcellular Morphologies. *Cell Host & Microbe*, *28*(6), 853-866.e5. https://doi.org/10.1016/j.chom.2020.11.003

Corton, J. M., Gillespie, J. G., & Hardie, D. G. (1994). Role of the AMP-activated protein kinase in the cellular stress response. *Current Biology : CB*, *4*(4), 315–324. https://doi.org/10.1016/s0960-9822(00)00070-1

Côté, P. D., Moukhles, H., Lindenbaum, M., & Carbonetto, S. (1999). Chimaeric mice deficient in dystroglycans develop muscular dystrophy and have disrupted myoneural synapses. *Nature Genetics*, *23*(3), 338–342. https://doi.org/10.1038/15519

Cover, C. M., Hsieh, S. J., Cram, E. J., Hong, C., Riby, J. E., Bjeldanes, L. F., & Firestone, G. L. (1999). Indole-3-carbinol and tamoxifen cooperate to arrest the cell cycle of MCF-7 human breast cancer cells. *Cancer Research*, *59*(6), 1244–1251.

Cover, C. M., Hsieh, S. J., Tran, S. H., Hallden, G., Kim, G. S., Bjeldanes, L. F., & Firestone, G. L. (1998). Indole-3-carbinol inhibits the expression of cyclin-dependent kinase-6 and induces a G1 cell cycle arrest of human breast cancer cells independent of estrogen receptor signaling. *The Journal of Biological Chemistry*, *273*(7), 3838–3847. https://doi.org/10.1074/jbc.273.7.3838

D'Amours, D., Sallmann, F. R., Dixit, V. M., & Poirier, G. G. (2001). Gain-of-function of poly(ADP-ribose) polymerase-1 upon cleavage by apoptotic proteases: implications for apoptosis. *Journal of Cell Science*, *114*(Pt 20), 3771–3778.

Daina, A., Michielin, O., & Zoete, V. (2017). SwissADME: a free web tool to evaluate pharmacokinetics, drug-likeness and medicinal chemistry friendliness of small molecules. *Scientific Reports*, *7*, 42717. https://doi.org/10.1038/srep42717

Davis, A. P., Grondin, C. J., Johnson, R. J., Sciaky, D., Wiegers, J., Wiegers, T. C., & Mattingly, C. J. (2021). Comparative Toxicogenomics Database (CTD): update 2021. *Nucleic Acids Research*, *49*(D1), D1138–D1143. https://doi.org/10.1093/nar/gkaa891

De Filippis, F., Esposito, A., & Ercolini, D. (2022). Outlook on next-generation probiotics from the human gut. *Cellular and Molecular Life Sciences : CMLS*, *79*(2), 76. https://doi.org/10.1007/s00018-021-04080-6

De Filippo, C., Cavalieri, D., Di Paola, M., Ramazzotti, M., Poullet, J. B., Massart, S., Collini, S., Pieraccini, G., & Lionetti, P. (2010). Impact of diet in shaping gut microbiota revealed by a comparative study in children from Europe and rural Africa. *Proceedings of the National Academy of Sciences*, *107*(33), 14691 LP – 14696. https://doi.org/10.1073/pnas.1005963107

de Matos, P., Alcántara, R., Dekker, A., Ennis, M., Hastings, J., Haug, K., Spiteri, I., Turner, S., & Steinbeck, C. (2010). Chemical Entities of Biological Interest: an update. *Nucleic Acids Research*, *38*(Database issue), D249-54. https://doi.org/10.1093/nar/gkp886

Delgado, B., Bach, A., Guasch, I., González, C., Elcoso, G., Pryce, J. E., & Gonzalez-Recio, O. (2019). Whole rumen metagenome sequencing allows classifying and predicting feed efficiency and intake levels in cattle. *Scientific Reports*, *9*(1), 11. https://doi.org/10.1038/s41598-018-36673-w

Dell'Agnello, C., Leo, S., Agostino, A., Szabadkai, G., Tiveron, C., Zulian, A., Prelle, A., Roubertoux, P., Rizzuto, R., & Zeviani, M. (2007). Increased longevity and refractoriness to Ca2+-dependent neurodegeneration in Surf1 knockout mice. *Human Molecular Genetics*, *16*(4), 431–444. https://doi.org/10.1093/hmg/ddl477

Ding, L., Bailey, M. H., Porta-Pardo, E., Thorsson, V., Colaprico, A., Bertrand, D., Gibbs, D. L., Weerasinghe, A., Huang, K.-L., Tokheim, C., Cortés-Ciriano, I., Jayasinghe, R., Chen, F., Yu, L., Sun, S., Olsen, C., Kim, J., Taylor, A. M., Cherniack, A. D., … Getz, G. (2018). Perspective on Oncogenic Processes at the End of the Beginning of Cancer Genomics. *Cell*, *173*(2), 305-320.e10. https://doi.org/10.1016/j.cell.2018.03.033

Dobin, A., Davis, C. A., Schlesinger, F., Drenkow, J., Zaleski, C., Jha, S., Batut, P., Chaisson, M., & Gingeras, T. R. (2012). STAR: ultrafast universal RNA-seq aligner. *Bioinformatics*, *29*(1), 15–21. https://doi.org/10.1093/bioinformatics/bts635

Dong, D., Song, M., Wu, X., & Wang, W. (2020). NOL6, a new founding oncogene in human prostate cancer and targeted by miR-590-3p. *Cytotechnology*, *72*(3), 469–478. https://doi.org/10.1007/s10616-020-00394-8

Dong, S.-H., Liu, J., Ge, Y.-Z., Dong, L., Xu, C.-H., Ding, J., & Yue, J.-M. (2013). Chemical constituents from Brucea javanica. *Phytochemistry*, *85*, 175–184. https://doi.org/10.1016/j.phytochem.2012.08.018

Dong, Y., Hu, J., Fan, L., & Chen, Q. (2017). RNA-Seq-based transcriptomic and metabolomic analysis reveal stress responses and programmed cell death induced by acetic acid in Saccharomyces cerevisiae. *Scientific Reports*, *7*(1), 42659. https://doi.org/10.1038/srep42659

Du, Y., Gong, J., Tian, X., Yan, X., Guo, T., Huang, M., Zhang, B., Hu, X., Liu, H., Wang, Y., Li, J., & Li, M. (2015). Japonicone A inhibits the growth of non-small cell lung cancer cells via mitochondria-mediated pathways. *Tumour Biology : The Journal of the International Society for Oncodevelopmental Biology and Medicine*, *36*(10), 7473–7482. https://doi.org/10.1007/s13277-015-3439-6

Dumont, P., Ingrassia, L., Rouzeau, S., Ribaucour, F., Thomas, S., Roland, I., Darro, F., Lefranc, F., & Kiss, R. (2007). The Amaryllidaceae isocarbostyril narciclasine induces apoptosis by activation of the death receptor and/or mitochondrial pathways in cancer cells but not in normal fibroblasts. *Neoplasia (New York, N.Y.)*, *9*(9), 766–776. https://doi.org/10.1593/neo.07535

Dunckley, T., Tucker, M., & Parker, R. (2001). Two related proteins, Edc1p and Edc2p, stimulate mRNA decapping in Saccharomyces cerevisiae. *Genetics*, *157*(1), 27–37. https://pubmed.ncbi.nlm.nih.gov/11139489

Earnshaw, W. C., Sullivan, K. F., Machlin, P. S., Cooke, C. A., Kaiser, D. A., Pollard, T. D., Rothfield, N. F., & Cleveland, D. W. (1987). Molecular cloning of cDNA for CENP-B, the major human centromere autoantigen. *The Journal of Cell Biology*, *104*(4), 817–829. https://doi.org/10.1083/jcb.104.4.817

Eastwood, M. D., Cheung, S. W. T., Lee, K. Y., Moffat, J., & Meneghini, M. D. (2012). Developmentally programmed nuclear destruction during yeast gametogenesis. *Developmental Cell*, *23*(1), 35–44. https://doi.org/10.1016/j.devcel.2012.05.005

Eastwood, M. D., & Meneghini, M. D. (2015). Developmental Coordination of Gamete Differentiation with Programmed Cell Death in Sporulating Yeast. *Eukaryotic Cell*, *14*(9), 858–867. https://doi.org/10.1128/EC.00068-15

Egan, W. J., Merz, K. M. J., & Baldwin, J. J. (2000). Prediction of drug absorption using multivariate statistics. *Journal of Medicinal Chemistry*, *43*(21), 3867–3877. https://doi.org/10.1021/jm000292e

Ehrenreich, I. M. (2020). Evolution after genome duplication. *Science*, *368*(6498), 1424 LP – 1425. https://doi.org/10.1126/science.abc1796

Engbrecht, M., & Mangerich, A. (2020). The Nucleolus and PARP1 in Cancer Biology. *Cancers*, *12*(7). https://doi.org/10.3390/cancers12071813

Enyenihi, A. H., & Saunders, W. S. (2003). Large-scale functional genomic analysis of sporulation and meiosis in Saccharomyces cerevisiae. *Genetics*, *163*(1), 47–54.

Ercolini, D. (2020). Secrets of the cheese microbiome. *Nature Food*, *1*(8), 466–467. https://doi.org/10.1038/s43016-020-0131-9

Eriksson, M., Peña-Martínez, P., Ramakrishnan, R., Chapellier, M., Högberg, C., Glowacki, G., Orsmark-Pietras, C., Velasco-Hernández, T., Lazarević, V. L., Juliusson, G., Cammenga, J., Mulloy, J. C., Richter, J., Fioretos, T., Ebert, B. L., & Järås, M. (2017). Agonistic targeting of TLR1/TLR2 induces p38 MAPK-dependent apoptosis and NFκB-dependent differentiation of AML cells. *Blood Advances*, *1*(23), 2046–2057. https://doi.org/10.1182/bloodadvances.2017006148

Falcone, C., & Mazzoni, C. (2016). External and internal triggers of cell death in yeast. *Cellular and Molecular Life Sciences*, *73*(11), 2237–2250. https://doi.org/10.1007/s00018-016-2197-y

Fan, J., Ren, D., Wang, J., Liu, X., Zhang, H., Wu, M., & Yang, G. (2020). Bruceine D induces lung cancer cell apoptosis and autophagy via the ROS/MAPK signaling pathway in vitro and in vivo. *Cell Death & Disease*, *11*(2), 126.

https://doi.org/10.1038/s41419-020-2317-3
Fast, D. (1973). Sporulation synchrony of Saccharomyces cerevisiae grown in various carbon sources. *Journal of Bacteriology*, *116*(2), 925–930. https://doi.org/10.1128/JB.116.2.925-930.1973
Fatokun, A. A., Dawson, V. L., & Dawson, T. M. (2014). Parthanatos: mitochondrial-linked mechanisms and therapeutic opportunities. *British Journal of Pharmacology*, *171*(8), 2000–2016. https://doi.org/10.1111/bph.12416
Fernandes, A. R., Mira, N. P., Vargas, R. C., Canelhas, I., & Sá-Correia, I. (2005). Saccharomyces cerevisiae adaptation to weak acids involves the transcription factor Haa1p and Haa1p-regulated genes. *Biochemical and Biophysical Research Communications*, *337*(1), 95–103. https://doi.org/10.1016/j.bbrc.2005.09.010
Filardo, S., Di Pietro, M., Mastromarino, P., & Sessa, R. (2020). Therapeutic potential of resveratrol against emerging respiratory viral infections. *Pharmacology & Therapeutics*, *214*, 107613. https://doi.org/10.1016/j.pharmthera.2020.107613
Florey, O., Kim, S. E., & Overholtzer, M. (2015). Entosis: Cell-in-Cell Formation that Kills Through Entotic Cell Death. *Current Molecular Medicine*, *15*(9), 861–866. https://doi.org/10.2174/1566524015666151026100042
Fuchs, T. A., Abed, U., Goosmann, C., Hurwitz, R., Schulze, I., Wahn, V., Weinrauch, Y., Brinkmann, V., & Zychlinsky, A. (2007). Novel cell death program leads to neutrophil extracellular traps. *The Journal of Cell Biology*, *176*(2), 231–241. https://doi.org/10.1083/jcb.200606027
Fujioka, N., Fritz, V., Upadhyaya, P., Kassie, F., & Hecht, S. S. (2016). Research on cruciferous vegetables, indole-3-carbinol, and cancer prevention: A tribute to Lee W. Wattenberg. *Molecular Nutrition & Food Research*, *60*(6), 1228–1238. https://doi.org/10.1002/mnfr.201500889
Galluzzi, Lorenzo, Baehrecke, E. H., Ballabio, A., Boya, P., Bravo-San Pedro, J. M., Cecconi, F., Choi, A. M., Chu, C. T., Codogno, P., Colombo, M. I., Cuervo, A. M., Debnath, J., Deretic, V., Dikic, I., Eskelinen, E.-L., Fimia, G. M., Fulda, S., Gewirtz, D. A., Green, D. R., … Kroemer, G. (2017). Molecular definitions of autophagy and related processes. *The EMBO Journal*, *36*(13), 1811–1836. https://doi.org/10.15252/embj.201796697
Galluzzi, Lorenzo, Buqué, A., Kepp, O., Zitvogel, L., & Kroemer, G. (2017). Immunogenic cell death in cancer and infectious disease. *Nature Reviews Immunology*, *17*(2), 97–111. https://doi.org/10.1038/nri.2016.107
Galluzzi, Lorenzo, Pietrocola, F., Levine, B., & Kroemer, G. (2014). Metabolic control of autophagy. *Cell*, *159*(6), 1263–1276. https://doi.org/10.1016/j.cell.2014.11.006
Galluzzi, Lorenzo, Vitale, I., Aaronson, S. A., Abrams, J. M., Adam, D., Agostinis, P., Alnemri, E. S., Altucci, L., Amelio, I., Andrews, D. W., Annicchiarico-Petruzzelli, M., Antonov, A. V, Arama, E., Baehrecke, E. H., Barlev, N. A., Bazan, N. G., Bernassola, F., Bertrand, M. J. M., Bianchi, K., … Kroemer, G. (2018). Molecular mechanisms of cell death: recommendations of the Nomenclature Committee on Cell Death 2018. *Cell Death & Differentiation*, *25*(3), 486–541. https://doi.org/10.1038/s41418-017-0012-4
Galluzzi, Lorenzo, Yamazaki, T., & Kroemer, G. (2018). Linking cellular stress responses to systemic homeostasis. *Nature Reviews. Molecular Cell Biology*, *19*(11), 731–745. https://doi.org/10.1038/s41580-018-0068-0
Galluzzi, Luca, De Santi, M., Crinelli, R., De Marco, C., Zaffaroni, N., Duranti, A., Brandi, G., & Magnani, M. (2012). Induction of endoplasmic reticulum stress response by the indole-3-carbinol cyclic tetrameric derivative CTet in human breast cancer cell lines. *PloS One*, *7*(8), e43249. https://doi.org/10.1371/journal.pone.0043249
Gao, X, Xu, Y. X., Janakiraman, N., Chapman, R. A., & Gautam, S. C. (2001). Immunomodulatory activity of resveratrol: suppression of lymphocyte proliferation,

development of cell-mediated cytotoxicity, and cytokine production. *Biochemical Pharmacology*, *62*(9), 1299–1308. https://doi.org/10.1016/s0006-2952(01)00775-4
Gao, Xin, Liu, Y., Zou, S., Liu, P., Zhao, J., Yang, C., Liang, M., & Yang, J. (2021). Genome-wide screening of SARS-CoV-2 infection-related genes based on the blood leukocytes sequencing data set of patients with COVID-19. *Journal of Medical Virology*, *93*(9), 5544–5554. https://doi.org/10.1002/jmv.27093
Gaulton, A., Bellis, L. J., Bento, A. P., Chambers, J., Davies, M., Hersey, A., Light, Y., McGlinchey, S., Michalovich, D., Al-Lazikani, B., & Overington, J. P. (2012). ChEMBL: a large-scale bioactivity database for drug discovery. *Nucleic Acids Research*, *40*(Database issue), D1100-7. https://doi.org/10.1093/nar/gkr777
Ge, X., Fares, F. A., & Yannai, S. (1999). Induction of apoptosis in MCF-7 cells by indole-3-carbinol is independent of p53 and bax. *Anticancer Research*, *19*(4B), 3199–3203.
Gerbasi, V. R., Weaver, C. M., Hill, S., Friedman, D. B., & Link, A. J. (2004). Yeast Asc1p and mammalian RACK1 are functionally orthologous core 40S ribosomal proteins that repress gene expression. *Molecular and Cellular Biology*, *24*(18), 8276–8287. https://doi.org/10.1128/MCB.24.18.8276-8287.2004
Ghose, A. K., Viswanadhan, V. N., & Wendoloski, J. J. (1999). A knowledge-based approach in designing combinatorial or medicinal chemistry libraries for drug discovery. 1. A qualitative and quantitative characterization of known drug databases. *Journal of Combinatorial Chemistry*, *1*(1), 55–68. https://doi.org/10.1021/cc9800071
Ghulam, M. M., Catala, M., & Abou Elela, S. (2019). Differential expression of duplicated ribosomal protein genes modifies ribosome composition in response to stress. *Nucleic Acids Research*, *48*(4), 1954–1968. https://doi.org/10.1093/nar/gkz1183
Gibert, B., & Mehlen, P. (2015). Dependence Receptors and Cancer: Addiction to Trophic Ligands. *Cancer Research*, *75*(24), 5171 LP – 5175. https://doi.org/10.1158/0008-5472.CAN-14-3652
Gibson, B. A., & Kraus, W. L. (2012). New insights into the molecular and cellular functions of poly(ADP-ribose) and PARPs. *Nature Reviews Molecular Cell Biology*, *13*(7), 411–424. https://doi.org/10.1038/nrm3376
Gimeno, A., Ojeda-Montes, M. J., Tomás-Hernández, S., Cereto-Massagué, A., Beltrán-Debón, R., Mulero, M., Pujadas, G., & Garcia-Vallvé, S. (2019). The Light and Dark Sides of Virtual Screening: What Is There to Know? *International Journal of Molecular Sciences*, *20*(6). https://doi.org/10.3390/ijms20061375
Gong, J., Li, Y., Liu, C.-J., Xiang, Y., Li, C., Ye, Y., Zhang, Z., Hawke, D. H., Park, P. K., Diao, L., Putkey, J. A., Yang, L., Guo, A.-Y., Lin, C., & Han, L. (2017). A Pan-cancer Analysis of the Expression and Clinical Relevance of Small Nucleolar RNAs in Human Cancer. *Cell Reports*, *21*(7), 1968–1981. https://doi.org/10.1016/j.celrep.2017.10.070
Gordon, D. E., Jang, G. M., Bouhaddou, M., Xu, J., Obernier, K., White, K. M., O'Meara, M. J., Rezelj, V. V, Guo, J. Z., Swaney, D. L., Tummino, T. A., Hüttenhain, R., Kaake, R. M., Richards, A. L., Tutuncuoglu, B., Foussard, H., Batra, J., Haas, K., Modak, M., … Krogan, N. J. (2020). A SARS-CoV-2 protein interaction map reveals targets for drug repurposing. *Nature*, *583*(7816), 459–468. https://doi.org/10.1038/s41586-020-2286-9
Green, D. R., Galluzzi, L., & Kroemer, G. (2011). Mitochondria and the autophagy-inflammation-cell death axis in organismal aging. *Science (New York, N.Y.)*, *333*(6046), 1109–1112. https://doi.org/10.1126/science.1201940
Grilo, A. L., & Mantalaris, A. (2019). Apoptosis: A mammalian cell bioprocessing perspective. *Biotechnology Advances*, *37*(3), 459–475. https://doi.org/10.1016/j.biotechadv.2019.02.012
Grin, B., Mahammad, S., Wedig, T., Cleland, M. M., Tsai, L., Herrmann, H., & Goldman, R. D. (2012). Withaferin a alters intermediate filament organization, cell shape and

behavior. *PloS One*, *7*(6), e39065. https://doi.org/10.1371/journal.pone.0039065
Guibal, F. C., Moog-Lutz, C., Smolewski, P., Di Gioia, Y., Darzynkiewicz, Z., Lutz, P. G., & Cayre, Y. E. (2002). ASB-2 inhibits growth and promotes commitment in myeloid leukemia cells. *The Journal of Biological Chemistry*, *277*(1), 218–224. https://doi.org/10.1074/jbc.M108476200
Hanahan, D., & Weinberg, R. A. (2011). Hallmarks of Cancer: The Next Generation. *Cell*, *144*(5), 646–674. https://doi.org/10.1016/j.cell.2011.02.013
Haque, A., Brazeau, D., & Amin, A. R. (2021). Perspectives on natural compounds in chemoprevention and treatment of cancer: an update with new promising compounds. *European Journal of Cancer (Oxford, England : 1990)*, *149*, 165–183. https://doi.org/10.1016/j.ejca.2021.03.009
Herwig, R., Hardt, C., Lienhard, M., & Kamburov, A. (2016). Analyzing and interpreting genome data at the network level with ConsensusPathDB. *Nature Protocols*, *11*(10), 1889–1907. https://doi.org/10.1038/nprot.2016.117
Hetz, C., & Papa, F. R. (2018). The Unfolded Protein Response and Cell Fate Control. *Molecular Cell*, *69*(2), 169–181. https://doi.org/10.1016/j.molcel.2017.06.017
Hoadley, K. A., Yau, C., Hinoue, T., Wolf, D. M., Lazar, A. J., Drill, E., Shen, R., Taylor, A. M., Cherniack, A. D., Thorsson, V., Akbani, R., Bowlby, R., Wong, C. K., Wiznerowicz, M., Sanchez-Vega, F., Robertson, A. G., Schneider, B. G., Lawrence, M. S., Noushmehr, H., … Laird, P. W. (2018). Cell-of-Origin Patterns Dominate the Molecular Classification of 10,000 Tumors from 33 Types of Cancer. *Cell*, *173*(2), 291-304.e6. https://doi.org/10.1016/j.cell.2018.03.022
Hoadley, K. A., Yau, C., Wolf, D. M., Cherniack, A. D., Tamborero, D., Ng, S., Leiserson, M. D. M., Niu, B., McLellan, M. D., Uzunangelov, V., Zhang, J., Kandoth, C., Akbani, R., Shen, H., Omberg, L., Chu, A., Margolin, A. A., Van't Veer, L. J., Lopez-Bigas, N., … Stuart, J. M. (2014). Multiplatform analysis of 12 cancer types reveals molecular classification within and across tissues of origin. *Cell*, *158*(4), 929–944. https://doi.org/10.1016/j.cell.2014.06.049
Hoffmann, M., Kleine-Weber, H., Schroeder, S., Krüger, N., Herrler, T., Erichsen, S., Schiergens, T. S., Herrler, G., Wu, N.-H., Nitsche, A., Müller, M. A., Drosten, C., & Pöhlmann, S. (2020). SARS-CoV-2 Cell Entry Depends on ACE2 and TMPRSS2 and Is Blocked by a Clinically Proven Protease Inhibitor. *Cell*, *181*(2), 271-280.e8. https://doi.org/10.1016/j.cell.2020.02.052
Holze, C., Michaudel, C., Mackowiak, C., Haas, D. A., Benda, C., Hubel, P., Pennemann, F. L., Schnepf, D., Wettmarshausen, J., Braun, M., Leung, D. W., Amarasinghe, G. K., Perocchi, F., Staeheli, P., Ryffel, B., & Pichlmair, A. (2018). Oxeiptosis, a ROS-induced caspase-independent apoptosis-like cell-death pathway. *Nature Immunology*, *19*(2), 130–140. https://doi.org/10.1038/s41590-017-0013-y
Howe, K. L., Achuthan, P., Allen, J., Allen, J., Alvarez-Jarreta, J., Amode, M. R., Armean, I. M., Azov, A. G., Bennett, R., Bhai, J., Billis, K., Boddu, S., Charkhchi, M., Cummins, C., Da Rin Fioretto, L., Davidson, C., Dodiya, K., El Houdaigui, B., Fatima, R., … Flicek, P. (2021). Ensembl 2021. *Nucleic Acids Research*, *49*(D1), D884–D891. https://doi.org/10.1093/nar/gkaa942
Iglesias-Bartolome, R., Uchiyama, A., Molinolo, A. A., Abusleme, L., Brooks, S. R., Callejas-Valera, J. L., Edwards, D., Doci, C., Asselin-Labat, M.-L., Onaitis, M. W., Moutsopoulos, N. M., Gutkind, J. S., & Morasso, M. I. (2018). Transcriptional signature primes human oral mucosa for rapid wound healing. *Science Translational Medicine*, *10*(451). https://doi.org/10.1126/scitranslmed.aap8798
Izzo, V., Bravo-San Pedro, J. M., Sica, V., Kroemer, G., & Galluzzi, L. (2016). Mitochondrial Permeability Transition: New Findings and Persisting Uncertainties. *Trends in Cell*

Biology, *26*(9), 655–667. https://doi.org/10.1016/j.tcb.2016.04.006
Jang, M., Cai, L., Udeani, G. O., Slowing, K. V, Thomas, C. F., Beecher, C. W., Fong, H. H., Farnsworth, N. R., Kinghorn, A. D., Mehta, R. G., Moon, R. C., & Pezzuto, J. M. (1997). Cancer chemopreventive activity of resveratrol, a natural product derived from grapes. *Science (New York, N.Y.)*, *275*(5297), 218–220. https://doi.org/10.1126/science.275.5297.218
Jindal, S., & Malkovsky, M. (1994). Stress responses to viral infection. *Trends in Microbiology*, *2*(3), 89–91. https://doi.org/10.1016/0966-842X(94)90540-1
Jorgensen, I., & Miao, E. A. (2015). Pyroptotic cell death defends against intracellular pathogens. *Immunological Reviews*, *265*(1), 130–142. https://doi.org/10.1111/imr.12287
Kanehisa, M., Sato, Y., Kawashima, M., Furumichi, M., & Tanabe, M. (2016). KEGG as a reference resource for gene and protein annotation. *Nucleic Acids Research*, *44*(D1), D457-62. https://doi.org/10.1093/nar/gkv1070
Karami, H., Derakhshani, A., Fereidouni, M., Miri-Moghaddam, E., Baradaran, B., Silvestris, N., Paradiso, A. V., Safarpour, H., & Summa, S. De. (2022). Transcriptional analysis of lung epithelial cells using WGCNA revealed the role of IRF9 and IFI6 genes in SARS-CoV-2 pathogenicity. *Research Square*. https://doi.org/10.21203/rs.3.rs-31167/v1
Katz, E., Nisani, S., & Chamovitz, D. A. (2018). Indole-3-carbinol: a plant hormone combatting cancer. *F1000Research*, *7*. https://doi.org/10.12688/f1000research.14127.1
Kellis, M., Birren, B. W., & Lander, E. S. (2004). Proof and evolutionary analysis of ancient genome duplication in the yeast Saccharomyces cerevisiae. *Nature*, *428*(6983), 617–624. https://doi.org/10.1038/nature02424
Kerr, J. F., Wyllie, A. H., & Currie, A. R. (1972). Apoptosis: a basic biological phenomenon with wide-ranging implications in tissue kinetics. *British Journal of Cancer*, *26*(4), 239–257. https://doi.org/10.1038/bjc.1972.33
Kessel, D. H., Price, M., & Reiners, J. J. J. (2012). ATG7 deficiency suppresses apoptosis and cell death induced by lysosomal photodamage. *Autophagy*, *8*(9), 1333–1341. https://doi.org/10.4161/auto.20792
Kharbanda, K. K., Rogers, D. D. 2nd, Mailliard, M. E., Siford, G. L., Barak, A. J., Beckenhauer, H. C., Sorrell, M. F., & Tuma, D. J. (2005). Role of elevated S-adenosylhomocysteine in rat hepatocyte apoptosis: protection by betaine. *Biochemical Pharmacology*, *70*(12), 1883–1890. https://doi.org/10.1016/j.bcp.2005.09.021
Kim, S., Chen, J., Cheng, T., Gindulyte, A., He, J., He, S., Li, Q., Shoemaker, B. A., Thiessen, P. A., Yu, B., Zaslavsky, L., Zhang, J., & Bolton, E. E. (2021). PubChem in 2021: new data content and improved web interfaces. *Nucleic Acids Research*, *49*(D1), D1388–D1395. https://doi.org/10.1093/nar/gkaa971
Kim, Y. C., & Guan, K.-L. (2015). mTOR: a pharmacologic target for autophagy regulation. *The Journal of Clinical Investigation*, *125*(1), 25–32. https://doi.org/10.1172/JCI73939
Kiss, T., Fayet-Lebaron, E., & Jády, B. E. (2010). Box H/ACA small ribonucleoproteins. *Molecular Cell*, *37*(5), 597–606. https://doi.org/10.1016/j.molcel.2010.01.032
Kleerebezem, M., Boekhorst, J., van Kranenburg, R., Molenaar, D., Kuipers, O. P., Leer, R., Tarchini, R., Peters, S. A., Sandbrink, H. M., Fiers, M. W. E. J., Stiekema, W., Lankhorst, R. M. K., Bron, P. A., Hoffer, S. M., Groot, M. N. N., Kerkhoven, R., de Vries, M., Ursing, B., de Vos, W. M., & Siezen, R. J. (2003). Complete genome sequence of Lactobacillus plantarum WCFS1. *Proceedings of the National Academy of Sciences of the United States of America*, *100*(4), 1990–1995. https://doi.org/10.1073/pnas.0337704100
Klionsky, D. J., Abdelmohsen, K., Abe, A., Abedin, M. J., Abeliovich, H., Acevedo Arozena, A., Adachi, H., Adams, C. M., Adams, P. D., Adeli, K., Adhihetty, P. J., Adler, S. G., Agam, G., Agarwal, R., Aghi, M. K., Agnello, M., Agostinis, P., Aguilar, P. V, Aguirre-

Ghiso, J., … Zughaier, S. M. (2016). Guidelines for the use and interpretation of assays for monitoring autophagy (3rd edition). *Autophagy*, *12*(1), 1–222. https://doi.org/10.1080/15548627.2015.1100356

Kobayashi, K., Yamaguchi, M., Miyazaki, K., Imai, H., Yokoe, K., Ono, R., Nosaka, T., & Katayama, N. (2016). Expressions of SH3BP5, LMO3, and SNAP25 in diffuse large B-cell lymphoma cells and their association with clinical features. *Cancer Medicine*, *5*(8), 1802–1809. https://doi.org/10.1002/cam4.753

Krampe, B., & Al-Rubeai, M. (2010). Cell death in mammalian cell culture: molecular mechanisms and cell line engineering strategies. *Cytotechnology*, *62*(3), 175–188. https://doi.org/10.1007/s10616-010-9274-0

Kroemer, G, Galluzzi, L., Vandenabeele, P., Abrams, J., Alnemri, E. S., Baehrecke, E. H., Blagosklonny, M. V, El-Deiry, W. S., Golstein, P., Green, D. R., Hengartner, M., Knight, R. A., Kumar, S., Lipton, S. A., Malorni, W., Nuñez, G., Peter, M. E., Tschopp, J., Yuan, J., … Melino, G. (2009). Classification of cell death: recommendations of the Nomenclature Committee on Cell Death 2009. *Cell Death and Differentiation*, *16*(1), 3–11. https://doi.org/10.1038/cdd.2008.150

Kroemer, Guido, Mariño, G., & Levine, B. (2010). Autophagy and the integrated stress response. *Molecular Cell*, *40*(2), 280–293. https://doi.org/10.1016/j.molcel.2010.09.023

Kubli, D. A., & Gustafsson, Å. B. (2012). Mitochondria and mitophagy: the yin and yang of cell death control. *Circulation Research*, *111*(9), 1208–1221. https://doi.org/10.1161/CIRCRESAHA.112.265819

Kuleshov, M. V, Stein, D. J., Clarke, D. J. B., Kropiwnicki, E., Jagodnik, K. M., Bartal, A., Evangelista, J. E., Hom, J., Cheng, M., Bailey, A., Zhou, A., Ferguson, L. B., Lachmann, A., & Ma'ayan, A. (2020). The COVID-19 Drug and Gene Set Library. *Patterns*, *1*(6), 100090. https://doi.org/https://doi.org/10.1016/j.patter.2020.100090

Kurimoto, R., Chiba, T., Ito, Y., Matsushima, T., Yano, Y., Miyata, K., Yashiro, Y., Suzuki, T., Tomita, K., & Asahara, H. (2020). The tRNA pseudouridine synthase TruB1 regulates the maturation of let-7 miRNA. *The EMBO Journal*, *39*(20), e104708. https://doi.org/10.15252/embj.2020104708

Kuwabara, N., Manya, H., Yamada, T., Tateno, H., Kanagawa, M., Kobayashi, K., Akasaka-Manya, K., Hirose, Y., Mizuno, M., Ikeguchi, M., Toda, T., Hirabayashi, J., Senda, T., Endo, T., & Kato, R. (2016). Carbohydrate-binding domain of the POMGnT1 stem region modulates O-mannosylation sites of α-dystroglycan. *Proceedings of the National Academy of Sciences of the United States of America*, *113*(33), 9280–9285. https://doi.org/10.1073/pnas.1525545113

Landeras-Bueno, S., Fernández, Y., Falcón, A., Oliveros, J. C., & Ortín, J. (2016). Chemical Genomics Identifies the PERK-Mediated Unfolded Protein Stress Response as a Cellular Target for Influenza Virus Inhibition. *MBio*, *7*(2), e00085-16. https://doi.org/10.1128/mBio.00085-16

Langfelder, P. (2018). *"anRichment tutorial."*

Langfelder, P., & Horvath, S. (2008). WGCNA: an R package for weighted correlation network analysis. *BMC Bioinformatics*, *9*, 559. https://doi.org/10.1186/1471-2105-9-559

Lau, S. T., Lin, Z. X., & Leung, P. S. (2010). Role of reactive oxygen species in brucein D-mediated p38-mitogen-activated protein kinase and nuclear factor-kappaB signalling pathways in human pancreatic adenocarcinoma cells. *British Journal of Cancer*, *102*(3), 583–593. https://doi.org/10.1038/sj.bjc.6605487

Lee, H.-E., Shin, J.-A., Jeong, J. H., Jeon, J.-G., Lee, M.-H., & Cho, S.-D. (2016). Anticancer activity of Ashwagandha against human head and neck cancer cell lines. *Journal of Oral Pathology & Medicine : Official Publication of the International Association of Oral Pathologists and the American Academy of Oral Pathology*, *45*(3), 193–201.

https://doi.org/10.1111/jop.12353
Legrand, J., Bolotin-Fukuhara, M., Bourgais, A., Fairhead, C., & Sicard, D. (2016). Life-history strategies and carbon metabolism gene dosage in the Nakaseomyces yeasts. *FEMS Yeast Research*, *16*(2). https://doi.org/10.1093/femsyr/fov112
Leinonen, R., Sugawara, H., Shumway, M., & Collaboration, on behalf of the I. N. S. D. (2010). The Sequence Read Archive. *Nucleic Acids Research*, *39*(suppl_1), D19–D21. https://doi.org/10.1093/nar/gkq1019
Levine, B., & Kroemer, G. (2008). Autophagy in the pathogenesis of disease. *Cell*, *132*(1), 27–42. https://doi.org/10.1016/j.cell.2007.12.018
Li, G., & De Clercq, E. (2020). Therapeutic options for the 2019 novel coronavirus (2019-nCoV). In *Nature reviews. Drug discovery* (Vol. 19, Issue 3, pp. 149–150). https://doi.org/10.1038/d41573-020-00016-0
Li, M., Hao, S., Li, C., Xiao, H., Sun, L., Yu, Z., Zhang, N., Xiong, Y., Zhao, D., & Yin, Y. (2019). Elevated SH3BP5 Correlates with Poor Outcome and Contributes to the Growth of Acute Myeloid Leukemia Cells. *Biomolecules*, *9*(9). https://doi.org/10.3390/biom9090505
Li, X., Yang, X., Liu, Y., Gong, N., Yao, W., Chen, P., Qin, J., Jin, H., Li, J., Chu, R., Shan, L., Zhang, R., Zhang, W., & Wang, H. (2013). Japonicone A suppresses growth of Burkitt lymphoma cells through its effect on NF-κB. *Clinical Cancer Research : An Official Journal of the American Association for Cancer Research*, *19*(11), 2917–2928. https://doi.org/10.1158/1078-0432.CCR-12-3258
Liao, Y., Smyth, G. K., & Shi, W. (2013). The Subread aligner: fast, accurate and scalable read mapping by seed-and-vote. *Nucleic Acids Research*, *41*(10), e108–e108. https://doi.org/10.1093/nar/gkt214
Liberio, M. S., Sadowski, M. C., Davis, R. A., Rockstroh, A., Vasireddy, R., Lehman, M. L., & Nelson, C. C. (2015). The ascidian natural product eusynstyelamide B is a novel topoisomerase II poison that induces DNA damage and growth arrest in prostate and breast cancer cells. *Oncotarget*, *6*(41), 43944–43963. https://doi.org/10.18632/oncotarget.6267
Liberio, M. S., Sadowski, M. C., Nelson, C. C., & Davis, R. A. (2014). Identification of eusynstyelamide B as a potent cell cycle inhibitor following the generation and screening of an ascidian-derived extract library using a real time cell analyzer. *Marine Drugs*, *12*(10), 5222–5239. https://doi.org/10.3390/md12105222
Liberzon, A., Subramanian, A., Pinchback, R., Thorvaldsdóttir, H., Tamayo, P., & Mesirov, J. P. (2011). Molecular signatures database (MSigDB) 3.0. *Bioinformatics (Oxford, England)*, *27*(12), 1739–1740. https://doi.org/10.1093/bioinformatics/btr260
Lin, S.-C., Ho, C.-T., Chuo, W.-H., Li, S., Wang, T. T., & Lin, C.-C. (2017). Effective inhibition of MERS-CoV infection by resveratrol. *BMC Infectious Diseases*, *17*(1), 144. https://doi.org/10.1186/s12879-017-2253-8
Linkermann, A., & Green, D. R. (2014). Necroptosis. *The New England Journal of Medicine*, *370*(5), 455–465. https://doi.org/10.1056/NEJMra1310050
Lipinski, C. A., Lombardo, F., Dominy, B. W., & Feeney, P. J. (2001). Experimental and computational approaches to estimate solubility and permeability in drug discovery and development settings. *Advanced Drug Delivery Reviews*, *46*(1–3), 3–26. https://doi.org/10.1016/s0169-409x(00)00129-0
Liston, P., Fong, W. G., Kelly, N. L., Toji, S., Miyazaki, T., Conte, D., Tamai, K., Craig, C. G., McBurney, M. W., & Korneluk, R. G. (2001). Identification of XAF1 as an antagonist of XIAP anti-Caspase activity. *Nature Cell Biology*, *3*(2), 128–133. https://doi.org/10.1038/35055027
Liu, Yang, Shoji-Kawata, S., Sumpter, R. M. J., Wei, Y., Ginet, V., Zhang, L., Posner, B.,

Tran, K. A., Green, D. R., Xavier, R. J., Shaw, S. Y., Clarke, P. G. H., Puyal, J., & Levine, B. (2013). Autosis is a Na+,K+-ATPase-regulated form of cell death triggered by autophagy-inducing peptides, starvation, and hypoxia-ischemia. *Proceedings of the National Academy of Sciences of the United States of America*, *110*(51), 20364–20371. https://doi.org/10.1073/pnas.1319661110

Liu, Yun, Chang, Y., He, X., Cai, Y., Jiang, H., Jia, R., & Leng, J. (2020). CD47 Enhances Cell Viability and Migration Ability but Inhibits Apoptosis in Endometrial Carcinoma Cells via the PI3K/Akt/mTOR Signaling Pathway. *Frontiers in Oncology*, *10*, 1525. https://doi.org/10.3389/fonc.2020.01525

Lu, S., Wei, F., & Li, G. (2021). The evolution of the concept of stress and the framework of the stress system. *Cell Stress*, *5*(6), 76–85. https://doi.org/10.15698/cst2021.06.250

Ludovico, P., Sousa, M. J., Silva, M. T., Leão, C., & Côrte-Real, M. (2001). Saccharomyces cerevisiae commits to a programmed cell death process in response to acetic acid. *Microbiology*, *147*(9), 2409–2415. https://doi.org/10.1099/00221287-147-9-2409

Luo, C., Wang, Y., Wei, C., Chen, Y., & Ji, Z. (2020). The anti-migration and anti-invasion effects of Bruceine D in human triple-negative breast cancer MDA-MB-231 cells. *Experimental and Therapeutic Medicine*, *19*(1), 273–279. https://doi.org/10.3892/etm.2019.8187

Mace, K., Krakowiak, J., El-Samad, H., & Pincus, D. (2020). Multi-kinase control of environmental stress responsive transcription. *PloS One*, *15*(3), e0230246. https://doi.org/10.1371/journal.pone.0230246

Madeo, F., Fröhlich, E., Ligr, M., Grey, M., Sigrist, S. J., Wolf, D. H., & Fröhlich, K.-U. (1999). Oxygen Stress: A Regulator of Apoptosis in Yeast . *Journal of Cell Biology*, *145*(4), 757–767. https://doi.org/10.1083/jcb.145.4.757

Maiti, S., Mallick, S. K., Bhutia, S. K., Behera, B., Mandal, M., & Maiti, T. K. (2011). Antitumor effect of culinary-medicinal oyster mushroom, Pleurotus ostreatus (Jacq.: Fr.) P. Kumm., derived protein fraction on tumor-bearing mice models. *International Journal of Medicinal Mushrooms*, *13*(5), 427–440. https://doi.org/10.1615/intjmedmushr.v13.i5.20

Malik, F., Kumar, A., Bhushan, S., Khan, S., Bhatia, A., Suri, K. A., Qazi, G. N., & Singh, J. (2007). Reactive oxygen species generation and mitochondrial dysfunction in the apoptotic cell death of human myeloid leukemia HL-60 cells by a dietary compound withaferin A with concomitant protection by N-acetyl cysteine. *Apoptosis : An International Journal on Programmed Cell Death*, *12*(11), 2115–2133. https://doi.org/10.1007/s10495-007-0129-x

Mansouri, L., Xie, Y., & Rappolee, D. A. (2012). Adaptive and Pathogenic Responses to Stress by Stem Cells during Development. *Cells*, *1*(4), 1197–1224. https://doi.org/10.3390/cells1041197

Marais, T. L. Des, Kluz, T., Xu, D., Zhang, X., Gesumaria, L., Matsui, M. S., Costa, M., & Sun, H. (2017). Transcription factors and stress response gene alterations in human keratinocytes following Solar Simulated Ultra Violet Radiation. *Scientific Reports*, *7*(1), 13622. https://doi.org/10.1038/s41598-017-13765-7

Mari, A., Scala, E., Palazzo, P., Ridolfi, S., Zennaro, D., & Carabella, G. (2006). Bioinformatics applied to allergy: allergen databases, from collecting sequence information to data integration. The Allergome platform as a model. *Cellular Immunology*, *244*(2), 97–100. https://doi.org/10.1016/j.cellimm.2007.02.012

Mariño, G., Niso-Santano, M., Baehrecke, E. H., & Kroemer, G. (2014). Self-consumption: the interplay of autophagy and apoptosis. *Nature Reviews. Molecular Cell Biology*, *15*(2), 81–94. https://doi.org/10.1038/nrm3735

Martín-Hernández, R., Reglero, G., Ordovás, J. M., & Dávalos, A. (2019). NutriGenomeDB:

a nutrigenomics exploratory and analytical platform. *Database : The Journal of Biological Databases and Curation*, *2019*. https://doi.org/10.1093/database/baz097

Martins, I., Raza, S. Q., Voisin, L., Dakhli, H., Law, F., De Jong, D., Allouch, A., Thoreau, M., Brenner, C., Deutsch, E., & Perfettini, J.-L. (2017). Entosis: The emerging face of non-cell-autonomous type IV programmed death. *Biomedical Journal*, *40*(3), 133–140. https://doi.org/10.1016/j.bj.2017.05.001

Mazzio, E. A., & Soliman, K. F. A. (2018). Whole-transcriptomic Profile of SK-MEL-3 Melanoma Cells Treated with the Histone Deacetylase Inhibitor: Trichostatin A. *Cancer Genomics & Proteomics*, *15*(5), 349–364. https://doi.org/10.21873/cgp.20094

Meerovich, I. G., Yang, M., Jiang, P., Hoffman, R. M., Gerasimenya, V. P., Orlov, A. E., Savitsky, A. P., & Popov, V. O. (2005). Study of action of cyclophosphamide and extract of mycelium of Pleurotus ostreatus in vivo on mice, bearing melanoma B16-F0-GFP. In D. J. Bornhop, S. I. Achilefu, R. Raghavachari, & A. P. Savitsky (Eds.), *Genetically Engineered and Optical Probes for Biomedical Applications III* (Vol. 5704, pp. 214–221). SPIE. https://doi.org/10.1117/12.592546

Meslier, V., Laiola, M., Roager, H. M., De Filippis, F., Roume, H., Quinquis, B., Giacco, R., Mennella, I., Ferracane, R., Pons, N., Pasolli, E., Rivellese, A., Dragsted, L. O., Vitaglione, P., Ehrlich, S. D., & Ercolini, D. (2020). Mediterranean diet intervention in overweight and obese subjects lowers plasma cholesterol and causes changes in the gut microbiome and metabolome independently of energy intake. *Gut*, *69*(7), 1258–1268. https://doi.org/10.1136/gutjnl-2019-320438

Michel, V., & Bakovic, M. (2009). The solute carrier 44A1 is a mitochondrial protein and mediates choline transport. *FASEB Journal : Official Publication of the Federation of American Societies for Experimental Biology*, *23*(8), 2749–2758. https://doi.org/10.1096/fj.08-121491

Mira, N. P., Henriques, S. F., Keller, G., Teixeira, M. C., Matos, R. G., Arraiano, C. M., Winge, D. R., & Sá-Correia, I. (2011). Identification of a DNA-binding site for the transcription factor Haa1, required for Saccharomyces cerevisiae response to acetic acid stress. *Nucleic Acids Research*, *39*(16), 6896–6907. https://doi.org/10.1093/nar/gkr228

Mizushima, N., Yoshimori, T., & Levine, B. (2010). Methods in Mammalian Autophagy Research. *Cell*, *140*(3), 313–326. https://doi.org/https://doi.org/10.1016/j.cell.2010.01.028

Mizushima, N., Yoshimori, T., & Ohsumi, Y. (2011). The role of Atg proteins in autophagosome formation. *Annual Review of Cell and Developmental Biology*, *27*, 107–132. https://doi.org/10.1146/annurev-cellbio-092910-154005

Mohammed, S. (2020). Cytotoxicity Assay of Agaricus Bisporus Extract , Oxaliplatin and Combination of both on Melanoma-B16 and Vero-101 Cell line:An in Vitro study. *University of Thi-Qar Journal of Science*, *7*(2 SE-Articles). http://jsci.utq.edu.iq/index.php/main/article/view/702

Mohan, R., & Bargagna-Mohan, P. (2016). The Use of Withaferin A to Study Intermediate Filaments. *Methods in Enzymology*, *568*, 187–218. https://doi.org/10.1016/bs.mie.2015.09.025

Mongioì, L. M., Perelli, S., Condorelli, R. A., Barbagallo, F., Crafa, A., Cannarella, R., La Vignera, S., & Calogero, A. E. (2021). The Role of Resveratrol in Human Male Fertility. *Molecules (Basel, Switzerland)*, *26*(9). https://doi.org/10.3390/molecules26092495

Monticolo, F., Palomba, E., & Chiusano, M. L. (2021). Translation machinery reprogramming in programmed cell death in Saccharomyces cerevisiae. *Cell Death Discovery*, *7*(1). https://doi.org/10.1038/s41420-020-00392-x

Monticolo, Francesco, & Chiusano, M. L. (2021). Computational Approaches for Cancer-Fighting: From Gene Expression to Functional Foods. *Cancers*, *13*(16).

https://doi.org/10.3390/cancers13164207
Monticolo, Francesco, Palomba, E., & Chiusano, M. L. (2020). Identification of Novel Potential Genes Involved in Cancer by Integrated Comparative Analyses. *International Journal of Molecular Sciences*, *21*(24). https://doi.org/10.3390/ijms21249560
Moore, J., Yousef, M., & Tsiani, E. (2016). Anticancer Effects of Rosemary (Rosmarinus officinalis L.) Extract and Rosemary Extract Polyphenols. *Nutrients*, *8*(11). https://doi.org/10.3390/nu8110731
Muegge, I., Heald, S. L., & Brittelli, D. (2001). Simple selection criteria for drug-like chemical matter. *Journal of Medicinal Chemistry*, *44*(12), 1841–1846. https://doi.org/10.1021/jm015507e
Muhammad, B. A., Almozyan, S., Babaei-Jadidi, R., Onyido, E. K., Saadeddin, A., Kashfi, S. H., Spencer-Dene, B., Ilyas, M., Lourdusamy, A., Behrens, A., & Nateri, A. S. (2018). FLYWCH1, a Novel Suppressor of Nuclear β-Catenin, Regulates Migration and Morphology in Colorectal Cancer. *Molecular Cancer Research : MCR*, *16*(12), 1977–1990. https://doi.org/10.1158/1541-7786.MCR-18-0262
Müller, M., & Kersten, S. (2003). Nutrigenomics: goals and strategies. *Nature Reviews. Genetics*, *4*(4), 315–322. https://doi.org/10.1038/nrg1047
Munagala, R., Kausar, H., Munjal, C., & Gupta, R. C. (2011). Withaferin A induces p53-dependent apoptosis by repression of HPV oncogenes and upregulation of tumor suppressor proteins in human cervical cancer cells. *Carcinogenesis*, *32*(11), 1697–1705. https://doi.org/10.1093/carcin/bgr192
Naciff, J. M., Khambatta, Z. S., Carr, G. J., Tiesman, J. P., Singleton, D. W., Khan, S. A., & Daston, G. P. (2016). Dose- and Time-Dependent Transcriptional Response of Ishikawa Cells Exposed to Genistein. *Toxicological Sciences : An Official Journal of the Society of Toxicology*, *151*(1), 71–87. https://doi.org/10.1093/toxsci/kfw024
Naik, R., Nixon, S., Lopes, A., Godfrey, K., Hatem, M. H., & Monaghan, J. M. (2006). A randomized phase II trial of indole-3-carbinol in the treatment of vulvar intraepithelial neoplasia. *International Journal of Gynecological Cancer : Official Journal of the International Gynecological Cancer Society*, *16*(2), 786–790. https://doi.org/10.1111/j.1525-1438.2006.00386.x
Nakagawa, K., Lokugamage, K. G., & Makino, S. (2016). Viral and Cellular mRNA Translation in Coronavirus-Infected Cells. *Advances in Virus Research*, *96*, 165–192. https://doi.org/10.1016/bs.aivir.2016.08.001
Napolitano, F., Carrella, D., Gao, X., & di Bernardo, D. (2019). gep2pep: a Bioconductor package for the creation and analysis of pathway-based expression profiles. *Bioinformatics (Oxford, England)*. https://doi.org/10.1093/bioinformatics/btz803
Neef, D. W., & Thiele, D. J. (2009). Enhancer of decapping proteins 1 and 2 are important for translation during heat stress in Saccharomyces cerevisiae. *Molecular Microbiology*, *73*(6), 1032–1042. https://doi.org/10.1111/j.1365-2958.2009.06827.x
Network, T. C. G. A. R. (2013). Corrigendum: Comprehensive genomic characterization defines human glioblastoma genes and core pathways. *Nature*, *494*(7438), 506. https://doi.org/10.1038/nature11903
Nezis, I. P., Shravage, B. V, Sagona, A. P., Lamark, T., Bjørkøy, G., Johansen, T., Rusten, T. E., Brech, A., Baehrecke, E. H., & Stenmark, H. (2010). Autophagic degradation of dBruce controls DNA fragmentation in nurse cells during late Drosophila melanogaster oogenesis. *The Journal of Cell Biology*, *190*(4), 523–531. https://doi.org/10.1083/jcb.201002035
Ni, H.-T., & LaPorte, D. C. (1995). Response of a yeast glycogen synthase gene to stress. *Molecular Microbiology*, *16*(6), 1197–1205. https://doi.org/10.1111/j.1365-2958.1995.tb02342.x

Nienhold, R., Ciani, Y., Koelzer, V. H., Tzankov, A., Haslbauer, J. D., Menter, T., Schwab, N., Henkel, M., Frank, A., Zsikla, V., Willi, N., Kempf, W., Hoyler, T., Barbareschi, M., Moch, H., Tolnay, M., Cathomas, G., Demichelis, F., Junt, T., & Mertz, K. D. (2020). Two distinct immunopathological profiles in autopsy lungs of COVID-19. *Nature Communications*, *11*(1), 5086. https://doi.org/10.1038/s41467-020-18854-2

Nishikawa, Y., Okuzaki, D., Fukushima, K., Mukai, S., Ohno, S., Ozaki, Y., Yabuta, N., & Nojima, H. (2015). Withaferin A Induces Cell Death Selectively in Androgen-Independent Prostate Cancer Cells but Not in Normal Fibroblast Cells. *PloS One*, *10*(7), e0134137. https://doi.org/10.1371/journal.pone.0134137

Oh, Y., Zhang, F., Wang, Y., Lee, E. M., Choi, I. Y., Lim, H., Mirakhori, F., Li, R., Huang, L., Xu, T., Wu, H., Li, C., Qin, C.-F., Wen, Z., Wu, Q.-F., Tang, H., Xu, Z., Jin, P., Song, H., … Lee, G. (2017). Zika virus directly infects peripheral neurons and induces cell death. *Nature Neuroscience*, *20*(9), 1209–1212. https://doi.org/10.1038/nn.4612

Ohno, S. (1970). Evolution by Gene Duplication. In *Evolution by Gene Duplication*. https://doi.org/10.1007/978-3-642-86659-3

Orozco, J., Villa, E., Manes, C.-L., Medlin, L. K., & Guillebault, D. (2016). Electrochemical RNA genosensors for toxic algal species: enhancing selectivity and sensitivity. *Talanta*, *161*, 560–566. https://doi.org/10.1016/j.talanta.2016.08.073

Ostaszewski, M., Mazein, A., Gillespie, M. E., Kuperstein, I., Niarakis, A., Hermjakob, H., Pico, A. R., Willighagen, E. L., Evelo, C. T., Hasenauer, J., Schreiber, F., Dräger, A., Demir, E., Wolkenhauer, O., Furlong, L. I., Barillot, E., Dopazo, J., Orta-Resendiz, A., Messina, F., … Schneider, R. (2020). COVID-19 Disease Map, building a computational repository of SARS-CoV-2 virus-host interaction mechanisms. *Scientific Data*, *7*(1), 136. https://doi.org/10.1038/s41597-020-0477-8

Palomera-Ávalos, V., Griñán-Ferré, C., Izquierdo, V., Camins, A., Sanfeliu, C., & Pallàs, M. (2017). Metabolic Stress Induces Cognitive Disturbances and Inflammation in Aged Mice: Protective Role of Resveratrol. *Rejuvenation Research*, *20*(3), 202–217. https://doi.org/10.1089/rej.2016.1885

Pascal, J. M. (2018). The comings and goings of PARP-1 in response to DNA damage. *DNA Repair*, *71*, 177–182. https://doi.org/10.1016/j.dnarep.2018.08.022

Pasolli, E., De Filippis, F., Mauriello, I. E., Cumbo, F., Walsh, A. M., Leech, J., Cotter, P. D., Segata, N., & Ercolini, D. (2020). Large-scale genome-wide analysis links lactic acid bacteria from food with the gut microbiome. *Nature Communications*, *11*(1), 2610. https://doi.org/10.1038/s41467-020-16438-8

Pasquereau, S., Nehme, Z., Haidar Ahmad, S., Daouad, F., Van Assche, J., Wallet, C., Schwartz, C., Rohr, O., Morot-Bizot, S., & Herbein, G. (2021). Resveratrol Inhibits HCoV-229E and SARS-CoV-2 Coronavirus Replication In Vitro. *Viruses*, *13*(2). https://doi.org/10.3390/v13020354

Penet, M.-F., Shah, T., Bharti, S., Krishnamachary, B., Artemov, D., Mironchik, Y., Wildes, F., Maitra, A., & Bhujwalla, Z. M. (2015). Metabolic imaging of pancreatic ductal adenocarcinoma detects altered choline metabolism. *Clinical Cancer Research : An Official Journal of the American Association for Cancer Research*, *21*(2), 386–395. https://doi.org/10.1158/1078-0432.CCR-14-0964

Poljšak, B., & Milisav, I. (2012). Clinical implications of cellular stress responses. *Bosnian Journal of Basic Medical Sciences*, *12*(2), 122–126. https://doi.org/10.17305/bjbms.2012.2510

Prasad, K., Khatoon, F., Rashid, S., Ali, N., AlAsmari, A. F., Ahmed, M. Z., Alqahtani, A. S., Alqahtani, M. S., & Kumar, V. (2020). Targeting hub genes and pathways of innate immune response in COVID-19: A network biology perspective. *International Journal of Biological Macromolecules*, *163*, 1–8. https://doi.org/10.1016/j.ijbiomac.2020.06.228

Primig, M., Williams, R. M., Winzeler, E. A., Tevzadze, G. G., Conway, A. R., Hwang, S. Y., Davis, R. W., & Esposito, R. E. (2000). The core meiotic transcriptome in budding yeasts. *Nature Genetics*, *26*(4), 415–423. https://doi.org/10.1038/82539

Pulikkan, J. A., Hegde, M., Ahmad, H. M., Belaghzal, H., Illendula, A., Yu, J., O'Hagan, K., Ou, J., Muller-Tidow, C., Wolfe, S. A., Zhu, L. J., Dekker, J., Bushweller, J. H., & Castilla, L. H. (2018). CBFβ-SMMHC Inhibition Triggers Apoptosis by Disrupting MYC Chromatin Dynamics in Acute Myeloid Leukemia. *Cell*, *174*(5), 1325. https://doi.org/10.1016/j.cell.2018.08.014

Qi, C., Wang, C., Zhao, L., Zhu, Z., Wang, P., Zhang, S., Cheng, L., & Zhang, X. (2021). SCovid: single-cell atlases for exposing molecular characteristics of COVID-19 across 10 human tissues. *Nucleic Acids Research*. https://doi.org/10.1093/nar/gkab881

Qin, J.-J., Wang, W., Voruganti, S., Wang, H., Zhang, W.-D., & Zhang, R. (2015). Identification of a new class of natural product MDM2 inhibitor: In vitro and in vivo anti-breast cancer activities and target validation. *Oncotarget*, *6*(5), 2623–2640. https://doi.org/10.18632/oncotarget.3098

Quirós, P. M., Prado, M. A., Zamboni, N., D'Amico, D., Williams, R. W., Finley, D., Gygi, S. P., & Auwerx, J. (2017). Multi-omics analysis identifies ATF4 as a key regulator of the mitochondrial stress response in mammals. *The Journal of Cell Biology*, *216*(7), 2027–2045. https://doi.org/10.1083/jcb.201702058

Rahman, K. M. W., Aranha, O., & Sarkar, F. H. (2003). Indole-3-carbinol (I3C) induces apoptosis in tumorigenic but not in nontumorigenic breast epithelial cells. *Nutrition and Cancer*, *45*(1), 101–112. https://doi.org/10.1207/S15327914NC4501_12

Rajman, L., Chwalek, K., & Sinclair, D. A. (2018). Therapeutic Potential of NAD-Boosting Molecules: The In Vivo Evidence. *Cell Metabolism*, *27*(3), 529–547. https://doi.org/10.1016/j.cmet.2018.02.011

Ranjbar, A., Jamshidi, M., & Torabi, S. (2020). Molecular modelling of the antiviral action of Resveratrol derivatives against the activity of two novel SARS CoV-2 and 2019-nCoV receptors. *European Review for Medical and Pharmacological Sciences*, *24*(14), 7834–7844. https://doi.org/10.26355/eurrev_202007_22288

Raudvere, U., Kolberg, L., Kuzmin, I., Arak, T., Adler, P., Peterson, H., & Vilo, J. (2019). g:Profiler: a web server for functional enrichment analysis and conversions of gene lists (2019 update). *Nucleic Acids Research*, *47*(W1), W191–W198. https://doi.org/10.1093/nar/gkz369

Ravindra, N. G., Alfajaro, M. M., Gasque, V., Huston, N. C., Wan, H., Szigeti-Buck, K., Yasumoto, Y., Greaney, A. M., Habet, V., Chow, R. D., Chen, J. S., Wei, J., Filler, R. B., Wang, B., Wang, G., Niklason, L. E., Montgomery, R. R., Eisenbarth, S. C., Chen, S., … Wilen, C. B. (2021). Single-cell longitudinal analysis of SARS-CoV-2 infection in human airway epithelium identifies target cells, alterations in gene expression, and cell state changes. *PLoS Biology*, *19*(3), e3001143. https://doi.org/10.1371/journal.pbio.3001143

Reed, G. A., Arneson, D. W., Putnam, W. C., Smith, H. J., Gray, J. C., Sullivan, D. K., Mayo, M. S., Crowell, J. A., & Hurwitz, A. (2006). Single-dose and multiple-dose administration of indole-3-carbinol to women: pharmacokinetics based on 3,3'-diindolylmethane. *Cancer Epidemiology, Biomarkers & Prevention : A Publication of the American Association for Cancer Research, Cosponsored by the American Society of Preventive Oncology*, *15*(12), 2477–2481. https://doi.org/10.1158/1055-9965.EPI-06-0396

Reed, G. A., Peterson, K. S., Smith, H. J., Gray, J. C., Sullivan, D. K., Mayo, M. S., Crowell, J. A., & Hurwitz, A. (2005). A phase I study of indole-3-carbinol in women: tolerability and effects. *Cancer Epidemiology, Biomarkers & Prevention : A Publication of the*

American Association for Cancer Research, Cosponsored by the American Society of Preventive Oncology, *14*(8), 1953–1960. https://doi.org/10.1158/1055-9965.EPI-05-0121

Rendleman, J., Cheng, Z., Maity, S., Kastelic, N., Munschauer, M., Allgoewer, K., Teo, G., Zhang, Y. B. M., Lei, A., Parker, B., Landthaler, M., Freeberg, L., Kuersten, S., Choi, H., & Vogel, C. (2018). New insights into the cellular temporal response to proteostatic stress. *ELife*, *7*. https://doi.org/10.7554/eLife.39054

Renehan, A. G., Booth, C., & Potten, C. S. (2001). What is apoptosis, and why is it important? *BMJ (Clinical Research Ed.)*, *322*(7301), 1536–1538. https://doi.org/10.1136/bmj.322.7301.1536

Robinson, M. D., McCarthy, D. J., & Smyth, G. K. (2009). edgeR: A Bioconductor package for differential expression analysis of digital gene expression data. *Bioinformatics*, *26*(1), 139–140. https://doi.org/10.1093/bioinformatics/btp616

Ross, E. M., Petrovski, S., Moate, P. J., & Hayes, B. J. (2013). Metagenomics of rumen bacteriophage from thirteen lactating dairy cattle. *BMC Microbiology*, *13*(1), 242. https://doi.org/10.1186/1471-2180-13-242

Rouhimoghadam, M., Safarian, S., Carroll, J. S., Sheibani, N., & Bidkhori, G. (2018). Tamoxifen-Induced Apoptosis of MCF-7 Cells via GPR30/PI3K/MAPKs Interactions: Verification by ODE Modeling and RNA Sequencing. *Frontiers in Physiology*, *9*, 907. https://doi.org/10.3389/fphys.2018.00907

Rubinstein, A. D., Eisenstein, M., Ber, Y., Bialik, S., & Kimchi, A. (2011). The autophagy protein Atg12 associates with antiapoptotic Bcl-2 family members to promote mitochondrial apoptosis. *Molecular Cell*, *44*(5), 698–709. https://doi.org/10.1016/j.molcel.2011.10.014

Ruskovska, T., Massaro, M., Carluccio, M. A., Arola-Arnal, A., Muguerza, B., Vanden Berghe, W., Declerck, K., Bravo, F. I., Calabriso, N., Combet, E., Gibney, E. R., Gomes, A., Gonthier, M.-P., Kistanova, E., Krga, I., Mena, P., Morand, C., Nunes Dos Santos, C., de Pascual-Teresa, S., … Milenkovic, D. (2020). Systematic bioinformatic analysis of nutrigenomic data of flavanols in cell models of cardiometabolic disease. *Food & Function*, *11*(6), 5040–5064. https://doi.org/10.1039/d0fo00701c

Safa, M., Jafari, L., Alikarami, F., Manafi Shabestari, R., & Kazemi, A. (2017). Indole-3-carbinol induces apoptosis of chronic myelogenous leukemia cells through suppression of STAT5 and Akt signaling pathways. *Tumour Biology : The Journal of the International Society for Oncodevelopmental Biology and Medicine*, *39*(6), 1010428317705768. https://doi.org/10.1177/1010428317705768

Safra, M., Nir, R., Farouq, D., Vainberg Slutskin, I., & Schwartz, S. (2017). Corrigendum: TRUB1 is the predominant pseudouridine synthase acting on mammalian mRNA via a predictable and conserved code. *Genome Research*, *27*(8), 1460. https://doi.org/10.1101/gr.225870.117

Sales, N. M. R., Pelegrini, P. B., & Goersch, M. C. (2014). Nutrigenomics: Definitions and Advances of This New Science. *Journal of Nutrition and Metabolism*, *2014*, 202759. https://doi.org/10.1155/2014/202759

Sant, D. W., Mustafi, S., Gustafson, C. B., Chen, J., Slingerland, J. M., & Wang, G. (2018). Vitamin C promotes apoptosis in breast cancer cells by increasing TRAIL expression. *Scientific Reports*, *8*(1), 5306. https://doi.org/10.1038/s41598-018-23714-7

Sareddy, G. R., Viswanadhapalli, S., Surapaneni, P., Suzuki, T., Brenner, A., & Vadlamudi, R. K. (2017). Novel KDM1A inhibitors induce differentiation and apoptosis of glioma stem cells via unfolded protein response pathway. *Oncogene*, *36*(17), 2423–2434. https://doi.org/10.1038/onc.2016.395

Sari, A. N., Bhargava, P., Dhanjal, J. K., Putri, J. F., Radhakrishnan, N., Shefrin, S., Ishida, Y., Terao, K., Sundar, D., Kaul, S. C., & Wadhwa, R. (2020). Combination of

Withaferin-A and CAPE Provides Superior Anticancer Potency: Bioinformatics and Experimental Evidence to Their Molecular Targets and Mechanism of Action. *Cancers*, *12*(5). https://doi.org/10.3390/cancers12051160

Schell, M. A., Karmirantzou, M., Snel, B., Vilanova, D., Berger, B., Pessi, G., Zwahlen, M.-C., Desiere, F., Bork, P., Delley, M., Pridmore, R. D., & Arigoni, F. (2002). The genome sequence of Bifidobacterium longum reflects its adaptation to the human gastrointestinal tract. *Proceedings of the National Academy of Sciences of the United States of America*, *99*(22), 14422–14427. https://doi.org/10.1073/pnas.212527599

Schoeman, D., & Fielding, B. C. (2019). Coronavirus envelope protein: current knowledge. *Virology Journal*, *16*(1), 69. https://doi.org/10.1186/s12985-019-1182-0

Schoggins, J. W., & Rice, C. M. (2011). Interferon-stimulated genes and their antiviral effector functions. *Current Opinion in Virology*, *1*(6), 519–525. https://doi.org/10.1016/j.coviro.2011.10.008

Schwartz, D., Decker, C. J., & Parker, R. (2003). The enhancer of decapping proteins, Edc1p and Edc2p, bind RNA and stimulate the activity of the decapping enzyme. *RNA (New York, N.Y.)*, *9*(2), 239–251. https://doi.org/10.1261/rna.2171203

Schwarz, K. B. (1996). Oxidative stress during viral infection: a review. *Free Radical Biology & Medicine*, *21*(5), 641–649. https://doi.org/10.1016/0891-5849(96)00131-1

Schweichel, J. U., & Merker, H. J. (1973). The morphology of various types of cell death in prenatal tissues. *Teratology*, *7*(3), 253–266. https://doi.org/10.1002/tera.1420070306

Segev, N., & Gerst, J. E. (2017). Specialized ribosomes and specific ribosomal protein paralogs control translation of mitochondrial proteins. *Journal of Cell Biology*, *217*(1), 117–126. https://doi.org/10.1083/jcb.201706059

Sgambato, A., & Brancaccio, A. (2005). The dystroglycan complex: from biology to cancer. *Journal of Cellular Physiology*, *205*(2), 163–169. https://doi.org/10.1002/jcp.20411

Shefchek, K. A., Harris, N. L., Gargano, M., Matentzoglu, N., Unni, D., Brush, M., Keith, D., Conlin, T., Vasilevsky, N., Zhang, X. A., Balhoff, J. P., Babb, L., Bello, S. M., Blau, H., Bradford, Y., Carbon, S., Carmody, L., Chan, L. E., Cipriani, V., … Osumi-Sutherland, D. (2020). The Monarch Initiative in 2019: an integrative data and analytic platform connecting phenotypes to genotypes across species. *Nucleic Acids Research*, *48*(D1), D704–D715. https://doi.org/10.1093/nar/gkz997

Shen, H.-M., & Codogno, P. (2011). Autophagic cell death: Loch Ness monster or endangered species? *Autophagy*, *7*(5), 457–465. https://doi.org/10.4161/auto.7.5.14226

Shen, X., Sun, X., Sun, B., Li, T., Wu, G., Li, Y., Chen, L., Liu, Q., Cui, M., & Zhou, Z. (2018). ARRDC3 suppresses colorectal cancer progression through destabilizing the oncoprotein YAP. *FEBS Letters*, *592*(4), 599–609. https://doi.org/10.1002/1873-3468.12986

Shi, L., & Tu, B. P. (2015). Acetyl-CoA and the regulation of metabolism: mechanisms and consequences. *Current Opinion in Cell Biology*, *33*, 125–131. https://doi.org/10.1016/j.ceb.2015.02.003

Shi, P., & Zhang, J. (2006). Contrasting modes of evolution between vertebrate sweet/umami receptor genes and bitter receptor genes. *Molecular Biology and Evolution*, *23*(2), 292–300. https://doi.org/10.1093/molbev/msj028

Shpilka, T., & Haynes, C. M. (2018). The mitochondrial UPR: mechanisms, physiological functions and implications in ageing. *Nature Reviews. Molecular Cell Biology*, *19*(2), 109–120. https://doi.org/10.1038/nrm.2017.110

Shu, Y., & McCauley, J. (2017). GISAID: Global initiative on sharing all influenza data - from vision to reality. In *Euro surveillance : bulletin Europeen sur les maladies transmissibles = European communicable disease bulletin* (Vol. 22, Issue 13). https://doi.org/10.2807/1560-7917.ES.2017.22.13.30494

Sick, E., Jeanne, A., Schneider, C., Dedieu, S., Takeda, K., & Martiny, L. (2012). CD47 update: a multifaceted actor in the tumour microenvironment of potential therapeutic interest. *British Journal of Pharmacology*, *167*(7), 1415–1430. https://doi.org/10.1111/j.1476-5381.2012.02099.x

Siemann, E. H., & Creasy, L. L. (1992). Concentration of the Phytoalexin Resveratrol in Wine. *American Journal of Enology and Viticulture*, *43*(1), 49 LP – 52. http://www.ajevonline.org/content/43/1/49.abstract

Sin, Z. W., Bhardwaj, V., Pandey, A. K., & Garg, M. (2020). A brief overview of antitumoral actions of bruceine D. *Exploration of Targeted Anti-Tumor Therapy*, *1*(4), 200–217. https://doi.org/10.37349/etat.2020.00013

Singh, K. M., Ahir, V. B., Tripathi, A. K., Ramani, U. V, Sajnani, M., Koringa, P. G., Jakhesara, S., Pandya, P. R., Rank, D. N., Murty, D. S., Kothari, R. K., & Joshi, C. G. (2012). Metagenomic analysis of Surti buffalo (Bubalus bubalis) rumen: a preliminary study. *Molecular Biology Reports*, *39*(4), 4841–4848. https://doi.org/10.1007/s11033-011-1278-0

Sirotkin, A. V. (2021). Effects of resveratrol on female reproduction: A review. *Phytotherapy Research : PTR*, *35*(10), 5502–5513. https://doi.org/10.1002/ptr.7185

Slenter, D. N., Kutmon, M., Hanspers, K., Riutta, A., Windsor, J., Nunes, N., Mélius, J., Cirillo, E., Coort, S. L., Digles, D., Ehrhart, F., Giesbertz, P., Kalafati, M., Martens, M., Miller, R., Nishida, K., Rieswijk, L., Waagmeester, A., Eijssen, L. M. T., … Willighagen, E. L. (2018). WikiPathways: a multifaceted pathway database bridging metabolomics to other omics research. *Nucleic Acids Research*, *46*(D1), D661–D667. https://doi.org/10.1093/nar/gkx1064

Smedley, D., Haider, S., Ballester, B., Holland, R., London, D., Thorisson, G., & Kasprzyk, A. (2009). BioMart--biological queries made easy. *BMC Genomics*, *10*, 22. https://doi.org/10.1186/1471-2164-10-22

Song, X., Zhu, S., Xie, Y., Liu, J., Sun, L., Zeng, D., Wang, P., Ma, X., Kroemer, G., Bartlett, D. L., Billiar, T. R., Lotze, M. T., Zeh, H. J., Kang, R., & Tang, D. (2018). JTC801 Induces pH-dependent Death Specifically in Cancer Cells and Slows Growth of Tumors in Mice. *Gastroenterology*, *154*(5), 1480–1493. https://doi.org/10.1053/j.gastro.2017.12.004

Soung, Y. H., Pruitt, K., & Chung, J. (2014). Epigenetic silencing of ARRDC3 expression in basal-like breast cancer cells. *Scientific Reports*, *4*, 3846. https://doi.org/10.1038/srep03846

Spacková, N., Réblová, K., & Sponer, J. (2010). Structural dynamics of the box C/D RNA kink-turn and its complex with proteins: the role of the A-minor 0 interaction, long-residency water bridges, and structural ion-binding sites revealed by molecular simulations. *The Journal of Physical Chemistry. B*, *114*(32), 10581–10593. https://doi.org/10.1021/jp102572k

Stan, S. D., Zeng, Y., & Singh, S. V. (2008). Ayurvedic medicine constituent withaferin a causes G2 and M phase cell cycle arrest in human breast cancer cells. *Nutrition and Cancer*, *60 Suppl 1*(Suppl 1), 51–60. https://doi.org/10.1080/01635580802381477

Stawowczyk, M., Van Scoy, S., Kumar, K. P., & Reich, N. C. (2011). The interferon stimulated gene 54 promotes apoptosis. *The Journal of Biological Chemistry*, *286*(9), 7257–7266. https://doi.org/10.1074/jbc.M110.207068

Stobiecka, M., Ratajczak, K., & Jakiela, S. (2019). Toward early cancer detection: Focus on biosensing systems and biosensors for an anti-apoptotic protein survivin and survivin mRNA. *Biosensors & Bioelectronics*, *137*, 58–71. https://doi.org/10.1016/j.bios.2019.04.060

Su, S., Wong, G., Shi, W., Liu, J., Lai, A. C. K., Zhou, J., Liu, W., Bi, Y., & Gao, G. F.

(2016). Epidemiology, Genetic Recombination, and Pathogenesis of Coronaviruses. *Trends in Microbiology*, *24*(6), 490–502. https://doi.org/https://doi.org/10.1016/j.tim.2016.03.003

Subramanian, S., Iles, T., Ikramuddin, S., & Steer, C. J. (2020). Merit of an Ursodeoxycholic Acid Clinical Trial in COVID-19 Patients. *Vaccines*, *8*(2). https://doi.org/10.3390/vaccines8020320

Suman, S., Das, T. P., Sirimulla, S., Alatassi, H., Ankem, M. K., & Damodaran, C. (2016). Withaferin-A suppress AKT induced tumor growth in colorectal cancer cells. *Oncotarget*, *7*(12), 13854–13864. https://doi.org/10.18632/oncotarget.7351

Sun, G., Guzman, E., Balasanyan, V., Conner, C. M., Wong, K., Zhou, H. R., Kosik, K. S., & Montell, D. J. (2017). A molecular signature for anastasis, recovery from the brink of apoptotic cell death. *The Journal of Cell Biology*, *216*(10), 3355–3368. https://doi.org/10.1083/jcb.201706134

Sundar, D., Yu, Y., Katiyar, S. P., Putri, J. F., Dhanjal, J. K., Wang, J., Sari, A. N., Kolettas, E., Kaul, S. C., & Wadhwa, R. (2019). Wild type p53 function in p53(Y220C) mutant harboring cells by treatment with Ashwagandha derived anticancer withanolides: bioinformatics and experimental evidence. *Journal of Experimental & Clinical Cancer Research : CR*, *38*(1), 103. https://doi.org/10.1186/s13046-019-1099-x

Suomalainen, A., & Battersby, B. J. (2018). Mitochondrial diseases: the contribution of organelle stress responses to pathology. *Nature Reviews. Molecular Cell Biology*, *19*(2), 77–92. https://doi.org/10.1038/nrm.2017.66

Szarc vel Szic, K., Op de Beeck, K., Ratman, D., Wouters, A., Beck, I. M., Declerck, K., Heyninck, K., Fransen, E., Bracke, M., De Bosscher, K., Lardon, F., Van Camp, G., & Vanden Berghe, W. (2014). Pharmacological levels of Withaferin A (Withania somnifera) trigger clinically relevant anticancer effects specific to triple negative breast cancer cells. *PloS One*, *9*(2), e87850. https://doi.org/10.1371/journal.pone.0087850

Szklarczyk, D., Gable, A. L., Lyon, D., Junge, A., Wyder, S., Huerta-Cepas, J., Simonovic, M., Doncheva, N. T., Morris, J. H., Bork, P., Jensen, L. J., & Mering, C. von. (2019). STRING v11: protein-protein association networks with increased coverage, supporting functional discovery in genome-wide experimental datasets. *Nucleic Acids Research*, *47*(D1), D607–D613. https://doi.org/10.1093/nar/gky1131

Tajan, M., Hock, A. K., Blagih, J., Robertson, N. A., Labuschagne, C. F., Kruiswijk, F., Humpton, T. J., Adams, P. D., & Vousden, K. H. (2018). A Role for p53 in the Adaptation to Glutamine Starvation through the Expression of SLC1A3. *Cell Metabolism*, *28*(5), 721-736.e6. https://doi.org/10.1016/j.cmet.2018.07.005

Talevi, A., Enrique, A. V, & Bruno-Blanch, L. E. (2012). Anticonvulsant activity of artificial sweeteners: a structural link between sweet-taste receptor T1R3 and brain glutamate receptors. *Bioorganic & Medicinal Chemistry Letters*, *22*(12), 4072–4074. https://doi.org/10.1016/j.bmcl.2012.04.076

Tan, B., Huang, Y., Lan, L., Zhang, B., Ye, L., Yan, W., Wang, F., & Lin, N. (2019). Bruceine D induces apoptosis in human non-small cell lung cancer cells through regulating JNK pathway. *Biomedicine & Pharmacotherapy = Biomedecine & Pharmacotherapie*, *117*, 109089. https://doi.org/10.1016/j.biopha.2019.109089

Tan, B. L., Norhaizan, M. E., & Liew, W.-P.-P. (2018). Nutrients and Oxidative Stress: Friend or Foe? *Oxidative Medicine and Cellular Longevity*, *2018*, 9719584. https://doi.org/10.1155/2018/9719584

Tang, Y. T., Hu, T., Arterburn, M., Boyle, B., Bright, J. M., Emtage, P. C., & Funk, W. D. (2005). PAQR proteins: a novel membrane receptor family defined by an ancient 7-transmembrane pass motif. *Journal of Molecular Evolution*, *61*(3), 372–380. https://doi.org/10.1007/s00239-004-0375-2

Tang, Z., Kang, B., Li, C., Chen, T., & Zhang, Z. (2019). GEPIA2: an enhanced web server for large-scale expression profiling and interactive analysis. *Nucleic Acids Research*, *47*(W1), W556–W560. https://doi.org/10.1093/nar/gkz430

Tao, Y., Zhang, M.-L., Ma, P.-C., Sun, J.-F., Zhou, W.-Q., Cao, Y.-P., & Li, L.-J. (2012). Triptolide inhibits proliferation and induces apoptosis of human melanoma A375 cells. *Asian Pacific Journal of Cancer Prevention : APJCP*, *13*(4), 1611–1615. https://doi.org/10.7314/apjcp.2012.13.4.1611

Tapiolas, D. M., Bowden, B. F., Abou-Mansour, E., Willis, R. H., Doyle, J. R., Muirhead, A. N., Liptrot, C., Llewellyn, L. E., Wolff, C. W. W., Wright, A. D., & Motti, C. A. (2009). Eusynstyelamides A, B, and C, nNOS inhibitors, from the ascidian Eusynstyela latericius. *Journal of Natural Products*, *72*(6), 1115–1120. https://doi.org/10.1021/np900099j

Tatehashi, Y., Watanabe, D., & Takagi, H. (2016). γ-Glutamyl kinase is involved in selective autophagy of ribosomes in Saccharomyces cerevisiae. In *FEBS letters* (Vol. 590, Issue 17, pp. 2906–2914). https://doi.org/10.1002/1873-3468.12318

Teague, S. J., Davis, A. M., Leeson, P. D., & Oprea, T. (1999). The Design of Leadlike Combinatorial Libraries. *Angewandte Chemie (International Ed. in English)*, *38*(24), 3743–3748. https://doi.org/10.1002/(SICI)1521-3773(19991216)38:24<3743::AID-ANIE3743>3.0.CO;2-U

Thaiparambil, J. T., Bender, L., Ganesh, T., Kline, E., Patel, P., Liu, Y., Tighiouart, M., Vertino, P. M., Harvey, R. D., Garcia, A., & Marcus, A. I. (2011). Withaferin A inhibits breast cancer invasion and metastasis at sub-cytotoxic doses by inducing vimentin disassembly and serine 56 phosphorylation. *International Journal of Cancer*, *129*(11), 2744–2755. https://doi.org/10.1002/ijc.25938

Thomas, D., Becker, A., & Surdin-Kerjan, Y. (2000). Reverse methionine biosynthesis from S-adenosylmethionine in eukaryotic cells. *The Journal of Biological Chemistry*, *275*(52), 40718–40724. https://doi.org/10.1074/jbc.M005967200

Torre, D., Lachmann, A., & Ma'ayan, A. (2018). BioJupies: Automated Generation of Interactive Notebooks for RNA-Seq Data Analysis in the Cloud. *Cell Systems*, *7*(5), 556-561.e3. https://doi.org/10.1016/j.cels.2018.10.007

Tran, V., Ledwith, M. P., Thamamongood, T., Higgins, C. A., Tripathi, S., Chang, M. W., Benner, C., García-Sastre, A., Schwemmle, M., Boon, A. C. M., Diamond, M. S., & Mehle, A. (2020). Influenza virus repurposes the antiviral protein IFIT2 to promote translation of viral mRNAs. *Nature Microbiology*, *5*(12), 1490–1503. https://doi.org/10.1038/s41564-020-0778-x

Triana, S., Metz-Zumaran, C., Ramirez, C., Kee, C., Doldan, P., Shahraz, M., Schraivogel, D., Gschwind, A. R., Sharma, A. K., Steinmetz, L. M., Herrmann, C., Alexandrov, T., Boulant, S., & Stanifer, M. L. (2021). Single-cell analyses reveal SARS-CoV-2 interference with intrinsic immune response in the human gut. *Molecular Systems Biology*, *17*(4), e10232. https://doi.org/10.15252/msb.202110232

Tripathi, S. K., Feng, Q., Liu, L., Levin, D. E., Roy, K. K., Doerksen, R. J., Baerson, S. R., Shi, X., Pan, X., Xu, W.-H., Li, X.-C., Clark, A. M., & Agarwal, A. K. (2020). Puupehenone, a Marine-Sponge-Derived Sesquiterpene Quinone, Potentiates the Antifungal Drug Caspofungin by Disrupting Hsp90 Activity and the Cell Wall Integrity Pathway. *MSphere*, *5*(1). https://doi.org/10.1128/mSphere.00818-19

Utama, B., Kennedy, D., Ru, K., & Mattick, J. S. (2002). Isolation and characterization of a new nucleolar protein, Nrap, that is conserved from yeast to humans. *Genes to Cells : Devoted to Molecular & Cellular Mechanisms*, *7*(2), 115–132. https://doi.org/10.1046/j.1356-9597.2001.00507.x

Veber, D. F., Johnson, S. R., Cheng, H.-Y., Smith, B. R., Ward, K. W., & Kopple, K. D.

(2002). Molecular properties that influence the oral bioavailability of drug candidates. *Journal of Medicinal Chemistry*, *45*(12), 2615–2623. https://doi.org/10.1021/jm020017n

Vidoni, C., Fuzimoto, A., Ferraresi, A., & Isidoro, C. (2021). Targeting autophagy with natural products to prevent SARS-CoV-2 infection. *Journal of Traditional and Complementary Medicine*. https://doi.org/10.1016/j.jtcme.2021.10.003

Vilela-Moura, A., Schuller, D., Mendes-Faia, A., Silva, R. D., Chaves, S. R., Sousa, M. J., & Côrte-Real, M. (2011). The impact of acetate metabolism on yeast fermentative performance and wine quality: reduction of volatile acidity of grape musts and wines. *Applied Microbiology and Biotechnology*, *89*(2), 271–280. https://doi.org/10.1007/s00253-010-2898-3

Wahedi, H. M., Ahmad, S., & Abbasi, S. W. (2021). Stilbene-based natural compounds as promising drug candidates against COVID-19. *Journal of Biomolecular Structure & Dynamics*, *39*(9), 3225–3234. https://doi.org/10.1080/07391102.2020.1762743

Wang, J., Gu, Q., Li, M., Zhang, W., Yang, M., Zou, B., Chan, S., Qiao, L., Jiang, B., Tu, S., Ma, J., Hung, I. F., Lan, H. Y., & Wong, B. C. Y. (2009). Identification of XAF1 as a novel cell cycle regulator through modulating G(2)/M checkpoint and interaction with checkpoint kinase 1 in gastrointestinal cancer. *Carcinogenesis*, *30*(9), 1507–1516. https://doi.org/10.1093/carcin/bgp155

Wang, Q., Xu, J., Rottinghaus, G. E., Simonyi, A., Lubahn, D., Sun, G. Y., & Sun, A. Y. (2002). Resveratrol protects against global cerebral ischemic injury in gerbils. *Brain Research*, *958*(2), 439–447. https://doi.org/10.1016/s0006-8993(02)03543-6

Wang, S., Hu, H., Zhong, B., Shi, D., Qing, X., Cheng, C., Deng, X., Zhang, Z., & Shao, Z. (2019). Bruceine D inhibits tumor growth and stem cell-like traits of osteosarcoma through inhibition of STAT3 signaling pathway. *Cancer Medicine*, *8*(17), 7345–7358. https://doi.org/10.1002/cam4.2612

Wang, Z., Wilson, W. A., Fujino, M. A., & Roach, P. J. (2001). Antagonistic controls of autophagy and glycogen accumulation by Snf1p, the yeast homolog of AMP-activated protein kinase, and the cyclin-dependent kinase Pho85p. *Molecular and Cellular Biology*, *21*(17), 5742–5752. https://doi.org/10.1128/mcb.21.17.5742-5752.2001

Weng, J.-R., Tsai, C.-H., Kulp, S. K., & Chen, C.-S. (2008). Indole-3-carbinol as a chemopreventive and anti-cancer agent. *Cancer Letters*, *262*(2), 153–163. https://doi.org/10.1016/j.canlet.2008.01.033

Wesselborg, S., & Stork, B. (2015). Autophagy signal transduction by ATG proteins: from hierarchies to networks. *Cellular and Molecular Life Sciences : CMLS*, *72*(24), 4721–4757. https://doi.org/10.1007/s00018-015-2034-8

Widodo, N., Priyandoko, D., Shah, N., Wadhwa, R., & Kaul, S. C. (2010). Selective killing of cancer cells by Ashwagandha leaf extract and its component Withanone involves ROS signaling. *PloS One*, *5*(10), e13536. https://doi.org/10.1371/journal.pone.0013536

Wishart, D. S., Feunang, Y. D., Marcu, A., Guo, A. C., Liang, K., Vázquez-Fresno, R., Sajed, T., Johnson, D., Li, C., Karu, N., Sayeeda, Z., Lo, E., Assempour, N., Berjanskii, M., Singhal, S., Arndt, D., Liang, Y., Badran, H., Grant, J., … Scalbert, A. (2018). HMDB 4.0: the human metabolome database for 2018. *Nucleic Acids Research*, *46*(D1), D608–D617. https://doi.org/10.1093/nar/gkx1089

Wolf, A. S., & Grayhack, E. J. (2015). Asc1, homolog of human RACK1, prevents frameshifting in yeast by ribosomes stalled at CGA codon repeats. *RNA* , *21*(5), 935–945. https://doi.org/10.1261/rna.049080.114

Wolfe, K. (2000). Robustness—it's not where you think it is. *Nature Genetics*, *25*(1), 3–4. https://doi.org/10.1038/75560

Xiang, Y., Yao, X., Chen, K., Wang, X., Zhou, J., Gong, W., Yoshimura, T., Huang, J., Wang, R., Wu, Y., Shi, G., Bian, X., & Wang, J. (2016). The G-protein coupled

chemoattractant receptor FPR2 promotes malignant phenotype of human colon cancer cells. *American Journal of Cancer Research*, *6*(11), 2599–2610.

Xiao, J., Shi, Q., Li, W., Mu, X., Peng, J., Li, M., Chen, M., Huang, H., Wang, C., Gao, K., & Fan, J. (2018). ARRDC1 and ARRDC3 act as tumor suppressors in renal cell carcinoma by facilitating YAP1 degradation. *American Journal of Cancer Research*, *8*(1), 132–143.

Yadav, R., Choudhury, C., Kumar, Y., & Bhatia, A. (2020). Virtual repurposing of ursodeoxycholate and chenodeoxycholate as lead candidates against SARS-Cov2-Envelope protein: A molecular dynamics investigation. *Journal of Biomolecular Structure & Dynamics*, 1–12. https://doi.org/10.1080/07391102.2020.1868339

Yan, Y.; Shen, X.; Cao, Y.; Zhang, J.; Wang, Y.; Cheng, Y. (2020). Discovery of Anti-2019-nCoV Agents from 38 Chinese Patent Drugs toward Respiratory Diseases via Docking Screening. *Preprints*, *2020020254 (doi: 10.20944/preprints202002.0254.v2)*.

Yang, J., Yan, Y., & Zhong, W. (2021). Application of omics technology to combat the COVID-19 pandemic. *MedComm*, *2*(3), 381–401. https://doi.org/10.1002/mco2.90

Yang, M., Wei, J., Huang, T., Lei, L., Shen, C., Lai, J., Yang, M., Liu, L., Yang, Y., Liu, G., & Liu, Y. (2021). Resveratrol inhibits the replication of severe acute respiratory syndrome coronavirus 2 (SARS-CoV-2) in cultured Vero cells. In *Phytotherapy research : PTR* (Vol. 35, Issue 3, pp. 1127–1129). https://doi.org/10.1002/ptr.6916

Yang, W. S., & Stockwell, B. R. (2016). Ferroptosis: Death by Lipid Peroxidation. *Trends in Cell Biology*, *26*(3), 165–176. https://doi.org/10.1016/j.tcb.2015.10.014

Yang, Z., & Klionsky, D. J. (2010). Mammalian autophagy: core molecular machinery and signaling regulation. *Current Opinion in Cell Biology*, *22*(2), 124–131. https://doi.org/10.1016/j.ceb.2009.11.014

Ye, R. D., Boulay, F., Wang, J. M., Dahlgren, C., Gerard, C., Parmentier, M., Serhan, C. N., & Murphy, P. M. (2009). International Union of Basic and Clinical Pharmacology. LXXIII. Nomenclature for the formyl peptide receptor (FPR) family. *Pharmacological Reviews*, *61*(2), 119–161. https://doi.org/10.1124/pr.109.001578

Yoshida, A., Kobayashi, K., Manya, H., Taniguchi, K., Kano, H., Mizuno, M., Inazu, T., Mitsuhashi, H., Takahashi, S., Takeuchi, M., Herrmann, R., Straub, V., Talim, B., Voit, T., Topaloglu, H., Toda, T., & Endo, T. (2001). Muscular dystrophy and neuronal migration disorder caused by mutations in a glycosyltransferase, POMGnT1. *Developmental Cell*, *1*(5), 717–724. https://doi.org/10.1016/s1534-5807(01)00070-3

Young, M. M., Takahashi, Y., Khan, O., Park, S., Hori, T., Yun, J., Sharma, A. K., Amin, S., Hu, C.-D., Zhang, J., Kester, M., & Wang, H.-G. (2012). Autophagosomal membrane serves as platform for intracellular death-inducing signaling complex (iDISC)-mediated caspase-8 activation and apoptosis. *The Journal of Biological Chemistry*, *287*(15), 12455–12468. https://doi.org/10.1074/jbc.M111.309104

Yu, Y., Katiyar, S. P., Sundar, D., Kaul, Z., Miyako, E., Zhang, Z., Kaul, S. C., Reddel, R. R., & Wadhwa, R. (2017). Withaferin-A kills cancer cells with and without telomerase: chemical, computational and experimental evidences. *Cell Death & Disease*, *8*(4), e2755. https://doi.org/10.1038/cddis.2017.33

Zhang, J.-Y., Lin, M.-T., Tung, H.-Y., Tang, S.-L., Yi, T., Zhang, Y.-Z., Tang, Y.-N., Zhao, Z.-Z., & Chen, H.-B. (2016). Bruceine D induces apoptosis in human chronic myeloid leukemia K562 cells via mitochondrial pathway. *American Journal of Cancer Research*, *6*(4), 819–826.

Zhang, Jianzhi. (2003). Evolution by gene duplication: an update. *Trends in Ecology & Evolution*, *18*(6), 292–298. https://doi.org/https://doi.org/10.1016/S0169-5347(03)00033-8

Zhang, Joann, Hsu B A, J. C., Kinseth B A, M. A., Bjeldanes, L. F., & Firestone, G. L.

(2003). Indole-3-carbinol induces a G1 cell cycle arrest and inhibits prostate-specific antigen production in human LNCaP prostate carcinoma cells. *Cancer*, *98*(11), 2511–2520. https://doi.org/10.1002/cncr.11844

Zhang, L., Lin, D., Sun, X., Curth, U., Drosten, C., Sauerhering, L., Becker, S., Rox, K., & Hilgenfeld, R. (2020). Crystal structure of SARS-CoV-2 main protease provides a basis for design of improved α-ketoamide inhibitors. *Science*. https://doi.org/10.1126/science.abb3405

Zhang, Y., Wang, D., Peng, M., Tang, L., Ouyang, J., Xiong, F., Guo, C., Tang, Y., Zhou, Y., Liao, Q., Wu, X., Wang, H., Yu, J., Li, Y., Li, X., Li, G., Zeng, Z., Tan, Y., & Xiong, W. (2021). Single-cell RNA sequencing in cancer research. *Journal of Experimental & Clinical Cancer Research : CR*, *40*(1), 81. https://doi.org/10.1186/s13046-021-01874-1

Zheng, Y., Lin, Z.-Y., Xie, J.-J., Jiang, F.-N., Chen, C.-J., Li, J.-X., Zhou, X., & Zhong, W.-D. (2017). ARRDC3 Inhibits the Progression of Human Prostate Cancer Through ARRDC3-ITGβ4 Pathway. *Current Molecular Medicine*, *17*(3), 221–229. https://doi.org/10.2174/1566524017666170807144711

Zhou, S., Xie, Y., Puscheck, E. E., & Rappolee, D. A. (2011). Oxygen levels that optimize TSC culture are identified by maximizing growth rates and minimizing stress. *Placenta*, *32*(6), 475–481. https://doi.org/10.1016/j.placenta.2011.03.013

Zhou, Z., Ren, L., Zhang, L., Zhong, J., Xiao, Y., Jia, Z., Guo, L., Yang, J., Wang, C., Jiang, S., Yang, D., Zhang, G., Li, H., Chen, F., Xu, Y., Chen, M., Gao, Z., Yang, J., Dong, J., … Wang, J. (2020). Heightened Innate Immune Responses in the Respiratory Tract of COVID-19 Patients. *Cell Host & Microbe*, *27*(6), 883-890.e2. https://doi.org/10.1016/j.chom.2020.04.017

Zhu, L., Yang, P., Zhao, Y., Zhuang, Z., Wang, Z., Song, R., Zhang, J., Liu, C., Gao, Q., Xu, Q., Wei, X., Sun, H.-X., Ye, B., Wu, Y., Zhang, N., Lei, G., Yu, L., Yan, J., Diao, G., … Liu, W. J. (2020). Single-Cell Sequencing of Peripheral Mononuclear Cells Reveals Distinct Immune Response Landscapes of COVID-19 and Influenza Patients. *Immunity*, *53*(3), 685-696.e3. https://doi.org/10.1016/j.immuni.2020.07.009

Zoete, V., Daina, A., Bovigny, C., & Michielin, O. (2016). SwissSimilarity: A Web Tool for Low to Ultra High Throughput Ligand-Based Virtual Screening. *Journal of Chemical Information and Modeling*, *56*(8), 1399–1404. https://doi.org/10.1021/acs.jcim.6b00174

Zou, M., Yang, W., Niu, L., Sun, Y., Luo, R., Wang, Y., & Peng, X. (2020). Polydatin attenuates Mycoplasma gallisepticum (HS strain)-induced inflammation injury via inhibiting the TLR6/ MyD88/NF-κB pathway. *Microbial Pathogenesis*, *149*, 104552. https://doi.org/10.1016/j.micpath.2020.104552

Zou, P., Yang, Y., Xu, X., Liu, B., Mei, F., You, J., Liu, Q., & Pei, F. (2018). Silencing of vacuolar ATPase c subunit ATP6V0C inhibits the invasion of prostate cancer cells through a LASS2/TMSG1-independent manner. *Oncology Reports*, *39*(1), 298–306. https://doi.org/10.3892/or.2017.6092

Zumla, A., Chan, J. F. W., Azhar, E. I., Hui, D. S. C., & Yuen, K.-Y. (2016). Coronaviruses - drug discovery and therapeutic options. *Nature Reviews. Drug Discovery*, *15*(5), 327–347. https://doi.org/10.1038/nrd.2015.37

Supplementary Tables

Supplementary Table S1: List of differentially expressed genes (DEGs) of yeast cells treated with acetic acid.
Gene ID, Gene name, the log2 fold change (log2FC) of significant DEGs at each time points after acetic acid treatments (45, 120 and 200 min) are reported.

Gene ID	Gene name	log2FC		
		45 min	120 min	200 min
ETS1-1		3,006	1,992	-
ETS1-2		3,182	2,095	-
ITS1-1		1,702	-	-
ITS1-2		1,637	-	-
ITS2-1		1,326	-	-
ITS2-2		1,460	-	-
LSR1		-	-	-1,826
Q0045	COX1	-	-	-1,364
Q0060	AI3	-	-	-1,226
Q0065	AI4	-	-	-1,261
Q0070	AI5_ALPHA	-	-	-1,280
Q0075	AI5_BETA	-	-	-1,083
Q0130	OLI1	-	-	-2,211
RDN18-1		1,093	-	-
RDN18-2		1,085	-	-
RDN58-1		1,056	-	-
RDN58-2		1,056	-	-
RNA170		-	-1,852	-1,128
RPR1		-	-2,203	-1,980
SCR1		-	-2,091	-1,922
snR10		-	-2,982	-
snR11		-	-1,642	-1,277
snR128		-	-1,977	-
snR13		1,049	-	-
snR161		-1,102	-	-
snR17b		1,180	-	-

Gene ID	Gene name	log2FC		
		45 min	120 min	200 min
snR19		-	-	-1,142
snR191		-	-1,813	-
snR24		-1,106	-	-
snR30		-	-1,769	-
snR31		-	-1,745	-1,384
snR34		-	-2,254	-
snR36		-	-1,587	-
snR37		1,351	-	-
snR39		-	-	-1,528
snR42		-	-1,339	-
snR44		-	-1,438	-1,684
snR45		1,345	-2,395	-
snR5		1,580	-	1,094
snR54		-	-	-1,233
snR64		-1,048	-1,936	-
snR67		1,725	-	-
snR70		-	-2,586	-1,171
snR8		-	-1,435	-
snR81		-	-2,628	-
snR82		1,612	-	1,559
snR86		1,151	-	-
snR87		-	-1,464	-
snR9		-	-1,780	-1,395
tD(GUC)I1		-	-1,623	-1,967
tD(GUC)N		-	-	1,111
tD(GUC)O		-	-1,669	-1,992
tF(GAA)H1		-	-	-1,078
tM(CAU)M		-	-1,444	-
tN(GUU)C		-	-	-1,048
tP(UGG)O1		-2,225	-2,879	-1,977

Gene ID	Gene name	log2FC		
		45 min	120 min	200 min
tY(GUA)D		-1,199	-1,837	-
YAL004W		-	-	1,080
YAL005C	SSA1	-	-	1,067
YAL010C	MDM10	1,049	-	1,066
YAL012W	CYS3	-1,828	-	-
YAL016C-B		-	1,089	-
YAL018C	LDS1	2,003	1,704	1,433
YAL022C	FUN26	-1,441	-1,844	-1,923
YAL023C	PMT2	-	-	-1,163
YAL025C	MAK16	1,196	-	-
YAL034C	FUN19	-	-	1,290
YAL034W-A	MTW1	-1,101	-	-
YAL035W	FUN12	1,208	-	-
YAL037C-A		-	-1,848	-1,629
YAL037C-B		-	-	-1,160
YAL038W	CDC19	-	-1,032	-1,228
YAL040C	CLN3	-	-	-1,018
YAL053W	FLC2	-1,063	-	-
YAL059C-A		1,720	-	-
YAL059W	ECM1	1,694	-	-
YAL060W	BDH1	-1,116	-	-
YAL062W	GDH3	-2,191	-1,253	-
YAL065C		-	1,422	1,227
YAL067C	SEO1	-8,032	-3,689	-3,602
YAR002W	NUP60	1,201	-	-
YAR003W	SWD1	-1,479	-	-
YAR007C	RFA1	-	1,370	1,234
YAR023C		-	-	1,206
YAR035W	YAT1	-1,960	-1,034	-1,723

Gene ID	Gene name	log2FC		
		45 min	120 min	200 min
YAR042W	SWH1	1,024	1,054	-
YBL002W	HTB2	1,174	-	-
YBL003C	HTA2	-	1,165	-
YBL004W	UTP20	-	-	-1,055
YBL007C	SLA1	-1,183	-	-
YBL010C		-	1,048	1,032
YBL013W	FMT1	-1,168	-	-
YBL015W	ACH1	-	-	-1,123
YBL020W	RFT1	-	-	-1,019
YBL022C	PIM1	-	1,197	1,022
YBL027W	RPL19B	-	-1,279	-1,734
YBL039C	URA7	1,034	-	-
YBL043W	ECM13	-1,538	-1,514	-1,367
YBL046W	PSY4	-	-	1,106
YBL049W	MOH1	-1,383	-	-
YBL054W	TOD6	1,066	-	-
YBL058W	SHP1	-	-	1,259
YBL059C-A	CMC2	1,139	-	-
YBL064C	PRX1	-	1,098	1,298
YBL071C-B		-	-1,276	-
YBL075C	SSA3	1,729	2,208	2,413
YBL078C	ATG8	-	1,588	1,589
YBL084C	CDC27	1,284	1,338	1,243
YBL086C		1,378	1,106	1,594
YBL090W	MRP21	1,011	-	-
YBL092W	RPL32	-	-1,107	-1,695
YBL098W	BNA4	-2,211	-2,048	-1,968
YBL099W	ATP1	-	-	-1,378
YBL100C		-	-	-1,337

Gene ID	Gene name	log2FC		
		45 min	120 min	200 min
YBL113C		-1,718	-1,185	-
YBL113W-A		-1,718	-1,188	-
YBR002C	RER2	-	-1,167	-1,365
YBR005W	RCR1	1,507	1,575	2,393
YBR010W	HHT1	1,126	-	-
YBR018C	GAL7	2,592	-	-
YBR025C	OLA1	1,662	-	-
YBR029C	CDS1	-	-	-1,443
YBR033W	EDS1	-1,195	-1,088	-
YBR043C	QDR3	-1,736	-2,368	-1,377
YBR046C	ZTA1	-1,061	-	-
YBR048W	RPS11B	-	-	-1,165
YBR050C	REG2	-1,173	-	-
YBR051W		-1,998	-1,384	-
YBR054W	YRO2	1,984	-	-1,167
YBR061C	TRM7	1,126	-	-
YBR062C		1,109	1,309	1,686
YBR063C		1,063	1,010	1,020
YBR064W		1,155	1,218	1,302
YBR065C	ECM2	-	1,072	1,081
YBR066C	NRG2	1,030	-	-
YBR067C	TIP1	2,891	2,684	3,468
YBR069C	TAT1	-	-1,232	-1,607
YBR071W		1,386	1,621	1,451
YBR072W	HSP26	1,472	-	-
YBR073W	RDH54	-	1,463	1,429
YBR083W	TEC1	1,039	-	-
YBR084C-A	RPL19A	-	-1,094	-1,349
YBR085W	AAC3	1,836	1,880	2,429

Gene ID	Gene name	log2FC		
		45 min	120 min	200 min
YBR088C	POL30	-	1,496	1,236
YBR089W		-	1,506	1,267
YBR092C	PHO3	2,025	-	-
YBR097W	VPS15	-	1,048	-
YBR101C	FES1	2,106	1,258	1,839
YBR107C	IML3	-1,726	-1,529	-1,140
YBR115C	LYS2	-	-2,321	-1,564
YBR116C		-1,644	-	-1,091
YBR117C	TKL2	-2,529	-1,159	-1,494
YBR119W	MUD1	-1,231	-1,229	-1,402
YBR121C	GRS1	-	-	-1,028
YBR126W-A	MEO1	-1,402	-1,857	-1,761
YBR126W-B		-1,402	-1,860	-1,769
YBR133C	HSL7	-1,860	-1,795	-1,947
YBR134W		-	-1,103	-1,551
YBR137W		-	1,185	1,079
YBR141C	BMT2	1,353	-	-
YBR142W	MAK5	1,007	-	-
YBR145W	ADH5	-	-1,701	-
YBR147W	RTC2	-1,601	-2,403	-1,025
YBR148W	YSW1	-1,737	-1,913	-1,060
YBR158W	AMN1	1,272	-	-
YBR161W	CSH1	-1,465	-1,249	-1,025
YBR162C	TOS1	-	-	-1,100
YBR163W	EXO5	-1,253	-1,229	-
YBR173C	UMP1	1,136	1,201	1,471
YBR174C		-1,327	-1,169	-
YBR175W	SWD3	-	-1,029	-
YBR181C	RPS6B	-	-1,044	-1,613

Gene ID	Gene name	log2FC		
		45 min	120 min	200 min
YBR182C	SMP1	-1,860	-1,041	-1,219
YBR187W	GDT1	-1,502	-1,322	-1,514
YBR189W	RPS9B	-	-1,134	-1,857
YBR190W		-	-1,260	-1,806
YBR191W	RPL21A	-	-1,224	-1,831
YBR191W-A		-	-	-1,640
YBR196C-A		-	-	-1,176
YBR196C-B		-	-1,431	-
YBR197C		-1,166	-1,364	-1,072
YBR201C-A		1,178	1,825	1,452
YBR208C	DUR1,2	-1,536	-	-
YBR213W	MET8	-2,794	-	-
YBR214W	SDS24	-	-	1,524
YBR219C		-1,047	-1,126	-1,325
YBR220C		-1,108	-1,305	-1,539
YBR235W	VHC1	-1,745	-	-
YBR236C	ABD1	1,016	-	-
YBR241C		-1,093	-	-
YBR249C	ARO4	-	-2,131	-1,805
YBR250W	SPO23	-	-1,070	-
YBR251W	MRPS5	1,308	-	-
YBR256C	RIB5	-	-1,350	-
YBR280C	SAF1	-	-	1,338
YBR281C	DUG2	-1,424	-	-
YBR285W		-	1,270	1,576
YBR291C	CTP1	-1,451	-2,733	-2,580
YBR293W	VBA2	-1,184	-	-
YBR294W	SUL1	-5,412	-2,664	-2,758
YBR295W	PCA1	-1,413	-1,084	-1,089

Gene ID	Gene name	log2FC		
		45 min	120 min	200 min
YBR296C	PHO89	-1,058	-	-
YBR297W	MAL33	-1,205	-	-
YBR301W	PAU24	1,448	-	-
YBR302C	COS2	-	-	-1,017
YCL001W	RER1	-1,395	-1,184	-1,238
YCL009C	ILV6	-	-1,497	-
YCL010C	SGF29	-1,782	-1,468	-1,106
YCL011C	GBP2	-1,201	-1,159	-1,158
YCL014W	BUD3	-	-	-1,013
YCL018W	LEU2	1,781	1,605	1,772
YCL023C		-1,363	-	-
YCL024W	KCC4	-1,077	-	-
YCL025C	AGP1	-3,557	-3,057	-2,715
YCL026C-B	HBN1	-2,853	-1,311	-1,340
YCL027W	FUS1	-	1,577	2,107
YCL030C	HIS4	-2,246	-2,457	-1,191
YCL036W	GFD2	1,040	-	-
YCL038C	ATG22	-	-1,173	-
YCL040W	GLK1	-1,665	-1,717	-1,077
YCL042W		-1,404	-1,650	-
YCL044C	MGR1	1,018	-	1,469
YCL048W-A		-1,782	-	-
YCL049C		-1,386	-	-
YCL050C	APA1	1,617	1,077	1,044
YCL055W	KAR4	1,411	1,529	1,502
YCL059C	KRR1	1,261	-	-
YCL061C	MRC1	-	1,045	-
YCL064C	CHA1	3,200	3,231	4,010
YCR001W		-1,380	-	-

Gene ID	Gene name	log2FC		
		45 min	120 min	200 min
YCR016W		1,135	-	-
YCR021C	HSP30	3,275	3,268	2,755
YCR025C		-1,845	-	-
YCR031C	RPS14A	-	-	-1,016
YCR034W	ELO2	-	-	-1,298
YCR043C		-	-	-1,180
YCR045C	RRT12	-1,315	-	-
YCR045W-A		-1,366	-	-
YCR061W		-1,929	-1,459	-1,057
YCR063W	BUD31	-	-	-1,013
YCR065W	HCM1	-1,212	-	-
YCR068W	ATG15	-1,014	-	-
YCR071C	IMG2	1,164	-	-
YCR073C	SSK22	-	1,135	1,502
YCR075C	ERS1	-1,127	-	-
YCR081C-A		1,046	1,435	1,247
YCR082W	AHC2	1,098	1,424	1,362
YCR087C-A		1,465	-	-
YCR087W		1,443	-	-
YCR091W	KIN82	-	-	1,162
YCR098C	GIT1	-2,626	-1,288	-1,835
YCR099C		1,283	1,555	2,083
YCR100C		1,386	1,742	2,022
YCR101C		1,659	1,886	2,245
YCR102C		1,793	2,238	2,769
YCR104W	PAU3	1,849	-	-
YCR105W	ADH7	-	-	1,421
YDL001W	RMD1	-	-1,100	-
YDL003W	MCD1	-	1,636	1,372

Gene ID	Gene name	log2FC		
		45 min	120 min	200 min
YDL007W	RPT2	-	-	1,109
YDL008W	APC11	-	1,090	-
YDL009C		-1,025	-	-
YDL014W	NOP1	-	-	-1,046
YDL018C	ERP3	-1,225	-	-
YDL020C	RPN4	-	-	1,011
YDL022W	GPD1	-	-1,234	-
YDL023C		-	-1,260	-
YDL037C	BSC1	1,227	-	-
YDL039C	PRM7	1,070	-	-
YDL045C	FAD1	-	1,220	1,166
YDL048C	STP4	-	1,017	1,236
YDL052C	SLC1	-1,095	-1,113	-
YDL053C	PBP4	-	-1,006	-
YDL055C	PSA1	-1,270	-	-1,385
YDL059C	RAD59	-3,382	-	-1,198
YDL061C	RPS29B	-	-	-1,391
YDL062W		1,611	-	-
YDL063C	SYO1	1,371	-	-
YDL066W	IDP1	-	-1,814	-1,049
YDL075W	RPL31A	-	-	-1,449
YDL082W	RPL13A	-	-1,010	-1,276
YDL083C	RPS16B	-	-1,567	-1,959
YDL085W	NDE2	-2,384	-1,751	-
YDL089W	NUR1	-	1,167	1,331
YDL090C	RAM1	1,435	1,249	1,566
YDL091C	UBX3	-	1,337	1,354
YDL096C	OPI6	-	-1,024	-1,191
YDL097C	RPN6	-	1,248	1,513

Gene ID	Gene name	log2FC		
		45 min	120 min	200 min
YDL099W	BUG1	1,121	1,242	1,398
YDL106C	PHO2	-	-	1,164
YDL112W	TRM3	1,140	-	-
YDL114W-A		-	-	1,375
YDL115C	IWR1	-	-	1,215
YDL118W		1,112	-	-
YDL119C	HEM25	1,035	-	-
YDL121C		1,367	-	-
YDL124W		-1,426	-	-
YDL128W	VCX1	-	-1,143	-
YDL131W	LYS21	-1,291	-3,055	-2,367
YDL132W	CDC53	-	1,072	1,172
YDL133C-A	RPL41B	1,186	-	-1,208
YDL136W	RPL35B	-	-	-1,156
YDL146W	LDB17	-1,188	-	-1,022
YDL147W	RPN5	-	1,339	1,373
YDL148C	NOP14	1,468	-	-
YDL152W		1,136	-	-
YDL153C	SAS10	1,250	-	-
YDL154W	MSH5	-	-	1,156
YDL157C		1,363	1,193	-
YDL163W		-1,061	-	-
YDL171C	GLT1	-2,422	-1,779	-1,820
YDL179W	PCL9	1,112	-	-
YDL180W		-2,124	-1,322	-1,178
YDL181W	INH1	-	-	-1,454
YDL182W	LYS20	-	-3,263	-2,296
YDL184C	RPL41A	1,149	-	-
YDL185C-A		-1,192	-1,235	-1,225

Gene ID	Gene name	log2FC		
		45 min	120 min	200 min
YDL185W	VMA1	-1,170	-1,107	-1,211
YDL188C	PPH22	-	-1,072	-1,017
YDL196W		-1,341	-	-
YDL197C	ASF2	-1,052	-	-
YDL198C	GGC1	-1,253	-1,486	-
YDL199C		-1,250	-	-
YDL210W	UGA4	-1,628	-1,414	-
YDL211C		-1,181	-	-1,010
YDL215C	GDH2	-1,263	-1,056	-
YDL220C	CDC13	-1,759	-1,348	-1,211
YDL221W		-1,903	-1,616	-1,452
YDL222C	FMP45	-2,648	-1,919	-1,685
YDL223C	HBT1	-3,210	-1,331	-1,279
YDL227C	HO	-	-	1,348
YDL229W	SSB1	-	-	-1,010
YDL232W	OST4	1,418	1,201	1,043
YDL234C	GYP7	-	-	1,081
YDL238C	GUD1	-1,685	-	-
YDL239C	ADY3	-2,445	-1,139	-
YDL241W		3,822	3,208	3,736
YDL243C	AAD4	-	-	1,233
YDL244W	THI13	-	1,523	1,415
YDR004W	RAD57	-1,314	-	-
YDR010C		-1,422	-	-
YDR012W	RPL4B	-1,257	-1,712	-1,829
YDR018C		-1,337	-1,474	-
YDR019C	GCV1	-1,873	-	-
YDR020C	DAS2	-	-1,018	-
YDR021W	FAL1	1,842	1,119	-

Gene ID	Gene name	log2FC		
		45 min	120 min	200 min
YDR024W	FYV1	-	-1,379	-1,531
YDR025W	RPS11A	-	-1,114	-1,615
YDR033W	MRH1	-	-2,052	-2,521
YDR034C	LYS14	-	-1,375	-1,226
YDR034W-B		-1,041	-	-
YDR036C	EHD3	-	1,008	1,090
YDR039C	ENA2	-	-	-1,027
YDR040C	ENA1	-1,199	-	-
YDR044W	HEM13	1,657	1,965	1,945
YDR046C	BAP3	-	-1,298	-1,482
YDR060W	MAK21	1,093	-	-
YDR064W	RPS13	-	-1,231	-1,768
YDR065W	RRG1	-1,001	-	-
YDR071C	PAA1	1,172	1,017	-
YDR072C	IPT1	-1,704	-1,882	-1,865
YDR077W	SED1	-	-1,599	-1,360
YDR083W	RRP8	1,122	-	-
YDR087C	RRP1	1,311	-	-
YDR089W	VTC5	-1,703	-	-
YDR101C	ARX1	1,640	-	-
YDR110W	FOB1	-	-	-1,027
YDR111C	ALT2	-2,488	-1,576	-1,592
YDR112W	IRC2	-1,665	-1,532	-1,878
YDR119W-A	COX26	-	-	1,235
YDR127W	ARO1	-1,340	-1,885	-1,497
YDR133C		-	1,123	1,896
YDR135C	YCF1	-1,211	-	-
YDR146C	SWI5	-	-1,326	-1,670
YDR152W	GIR2	1,379	-	-

Gene ID	Gene name	log2FC		
		45 min	120 min	200 min
YDR154C		1,132	1,019	1,099
YDR155C	CPR1	1,190	-	1,113
YDR158W	HOM2	-	-1,045	-
YDR161W	ACL4	1,329	-	-
YDR165W	TRM82	1,047	-	-
YDR168W	CDC37	-	1,121	-
YDR171W	HSP42	1,817	1,328	2,040
YDR185C	UPS3	-1,459	-1,487	-1,269
YDR202C	RAV2	-	-	1,087
YDR209C		1,759	1,488	1,435
YDR210C-C		-	1,044	1,092
YDR210C-D		-	1,229	1,065
YDR210W		1,781	1,492	1,467
YDR224C	HTB1	1,674	1,626	1,070
YDR234W	LYS4	-	-1,975	-1,647
YDR237W	MRPL7	1,125	-	-
YDR246W	TRS23	-	-	1,135
YDR253C	MET32	-3,248	-1,458	-1,367
YDR254W	CHL4	-1,325	-	-
YDR258C	HSP78	2,195	1,126	1,986
YDR261C	EXG2	-1,078	-	-
YDR261C-D		-	1,232	1,045
YDR261W-A		-	1,016	-
YDR263C	DIN7	-1,163	-	-
YDR265W	PEX10	-	1,157	1,326
YDR269C		1,182	1,231	1,565
YDR271C		1,030	1,403	1,518
YDR285W	ZIP1	-	-	1,087
YDR289C	RTT103	1,257	1,266	1,219

Gene ID	Gene name	log2FC		
		45 min	120 min	200 min
YDR290W		1,179	1,423	1,107
YDR295C	HDA2	-	1,170	1,004
YDR299W	BFR2	1,623	-	-
YDR300C	PRO1	1,097	-	-
YDR305C	HNT2	-1,083	-	-
YDR329C	PEX3	1,253	1,202	1,302
YDR330W	UBX5	1,061	1,351	1,676
YDR334W	SWR1	1,324	1,906	1,432
YDR339C	FCF1	2,061	1,247	1,283
YDR341C		-	-	-1,079
YDR342C	HXT7	2,433	1,956	1,916
YDR343C	HXT6	2,426	1,928	1,662
YDR345C	HXT3	-	-	-1,238
YDR351W	SBE2	-	1,121	1,160
YDR354C-A		-	-1,090	-
YDR354W	TRP4	-	-1,031	-
YDR355C		-1,127	-	-
YDR357C	CNL1	-1,176	-	-1,307
YDR358W	GGA1	-	-	1,239
YDR361C	BCP1	-	-	-1,007
YDR363W-A	SEM1	-	1,175	1,202
YDR381C-A		-	-1,059	-
YDR382W	RPP2B	-	-	-1,189
YDR384C	ATO3	-1,945	-2,823	-1,929
YDR385W	EFT2	-	-1,354	-1,867
YDR394W	RPT3	-	-	1,169
YDR398W	UTP5	-	-	-1,098
YDR399W	HPT1	-2,444	-1,864	-2,333
YDR402C	DIT2	-1,059	-	-

Gene ID	Gene name	log2FC		
		45 min	120 min	200 min
YDR408C	ADE8	-1,152	-	-
YDR417C		-	-1,213	-1,611
YDR418W	RPL12B	-	-1,190	-1,624
YDR419W	RAD30	-1,464	-1,300	-
YDR422C	SIP1	-1,185	-1,121	-
YDR425W	SNX41	-	1,143	1,458
YDR426C		-	1,020	1,609
YDR427W	RPN9	1,136	1,464	1,517
YDR429C	TIF35	1,157	-	-
YDR431W		1,305	1,103	1,042
YDR437W	GPI19	-1,024	-	-
YDR446W	ECM11	1,376	1,484	-
YDR447C	RPS17B	-	-	-1,289
YDR448W	ADA2	-1,198	-1,115	-
YDR450W	RPS18A	-	-	-1,171
YDR451C	YHP1	-	-	-1,123
YDR454C	GUK1	1,045	-	-
YDR459C	PFA5	-1,445	-1,116	-1,008
YDR461C-A		-1,103	-	-
YDR465C	RMT2	1,251	-	-
YDR468C	TLG1	-	-	-1,041
YDR471W	RPL27B	-	-1,395	-1,812
YDR478W	SNM1	1,097	-	-
YDR488C	PAC11	-1,183	-	-
YDR489W	SLD5	-1,192	-	-1,095
YDR490C	PKH1	-1,288	-1,233	-
YDR497C	ITR1	-2,388	-3,006	-3,905
YDR501W	PLM2	-1,241	-	-
YDR502C	SAM2	-2,989	-2,316	-3,374

Gene ID	Gene name	log2FC		
		45 min	120 min	200 min
YDR506C	GMC1	1,018	-	-
YDR508C	GNP1	-1,521	-2,323	-2,194
YDR509W		-1,603	-2,357	-2,065
YDR515W	SLF1	1,821	2,087	1,489
YDR516C	EMI2	1,539	1,198	1,838
YDR523C	SPS1	-2,350	-2,440	-1,959
YDR524W-C		-	1,195	-
YDR525W	API2	-1,756	-2,051	-1,171
YDR529C	QCR7	-	-	-1,095
YDR533C	HSP31	-1,128	-1,168	-
YDR540C	IRC4	-	1,237	1,127
YEL008W		-	-	1,065
YEL011W	GLC3	-	1,207	1,776
YEL017C-A	PMP2	-	-1,068	-
YEL017W	GTT3	-1,050	-1,547	-1,359
YEL020C	PXP1	-	-	1,142
YEL021W	URA3	1,722	1,729	1,693
YEL032C-A		-1,311	-1,049	-1,007
YEL032W	MCM3	-1,085	-	-
YEL039C	CYC7	2,885	2,366	3,339
YEL040W	UTR2	1,141	-	-
YEL041W	YEF1	-1,401	-1,003	-
YEL046C	GLY1	-	-1,597	-1,313
YEL047C	FRD1	-1,311	-	-
YEL050W-A		1,005	-	-
YEL053W-A		-	-1,492	-1,951
YEL054C	RPL12A	-	-1,472	-1,963
YEL060C	PRB1	-2,257	-1,389	-1,226
YEL063C	CAN1	-1,959	-1,791	-1,229

Gene ID	Gene name	log2FC		
		45 min	120 min	200 min
YEL065W	SIT1	-1,311	-	-
YEL069C	HXT13	1,198	1,043	1,584
YEL070W	DSF1	1,867	2,742	2,592
YEL072W	RMD6	-3,253	-1,481	-1,139
YEL073C		-1,270	-1,972	-2,427
YEL077C		-1,881	-	-
YEL077W-A		-1,782	-	-
YER001W	MNN1	-1,140	-	-
YER005W	YND1	-1,033	-	-
YER006C-A		-1,662	-1,879	-1,711
YER006W	NUG1	1,282	-	-
YER007W	PAC2	-1,140	-1,139	-
YER009W	NTF2	1,245	-	-
YER011W	TIR1	2,681	3,612	4,314
YER012W	PRE1	-	1,292	1,353
YER018C	SPC25	-2,528	-2,128	-2,148
YER019W	ISC1	-1,923	-1,562	-1,483
YER021W	RPN3	-	1,155	1,403
YER024W	YAT2	-	-1,093	-
YER026C	CHO1	-	-1,489	-1,859
YER028C	MIG3	-2,146	-1,401	-1,097
YER033C	ZRG8	-	-	1,119
YER037W	PHM8	-2,204	-1,984	-1,700
YER038C	KRE29	-1,313	-1,080	-1,061
YER038W-A	FMP49	-1,854	-2,455	-1,091
YER039C	HVG1	-2,041	-2,319	-1,238
YER039C-A		-2,214	-2,509	-1,508
YER042W	MXR1	-2,883	-	-
YER043C	SAH1	-	-1,212	-1,940

Gene ID	Gene name	log2FC		
		45 min	120 min	200 min
YER044C	ERG28	-	1,380	1,290
YER046W	SPO73	-1,442	-1,179	-1,522
YER050C	RSM18	1,450	1,145	-
YER053C-A		3,559	2,805	2,786
YER056C	FCY2	-1,080	-	-1,348
YER056C-A	RPL34A	-	-1,410	-1,593
YER060W-A	FCY22	-1,162	-	-
YER065C	ICL1	-1,191	-	-
YER066C-A		3,945	3,521	3,736
YER067C-A		4,104	3,654	3,997
YER067W	RGI1	4,166	3,611	3,885
YER068C-A		-3,652	-3,598	-1,522
YER069W	ARG5,6	-3,381	-3,194	-1,517
YER073W	ALD5	-	-1,822	-1,637
YER074W	RPS24A	-	-	-1,236
YER077C	MRX1	-	-1,133	-1,342
YER079W		-	1,063	1,854
YER081W	SER3	-1,582	-1,118	-1,051
YER082C	UTP7	1,053	-	-
YER084W-A		-1,064	-	-
YER086W	ILV1	-1,128	-1,557	-1,474
YER088C	DOT6	-1,396	-	-
YER088C-A		-2,079	-2,441	-2,155
YER088W-B		-1,694	-2,017	-1,752
YER089C	PTC2	-1,245	-1,395	-1,315
YER090C-A		1,416	-	1,210
YER090W	TRP2	1,298	-	-
YER091C	MET6	-4,369	-3,013	-3,439
YER092W	IES5	-1,397	-1,051	-

Gene ID	Gene name	log2FC		
		45 min	120 min	200 min
YER095W	RAD51	-1,487	-	-1,115
YER096W	SHC1	-	1,055	1,350
YER100W	UBC6	-	-	1,014
YER102W	RPS8B	-	-	-1,278
YER103W	SSA4	1,948	1,942	2,377
YER110C	KAP123	1,120	-	-
YER117W	RPL23B	-	-1,697	-2,064
YER119C	AVT6	-1,687	-	-
YER125W	RSP5	-1,089	-	-1,093
YER126C	NSA2	1,271	-	-
YER130C	COM2	1,342	1,222	-
YER131W	RPS26B	-	-	-1,471
YER138W-A		-	1,503	-
YER142C		-	2,044	2,253
YER143W	DDI1	1,653	1,907	2,326
YER150W	SPI1	1,017	-	-
YER152C		-1,445	-1,163	-1,294
YER152W-A		-1,407	-1,114	-1,212
YER153C	PET122	-1,188	-	-1,187
YER155C	BEM2	-	1,106	-
YER158W-A		1,077	-	1,043
YER159C	BUR6	1,114	1,095	1,193
YER179W	DMC1	-	1,046	1,252
YER187W		-	-	1,026
YER188W		1,381	1,525	2,220
YFL001W	DEG1	-	-1,066	-1,038
YFL008W	SMC1	-	1,109	-
YFL014W	HSP12	-3,788	-1,975	-1,377
YFL015C		-	-1,045	-

Gene ID	Gene name	log2FC		
		45 min	120 min	200 min
YFL015W-A		-1,936	-1,791	-1,063
YFL020C	PAU5	-	1,783	2,570
YFL024C	EPL1	-1,355	-1,273	-1,136
YFL030W	AGX1	-1,475	-1,891	-2,009
YFL031C-A		-1,755	-2,138	-2,132
YFL031W	HAC1	-1,821	-2,467	-2,608
YFL032W		-1,769	-2,577	-2,567
YFL033C	RIM15	-	1,118	1,075
YFL034C-A	RPL22B	-1,931	-2,061	-2,832
YFL036W	RPO41	-	1,080	-
YFL041W-A		-	1,088	-
YFL044C	OTU1	-	-	1,190
YFL055W	AGP3	-4,836	-2,296	-1,797
YFL056C		-	1,198	1,508
YFL060C	SNO3	-1,096	-	-
YFL064C		-1,025	-	-
YFL065C		-1,619	-	-
YFL066C		-1,892	-	-
YFL067W		-1,957	-1,098	-
YFR003C	YPI1	1,233	1,449	1,787
YFR010W	UBP6	-	1,044	1,334
YFR015C	GSY1	1,724	1,853	2,111
YFR017C	IGD1	-	-	1,370
YFR018C		-1,005	-	-
YFR020W	CSS2	-	-	1,333
YFR021W	ATG18	-	-	1,223
YFR024C-A	LSB3	-	-	1,258
YFR026C	ULI1	-	1,040	1,102
YFR030W	MET10	-4,174	-2,270	-2,277

Gene ID	Gene name	log2FC		
		45 min	120 min	200 min
YFR031C-A	RPL2A	-	-1,577	-2,222
YFR032C	RRT5	-1,482	-1,992	-1,990
YFR032C-A	RPL29	-	-	-1,551
YFR032C-B		-	-1,032	-1,091
YFR034C	PHO4	-1,092	-	-
YFR036W	CDC26	-	-1,264	-1,104
YFR045W		1,096	1,111	1,109
YFR050C	PRE4	-	1,054	1,395
YFR052C-A		1,687	-	1,195
YFR052W	RPN12	-	-	1,052
YFR053C	HXK1	1,968	1,152	1,344
YGL008C	PMA1	-1,725	-2,859	-2,981
YGL009C	LEU1	1,391	-	-
YGL011C	SCL1	1,089	1,472	1,797
YGL015C		1,422	-	-
YGL021W	ALK1	-	-1,346	-1,715
YGL027C	CWH41	-1,385	-1,131	-1,005
YGL028C	SCW11	-	-1,237	-1,712
YGL030W	RPL30	-	-	-1,363
YGL031C	RPL24A	-	-1,307	-1,842
YGL035C	MIG1	-	1,138	1,098
YGL037C	PNC1	1,206	-	1,547
YGL039W		1,244	1,610	1,671
YGL045W	RIM8	-1,671	-	-
YGL048C	RPT6	-	-	1,069
YGL050W	TYW3	-	-1,119	-1,223
YGL052W		-1,085	-1,034	-
YGL056C	SDS23	-	-1,022	-
YGL058W	RAD6	1,031	-	-

Gene ID	Gene name	log2FC		
		45 min	120 min	200 min
YGL063C-A		-	-1,431	-1,545
YGL063W	PUS2	-1,101	-1,533	-1,605
YGL073W	HSF1	-	-	1,104
YGL074C		-	-	1,005
YGL075C	MPS2	-	1,009	-
YGL076C	RPL7A	-	-	-1,267
YGL077C	HNM1	-1,940	-2,212	-2,362
YGL088W		-	-2,938	-
YGL094C	PAN2	-	1,318	1,044
YGL096W	TOS8	-	-	1,242
YGL102C		-	-1,063	-1,488
YGL103W	RPL28	-	-1,075	-1,495
YGL111W	NSA1	1,054	-	-
YGL123C-A		-	-1,040	-1,792
YGL123W	RPS2	-	-1,102	-1,892
YGL125W	MET13	-3,562	-3,365	-3,319
YGL126W	SCS3	-1,938	-1,763	-1,942
YGL129C	RSM23	1,449	-	-
YGL135W	RPL1B	-1,056	-1,554	-2,035
YGL138C		1,916	-	-
YGL140C		-1,137	-	-
YGL141W	HUL5	1,121	1,399	1,433
YGL144C	ROG1	-1,243	-1,143	-1,128
YGL146C	RRT6	-1,837	-1,444	-
YGL147C	RPL9A	-	-1,045	-1,815
YGL157W	ARI1	-1,171	-	-
YGL166W	CUP2	-	-1,069	-
YGL170C	SPO74	-	-1,194	-
YGL174W	BUD13	-	1,119	-

Gene ID	Gene name	log2FC		
		45 min	120 min	200 min
YGL183C	MND1	-2,018	-	-
YGL184C	STR3	-4,828	-2,664	-1,591
YGL186C	TPN1	-1,709	-1,272	-
YGL188C-A		-2,043	-2,312	-1,474
YGL189C	RPS26A	-	-	-1,199
YGL191W	COX13	1,094	-	-
YGL196W	DSD1	-1,835	-	-
YGL197W	MDS3	-1,288	-	-
YGL202W	ARO8	-	-1,437	-
YGL203C	KEX1	-1,214	-	-
YGL205W	POX1	-1,009	-1,130	-1,180
YGL208W	SIP2	-1,348	-1,160	-
YGL209W	MIG2	-1,358	-	-1,259
YGL215W	CLG1	-	-	-1,036
YGL217C		-1,030	-	-
YGL222C	EDC1	-	-	1,167
YGL224C	SDT1	-1,742	-1,606	-
YGL234W	ADE5,7	-2,396	-2,030	-1,661
YGL240W	DOC1	-	1,159	1,706
YGL247W	BRR6	-1,306	-1,270	-1,472
YGR001C	EFM5	-	-1,019	-
YGR027C	RPS25A	-	-	-1,229
YGR029W	ERV1	-	-1,127	-
YGR031C-A	NAG1	-1,075	-	-
YGR031W	IMO32	-	-1,022	-
YGR032W	GSC2	-3,609	-3,345	-3,620
YGR034W	RPL26B	-	-	-1,226
YGR035C		2,554	1,544	2,991
YGR035W-A		-	-1,055	-

Gene ID	Gene name	log2FC		
		45 min	120 min	200 min
YGR040W	KSS1	-	-1,077	-1,319
YGR041W	BUD9	-1,296	-	-
YGR043C	NQM1	-2,279	-	-
YGR048W	UFD1	-	1,436	1,459
YGR050C		-1,711	-2,046	-1,513
YGR051C		-1,863	-1,828	-1,338
YGR052W	FMP48	1,493	1,134	1,487
YGR053C		-	1,193	1,244
YGR055W	MUP1	-2,443	-1,415	-1,333
YGR060W	ERG25	-	1,034	-
YGR061C	ADE6	-1,032	-	-
YGR066C		1,116	1,702	1,879
YGR076C	MRPL25	1,552	1,315	-
YGR079W		-1,838	-2,312	-2,230
YGR081C	SLX9	-	-1,147	-1,239
YGR085C	RPL11B	-	-	-1,349
YGR087C	PDC6	-5,871	-1,978	-1,137
YGR088W	CTT1	-1,187	-	-
YGR090W	UTP22	-	-1,092	-1,668
YGR092W	DBF2	-1,112	-1,580	-1,577
YGR103W	NOP7	1,475	-	-
YGR108W	CLB1	-1,896	-3,145	-3,833
YGR109W-A		-1,401	-1,494	-1,205
YGR112W	SHY1	1,036	-	-
YGR118W	RPS23A	-	-1,010	-1,603
YGR121C	MEP1	-1,311	-2,325	-2,164
YGR124W	ASN2	1,011	-	-
YGR125W		-1,610	-1,071	-
YGR131W	FHN1	1,085	-	1,087

Gene ID	Gene name	log2FC		
		45 min	120 min	200 min
YGR132C	PHB1	1,050	-	-
YGR135W	PRE9	-	-	1,076
YGR141W	VPS62	-1,589	-1,696	-1,156
YGR142W	BTN2	2,596	1,667	2,594
YGR145W	ENP2	1,118	-	-
YGR146C-A		-1,713	-1,655	-
YGR148C	RPL24B	-	-	-1,307
YGR154C	GTO1	-2,647	-	-
YGR155W	CYS4	-1,400	-	-
YGR157W	CHO2	-2,141	-2,001	-2,324
YGR159C	NSR1	1,238	-	-
YGR160W		1,227	-	-
YGR164W		-1,063	-	-
YGR168C		-1,236	-1,101	-
YGR176W		-	-	-1,107
YGR180C	RNR4	1,199	1,354	1,009
YGR190C		-	-1,451	-1,283
YGR191W	HIP1	-	-1,223	-1,144
YGR195W	SKI6	1,352	-	-
YGR199W	PMT6	-1,663	-1,444	-1,474
YGR200C	ELP2	-	-	-1,367
YGR201C		-1,117	-	-
YGR203W	YCH1	-1,261	-	-
YGR204W	ADE3	-1,358	-	-
YGR209C	TRX2	-	1,091	1,252
YGR210C		-1,131	-1,335	-
YGR211W	ZPR1	1,027	-	1,176
YGR214W	RPS0A	-	-1,186	-1,876
YGR223C	HSV2	-	-	1,121

Gene ID	Gene name	log2FC		
		45 min	120 min	200 min
YGR225W	AMA1	-1,223	-1,457	-1,871
YGR237C		1,258	1,040	1,409
YGR239C	PEX21	-1,378	-1,826	-1,308
YGR243W	MPC3	-	-1,993	-
YGR247W	CPD1	1,139	1,096	1,112
YGR249W	MGA1	1,752	2,078	2,247
YGR253C	PUP2	-	-	1,072
YGR254W	ENO1	-	-1,107	-1,327
YGR256W	GND2	-1,804	-1,215	-
YGR266W		-	-	1,217
YGR271C-A	EFG1	1,217	-	-
YGR276C	RNH70	1,104	1,077	1,006
YGR279C	SCW4	-	-1,062	-
YGR280C	PXR1	1,759	-	-
YGR285C	ZUO1	1,386	-	-
YGR286C	BIO2	1,869	2,049	2,003
YGR287C	IMA1	-	1,205	1,436
YGR289C	MAL11	-	1,130	1,458
YGR290W		-	1,228	1,394
YGR292W	MAL12	-	1,254	1,405
YGR293C		-	-	1,035
YGR294W	PAU12	-	-	1,796
YGR295C	COS6	-	-	-1,106
YHL001W	RPL14B	-	-1,026	-1,395
YHL003C	LAG1	-1,017	-1,156	-1,045
YHL006C	SHU1	-1,033	-	-
YHL008C		-	-1,079	-
YHL012W		-1,705	-2,270	-2,090
YHL014C	YLF2	-	-1,151	-

Gene ID	Gene name	log2FC		
		45 min	120 min	200 min
YHL015W	RPS20	-	-	-1,325
YHL016C	DUR3	-2,225	-1,627	-
YHL021C	AIM17	-	-	1,135
YHL025W	SNF6	-1,069	-	-1,157
YHL027W	RIM101	-1,163	-	-
YHL028W	WSC4	1,578	1,176	-
YHL030W	ECM29	-	1,744	1,853
YHL030W-A		1,060	1,279	1,072
YHL031C	GOS1	1,019	1,263	1,022
YHL033C	RPL8A	-	-2,495	-2,801
YHL036W	MUP3	-1,433	-	-
YHL050C		-1,758	-	-
YHL050W-A		-1,840	-1,142	-
YHR002W	LEU5	-1,155	-	-
YHR010W	RPL27A	-	-1,102	-1,765
YHR011W	DIA4	-1,236	-1,113	-1,311
YHR014W	SPO13	-1,215	-1,361	-
YHR015W	MIP6	-	-1,394	-1,159
YHR018C	ARG4	-	-1,178	-
YHR027C	RPN1	-	-	1,094
YHR029C	YHI9	-	-1,218	-
YHR033W		-1,684	-2,200	-2,485
YHR036W	BRL1	-1,088	-	-1,199
YHR041C	SRB2	-	-1,252	-1,387
YHR046C	INM1	1,236	-	-
YHR047C	AAP1	1,139	-	-
YHR048W	YHK8	-1,521	-1,419	-1,045
YHR054C		-1,436	-1,624	-1,331
YHR056W-A		-1,114	-1,010	-

Gene ID	Gene name	log2FC		
		45 min	120 min	200 min
YHR061C	GIC1	-2,516	-2,071	-1,755
YHR063W-A		1,198	-	-
YHR064C	SSZ1	1,083	-	-
YHR065C	RRP3	1,041	-	-
YHR067W	HTD2	-2,592	-2,936	-2,581
YHR071W	PCL5	-	-1,324	-
YHR081W	LRP1	1,141	-	-
YHR086W	NAM8	-1,021	-1,127	-1,163
YHR087W	RTC3	-	-1,079	-
YHR092C	HXT4	1,145	-	-
YHR093W	AHT1	-1,116	-	-
YHR094C	HXT1	-4,375	-4,731	-4,900
YHR096C	HXT5	-1,655	-1,453	-
YHR100C	GEP4	-	1,128	-
YHR112C		-1,314	-	-
YHR115C	DMA1	-1,097	-	-
YHR122W	CIA2	-	-1,026	-
YHR123W	EPT1	-	-	-1,055
YHR124W	NDT80	-1,034	-	-
YHR136C	SPL2	-2,091	-1,903	-
YHR137C-A		-	-	1,272
YHR137W	ARO9	-	-	1,338
YHR139C	SPS100	-1,629	-	-
YHR140W		-1,030	-	-
YHR141C	RPL42B	-	-	-1,645
YHR146W	CRP1	1,269	-	1,052
YHR147C	MRPL6	1,459	1,029	-
YHR148W	IMP3	1,186	-	-
YHR156C	LIN1	-	1,006	1,072

Gene ID	Gene name	log2FC		
		45 min	120 min	200 min
YHR159W	TDA11	-	1,362	1,295
YHR165C	PRP8	1,083	1,184	-
YHR165W-A		1,348	1,386	1,025
YHR169W	DBP8	-	-	-1,523
YHR170W	NMD3	-	-	-1,038
YHR175W	CTR2	-1,873	-1,398	-1,396
YHR175W-A		-1,981	-1,795	-
YHR176W	FMO1	-3,305	-1,553	-1,776
YHR190W	ERG9	-	-	1,129
YHR196W	UTP9	-	-1,200	-1,546
YHR199C	AIM46	-	-	1,200
YHR202W		-1,553	-1,065	-
YHR203C	RPS4B	-	-	-1,751
YHR213W-B		-	-	-2,170
YIL001W		-	-1,055	-
YIL002W-A		1,220	-	-
YIL007C	NAS2	-	-	1,103
YIL008W	URM1	1,253	-	-
YIL009W	FAA3	1,118	-	-
YIL011W	TIR3	1,932	2,662	3,044
YIL018W	RPL2B	-	-1,446	-1,942
YIL019W	FAF1	1,729	-	-
YIL020C	HIS6	1,005	-	-
YIL023C	YKE4	-1,666	-1,206	-1,126
YIL024C		-1,175	-	-
YIL027C	EMC5	1,110	1,093	-
YIL028W		-	-	1,348
YIL029C		-	1,738	2,434
YIL045W	PIG2	-	-	1,063

Gene ID	Gene name	log2FC		
		45 min	120 min	200 min
YIL046W	MET30	-1,601	-	-
YIL046W-A		-1,324	-1,837	-
YIL047C	SYG1	-2,839	-1,161	-1,694
YIL047C-A		-2,739	-1,009	-1,774
YIL051C	MMF1	1,043	-	-
YIL052C	RPL34B	-	-	-1,436
YIL054W		-1,752	-1,734	-1,531
YIL055C		-1,622	-1,365	-
YIL059C		-	-	1,470
YIL060W		-	1,034	1,607
YIL066W-A		-1,125	-	-
YIL069C	RPS24B	-	-1,457	-2,042
YIL074C	SER33	-3,477	-1,524	-1,471
YIL082W		-1,166	-	-
YIL088C	AVT7	-1,480	-	-
YIL089W		-1,356	-	-
YIL094C	LYS12	-	-1,439	-1,492
YIL096C	BMT5	1,703	-	-
YIL097W	FYV10	-	-	1,242
YIL098C	FMC1	1,000	1,070	-
YIL106W	MOB1	-	-1,044	-
YIL113W	SDP1	-	-	1,358
YIL116W	HIS5	-1,064	-1,326	-
YIL117C	PRM5	1,283	1,463	2,027
YIL120W	QDR1	-1,211	-	-
YIL121W	QDR2	-1,088	-	-
YIL123W	SIM1	-1,179	-	-1,106
YIL127C	RRT14	1,274	-	-
YIL132C	CSM2	-1,284	-	-

Gene ID	Gene name	log2FC		
		45 min	120 min	200 min
YIL133C	RPL16A	-	-1,457	-2,073
YIL145C	PAN6	-	-	-1,069
YIL146C	ATG32	-1,326	-1,223	-
YIL148W	RPL40A	-	-	-1,515
YIL149C	MLP2	1,038	-	-
YIL155C	GUT2	-1,695	-	-
YIL158W	AIM20	-	-1,069	-1,301
YIL163C		-1,885	-1,060	-
YIL164C	NIT1	-2,667	-1,916	-
YIL165C		-2,933	-1,935	-
YIL166C		-1,233	-	-
YIL170W		-	1,009	-
YIL173W	VTH1	-1,404	-	-
YIR013C	GAT4	-	-1,489	-
YIR014W		-	-	1,282
YIR017C	MET28	-1,599	-	-
YIR017W-A		-1,599	-	-
YIR018C-A		-1,058	-	-
YIR019C	FLO11	1,359	1,449	1,964
YIR024C	INA22	-	1,059	-
YIR025W	MND2	-	1,186	1,554
YIR027C	DAL1	-1,705	-	-
YIR028W	DAL4	-1,502	-1,420	-1,045
YIR029W	DAL2	-1,596	-	-
YIR030W-A		-1,548	-	-
YIR031C	DAL7	-1,725	-1,013	-
YIR032C	DAL3	-2,137	-1,547	-1,240
YIR034C	LYS1	-	-1,526	-
YIR035C		1,045	-	-

Gene ID	Gene name	log2FC		
		45 min	120 min	200 min
YIR039C	YPS6	-	1,199	1,640
YIR042C		-2,759	-	-
YJL001W	PRE3	-	1,187	1,410
YJL009W		-	1,097	1,021
YJL011C	RPC17	-	-	-1,160
YJL016W	TPH3	-1,019	-	-1,128
YJL019W	MPS3	-1,294	-	-
YJL020W-A		-1,036	-	-
YJL024C	APS3	1,154	1,028	-
YJL031C	BET4	1,279	1,641	1,533
YJL032W		1,228	1,648	1,470
YJL033W	HCA4	1,084	-	-
YJL034W	KAR2	1,112	-	-
YJL035C	TAD2	-	-1,068	-1,263
YJL036W	SNX4	1,508	1,747	1,899
YJL045W		-1,315	-	-
YJL051W	IRC8	-	-	-1,033
YJL057C	IKS1	-	-	1,016
YJL060W	BNA3	-2,783	-1,028	-
YJL077C	ICS3	-1,422	-	-
YJL077W-A		-1,439	-	-
YJL077W-B		-1,814	-	-
YJL078C	PRY3	-1,009	-	-
YJL085W	EXO70	-1,081	-	-1,062
YJL086C		-	-	-1,193
YJL088W	ARG3	-4,319	-4,764	-2,564
YJL089W	SIP4	-1,026	-	-
YJL091C	GWT1	-	-	-1,032
YJL093C	TOK1	-1,011	-	-

Gene ID	Gene name	log2FC		
		45 min	120 min	200 min
YJL096W	MRPL49	1,464	1,129	-
YJL101C	GSH1	-1,821	-	-
YJL105W		-	-	1,308
YJL119C		-1,066	-	-
YJL130C	URA2	1,213	-	-
YJL132W		-1,505	-1,094	-
YJL134W	LCB3	-1,165	-1,550	-1,255
YJL135W		-	-1,613	-1,320
YJL136C	RPS21B	-	-	-1,468
YJL137C	GLG2	-2,211	-1,724	-1,501
YJL139C	YUR1	-1,540	-1,351	-1,040
YJL144W		1,076	-	2,168
YJL151C	SNA3	-	1,015	-
YJL153C	INO1	-1,434	-3,309	-6,239
YJL157C	FAR1	-	-1,052	-1,555
YJL158C	CIS3	-	-1,012	-1,521
YJL159W	HSP150	-	-1,004	-
YJL160C	PIR5	-1,478	-1,245	-
YJL163C		-1,121	-	-
YJL168C		-1,141	-1,299	-1,360
YJL169W		-1,061	-1,231	-1,434
YJL172W	CPS1	-2,546	-1,600	-1,096
YJL177W	RPL17B	-	-	-1,024
YJL185C	ATG36	-1,793	-1,629	-1,218
YJL188C	BUD19	-	-	-1,182
YJL189W	RPL39	-	-	-1,180
YJL190C	RPS22A	-	-	-1,349
YJL191W	RPS14B	-1,677	-2,355	-2,444
YJL193W		-1,031	-	-

Gene ID	Gene name	log2FC		
		45 min	120 min	200 min
YJL196C	ELO1	-	1,000	1,505
YJL199C	MBB1	-1,115	-	-
YJL200C	ACO2	-	-1,719	-1,560
YJL204C	RCY1	-	1,007	1,094
YJL210W	PEX2	-1,148	-1,475	-
YJL211C		-	-1,328	-
YJL212C	OPT1	-3,085	-1,583	-1,700
YJL213W		1,409	1,847	2,549
YJL214W	HXT8	-	1,016	-
YJL217W	REE1	1,912	1,516	1,502
YJL218W		2,395	2,659	2,861
YJL219W	HXT9	-	1,020	1,453
YJL222W	VTH2	-	-1,530	-1,012
YJL225C		-1,692	-	-
YJR001W	AVT1	-1,432	-	-
YJR007W	SUI2	1,125	-	-
YJR008W	MHO1	-1,243	-1,295	-1,093
YJR010W	MET3	-5,231	-2,516	-3,082
YJR016C	ILV3	-	-1,157	-
YJR022W	LSM8	-	-	1,071
YJR025C	BNA1	-	-2,175	-
YJR044C	VPS55	-1,433	-	-
YJR045C	SSC1	1,473	1,050	1,031
YJR047C	ANB1	1,010	1,014	-
YJR048W	CYC1	1,063	-	-
YJR061W		-2,485	-2,400	-3,173
YJR063W	RPA12	1,183	-	-
YJR070C	LIA1	-	-1,109	-1,469
YJR071W		-	-1,044	-1,445

Gene ID	Gene name	log2FC		
		45 min	120 min	200 min
YJR073C	OPI3	-	-1,697	-2,332
YJR074W	MOG1	-	-1,298	-
YJR077C	MIR1	-	-1,151	-1,814
YJR078W	BNA2	-1,842	-1,699	-1,356
YJR091C	JSN1	1,134	1,443	1,371
YJR092W	BUD4	1,055	-	-
YJR094C	IME1	1,446	-	-
YJR094W-A	RPL43B	-	-	-1,735
YJR095W	SFC1	-1,642	-1,149	-1,826
YJR096W		-	-	1,095
YJR098C		-1,212	-1,338	-1,055
YJR105W	ADO1	-	-1,113	-1,474
YJR106W	ECM27	-1,130	-	-
YJR109C	CPA2	-1,109	-1,602	-
YJR116W	TDA4	-	-	1,359
YJR117W	STE24	-	1,304	1,332
YJR123W	RPS5	-	-1,408	-2,036
YJR125C	ENT3	-	-	1,006
YJR128W		-1,267	-1,289	-
YJR129C	EFM3	-	-	-1,681
YJR135W-A	TIM8	1,146	-	-
YJR137C	MET5	-3,986	-2,038	-2,761
YJR139C	HOM6	-1,693	-	-
YJR140W-A		-1,480	-	-
YJR145C	RPS4A	-	-1,139	-1,748
YJR146W		-1,189	-	-1,025
YJR148W	BAT2	1,263	1,305	1,335
YJR150C	DAN1	-	1,311	1,392
YJR152W	DAL5	-1,670	-	-

Gene ID	Gene name	log2FC		
		45 min	120 min	200 min
YJR156C	THI11	-	1,161	1,216
YJR159W	SOR1	-	1,216	1,661
YKL001C	MET14	-3,855	-1,943	-2,544
YKL003C	MRP17	1,156	-	-
YKL004W	AUR1	-	-1,097	-
YKL005C	BYE1	-1,751	-1,347	-
YKL006W	RPL14A	-	-1,357	-1,776
YKL009W	MRT4	1,412	-	-
YKL018C-A		-	-1,337	-1,264
YKL027W	TCD2	-	-	-1,039
YKL031W		-1,157	-1,589	-
YKL033W	TTI1	-1,025	-1,100	-1,111
YKL040C	NFU1	-	1,118	1,058
YKL043W	PHD1	2,126	2,278	2,137
YKL044W	MMO1	1,965	2,461	2,443
YKL048C	ELM1	1,281	1,246	1,107
YKL054C	DEF1	-1,205	-	-1,145
YKL056C	TMA19	1,197	-	-
YKL063C		-	1,372	-
YKL068W-A		-3,308	-2,098	-2,514
YKL082C	RRP14	1,043	-	-
YKL083W		1,072	-	-
YKL086W	SRX1	1,639	1,263	1,530
YKL089W	MIF2	-	1,011	-
YKL091C		-1,257	-1,104	-
YKL096W-A	CWP2	-	-	-1,401
YKL099C	UTP11	1,189	-	-
YKL102C		-2,132	-1,099	-
YKL110C	KTI12	1,653	1,087	-
YKL117W	SBA1	-	1,076	1,274

Gene ID	Gene name	log2FC		
		45 min	120 min	200 min
YKL120W	OAC1	1,910	1,313	-
YKL127W	PGM1	-1,182	-	-1,084
YKL130C	SHE2	1,050	-	-
YKL143W	LTV1	1,344	-	-
YKL145W	RPT1	-	1,270	1,683
YKL145W-A		-	1,366	1,869
YKL148C	SDH1	-	-	-1,299
YKL156C-A		-	-	-1,231
YKL156W	RPS27A	-	-	-1,222
YKL159C	RCN1	1,149	1,244	1,469
YKL162C		-	1,008	-
YKL163W	PIR3	-1,295	-1,860	-1,491
YKL164C	PIR1	-1,189	-2,333	-2,203
YKL172W	EBP2	1,517	-	-
YKL177W		-1,620	-1,057	-1,052
YKL178C	STE3	-1,466	-	-1,013
YKL180W	RPL17A	-	-	-1,167
YKL182W	FAS1	-1,017	-2,077	-2,292
YKL183C-A		-1,045	-	-1,741
YKL183W	LOT5	-	-1,260	-1,287
YKL186C	MTR2	1,214	1,030	1,097
YKL193C	SDS22	1,344	1,337	1,799
YKL201C	MNN4	-3,674	-2,190	-2,283
YKL202W		-3,157	-2,570	-1,557
YKL212W	SAC1	-	-	-1,517
YKL215C	OXP1	-1,169	-	-
YKL216W	URA1	2,434	2,315	1,920
YKL218C	SRY1	-2,191	-1,939	-
YKL220C	FRE2	-	-	1,021
YKL221W	MCH2	-	1,110	1,264

Gene ID	Gene name	log2FC		
		45 min	120 min	200 min
YKR004C	ECM9	-1,050	-	-1,414
YKR005C		-1,222	-	-
YKR006C	MRPL13	1,057	-	-
YKR010C	TOF2	-1,126	-1,139	-1,353
YKR011C		1,531	1,551	1,974
YKR017C	HEL1	-1,051	-	-
YKR020W	VPS51	1,052	1,172	1,547
YKR033C		-2,425	-	-
YKR034W	DAL80	-2,446	-	-
YKR039W	GAP1	-2,880	-2,299	-2,148
YKR042W	UTH1	1,316	-	-
YKR046C	PET10	-2,598	-2,256	-1,904
YKR050W	TRK2	-1,394	-	-
YKR053C	YSR3	-1,233	-	-
YKR055W	RHO4	-	1,249	1,246
YKR057W	RPS21A	-	-	-1,178
YKR059W	TIF1	1,034	-	-
YKR061W	KTR2	-	-1,012	-
YKR069W	MET1	-3,656	-1,419	-1,332
YKR077W	MSA2	-	-	1,029
YKR079C	TRZ1	1,002	-	-
YKR080W	MTD1	-2,547	-1,594	-1,109
YKR081C	RPF2	1,493	-	-
YKR083C	DAD2	1,124	1,587	1,187
YKR091W	SRL3	1,361	1,788	2,111
YKR093W	PTR2	-	1,338	1,228
YKR094C	RPL40B	-	-	-1,507
YKR097W	PCK1	-1,275	-	-1,247
YKR102W	FLO10	-	-	1,182
YKR106W	GEX2	-1,014	-	-

Gene ID	Gene name	log2FC		
		45 min	120 min	200 min
YLL005C	SPO75	-1,507	-1,140	-1,223
YLL006W	MMM1	1,274	1,177	1,272
YLL009C	COX17	1,954	1,332	-
YLL013C	PUF3	-	-	-1,161
YLL023C	POM33	-	-	1,275
YLL024C	SSA2	1,363	-	1,054
YLL026W	HSP104	2,173	1,320	1,826
YLL034C	RIX7	1,497	-	-
YLL039C	UBI4	-	1,032	1,343
YLL044W		-	-	-1,530
YLL045C	RPL8B	-	-	-1,561
YLL049W	LDB18	-	-1,304	-
YLL052C	AQY2	-	-1,515	-2,276
YLL053C		-	-1,393	-2,536
YLL055W	YCT1	-3,058	-	-
YLL056C		-1,949	-	-
YLL057C	JLP1	-2,392	-2,270	-2,292
YLL058W		-1,388	-	-
YLL059C		-1,164	-	-
YLL060C	GTT2	-	-	1,537
YLL061W	MMP1	-4,063	-1,354	-1,491
YLL062C	MHT1	-4,142	-1,590	-1,958
YLL066C		-1,678	-1,332	-1,344
YLL067C		-1,647	-1,373	-1,381
YLL067W-A		-	-	-1,036
YLR014C	PPR1	1,062	-	-
YLR029C	RPL15A	-1,680	-3,017	-3,132
YLR030W		-1,330	-1,098	-
YLR042C		-2,145	-1,630	-1,146
YLR044C	PDC1	-	-1,606	-2,039

Gene ID	Gene name	log2FC		
		45 min	120 min	200 min
YLR045C	STU2	-1,153	-	-
YLR048W	RPS0B	-	-	-1,608
YLR053C		-1,230	-	-
YLR058C	SHM2	-2,664	-1,159	-
YLR061W	RPL22A	-	-1,043	-2,059
YLR062C	BUD28	-	-1,030	-2,080
YLR064W	PER33	1,075	1,003	1,060
YLR068W	FYV7	1,182	-	-
YLR072W	LAM6	-1,287	-1,097	-
YLR073C	RFU1	-	-	-1,165
YLR075W	RPL10	-	-	-1,325
YLR076C		-	-	-1,278
YLR077W	FMP25	-1,051	-	-
YLR080W	EMP46	-1,066	-	-
YLR092W	SUL2	-4,219	-2,679	-2,749
YLR099C	ICT1	-	-1,547	-1,311
YLR099W-A	MIM2	-1,037	-1,805	-1,800
YLR106C	MDN1	-	-	-1,369
YLR110C	CCW12	-	-1,186	-1,261
YLR112W		-	-	1,212
YLR119W	SRN2	-	1,183	-
YLR120C	YPS1	-2,239	-2,089	-2,348
YLR120W-A		-1,885	-1,823	-2,125
YLR121C	YPS3	-1,379	-1,136	-1,688
YLR122C		-1,555	-1,092	-
YLR123C		-1,686	-1,229	-
YLR124W		-1,665	-1,415	-
YLR130C	ZRT2	-1,406	-	-1,095
YLR138W	NHA1	-1,102	-1,013	-1,033
YLR142W	PUT1	-1,481	-	-

Gene ID	Gene name	log2FC		
		45 min	120 min	200 min
YLR150W	STM1	1,032	-	-
YLR152C		-	-1,564	-
YLR154W-E		1,072	-	-
YLR154W-F		1,108	-	-
YLR157C-B		1,265	-	-
YLR162W		-	-1,155	-1,213
YLR164W	SHH4	-1,498	-1,345	-
YLR167W	RPS31	-	-1,470	-2,037
YLR168C	UPS2	-1,161	-1,831	-2,018
YLR173W		-1,872	-1,853	-1,945
YLR174W	IDP2	-3,314	-2,741	-2,586
YLR177W		-	-	1,262
YLR178C	TFS1	-1,843	-	-
YLR179C		-2,468	-1,909	-1,880
YLR180W	SAM1	-2,714	-1,351	-1,847
YLR185W	RPL37A	-	-1,019	-1,576
YLR187W	SKG3	-1,124	-1,165	-1,032
YLR190W	MMR1	-	-	-1,199
YLR194C	NCW2	-	-1,508	-1,554
YLR197W	NOP56	1,157	-	-
YLR198C		1,244	-	-
YLR200W	YKE2	1,340	-	-
YLR205C	HMX1	-	-	1,212
YLR209C	PNP1	-1,108	-	-
YLR216C	CPR6	3,044	2,515	2,726
YLR217W		3,101	2,511	2,789
YLR218C	COA4	1,200	1,054	1,028
YLR225C		-	-	1,229
YLR232W		-	-	-1,170
YLR244C	MAP1	1,139	-	-

Gene ID	Gene name	log2FC		
		45 min	120 min	200 min
YLR246W	ERF2	-1,031	-	-
YLR248W	RCK2	-1,069	-	-
YLR249W	YEF3	-	-	-1,552
YLR255C		-	-1,068	-
YLR259C	HSP60	1,813	1,183	1,183
YLR260W	LCB5	1,271	-	-
YLR262C-A	TMA7	1,436	-	-
YLR264W	RPS28B	-	-	-1,017
YLR276C	DBP9	1,116	-	-
YLR279W		-2,354	-2,401	-2,263
YLR280C		-2,538	-2,539	-2,289
YLR281C		-2,541	-2,630	-2,300
YLR287C-A	RPS30A	1,100	-	-
YLR297W		-	-	1,219
YLR299C-A		-1,820	-	-
YLR299W	ECM38	-1,712	-1,061	-
YLR300W	EXG1	-	-	-1,036
YLR302C		-4,256	-2,391	-2,320
YLR303W	MET17	-3,708	-1,986	-2,185
YLR304C	ACO1	-1,437	-	-
YLR305C	STT4	-	-	-1,163
YLR307C-A		-	1,116	1,220
YLR309C	IMH1	1,152	-	-
YLR312C	ATG39	-1,856	-1,134	-
YLR312W-A	MRPL15	1,038	-	-
YLR323C	CWC24	1,071	1,211	1,095
YLR324W	PEX30	-	1,204	1,557
YLR326W		-1,140	-	-
YLR327C	TMA10	-	-	2,027
YLR329W	REC102	-1,030	-1,020	-

Gene ID	Gene name	log2FC		
		45 min	120 min	200 min
YLR333C	RPS25B	-	-	-1,330
YLR336C	SGD1	1,017	-	-
YLR339C		-	-	-1,199
YLR340W	RPP0	-	-	-1,221
YLR342W	FKS1	-1,635	-	-1,053
YLR342W-A		-2,805	-1,590	-1,590
YLR343W	GAS2	-3,026	-2,493	-1,750
YLR344W	RPL26A	-	-1,612	-2,095
YLR354C	TAL1	-	-	-1,378
YLR355C	ILV5	-1,148	-1,245	-1,429
YLR356W	ATG33	-	-	1,294
YLR359W	ADE13	-1,189	-	-
YLR361C	DCR2	-1,139	-1,125	-
YLR362W	STE11	-	-	1,143
YLR363W-A		1,098	-	-
YLR364W	GRX8	-2,400	-	-1,120
YLR366W		-	-	-2,699
YLR367W	RPS22B	-	-	-2,412
YLR372W	ELO3	-	-	-1,106
YLR374C		-1,234	-1,116	-
YLR387C	REH1	-	1,002	1,457
YLR388W	RPS29A	-	-	-1,338
YLR402W		-1,724	-1,898	-1,373
YLR405W	DUS4	-	-1,377	-1,467
YLR406C	RPL31B	-1,126	-2,177	-2,407
YLR407W		-1,541	-1,807	-1,601
YLR413W	INA1	1,266	-	-
YLR415C		-1,474	-1,126	-
YLR416C		-1,671	-1,186	-
YLR419W		1,008	-	-

Gene ID	Gene name	log2FC		
		45 min	120 min	200 min
YLR420W	URA4	1,661	1,513	1,592
YLR430W	SEN1	-	-	-1,057
YLR432W	IMD3	-	-	-1,132
YLR435W	TSR2	1,133	-	-
YLR437C-A		-1,877	-1,570	-
YLR438W	CAR2	-1,635	-1,149	-1,145
YLR441C	RPS1A	-	-	-1,193
YLR448W	RPL6B	-	-	-1,324
YLR449W	FPR4	1,022	-	-
YLR450W	HMG2	-1,215	-	-
YLR451W	LEU3	-	-1,315	-1,227
YLR452C	SST2	-	1,245	1,487
YLR460C		1,941	2,125	2,461
YLR463C		-1,158	-1,066	-
YLR464W		-1,342	-1,069	-1,145
YLR465C	BSC3	-1,524	-1,105	-1,198
YLR466C-A		-1,491	-1,617	-1,239
YLR466W	YRF1-4	-1,661	-1,455	-1,355
YLR467C-A		-1,491	-1,625	-1,240
YLR467W	YRF1-5	-1,615	-1,429	-1,366
YML007C-A		-	-	1,135
YML017W	PSP2	-1,297	-1,154	-1,239
YML018C		-2,631	-1,240	-1,745
YML024W	RPS17A	-	-	-1,321
YML026C	RPS18B	-	-1,335	-2,014
YML027W	YOX1	-1,812	-	-1,210
YML028W	TSA1	-	1,011	1,035
YML042W	CAT2	-	1,040	-
YML048W	GSF2	-	-	1,096
YML049C	RSE1	-	1,095	1,016

Gene ID	Gene name	log2FC		
		45 min	120 min	200 min
YML050W	AIM32	1,022	1,022	-
YML054C-A		-1,398	-	-
YML058W-A	HUG1	-	1,069	-
YML063W	RPS1B	-	-1,311	-1,937
YML066C	SMA2	-1,247	-	-1,043
YML069W	POB3	-	1,052	-
YML072C	TCB3	-1,306	-	-1,169
YML073C	RPL6A	-	-1,400	-1,704
YML074C	FPR3	1,118	-	-
YML091C	RPM2	-	1,118	-
YML092C	PRE8	-	1,367	1,464
YML095C	RAD10	-	-	1,185
YML101C	CUE4	-	-1,342	-1,210
YML104C	MDM1	-1,285	-	-
YML116W	ATR1	-1,761	-1,228	-
YML123C	PHO84	-1,489	-1,237	-
YML125C	PGA3	1,468	1,647	1,526
YML128C	MSC1	-1,531	-	-
YML130C	ERO1	1,435	1,107	-
YMR001C	CDC5	-	-	-1,002
YMR001C-A		-	-1,085	-1,607
YMR003W	AIM34	-1,399	-1,443	-1,198
YMR004W	MVP1	1,160	1,373	1,337
YMR008C	PLB1	-	-1,166	-1,047
YMR009W	ADI1	-	-	1,484
YMR013C	SEC59	-1,158	-	-
YMR013C-A		-1,666	-	-
YMR018W	PEX9	-	-	-1,087
YMR032W	HOF1	-	-	-1,054
YMR040W	YET2	-	-	-1,366

Gene ID	Gene name	log2FC		
		45 min	120 min	200 min
YMR041C	ARA2	-	-1,009	-
YMR042W	ARG80	-	-1,130	-
YMR053C	STB2	-	1,027	1,214
YMR056C	AAC1	-1,187	-1,050	-
YMR062C	ARG7	-	-1,401	-
YMR067C	UBX4	-	1,000	1,255
YMR071C	TVP18	1,030	1,022	1,242
YMR081C	ISF1	-	1,316	1,709
YMR090W		-1,299	-	-
YMR095C	SNO1	-1,334	-2,090	-1,072
YMR096W	SNZ1	-1,799	-2,271	-
YMR115W	MGR3	1,531	1,623	1,456
YMR116C	ASC1	-	-1,140	-2,565
YMR117C	SPC24	-1,019	-	-
YMR119W-A		-1,497	-	-1,024
YMR120C	ADE17	-3,312	-1,831	-
YMR121C	RPL15B	-1,151	-1,419	-
YMR122C		-1,256	-	-
YMR122W-A		-	1,081	-
YMR128W	ECM16	1,603	-	-
YMR131C	RRB1	1,278	-	-
YMR133W	REC114	-1,678	-	-
YMR135C	GID8	-1,323	-1,045	-
YMR135W-A		-1,371	-1,068	-
YMR136W	GAT2	-	-	1,025
YMR141W-A		-2,059	-1,861	-1,843
YMR142C	RPL13B	-	-1,111	-1,723
YMR143W	RPS16A	-	-	-1,491
YMR144W	FDO1	-1,329	-	-
YMR155W		-1,004	-	-

Gene ID	Gene name	log2FC		
		45 min	120 min	200 min
YMR156C	TPP1	-	-	1,057
YMR161W	HLJ1	-	1,193	1,112
YMR166C	MME1	1,196	1,097	-
YMR169C	ALD3	-2,512	-1,275	-1,271
YMR170C	ALD2	-1,053	-	-
YMR175W	SIP18	-	-	-1,848
YMR186W	HSC82	1,751	1,179	1,089
YMR189W	GCV2	-2,463	-	-
YMR193C-A		-	-	-1,080
YMR194C-A		-2,079	-1,833	-1,520
YMR194W	RPL36A	-	-	-1,351
YMR195W	ICY1	1,333	1,191	1,451
YMR196W		-2,429	-	-
YMR197C	VTI1	-	1,169	1,141
YMR201C	RAD14	-	-	1,237
YMR206W		-1,282	-	-
YMR209C		1,005	-	-
YMR210W	MGL2	1,062	-	1,142
YMR217W	GUA1	1,025	-	-
YMR229C	RRP5	1,036	-	-
YMR230W	RPS10B	-	-	-1,213
YMR238W	DFG5	-1,307	-1,005	-
YMR241W	YHM2	-	-1,552	-2,096
YMR242C	RPL20A	-	-	-1,230
YMR242W-A		-1,057	-	-
YMR244W		-1,495	-1,154	-1,628
YMR246W	FAA4	1,187	-	-
YMR250W	GAD1	-1,243	-	-
YMR251W	GTO3	-1,122	-1,221	-
YMR252C		-1,090	-	-

Gene ID	Gene name	log2FC		
		45 min	120 min	200 min
YMR253C		-1,030	-	-
YMR254C		-1,157	-	-
YMR256C	COX7	1,428	1,256	-
YMR262W		-1,268	-1,254	-
YMR268C	PRP24	1,038	-	-
YMR276W	DSK2	-	-	1,043
YMR278W	PRM15	1,244	1,408	1,438
YMR290C	HAS1	1,886	-	-
YMR290W-A		1,876	-	-
YMR297W	PRC1	-1,118	-	-
YMR300C	ADE4	-1,358	-	-
YMR301C	ATM1	-1,103	-	-
YMR304W	UBP15	-1,021	-	-
YMR306C-A		-	-	1,446
YMR308C	PSE1	-	-	-1,223
YMR311C	GLC8	-	-	1,121
YMR312W	ELP6	1,086	-	-
YMR314W	PRE5	-	-	1,135
YMR316C-B		-1,293	-	-
YMR316W	DIA1	1,181	1,033	-
YMR319C	FET4	1,512	1,091	-
YNL007C	SIS1	-	-	1,330
YNL011C		-2,001	-1,689	-1,386
YNL013C		-1,153	-	-
YNL014W	HEF3	-1,117	-	-
YNL018C		-	-	1,220
YNL019C		-1,088	-	-
YNL024C	EFM6	-	-	-1,222
YNL028W		-1,158	-	-
YNL029C	KTR5	-1,041	-	-

Gene ID	Gene name	log2FC		
		45 min	120 min	200 min
YNL036W	NCE103	-1,845	-1,937	-1,229
YNL037C	IDH1	-1,413	-	-
YNL043C		-	-1,159	-2,057
YNL044W	YIP3	-	-1,076	-1,966
YNL057W		1,856	1,295	1,442
YNL058C		1,933	1,296	1,455
YNL061W	NOP2	1,587	-	-
YNL062C	GCD10	1,390	-	-
YNL064C	YDJ1	1,333	-	1,035
YNL067W	RPL9B	1,017	-1,276	-1,598
YNL069C	RPL16B	-	-1,089	-1,631
YNL080C	EOS1	-1,206	-1,301	-
YNL096C	RPS7B	-1,136	-1,768	-2,240
YNL097C-B		-2,690	-1,858	-1,326
YNL101W	AVT4	-1,222	-	-
YNL103W-A		-	-1,165	-
YNL104C	LEU4	-	-1,019	-
YNL107W	YAF9	1,091	-	-
YNL111C	CYB5	1,462	1,462	1,108
YNL112W	DBP2	-	-	-1,384
YNL113W	RPC19	1,101	-	-
YNL114C		1,100	-	-
YNL122C		1,179	1,045	-
YNL124W	NAF1	1,144	-	-
YNL130C-A	DGR1	-1,344	-	-1,028
YNL131W	TOM22	1,182	-	-
YNL132W	KRE33	1,340	-	-
YNL141W	AAH1	1,915	-	-
YNL142W	MEP2	-3,050	-3,172	-2,294
YNL144C		-	-	1,085

Gene ID	Gene name	log2FC		
		45 min	120 min	200 min
YNL144W-A		-	1,341	1,612
YNL146C-A		-1,292	-	-
YNL148C	ALF1	-1,085	-1,038	-
YNL149C	PGA2	-	-	1,157
YNL150W		-	-	1,148
YNL155W	CUZ1	-	1,068	1,289
YNL158W	PGA1	-	-1,053	-
YNL159C	ASI2	-1,277	-1,129	-
YNL160W	YGP1	-	-1,662	-1,689
YNL162W	RPL42A	-	-	-1,717
YNL169C	PSD1	-	-1,397	-1,770
YNL170W		-	-1,239	-1,530
YNL173C	MDG1	-	-	1,247
YNL174W		1,417	-	-
YNL175C	NOP13	1,312	-	-
YNL178W	RPS3	-	-1,776	-2,345
YNL185C	MRPL19	1,164	-	-
YNL186W	UBP10	-	-1,043	-1,433
YNL191W	DUG3	-1,445	-	-
YNL195C		-1,254	-	-
YNL196C	SLZ1	1,067	1,195	1,554
YNL208W		-1,324	-	-
YNL212W	VID27	-1,089	-	-
YNL214W	PEX17	1,007	-	-
YNL220W	ADE12	-1,563	-1,242	-
YNL226W		-	-1,238	-1,116
YNL230C	ELA1	-2,098	-1,883	-1,569
YNL234W		-	-	1,165
YNL241C	ZWF1	-2,219	-	-
YNL250W	RAD50	1,333	1,490	1,405

Gene ID	Gene name	log2FC		
		45 min	120 min	200 min
YNL252C	MRPL17	1,038	-	-
YNL256W	FOL1	-1,381	-1,076	-1,474
YNL259C	ATX1	-1,770	-2,055	-2,008
YNL263C	YIF1	-	1,099	1,096
YNL268W	LYP1	-1,181	-1,497	-1,385
YNL270C	ALP1	-1,911	-	-1,040
YNL274C	GOR1	-1,291	-	-
YNL276C		-2,644	-1,315	-1,691
YNL277W	MET2	-2,766	-1,502	-1,782
YNL278W	CAF120	-1,601	-	-
YNL281W	HCH1	1,400	-	-
YNL283C	WSC2	-1,307	-	-
YNL289W	PCL1	-1,408	-	-
YNL300W	TOS6	-	-	1,003
YNL301C	RPL18B	-2,184	-2,567	-2,688
YNL302C	RPS19B	-	-	-1,415
YNL308C	KRI1	1,145	-	-
YNL315C	ATP11	1,371	1,165	-
YNL332W	THI12	-	1,310	-
YNL334C	SNO2	-1,109	-	-
YNR002C	ATO2	-1,268	-1,004	-
YNR016C	ACC1	-1,197	-2,224	-2,533
YNR023W	SNF12	-	-	1,017
YNR034W	SOL1	1,075	-	1,064
YNR034W-A	EGO4	1,656	-	-
YNR043W	MVD1	-	1,047	1,137
YNR044W	AGA1	1,028	1,676	1,983
YNR050C	LYS9	-	-3,117	-2,332
YNR053C	NOG2	-	-	-1,195
YNR055C	HOL1	-	-	-1,174

Gene ID	Gene name	log2FC		
		45 min	120 min	200 min
YNR056C	BIO5	-1,262	-	-
YNR067C	DSE4	-	-	-1,106
YNR068C		-	-	1,555
YNR069C	BSC5	-	-	1,823
YOL013W-A		-2,299	-2,895	-2,009
YOL014W		3,113	2,593	3,212
YOL015W	IRC10	-	-	1,609
YOL016C	CMK2	1,049	1,317	1,285
YOL022C	TSR4	1,425	-	-
YOL032W	OPI10	1,933	1,500	2,097
YOL038C-A		-	-	1,275
YOL038W	PRE6	-	-	1,103
YOL039W	RPP2A	-	-1,086	-1,361
YOL040C	RPS15	-	-	-1,274
YOL052C-A	DDR2	-	-1,110	-
YOL056W	GPM3	-	1,102	-
YOL058W	ARG1	-3,785	-4,824	-2,935
YOL064C	MET22	-2,117	-	-
YOL070C	NBA1	1,068	-	-
YOL077C	BRX1	1,658	-	-
YOL077W-A	ATP19	-	-	-1,014
YOL079W		1,219	-	-
YOL080C	REX4	1,204	-	-
YOL084W	PHM7	-2,307	-2,031	-1,529
YOL085C		-1,716	-	-
YOL085W-A		-1,448	-	-
YOL086C	ADH1	-	-1,106	-1,309
YOL087C	DUF1	-1,214	-	-
YOL101C	IZH4	1,694	1,721	2,202
YOL104C	NDJ1	1,696	1,346	1,562

Gene ID	Gene name	log2FC		
		45 min	120 min	200 min
YOL107W		-1,122	-1,515	-1,611
YOL109W	ZEO1	2,680	2,138	2,272
YOL110W	SHR5	-1,949	-1,245	-1,457
YOL119C	MCH4	-1,916	-1,647	-
YOL120C	RPL18A	-	-2,088	-2,541
YOL121C	RPS19A	-	-	-1,230
YOL123W	HRP1	-	1,149	1,031
YOL124C	TRM11	-1,545	-2,441	-2,807
YOL126C	MDH2	1,556	2,009	2,298
YOL127W	RPL25	-	-1,366	-1,842
YOL128C	YGK3	-1,707	-1,713	-1,169
YOL133W	HRT1	-	-	1,146
YOL134C		-	-	1,180
YOL135C	MED7	-	-1,108	-
YOL138C	RTC1	-1,340	-1,215	-1,177
YOL139C	CDC33	1,224	-	-
YOL140W	ARG8	-1,692	-2,751	-1,099
YOL143C	RIB4	1,889	2,022	2,079
YOL144W	NOP8	1,229	-	-
YOL156W	HXT11	-	-	1,175
YOL157C	IMA2	-	-	1,068
YOL158C	ENB1	-	-	1,419
YOL162W		-3,769	-1,242	-
YOL163W		-3,878	-1,300	-
YOL164W	BDS1	-3,613	-	-1,332
YOR004W	UTP23	-	-	-1,228
YOR007C	SGT2	1,248	1,161	1,349
YOR008C-A		-	-	-1,131
YOR008W-B		-1,444	-	-1,123
YOR010C	TIR2	-	1,237	1,248

Gene ID	Gene name	log2FC		
		45 min	120 min	200 min
YOR020C	HSP10	1,956	1,186	1,009
YOR021C	SFM1	1,072	-	-
YOR025W	HST3	-	-1,364	-1,379
YOR027W	STI1	2,332	1,728	2,237
YOR028C	CIN5	1,071	1,072	1,325
YOR032C	HMS1	-	1,313	1,697
YOR032W-A		-2,728	-	-
YOR034C	AKR2	-1,518	-	-1,026
YOR034C-A		-1,715	-	-1,040
YOR036W	PEP12	-	-	1,066
YOR037W	CYC2	-	-	1,014
YOR040W	GLO4	-1,896	-1,301	-1,327
YOR044W	IRC23	-1,525	-1,371	-1,063
YOR052C	TMC1	1,392	1,765	1,869
YOR057W	SGT1	-	-	1,069
YOR059C	LPL1	-	-	1,021
YOR063W	RPL3	-1,441	-2,044	-2,355
YOR064C	YNG1	-1,004	-1,293	-
YOR067C	ALG8	-1,024	-1,135	-1,414
YOR072W		-1,794	-1,261	-1,336
YOR073W	SGO1	-	-	-1,334
YOR073W-A		-	-	1,002
YOR077W	RTS2	-	-1,414	-1,348
YOR092W	ECM3	-1,435	-1,463	-1,507
YOR095C	RKI1	-	-	-1,069
YOR096W	RPS7A	-	-	-1,503
YOR107W	RGS2	-1,131	-1,163	-
YOR109W	INP53	-1,350	-	-1,134
YOR117W	RPT5	1,016	1,325	1,604
YOR128C	ADE2	-1,505	-	-

Gene ID	Gene name	log2FC		
		45 min	120 min	200 min
YOR130C	ORT1	-	-1,196	-
YOR134W	BAG7	-	-1,700	-1,090
YOR142W	LSC1	-1,357	-	-
YOR148C	SPP2	-1,031	-1,349	-
YOR158W	PET123	1,166	-	-
YOR161C	PNS1	-	-1,232	-
YOR161C-C		-	-1,578	-
YOR161W-A		-	-1,116	-
YOR161W-B		-1,090	-1,245	-
YOR167C	RPS28A	1,504	-	-
YOR170W		-	1,181	-
YOR171C	LCB4	-	1,018	-
YOR173W	DCS2	-1,339	-1,042	-
YOR180C	DCI1	-1,334	-	-
YOR182C	RPS30B	-	-	-1,363
YOR185C	GSP2	-1,426	-	-
YOR200W		-	-1,035	-1,045
YOR201C	MRM1	-	-1,082	-1,040
YOR202W	HIS3	-1,240	-	-
YOR208W	PTP2	1,148	1,448	1,418
YOR210W	RPB10	1,189	-	-
YOR221C	MCT1	1,272	1,036	1,434
YOR222W	ODC2	-1,860	-2,726	-2,141
YOR224C	RPB8	1,160	-	-
YOR232W	MGE1	1,167	1,086	-
YOR234C	RPL33B	-	-1,194	-1,908
YOR235W	IRC13	-	-1,860	-
YOR237W	HES1	-2,909	-2,439	-1,553
YOR244W	ESA1	1,180	1,077	-
YOR257W	CDC31	1,208	1,010	1,058

Gene ID	Gene name	log2FC		
		45 min	120 min	200 min
YOR259C	RPT4	1,031	1,138	1,479
YOR261C	RPN8	-	1,350	1,315
YOR272W	YTM1	1,145	-	-
YOR274W	MOD5	1,354	-	-
YOR283W		-	-1,317	-
YOR284W	HUA2	-1,746	-	-
YOR287C	RRP36	1,537	-	-
YOR289W		-1,067	-1,351	-1,275
YOR293W	RPS10A	-	-	-1,518
YOR294W	RRS1	1,168	-	-
YOR298W	MUM3	-2,140	-1,585	-
YOR301W	RAX1	-1,133	-1,219	-1,243
YOR302W		-1,238	-1,290	-
YOR303W	CPA1	-1,430	-1,403	-
YOR312C	RPL20B	-	-	-1,742
YOR313C	SPS4	-	-	1,024
YOR315W	SFG1	-	-	-1,054
YOR327C	SNC2	-	1,026	-
YOR339C	UBC11	-1,432	-1,642	-1,685
YOR340C	RPA43	1,197	-	-
YOR343C		-2,128	-1,045	-
YOR345C		-	-1,028	-1,247
YOR346W	REV1	-	-	-1,079
YOR348C	PUT4	-4,744	-3,806	-3,012
YOR354C	MSC6	1,052	-	-
YOR355W	GDS1	-	-	-1,086
YOR359W	VTS1	-	-1,080	-1,452
YOR362C	PRE10	-	-	1,156
YOR365C		1,175	1,273	1,475
YOR366W		1,209	-	-

Gene ID	Gene name	log2FC		
		45 min	120 min	200 min
YOR369C	RPS12	-	-	-1,364
YOR374W	ALD4	-1,368	-	-
YOR375C	GDH1	-1,139	-1,679	-2,058
YOR376W		-1,087	-	-
YOR376W-A		-	-	1,151
YOR385W		1,985	1,746	1,692
YOR386W	PHR1	-	-	1,240
YOR387C		-1,001	-	-
YOR388C	FDH1	-	-	1,250
YOR389W		-1,387	-	-
YOR391C	HSP33	-2,242	-1,835	-1,971
YPL001W	HAT1	-	-1,387	-
YPL003W	ULA1	-1,387	-1,127	-
YPL004C	LSP1	-	-	1,186
YPL006W	NCR1	-1,344	-	-
YPL014W	CIP1	-	1,532	1,645
YPL017C	IRC15	-1,749	-	-
YPL018W	CTF19	-1,307	-	-
YPL024W	RMI1	-1,731	-1,059	-1,536
YPL025C		-1,724	-2,000	-
YPL035C		-	-	1,036
YPL036W	PMA2	-1,856	-2,303	-1,314
YPL038W-A		-1,045	-	-
YPL042C	SSN3	-	-	-1,045
YPL054W	LEE1	-4,160	-1,509	-
YPL061W	ALD6	-	-1,457	-1,437
YPL062W		-1,925	-1,107	-
YPL067C		-1,015	-1,244	-1,353
YPL079W	RPL21B	-	-	-1,263
YPL081W	RPS9A	-1,224	-3,078	-3,354

Gene ID	Gene name	log2FC		
		45 min	120 min	200 min
YPL090C	RPS6A	-	-	-1,599
YPL092W	SSU1	-	-1,235	-
YPL096W	PNG1	-	-	1,060
YPL106C	SSE1	1,953	1,301	1,310
YPL120W	VPS30	1,030	1,154	-
YPL125W	KAP120	-1,495	-1,390	-1,475
YPL131W	RPL5	-	-1,127	-1,584
YPL133C	RDS2	-	-1,024	-
YPL142C		-	-	-1,113
YPL143W	RPL33A	-	-	-1,114
YPL144W	POC4	-1,411	-1,246	-1,158
YPL148C	PPT2	-1,444	-1,121	-
YPL152W	RRD2	-	-	1,131
YPL153C	RAD53	-	1,330	1,035
YPL155C	KIP2	-	-1,004	-1,092
YPL163C	SVS1	-1,356	-	-
YPL170W	DAP1	1,415	1,490	1,810
YPL179W	PPQ1	-1,116	-1,256	-1,141
YPL183C	RTT10	-	-	-1,067
YPL189C-A	COA2	1,429	1,029	1,045
YPL191C		-1,265	-1,117	-1,158
YPL196W	OXR1	-	-	1,225
YPL197C		-	-2,777	-3,383
YPL198W	RPL7B	-1,508	-3,378	-3,916
YPL201C	YIG1	-1,275	-	-
YPL211W	NIP7	1,486	-	-
YPL219W	PCL8	-1,155.	-1,059	-
YPL220W	RPL1A	1,023	-	-
YPL221W	FLC1	-1,820	-1,632	-2,003
YPL222C-A		-1,826	-1,033	-

Gene ID	Gene name	log2FC		
		45 min	120 min	200 min
YPL222W	FMP40	-1,927	-1,113	-
YPL223C	GRE1	-3,728	-1,129	-1,164
YPL226W	NEW1	-	-	-1,020
YPL231W	FAS2	-1,088	-1,954	-1,989
YPL233W	NSL1	-1,196	-1,055	-1,045
YPL240C	HSP82	2,724	2,360	2,533
YPL249C-A	RPL36B	-	-	-1,164
YPL250W-A		-	-	-1,162
YPL256C	CLN2	-1,109	-	-
YPL263C	KEL3	1,029	-	-
YPL264C		-1,258	-	-
YPL265W	DIP5	-2,618	-1,435	-1,149
YPL266W	DIM1	1,439	-	-
YPL267W	ACM1	-	1,017	1,010
YPL273W	SAM4	1,362	-	-
YPL274W	SAM3	-3,113	-1,711	-1,873
YPL275W		-1,014	-	-
YPL277C		-2,100	-1,136	-1,334
YPL278C		-2,363	-	-1,241
YPL280W	HSP32	-	-1,394	-1,441
YPR002W	PDH1	-2,180	-1,278	-1,782
YPR010C	RPA135	-	-	-1,187
YPR012W		-	-	1,354
YPR013C	CMR3	-	1,576	2,035
YPR014C		-	1,379	1,692
YPR026W	ATH1	-	-	1,144
YPR027C		-	1,152	1,320
YPR036W-A	SPO24	-	-	1,179
YPR043W	RPL43A	-	-	-1,082
YPR044C	OPI11	-	-	-1,079

Gene ID	Gene name	log2FC		
		45 min	120 min	200 min
YPR050C		-1,446	-1,309	-1,438
YPR051W	MAK3	-1,425	-1,307	-1,439
YPR052C	NHP6A	1,281	1,127	-
YPR053C		1,180	1,040	-
YPR054W	SMK1	-1,096	-	-
YPR064W		-1,869	-	-
YPR066W	UBA3	-1,437	-1,032	-
YPR068C	HOS1	-1,794	-1,471	-
YPR074W-A		-	-1,153	-
YPR080W	TEF1	-	-	-1,274
YPR096C		-	1,020	1,008
YPR101W	SNT309	-1,082	-1,223	-
YPR103W	PRE2	-	1,046	1,201
YPR112C	MRD1	1,069	-	-
YPR116W	RRG8	1,284	1,069	1,232
YPR119W	CLB2	-	-	-1,345
YPR123C		-	-	-1,013
YPR125W	YLH47	1,046	-	-
YPR132W	RPS23B	-	-1,255	-1,735
YPR137W	RRP9	1,021	-	-
YPR145C-A		1,500	-	1,231
YPR149W	NCE102	1,240	-	-
YPR150W		-	1,449	2,234
YPR151C	SUE1	-	1,451	2,236
YPR155C	NCA2	-1,255	-	-
YPR156C	TPO3	-	-1,005	-1,293
YPR157W	TDA6	2,044	2,259	2,797
YPR159W	KRE6	-1,830	-1,613	-1,713
YPR160W	GPH1	-	-	-1,130
YPR160W-A		-1,062	-1,206	-1,173

Gene ID	Gene name	log2FC		
		45 min	120 min	200 min
YPR161C	SGV1	1,040	-	-
YPR167C	MET16	-2,777	-1,014	-
YPR176C	BET2	-1,468	-1,049	-
YPR184W	GDB1	-1,313	-	-
YPR192W	AQY1	-1,053	-	-
YPR193C	HPA2	-	1,219	1,713
YPR194C	OPT2	-1,214	-	-
YPR195C		-1,074	-	-
YPR202W		-1,542	-	-
YPR204W		-2,008	-1,052	-1,287

Supplementary Table S2: Pathways enrichment of yeast cells treated with acetic acid.
List of pathways (Pathway) enriched by significant down and up-regulated genes at each time point. P-values (p-value) are also indicated.

Pathways associated to down-regulated DEGs						Pathways associated to up-regulated DEGs					
45 min		120 min		200 min		45 min		120 min		200 min	
Pathway	**p-value**	**Pathway**	**p-value**	**Pathway**	**p-value**	**Pathway**	**p-value**	**Pathway**	**p-value**	**Pathway**	**p-value**
Metabolism of amino acids and derivatives	1,17E-08	GTP hydrolysis and joining of the 60S ribosomal subunit	2,89E-33	GTP hydrolysis and joining of the 60S ribosomal subunit	6,74E-105	Cellular responses to stress	2,41E-06	Proteasome	1,88E-11	Proteasome	3,52E-24
Superpathway of sulfur amino acid biosynthesis	3,97E-08	Formation of a pool of free 40S subunits	2,89E-33	Formation of a pool of free 40S subunits	6,74E-105	Cellular responses to external stimuli	4,88E-06	Ub-specific processing proteases	3,81E-08	Ub-specific processing proteases	8,86E-15
Metabolism	1,30E-06	Nonsense Mediated Decay independent of the Exon Junction Complex	2,04E-31	Nonsense Mediated Decay independent of the Exon Junction Complex	7,12E-98			Deubiquitination	1,44E-07	Deubiquitination	9,85E-15
Sulfur metabolism	1,80E-06	Nonsense Mediated Decay enhanced by the Exon Junction Complex	1,13E-30	Nonsense Mediated Decay enhanced by the Exon Junction Complex	2,76E-95					Post-translational protein modification	3,62E-07
Alanine, aspartate and glutamate metabolism	2,84E-06	Nonsense-Mediated Decay	1,13E-30	Nonsense-Mediated Decay	2,76E-95					Protein processing in endoplasmic reticulum	9,01E-07
Arginine biosynthesis	7,35E-06	L13a-mediated translational silencing of Ceruloplasmin expression	1,01E-29	L13a-mediated translational silencing of Ceruloplasmin expression	4,09E-92						
		Cap-dependent Translation Initiation	2,26E-28	Ribosome	3,96E-90						
		Eukaryotic Translation Initiation	3,71E-28	Cap-dependent Translation Initiation	7,83E-88						
		Translation	1,63E-27	Eukaryotic Translation Initiation	3,64E-87						
		Ribosome	1,15E-26	Translation	4,61E-86						
		Metabolism of RNA	6,19E-18	Metabolism of RNA	4,51E-57						
		Formation of the ternary complex, and subsequently, the 43S complex	1,25E-09	Formation of the ternary complex, and subsequently, the 43S complex	7,51E-34						

	Metabolism of proteins	2,74E-09	Ribosomal scanning and start codon recognition	5,69E-31			
	Lysine biosynthesis	7,38E-09	Metabolism of proteins	8,61E-31			
	Ribosomal scanning and start codon recognition	8,46E-09					
	Metabolism of amino acids and derivatives	8,23E-08					
	Arginine biosynthesis	4,88E-07					
	Lysine biosynthesis	9,34E-07					
	Arginine biosynthesis	1,34E-06					

Supplementary Table S3: Ribosomal protein genes details and paralog couples expression trends in acetic acid treatments.
List of ribosomal protein genes (RPGs), their expression as log2CPM in the control and in the treatments at the three acetic acid exposure times (45 minutes, A) (120 minutes, B) and (200 minutes, C), and their classification in terms of paralogy relationships as obtained from Ghulam et al. (Paralog classification) are reported (Major and Minor paralogs). Paralogs not described by Ghulam et al. are indicated as "Not defined", indicating that there is no information confirming the assignment to a Major or a Minor paralog. RPGs with no paralogs are reported as "No paralog". Significant DEGs and their up or down-regulation are also indicated (up/down). The log2 of the mean of CPMs for the two control samples (log2CPM Control) and the two treated samples (log2CPM Treatment) are also shown. Genes with log2CPM Treated/Control Ratio >1 are marked by "yes". The two ratios between log2CPMs of couple of paralogs are shown in control and treatment samples (log2 CPM paralog ratio Control and log2 CPM paralog ratio Treatment, respectively) to show the ratio and indicate the shift among paralogs (Paralog couple shift = yes/not).

A

		45 minutes						
RPGs	**Paralog classification**	**Significant DEGs**	**log2 CPM Control**	**log2 CPM Treatment**	**log2 CPM Treated/Control Ratio >1**	**log2 CPM paralogs ratio Control**	**log2 CPM paralogs ratio Treatment**	**Paralog couple shift**
RPL4A	Major		9,338	8,713	No	1,011	1,097	No
RPL4B	Minor	Down	9,233	7,943	No			
RPL7A	Major		8,954	9,190	Yes	1,447	1,978	No
RPL7B	Minor	Down	6,189	4,646	No			
RPL8B	Major		9,294	9,640	Yes	1,280	1,366	No
RPL8A	Minor		7,263	7,059	No			
RPL9A	Major		8,166	8,218	Yes	1,231	1,079	No
RPL9B	Minor	Up	6,633	7,617	Yes			
RPL14A	Major		8,483	7,831	No	1,060	1,052	No
RPL14B	Minor		8,001	7,444	No			
RPL16B	Major		8,714	8,445	No	1,097	1,206	No
RPL16A	Minor		7,943	7,004	No			
RPL17A	Major		8,792	8,595	No	1,060	1,001	No
RPL17B	Minor		8,293	8,586	Yes			
RPL21A	Major		8,281	7,997	No	1,011	0,978	**Yes**
RPL21B	Minor		8,194	8,177	No			
RPL22A	Major		7,993	7,860	No	1,500	2,338	No
RPL22B	Minor	Down	5,328	3,363	No			
RPL24A	Major		8,779	8,527	No	0,999	0,904	No
RPL24B	Minor		8,787	9,436	Yes			

RPGs	Paralog classification	Significant DEGs	log2 CPM Control	log2 CPM Treatment	log2 CPM Treated/Control Ratio >1	log2 CPM paralogs ratio Control	log2 CPM paralogs ratio Treatment	Paralog couple shift
RPL26B	Major		8,204	8,682	Yes	1,029	1,218	No
RPL26A	Minor		7,974	7,131	No			
RPL31A	Major		9,007	9,097	Yes	1,086	1,275	No
RPL31B	Minor	Down	8,297	7,137	No			
RPL33A	Major		8,234	8,549	Yes	1,208	1,401	No
RPL33B	Minor		6,816	6,103	No			
RPL36B	Major		9,535	10,111	Yes	1,429	1,602	No
RPL36A	Minor		6,672	6,312	No			
RPL37A	Major		7,362	7,043	No	0,855	0,766	No
RPL37B	Minor		8,614	9,192	Yes			
RPS1B	Major		9,137	8,564	No	1,022	0,936	**Yes**
RPS1A	Minor		8,939	9,147	Yes			
RPS7A	Major		8,319	8,249	No	1,035	1,201	No
RPS7B	Minor	Down	8,037	6,868	No			
RPS9B	Major		8,691	8,765	Yes	1,549	2,013	No
RPS9A	Minor	Down	5,612	4,355	No			
RPS21B	Major		8,136	8,701	Yes	1,002	0,994	**Yes**
RPS21A	Minor		8,118	8,756	Yes			
RPS28A	Major	Up	8,188	9,659	Yes	1,159	1,420	No
RPS28B	Minor		7,062	6,803	No			
RPL6A	Equal		8,357	7,812	No	1,108	1,047	No
RPL6B	Equal		7,543	7,464	No			
RPL34A	Equal		8,121	7,505	No	0,975	0,899	No
RPL34B	Equal		8,325	8,348	Yes			
RPS29A	Equal		7,077	7,581	Yes	0,893	0,962	No
RPS29B	Equal		7,927	7,877	No			
RPL1A	Not defined	Up	7,612	8,603	Yes	0,884	1,144	Yes
RPL1B	Not defined	Down	8,611	7,522	No			
RPL2A	Not defined		9,486	8,765	No	0,935	0,927	No
RPL2B	Not defined		10,143	9,457	No			
RPL11A	Not defined		7,823	8,202	Yes	0,970	1,050	Yes
RPL11B	Not defined		8,066	7,814	No			
RPL12A	Not defined		8,256	7,730	No	0,990	0,974	No
RPL12B	Not defined		8,341	7,933	No			

RPGs	Paralog classification	Significant DEGs	log2 CPM Control	log2 CPM Treatment	log2 CPM Treated/Control Ratio >1	log2 CPM paralogs ratio Control	log2 CPM paralogs ratio Treatment	Paralog couple shift
RPL13A	Not defined		8,520	8,060	No	0,984	0,944	No
RPL13B	Not defined		8,659	8,540	No			
RPL15A	Not defined	Down	10,418	8,705	No	1,634	1,676	No
RPL15B	Not defined	Down	6,377	5,193	No			
RPL18A	Not defined		8,883	8,111	No	1,206	1,575	No
RPL18B	Not defined	Down	7,369	5,151	No			
RPL19A	Not defined		9,255	9,080	No	1,012	1,043	No
RPL19B	Not defined		9,143	8,709	No			
RPL20A	Not defined		7,999	8,081	Yes	1,010	1,054	No
RPL20B	Not defined		7,920	7,668	No			
RPL23A	Not defined		7,910	8,676	Yes	0,892	1,076	Yes
RPL23B	Not defined		8,864	8,062	No			
RPL27A	Not defined		8,982	8,522	No	1,117	1,205	No
RPL27B	Not defined		8,039	7,069	No			
RPL35A	Not defined		8,658	8,704	Yes	1,153	1,183	No
RPL35B	Not defined		7,508	7,359	No			
RPL40A	Not defined		8,073	8,119	Yes	1,019	1,054	No
RPL40B	Not defined		7,922	7,699	No			
RPL41A	Not defined	Up	8,895	10,009	Yes	1,061	1,050	No
RPL41B	Not defined	Up	8,384	9,534	Yes			
RPL42A	Not defined		7,794	7,642	No	0,935	0,923	No
RPL42B	Not defined		8,334	8,278	No			
RPL43A	Not defined		8,944	9,223	Yes	1,112	1,155	No
RPL43B	Not defined		8,040	7,984	No			
RPP2A	Not defined		8,723	8,664	No	0,943	0,905	No
RPP2B	Not defined		9,253	9,577	Yes			
RPS0A	Not defined		8,908	8,756	No	0,998	1,025	Yes
RPS0B	Not defined		8,925	8,541	No			
RPS4A	Not defined		9,512	9,136	No	1,076	1,073	No
RPS4B	Not defined		8,836	8,513	No			
RPS6A	Not defined		8,931	8,857	No	1,102	1,124	No
RPS6B	Not defined		8,101	7,883	No			
RPS8A	Not defined		8,556	9,059	Yes	1,146	1,189	No
RPS8B	Not defined		7,466	7,619	Yes			

RPGs	Paralog classification	Significant DEGs	log2 CPM Control	log2 CPM Treatment	log2 CPM Treated/Control Ratio >1	log2 CPM paralogs ratio Control	log2 CPM paralogs ratio Treatment	Paralog couple shift
RPS10A	Not defined		8,432	8,530	Yes	1,156	1,126	No
RPS10B	Not defined		7,293	7,577	Yes			
RPS11A	Not defined		8,382	7,903	No	0,958	0,871	No
RPS11B	Not defined		8,747	9,078	Yes			
RPS14A	Not defined		9,278	9,640	Yes	1,285	1,751	No
RPS14B	Not defined	Down	7,219	5,506	No			
RPS16A	Not defined		8,261	8,051	No	0,971	1,041	Yes
RPS16B	Not defined		8,510	7,736	No			
RPS17A	Not defined		8,485	8,484	No	1,094	1,051	No
RPS17B	Not defined		7,756	8,072	Yes			
RPS18A	Not defined		8,784	9,130	Yes	1,031	1,168	No
RPS18B	Not defined		8,517	7,819	No			
RPS19A	Not defined		8,655	8,442	No	0,918	0,890	No
RPS19B	Not defined		9,431	9,486	Yes			
RPS22A	Not defined		8,321	8,346	Yes	1,699	1,709	No
RPS22B	Not defined		4,897	4,883	No			
RPS23A	Not defined		9,233	8,767	No	0,984	0,941	No
RPS23B	Not defined		9,381	9,317	No			
RPS24A	Not defined		8,887	9,031	Yes	1,118	1,277	No
RPS24B	Not defined		7,945	7,072	No			
RPS25A	Not defined		8,406	9,160	Yes	1,106	1,203	No
RPS25B	Not defined		7,598	7,614	Yes			
RPS26A	Not defined		8,800	9,259	Yes	1,058	1,108	No
RPS26B	Not defined		8,314	8,359	Yes			
RPS27A	Not defined		7,216	6,879	No	0,987	0,902	No
RPS27B	Not defined		7,312	7,627	Yes			
RPS30A	Not defined	Up	8,419	9,486	Yes	1,172	1,267	No
RPS30B	Not defined		7,183	7,487	Yes			
RPL3	No paralog	Down	11,318	9,843	No			
RPL5	No paralog		10,064	9,844	No			
RPL10	No paralog		10,698	10,135	No			
RPL25	No paralog		8,880	8,787	No			
RPL28	No paralog		9,828	9,527	No			
RPL29	No paralog		8,305	8,642	Yes			

RPGs	Paralog classification	Significant DEGs	log2 CPM Control	log2 CPM Treatment	log2 CPM Treated/Control Ratio >1	log2 CPM paralogs ratio Control	log2 CPM paralogs ratio Treatment	Paralog couple shift
RPL30	No paralog		8,979	9,141	Yes			
RPL32	No paralog		9,361	9,333	No			
RPL38	No paralog		8,426	9,011	Yes			
RPL39	No paralog		8,313	8,834	Yes			
RPP0	No paralog		9,508	9,737	Yes			
RPP1A	No paralog		8,388	8,978	Yes			
RPP1B	No paralog		8,705	9,314	Yes			
RPS2	No paralog		9,946	9,807	No			
RPS3	No paralog		9,498	8,608	No			
RPS5	No paralog		10,068	9,731	No			
RPS12	No paralog		9,098	9,803	Yes			
RPS13	No paralog		8,812	8,331	No			
RPS15	No paralog		9,279	9,315	Yes			
RPS20	No paralog		8,879	9,157	Yes			
RPS31	No paralog		9,950	9,652	No			

B

		120 minutes							
RPGs	**Paralog classification**	**log2 CPM Control**	**log2 CPM Treatment**	**log2 CPM Treated/Control Ratio >1**	**Significant Changes**	**Minor paralog more expressed than major paralog**	**log2 CPM Major/Minor Ratio Control**	**log2 CPM Major/Minor Ratio Treated**	**Paralog couple shifting**
RPL4A	Major	9,629	9,001	No	No	No	1,005	1,116	No
RPL4B	Minor	9,580	8,066	No	Down	No			
RPL7A	Major	9,715	9,060	No	No	No	1,224	1,906	No
RPL7B	Minor	7,936	4,753	No	Down	No			
RPL8B	Major	10,051	9,362	No	No	No	1,078	1,333	No
RPL8A	Minor	9,325	7,024	No	Down	No			
RPL9A	Major	8,885	8,029	No	Down	No	1,012	1,043	No
RPL9B	Minor	8,776	7,699	No	Down	No			
RPL14A	Major	9,146	7,984	No	Down	No	1,095	1,061	No
RPL14B	Minor	8,356	7,526	No	Down	No			
RPL16B	Major	9,248	8,356	No	Down	No	1,101	1,170	No
RPL16A	Minor	8,404	7,143	No	Down	No			
RPL17A	Major	9,142	8,510	No	No	No	1,056	1,020	No
RPL17B	Minor	8,656	8,342	No	No	No			
RPL21A	Major	8,737	7,706	No	Down	No	1,034	0,955	**Yes**
RPL21B	Minor	8,453	8,069	No	No	Yes			
RPL22A	Major	8,492	7,636	No	Down	No	1,570	2,153	No
RPL22B	Minor	5,410	3,547	No	Down	No			
RPL24A	Major	9,302	8,187	No	Down	No	0,996	0,926	No
RPL24B	Minor	9,338	8,839	No	No	Yes			
RPL26B	Major	8,686	8,308	No	No	No	1,046	1,207	No
RPL26A	Minor	8,301	6,884	No	Down	No			
RPL31A	Major	9,322	8,638	No	No	No	1,041	1,240	No
RPL31B	Minor	8,955	6,967	No	Down	No			
RPL33A	Major	8,558	8,274	No	No	No	1,248	1,413	No
RPL33B	Minor	6,855	5,857	No	Down	No			
RPL36B	Major	10,174	9,635	No	No	No	1,442	1,519	No
RPL36A	Minor	7,057	6,345	No	No	No			
RPL37A	Major	7,754	6,930	No	Down	No	0,871	0,789	No
RPL37B	Minor	8,904	8,780	No	No	Yes			

RPGs	Paralog classification	log2 CPM Control	log2 CPM Treatment	log2 CPM Treated/Control Ratio >1	Significant Changes	Minor paralog more expressed than major paralog	log2 CPM Major/Minor Ratio Control	log2 CPM Major/Minor Ratio Treated	Paralog couple shifting
RPS1B	Major	9,583	8,465	No	Down	No	1,020	0,926	**Yes**
RPS1A	Minor	9,398	9,141	No	No	Yes			
RPS7A	Major	8,676	8,027	No	No	No	1,043	1,190	No
RPS7B	Minor	8,321	6,747	No	Down	No			
RPS9B	Major	9,507	8,564	No	Down	No	1,251	1,817	No
RPS9A	Minor	7,597	4,714	No	Down	No			
RPS21B	Major	8,706	8,223	No	No	No	0,988	0,964	**Yes**
RPS21A	Minor	8,815	8,527	No	No	Yes			
RPS28A	Major	8,593	9,372	Yes	No	No	1,147	1,334	No
RPS28B	Minor	7,492	7,026	No	No	No			
RPL6A	Equal	9,007	7,800	No	Down	Equal	1,098	1,027	No
RPL6B	Equal	8,203	7,595	No	No	Equal			
RPL34A	Equal	8,509	7,292	No	Down	Equal	0,971	0,908	No
RPL34B	Equal	8,766	8,034	No	No	Equal			
RPS29A	Equal	7,644	7,134	No	No	Equal	0,914	0,931	No
RPS29B	Equal	8,367	7,662	No	No	Equal			
RPL1A	Not defined	8,046	8,457	Yes	No	Not defined	0,883	1,090	Yes
RPL1B	Not defined	9,110	7,756	No	Down	Not defined			
RPL2A	Not defined	9,698	8,304	No	Down	Not defined	0,920	0,894	No
RPL2B	Not defined	10,546	9,291	No	Down	Not defined			
RPL11A	Not defined	8,465	8,182	No	No	Not defined	0,999	1,054	Yes
RPL11B	Not defined	8,473	7,760	No	No	Not defined			
RPL12A	Not defined	9,004	7,726	No	Down	Not defined	1,028	0,995	Yes
RPL12B	Not defined	8,757	7,763	No	Down	Not defined			
RPL13A	Not defined	9,033	8,220	No	Down	Not defined	0,969	0,977	No
RPL13B	Not defined	9,325	8,409	No	Down	Not defined			
RPL15A	Not defined	11,529	8,708	No	Down	Not defined	1,760	1,633	No
RPL15B	Not defined	6,552	5,331	No	Down	Not defined			
RPL18A	Not defined	9,542	7,647	No	Down	Not defined	1,283	1,510	No
RPL18B	Not defined	7,435	5,063	No	Down	Not defined			
RPL19A	Not defined	9,585	8,684	No	Down	Not defined	1,001	1,023	No
RPL19B	Not defined	9,573	8,485	No	Down	Not defined			

RPGs	Paralog classification	log2 CPM Control	log2 CPM Treatment	log2 CPM Treated/Control Ratio >1	Significant Changes	Minor paralog more expressed than major paralog	log2 CPM Major/Minor Ratio Control	log2 CPM Major/Minor Ratio Treated	Paralog couple shifting
RPL20A	Not defined	8,520	8,010	No	No	Not defined	1,011	1,042	No
RPL20B	Not defined	8,429	7,690	No	No	Not defined			
RPL23A	Not defined	8,402	8,515	Yes	No	Not defined	0,889	1,072	Yes
RPL23B	Not defined	9,450	7,944	No	Down	Not defined			
RPL27A	Not defined	9,441	8,535	No	Down	Not defined	1,136	1,199	No
RPL27B	Not defined	8,311	7,116	No	Down	Not defined			
RPL35A	Not defined	9,232	8,658	No	No	Not defined	1,139	1,151	No
RPL35B	Not defined	8,106	7,524	No	No	Not defined			
RPL40A	Not defined	8,628	7,847	No	No	Not defined	1,026	1,026	No
RPL40B	Not defined	8,409	7,651	No	No	Not defined			
RPL41A	Not defined	9,962	10,335	Yes	No	Not defined	1,056	1,136	No
RPL41B	Not defined	9,431	9,101	No	No	Not defined			
RPL42A	Not defined	8,064	7,338	No	No	Not defined	0,938	0,930	No
RPL42B	Not defined	8,593	7,890	No	No	Not defined			
RPL43A	Not defined	9,412	8,923	No	No	Not defined	1,083	1,129	No
RPL43B	Not defined	8,689	7,901	No	No	Not defined			
RPP2A	Not defined	9,181	8,290	No	Down	Not defined	0,955	0,907	No
RPP2B	Not defined	9,614	9,139	No	No	Not defined			
RPS0A	Not defined	9,437	8,438	No	Down	Not defined	1,030	1,000	Yes
RPS0B	Not defined	9,160	8,441	No	No	Not defined			
RPS4A	Not defined	9,981	9,036	No	Down	Not defined	1,089	1,082	No
RPS4B	Not defined	9,162	8,354	No	No	Not defined			
RPS6A	Not defined	9,475	8,715	No	No	Not defined	1,084	1,104	No
RPS6B	Not defined	8,742	7,890	No	Down	Not defined			
RPS8A	Not defined	9,209	8,980	No	No	Not defined	1,131	1,167	No
RPS8B	Not defined	8,145	7,694	No	No	Not defined			
RPS10A	Not defined	9,108	8,320	No	No	Not defined	1,165	1,123	No
RPS10B	Not defined	7,819	7,410	No	No	Not defined			
RPS11A	Not defined	8,795	7,879	No	Down	Not defined	0,942	0,888	No
RPS11B	Not defined	9,338	8,874	No	No	Not defined			
RPS14A	Not defined	10,008	9,540	No	No	Not defined	1,311	1,744	No
RPS14B	Not defined	7,631	5,471	No	Down	Not defined			

RPGs	Paralog classification	log2 CPM Control	log2 CPM Treatment	log2 CPM Treated/Control Ratio >1	Significant Changes	Minor paralog more expressed than major paralog	log2 CPM Major/Minor Ratio Control	log2 CPM Major/Minor Ratio Treated	Paralog couple shifting
RPS16A	Not defined	8,742	7,942	No	No	Not defined	0,973	1,044	Yes
RPS16B	Not defined	8,983	7,610	No	Down	Not defined			
RPS17A	Not defined	8,967	8,362	No	No	Not defined	1,042	1,024	No
RPS17B	Not defined	8,605	8,166	No	No	Not defined			
RPS18A	Not defined	9,355	8,869	No	No	Not defined	1,052	1,144	No
RPS18B	Not defined	8,893	7,751	No	Down	Not defined			
RPS19A	Not defined	8,996	8,385	No	No	Not defined	0,912	0,909	No
RPS19B	Not defined	9,869	9,225	No	No	Not defined			
RPS22A	Not defined	8,830	8,275	No	No	Not defined	1,672	1,625	No
RPS22B	Not defined	5,281	5,094	No	No	Not defined			
RPS23A	Not defined	9,487	8,669	No	Down	Not defined	0,938	0,959	No
RPS23B	Not defined	10,109	9,043	No	Down	Not defined			
RPS24A	Not defined	9,167	8,757	No	No	Not defined	1,108	1,249	No
RPS24B	Not defined	8,277	7,014	No	Down	Not defined			
RPS25A	Not defined	9,045	8,608	No	No	Not defined	1,135	1,190	No
RPS25B	Not defined	7,972	7,234	No	No	Not defined			
RPS26A	Not defined	9,022	8,628	No	No	Not defined	1,014	1,040	No
RPS26B	Not defined	8,894	8,300	No	No	Not defined			
RPS27A	Not defined	7,391	6,963	No	No	Not defined	0,988	0,955	No
RPS27B	Not defined	7,481	7,288	No	No	Not defined			
RPS30A	Not defined	8,739	9,264	Yes	No	Not defined	1,150	1,314	No
RPS30B	Not defined	7,598	7,051	No	No	Not defined			
RPL3	No paralog	11,784	9,938	No	Down	No paralog			
RPL5	No paralog	10,525	9,593	No	Down	No paralog			
RPL10	No paralog	10,988	10,278	No	No	No paralog			
RPL25	No paralog	9,546	8,373	No	Down	No paralog			
RPL28	No paralog	10,091	9,205	No	Down	No paralog			
RPL29	No paralog	8,833	8,069	No	No	No paralog			
RPL30	No paralog	9,893	9,121	No	No	No paralog			
RPL32	No paralog	9,840	8,921	No	Down	No paralog			
RPL38	No paralog	8,885	8,942	Yes	No	No paralog			
RPL39	No paralog	8,559	8,227	No	No	No paralog			
RPP0	No paralog	10,274	9,802	No	No	No paralog			
RPP1A	No paralog	9,097	8,819	No	No	No paralog			

RPGs	Paralog classification	log2 CPM Control	log2 CPM Treatment	log2 CPM Treated/Control Ratio >1	Significant Changes	Minor paralog more expressed than major paralog	log2 CPM Major/Minor Ratio Control	log2 CPM Major/Minor Ratio Treated	Paralog couple shifting
RPP1B	No paralog	9,270	9,059	No	No	No paralog			
RPS2	No paralog	10,480	9,570	No	Down	No paralog			
RPS3	No paralog	10,244	8,666	No	Down	No paralog			
RPS5	No paralog	10,598	9,380	No	Down	No paralog			
RPS12	No paralog	9,701	9,496	No	No	No paralog			
RPS13	No paralog	9,240	8,201	No	Down	No paralog			
RPS15	No paralog	9,876	9,159	No	No	No paralog			
RPS20	No paralog	9,457	8,993	No	No	No paralog			
RPS31	No paralog	10,781	9,504	No	Down	No paralog			

C

		200 minutes							
RPGs	**Paralog classification**	**log2 CPM Control**	**log2 CPM Treatment**	**log2 CPM Treated/Control Ratio >1**	**Significant changes**	**Minor paralog more expressed than major paralog**	**log2 CPM Major/Minor Ratio Control**	**log2 CPM Major/Minor Ratio Treated**	**Paralog couple shifting**
RPL4A	Major	9,663	9,058	No	No	No	1,003	1,115	No
RPL4B	Minor	9,638	8,122	No	Down	No			
RPL7A	Major	10,037	9,075	No	Down	No	1,221	1,968	No
RPL7B	Minor	8,218	4,611	No	Down	No			
RPL8B	Major	10,580	9,331	No	Down	No	1,118	1,338	No
RPL8A	Minor	9,465	6,973	No	Down	No			
RPL9A	Major	9,426	7,923	No	Down	No	1,051	1,031	No
RPL9B	Minor	8,966	7,683	No	Down	No			
RPL14A	Major	9,370	7,902	No	Down	No	1,097	1,060	No
RPL14B	Minor	8,541	7,458	No	Down	No			
RPL16B	Major	9,628	8,308	No	Down	No	1,094	1,180	No
RPL16A	Minor	8,803	7,040	No	Down	No			
RPL17A	Major	9,365	8,511	No	Down	No	1,040	1,026	No
RPL17B	Minor	9,004	8,294	No	Down	No			
RPL21A	Major	9,256	7,739	No	Down	No	1,038	0,971	**Yes**
RPL21B	Minor	8,916	7,970	No	Down	Yes			
RPL22A	Major	9,284	7,536	No	Down	No	1,527	2,129	No
RPL22B	Minor	6,078	3,539	No	Down	No			
RPL24A	Major	9,678	8,142	No	Down	No	0,991	0,929	No
RPL24B	Minor	9,766	8,760	No	Down	Yes			
RPL26B	Major	9,119	8,202	No	Down	No	1,048	1,184	No
RPL26A	Minor	8,704	6,926	No	Down	No			
RPL31A	Major	9,767	8,633	No	Down	No	1,068	1,226	No
RPL31B	Minor	9,148	7,044	No	Down	No			
RPL33A	Major	8,975	8,172	No	Down	No	1,219	1,417	No
RPL33B	Minor	7,364	5,768	No	Down	No			
RPL36B	Major	10,527	9,665	No	Down	No	1,438	1,539	No
RPL36A	Minor	7,318	6,279	No	Down	No			
RPL37A	Major	8,141	6,874	No	Down	No	0,879	0,784	No
RPL37B	Minor	9,257	8,765	No	No	Yes			

RPGs	Paralog classification	log2 CPM Control	log2 CPM Treatment	log2 CPM Treated/Control Ratio >1	Significant changes	Minor paralog more expressed than major paralog	log2 CPM Major/Minor Ratio Control	log2 CPM Major/Minor Ratio Treated	Paralog couple shifting
RPS1B	Major	10,060	8,432	No	Down	No	1,012	0,931	**Yes**
RPS1A	Minor	9,939	9,059	No	Down	Yes			
RPS7A	Major	9,128	7,935	No	Down	No	1,060	1,188	No
RPS7B	Minor	8,607	6,678	No	Down	No			
RPS9B	Major	10,046	8,496	No	Down	No	1,311	1,843	No
RPS9A	Minor	7,662	4,609	No	Down	No			
RPS21B	Major	9,202	8,046	No	Down	No	0,990	0,955	**Yes**
RPS21A	Minor	9,291	8,422	No	Down	Yes			
RPS28A	Major	9,088	9,258	Yes	No	No	1,176	1,319	No
RPS28B	Minor	7,728	7,017	No	Down	No			
RPL6A	Equal	9,222	7,823	No	Down	Equal	1,073	1,032	No
RPL6B	Equal	8,596	7,579	No	Down	Equal			
RPL34A	Equal	8,669	7,382	No	Down	Equal	0,954	0,927	No
RPL34B	Equal	9,087	7,962	No	Down	Equal			
RPS29A	Equal	8,135	7,103	No	Down	Equal	0,936	0,933	No
RPS29B	Equal	8,695	7,615	No	Down	Equal			
RPL1A	Not defined	8,571	8,327	No	No	Not defined	0,915	1,089	Yes
RPL1B	Not defined	9,368	7,649	No	Down	Not defined			
RPL2A	Not defined	10,215	8,305	No	Down	Not defined	0,941	0,900	No
RPL2B	Not defined	10,860	9,231	No	Down	Not defined			
RPL11A	Not defined	8,690	8,161	No	No	Not defined	0,984	1,047	Yes
RPL11B	Not defined	8,835	7,795	No	Down	Not defined			
RPL12A	Not defined	9,326	7,673	No	Down	Not defined	1,026	0,986	Yes
RPL12B	Not defined	9,086	7,778	No	Down	Not defined			
RPL13A	Not defined	9,199	8,230	No	Down	Not defined	0,948	0,992	No
RPL13B	Not defined	9,706	8,297	No	Down	Not defined			
RPL15A	Not defined	11,463	8,639	No	Down	Not defined	1,941	1,569	No
RPL15B	Not defined	5,906	5,506	No	No	Not defined			
RPL18A	Not defined	9,876	7,646	No	Down	Not defined	1,317	1,492	No
RPL18B	Not defined	7,496	5,123	No	Down	Not defined			
RPL19A	Not defined	9,801	8,758	No	Down	Not defined	0,988	1,031	Yes
RPL19B	Not defined	9,917	8,497	No	Down	Not defined			

RPGs	Paralog classification	log2 CPM Control	log2 CPM Treatment	log2 CPM Treated/Control Ratio >1	Significant changes	Minor paralog more expressed than major paralog	log2 CPM Major/Minor Ratio Control	log2 CPM Major/Minor Ratio Treated	Paralog couple shifting
RPL20A	Not defined	8,909	7,990	No	Down	Not defined	0,994	1,060	Yes
RPL20B	Not defined	8,965	7,536	No	Down	Not defined			
RPL23A	Not defined	8,782	8,392	No	No	Not defined	0,908	1,060	Yes
RPL23B	Not defined	9,676	7,920	No	Down	Not defined			
RPL27A	Not defined	9,856	8,409	No	Down	Not defined	1,149	1,187	No
RPL27B	Not defined	8,580	7,084	No	Down	Not defined			
RPL35A	Not defined	9,329	8,643	No	No	Not defined	1,120	1,155	No
RPL35B	Not defined	8,330	7,480	No	Down	Not defined			
RPL40A	Not defined	8,941	7,738	No	Down	Not defined	1,017	1,018	No
RPL40B	Not defined	8,795	7,599	No	Down	Not defined			
RPL41A	Not defined	10,220	10,248	Yes	No	Not defined	1,069	1,183	No
RPL41B	Not defined	9,564	8,663	No	Down	Not defined			
RPL42A	Not defined	8,636	7,230	No	Down	Not defined	0,949	0,931	No
RPL42B	Not defined	9,102	7,768	No	Down	Not defined			
RPL43A	Not defined	9,682	8,912	No	Down	Not defined	1,052	1,145	No
RPL43B	Not defined	9,202	7,781	No	Down	Not defined			
RPP2A	Not defined	9,363	8,314	No	Down	Not defined	0,942	0,917	No
RPP2B	Not defined	9,934	9,065	No	Down	Not defined			
RPS0A	Not defined	9,908	8,341	No	Down	Not defined	1,020	0,991	Yes
RPS0B	Not defined	9,717	8,421	No	Down	Not defined			
RPS4A	Not defined	10,404	8,968	No	Down	Not defined	1,071	1,084	No
RPS4B	Not defined	9,716	8,277	No	Down	Not defined			
RPS6A	Not defined	9,922	8,629	No	Down	Not defined	1,086	1,102	No
RPS6B	Not defined	9,133	7,828	No	Down	Not defined			
RPS8A	Not defined	9,614	8,952	No	No	Not defined	1,118	1,173	No
RPS8B	Not defined	8,602	7,628	No	Down	Not defined			
RPS10A	Not defined	9,489	8,277	No	Down	Not defined	1,159	1,136	No
RPS10B	Not defined	8,188	7,285	No	Down	Not defined			
RPS11A	Not defined	9,205	7,905	No	Down	Not defined	0,950	0,895	No
RPS11B	Not defined	9,693	8,833	No	Down	Not defined			
RPS14A	Not defined	10,260	9,553	No	Down	Not defined	1,355	1,756	No
RPS14B	Not defined	7,570	5,440	No	Down	Not defined			

RPGs	Paralog classification	log2 CPM Control	log2 CPM Treatment	log2 CPM Treated/Control Ratio >1	Significant changes	Minor paralog more expressed than major paralog	log2 CPM Major/Minor Ratio Control	log2 CPM Major/Minor Ratio Treated	Paralog couple shifting
RPS16A	Not defined	9,049	7,867	No	Down	Not defined	0,972	1,027	Yes
RPS16B	Not defined	9,309	7,662	No	Down	Not defined			
RPS17A	Not defined	9,268	8,257	No	Down	Not defined	1,026	1,026	No
RPS17B	Not defined	9,029	8,051	No	Down	Not defined			
RPS18A	Not defined	9,663	8,799	No	Down	Not defined	1,033	1,150	No
RPS18B	Not defined	9,352	7,649	No	Down	Not defined			
RPS19A	Not defined	9,288	8,365	No	Down	Not defined	0,909	0,919	No
RPS19B	Not defined	10,212	9,106	No	Down	Not defined			
RPS22A	Not defined	9,228	8,188	No	Down	Not defined	1,290	1,622	No
RPS22B	Not defined	7,154	5,049	No	Down	Not defined			
RPS23A	Not defined	9,948	8,651	No	Down	Not defined	0,956	0,964	No
RPS23B	Not defined	10,409	8,974	No	Down	Not defined			
RPS24A	Not defined	9,597	8,672	No	Down	Not defined	1,102	1,244	No
RPS24B	Not defined	8,705	6,973	No	Down	Not defined			
RPS25A	Not defined	9,399	8,481	No	Down	Not defined	1,135	1,168	No
RPS25B	Not defined	8,278	7,261	No	Down	Not defined			
RPS26A	Not defined	9,453	8,569	No	Down	Not defined	1,001	1,035	No
RPS26B	Not defined	9,440	8,279	No	Down	Not defined			
RPS27A	Not defined	7,821	6,910	No	Down	Not defined	0,991	0,958	No
RPS27B	Not defined	7,894	7,212	No	No	Not defined			
RPS30A	Not defined	9,064	9,168	Yes	No	Not defined	1,129	1,314	No
RPS30B	Not defined	8,029	6,975	No	Down	Not defined			
RPL3	No paralog	11,986	9,945	No	Down	No paralog			
RPL5	No paralog	10,920	9,652	No	Down	No paralog			
RPL10	No paralog	11,213	10,203	No	Down	No paralog			
RPL25	No paralog	9,794	8,262	No	Down	No paralog			
RPL28	No paralog	10,287	9,099	No	Down	No paralog			
RPL29	No paralog	9,205	7,964	No	Down	No paralog			
RPL30	No paralog	10,174	9,114	No	Down	No paralog			
RPL32	No paralog	10,286	8,896	No	Down	No paralog			
RPL38	No paralog	9,460	8,897	No	No	No paralog			
RPL39	No paralog	8,996	8,128	No	Down	No paralog			
RPP0	No paralog	10,659	9,752	No	Down	No paralog			
RPP1A	No paralog	9,437	8,748	No	No	No paralog			

RPGs	Paralog classification	log2 CPM Control	log2 CPM Treatment	log2 CPM Treated/Control Ratio >1	Significant changes	Minor paralog more expressed than major paralog	log2 CPM Major/Minor Ratio Control	log2 CPM Major/Minor Ratio Treated	Paralog couple shifting
RPP1B	No paralog	9,616	8,992	No	No	No paralog			
RPS2	No paralog	11,041	9,467	No	Down	No paralog			
RPS3	No paralog	10,632	8,603	No	Down	No paralog			
RPS5	No paralog	11,093	9,367	No	Down	No paralog			
RPS12	No paralog	10,352	9,302	No	Down	No paralog			
RPS13	No paralog	9,580	8,119	No	Down	No paralog			
RPS15	No paralog	10,122	9,158	No	Down	No paralog			
RPS20	No paralog	9,895	8,882	No	Down	No paralog			
RPS31	No paralog	11,118	9,392	No	Down	No paralog			

Supplementary Table S4: Programmed cell death induced by acetic acid specific ohnologs replacement.
List of ohnologs (ohnologs 1 and ohnologs 2) and their expression as log2CPM in control and in treatments at the three exposure times (45 minutes, A), (120 minutes, B) and (200 minutes, C) are reported. The log2 of the mean of CPMs for the two control samples (log2CPM untreated cells) and the two treated samples (log2CPM treated cells) are also shown. The two ratios between log2CPMs of couple of ohnologs are shown in control and treatment samples (log2 CPM paralog ratio Control and log2 CPM paralog ratio Treatment, respectively) to show the ratio and indicate the shift among paralogs (Ratio changed).

A

Acetic acid 45 minutes

Ohnolog 1		LOG2 CPM		Ohnolog 2		LOG2 CPM		RATIO ohnologs			Differential expression	
Gene ID	**Gene name**	**untreated cells at 45 min**	**treated cells at 45 min**	**Gene ID**	**Gene name**	**untreated cells at 45 min**	**treated cells at 45 min**	**Ratio Ohnolog1/Ohnolog2 control**	**Ratio Ohnolog1/Ohnolog2 treated**	**Ratio changed**	**Ohnolog 1 DEGs**	**Ohnolog 2 DEGs**
YBR148W	YSW1	4,456570814	2,684427593	YOL091W	SPO21	3,419985325	3,163415509	1,303096473	0,848585203	Yes	-1,737	-
YJR115W		5,382714055	4,92668276	YBL043W	ECM13	5,893878365	4,323151288	0,913271995	1,139604523	Yes	-	-1,538
YNL225C	CNM67	5,676297649	4,910413252	YDL239C	ADY3	6,482629847	4,006247581	0,875616499	1,225688915	Yes	-	-2,445
YNL058C		6,597015131	8,497130637	YIL117C	PRM5	6,619177163	7,869161997	0,996651845	1,079801209	Yes	1,933	1,283
YKR095W	MLP1	8,229798977	8,462763602	YIL149C	MLP2	7,637960886	8,643203624	1,0774864	0,979123479	Yes	-	1,038
YOL089C	HAL9	5,590782001	5,059995515	YBR150C	TBS1	5,199620585	5,555277854	1,075228838	0,910844722	Yes	-	-
YNL278W	CAF120	7,263382632	5,627299038	YLR187W	SKG3	6,791666164	5,633834531	1,069455191	0,998839957	Yes	-1,601	-1,124
YLR046C		4,140686298	3,584828001	YGR213C	RTA1	4,284154922	3,395290861	0,966511803	1,055823536	Yes	-	-
YMR310C		5,161779274	6,108297486	YGR283C		5,7894264	6,10014512	0,891587338	1,001336422	Yes	-	-
YIL045W	PIG2	5,012085911	5,423343409	YER054C	GIP2	5,296278621	5,281972119	0,946341057	1,026764869	Yes	-	-
YMR016C	SOK2	7,47339973	6,683257796	YKL043W	PHD1	6,318789537	8,41235816	1,182726484	0,794457115	Yes	-	2,126
YHR080C	LAM4	7,065936856	6,397391089	YDR326C	YSP2	6,853514131	7,017220404	1,030994716	0,911670251	Yes	-	-
YKR034W	DAL80	7,301333178	4,820826948	YJL110C	GZF3	6,538625317	6,052514857	1,116646516	0,796499812	Yes	-2,446	-
YDL175C	AIR2	4,877765622	3,915556634	YIL079C	AIR1	4,688720404	5,235229985	1,040319149	0,747924474	Yes	-	-
YKL027W	TCD2	6,245917115	6,021352002	YHR003C	TCD1	6,182437585	6,360622009	1,010267719	0,946660876	Yes	-	-
YNL194C		4,135070887	4,088857718	YDL222C	FMP45	5,872890358	3,188303018	0,704094685	1,282455806	Yes	-	-2,648
YAR042W	SWH1	7,393144604	8,382714117	YDL019C	OSH2	8,143167867	7,435228601	0,907895395	1,127431928	Yes	1,024	-
YLR096W	KIN2	6,848768209	7,632727867	YDR122W	KIN1	7,843335352	7,418600007	0,873195892	1,028863648	Yes	-	-
YNR048W		5,098537676	4,339550925	YCR094W	CDC50	4,898154901	4,951372982	1,040909848	0,876433858	Yes	-	-

Gene ID	Gene name	untreated cells at 45 min	treated cells at 45 min	Gene ID	Gene name	untreated cells at 45 min	treated cells at 45 min	Ratio Ohnolog1/Ohnolog2 control	Ratio Ohnolog1/Ohnolog2 treated	Ratio changed	Ohnolog 1 DEGs	Ohnolog 2 DEGs
YPR157W	TDA6	3,445410377	5,460190347	YGR141W	VPS62	6,430872333	4,808169836	0,535760967	1,135606797	Yes	2,044	-1,589
YHR033W		6,114363024	4,393916554	YDR300C	PRO1	5,439172363	6,505020395	1,124134816	0,675465454	Yes	-1,684	1,097
YLL062C	MHT1	7,749181503	3,572098818	YPL273W	SAM4	6,134448981	7,463479612	1,263223727	0,478610381	Yes	-4,142	1,362
YKR018C		7,735728113	7,923006397	YJL082W	IML2	7,939471624	7,052758768	0,9743379	1,123391095	Yes	-	-
YDR009W	GAL3	3,586673697	2,56864299	YBR020W	GAL1	3,356367921	4,012243923	1,06861756	0,640201104	Yes	-	-
YPR138C	MEP3	6,868940423	6,214591166	YGR121C	MEP1	7,140983883	5,795660912	0,961903925	1,072283431	Yes	-	-1,311
YLR432W	IMD3	8,456597838	7,462571922	YML056C	IMD4	7,130264673	7,824616672	1,186014577	0,953730034	Yes	-	-
YDL192W	ARF1	7,794687062	8,249138767	YDL137W	ARF2	8,367930812	8,123965724	0,931495161	1,015407874	Yes	-	-
YNL074C	MLF3	7,472918461	7,89312234	YIL135C	VHS2	7,497581913	7,572381419	0,996710479	1,042356678	Yes	-	-
YHR056C	RSC30	6,020262618	5,325791982	YDR303C	RSC3	5,767083606	5,671666897	1,043900701	0,939017061	Yes	-	-
YGL222C	EDC1	6,201079448	6,675275122	YER035W	EDC2	6,458538271	5,620827559	0,960136673	1,187596498	Yes	-	-
YOR028C	CIN5	4,071771469	5,107895362	YDR259C	YAP6	4,922801578	4,59316385	0,82712484	1,112064696	Yes	1,071	-
YLR353W	BUD8	5,639806481	5,1302876	YGR041W	BUD9	6,225850319	4,895785567	0,90586927	1,047898755	Yes	-	-1,296
YOR295W	UAF30	4,298933232	3,999539997	YMR233W	TRI1	4,278785988	4,515031088	1,004708636	0,885827787	Yes	-	-
YPL053C	KTR6	7,849237757	7,876187742	YDR483W	KRE2	7,950482071	7,387373106	0,987265638	1,066168938	Yes	-	-
YNL004W	HRB1	8,022858111	7,841465874	YCL011C	GBP2	8,561855845	7,327718809	0,937046624	1,070110095	Yes	-	-1,201
YOR280C	FSH3	5,480472385	5,484904887	YMR222C	FSH2	5,383507946	5,596071443	1,018011386	0,980134893	Yes	-	-
YLR375W	STP3	7,600605194	6,710377794	YDL048C	STP4	6,574971405	7,487594245	1,155990608	0,896199443	Yes	-	-
YOR171C	LCB4	6,649632584	7,401059404	YLR260W	LCB5	6,547592729	7,785353312	1,015584331	0,950638861	Yes	-	1,271
YJL026W	RNR2	8,156046478	8,741814382	YGR180C	RNR4	8,103780358	9,26976009	1,006449597	0,943046454	Yes	-	1,199
YIL006W	YIA6	4,763285269	5,071785327	YEL006W	YEA6	5,657904979	4,884946416	0,841881454	1,038247894	Yes	-	-
YMR279C		4,416161146	4,294739955	YML116W	ATR1	5,938026036	4,143564767	0,74370862	1,036484331	Yes	-	-1,761
YOR299W	BUD7	6,977242812	6,576806521	YMR237W	BCH1	7,000528659	6,285119088	0,996673702	1,046409213	Yes	-	-
YNL116W	DMA2	6,172325451	6,657618612	YHR115C	DMA1	6,264658472	5,131657474	0,985261284	1,297362235	Yes	-	-1,097
YGL056C	SDS23	7,767899337	7,248336652	YBR214W	SDS24	7,500632451	8,394799593	1,03563258	0,863431768	Yes	-	-
YER089C	PTC2	8,223684732	6,944244929	YBL056W	PTC3	8,06127387	7,832384822	1,020147047	0,886606709	Yes	-1,245	-
YDR516C	EMI2	7,211987183	8,716967445	YCL040W	GLK1	10,26508575	8,565611253	0,70257447	1,017670215	Yes	1,539	-1,665
YDR046C	BAP3	7,640733776	6,884765566	YBR068C	BAP2	7,204378896	7,773257511	1,060568008	0,885698892	Yes	-	-
YPR111W	DBF20	5,380673669	5,164044343	YGR092W	DBF2	6,251733869	5,104823679	0,860669021	1,011600923	Yes	-	-1,112
YMR120C	ADE17	9,971509222	6,626397933	YLR028C	ADE16	8,862224369	8,564314846	1,125170026	0,773721897	Yes	-3,312	-
YIL074C	SER33	10,21626005	6,7047905	YER081W	SER3	8,89430561	7,279830613	1,148629302	0,921009136	Yes	-3,477	-1,582

Gene ID	Gene name	untreated cells at 45 min	treated cells at 45 min	Gene ID	Gene name	untreated cells at 45 min	treated cells at 45 min	Ratio Ohnolog1/Ohnolog2 control	Ratio Ohnolog1/Ohnolog2 treated	Ratio changed	Ohnolog 1 DEGs	Ohnolog 2 DEGs
YLR048W	RPS0B	8,925478671	8,540808938	YGR214W	RPS0A	8,907742546	8,75615471	1,001991091	0,975406354	Yes	-	-
YKR057W	RPS21A	8,11793691	8,756224398	YJL136C	RPS21B	8,135581707	8,700555044	0,997831157	1,006398368	Yes	-	-
YPR102C	RPL11A	7,823268739	8,20240027	YGR085C	RPL11B	8,065724013	7,814088467	0,969940048	1,049693807	Yes	-	-
YER117W	RPL23B	8,863701575	8,062095743	YBL087C	RPL23A	7,909635548	8,675577638	1,120620732	0,929286335	Yes	-	-

B

Acetic acid 120 minutes

Ohnolog 1		LOG2 CPM		Ohnolog 2		LOG2 CPM		RATIO ohnologs			Differential expression	
Gene ID	Gene name	untreated cells at 120 min	treated cells at 120 min	Gene ID	Gene name	untreated cells at 120 min	treated cells at 120 min	Ratio Ohnolog1/Ohnolog2 control	Ratio Ohnolog1/Ohnolog2 treated	Ratio changed	Ohnolog 1 DEGs	Ohnolog 2 DEGs
YBR148W	YSW1	4,681859751	2,965281112	YOL091W	SPO21	3,494075039	3,489100479	1,339942531	0,849869796	Yes	-1,913	-
YNR044W	AGA1	5,080552407	6,955959197	YCR089W	FIG2	5,18902554	5,925851298	0,979095664	1,173832897	Yes	1,676	-
YJR115W		5,12523751	4,952879716	YBL043W	ECM13	6,041560021	4,724249193	0,848330148	1,048395102	Yes	-	-1,514
YJL048C	UBX6	7,547963805	7,4941657	YBR273C	UBX7	6,998877227	7,84941942	1,078453523	0,954741402	Yes	-	-
YOL089C	HAL9	5,572086869	5,274496017	YBR150C	TBS1	5,292199961	6,081517339	1,052886684	0,867299347	Yes	-	-
YLR046C		4,106967727	3,897212091	YGR213C	RTA1	4,140586432	3,516693495	0,99188069	1,108203515	Yes	-	-
YMR310C		5,784821211	6,38920703	YGR283C		6,254336921	6,307141144	0,924929578	1,013011582	Yes	-	-
YIL045W	PIG2	4,670057377	5,682873177	YER054C	GIP2	4,802742759	5,458839179	0,972372998	1,041040593	Yes	-	-
YMR016C	SOK2	7,13363973	6,690370839	YKL043W	PHD1	5,82696721	8,296924675	1,224245731	0,806367552	Yes	-	2,278
YDR522C	SPS2	1,694963818	2,666985971	YCL048W	SPS22	1,718304298	2,048533601	0,986416562	1,301900037	Yes	-	-
YKL027W	TCD2	6,565460698	6,092373607	YHR003C	TCD1	6,308583862	6,546928515	1,040718621	0,930569746	Yes	-	-
YNL020C	ARK1	5,545010211	5,700048878	YIL095W	PRK1	5,245783062	5,742272988	1,057041465	0,992646795	Yes	-	-
YNL194C		4,009278461	4,15881417	YDL222C	FMP45	5,421417841	3,698963665	0,739525818	1,124318741	Yes	-	-1,919
YLR177W		6,165228313	7,06142017	YDR505C	PSP1	6,901523325	7,027990298	0,893314131	1,004756676	Yes	-	-
YAR042W	SWH1	7,254244317	8,502960096	YDL019C	OSH2	7,606428198	7,516563744	0,953699178	1,131229693	Yes	1,054	-
YLR096W	KIN2	6,671935034	7,802032039	YDR122W	KIN1	7,06883597	7,584945018	0,943852009	1,028620777	Yes	-	-
YNR048W		5,397907915	4,722339128	YCR094W	CDC50	5,054757083	5,339912547	1,067886711	0,884347653	Yes	-	-
YPR157W	TDA6	3,315665925	5,771813318	YGR141W	VPS62	6,298002452	4,797380621	0,526463105	1,203117654	Yes	2,259	-1,696
YHR033W		6,799974024	4,797258909	YDR300C	PRO1	6,16979297	6,686248326	1,102139741	0,717481415	Yes	-2,200	-
YPR154W	PIN3	7,315868208	7,533028244	YGR136W	LSB1	7,136581554	8,069320082	1,025122203	0,933539402	Yes	-	-
YKR018C		7,351561385	8,097850551	YJL082W	IML2	7,978665337	7,187414824	0,921402399	1,12667082	Yes	-	-
YOR120W	GCY1	7,096122907	6,436549785	YDR368W	YPR1	6,759712765	7,283333931	1,049766928	0,88373674	Yes	-	-
YPR058W	YMC1	6,273105007	5,685832777	YBR104W	YMC2	6,256025735	6,046097066	1,002730051	0,940413744	Yes	-	-
YPR138C	MEP3	7,133711106	6,357548626	YGR121C	MEP1	7,944933775	5,812521297	0,897894345	1,093767799	Yes	-	-2,325
YLR432W	IMD3	8,112835706	7,58276697	YML056C	IMD4	7,41779317	7,959664148	1,093699368	0,95264911	Yes	-	-

Gene ID	Gene name	untreated cells at 120 min	treated cells at 120 min	Gene ID	Gene name	untreated cells at 120 min	treated cells at 120 min	Ratio Ohnolog1/Ohnolog2 control	Ratio Ohnolog1/Ohnolog2 treated	Ratio changed	Ohnolog 1 DEGs	Ohnolog 2 DEGs
YLR180W	SAM1	9,923070767	8,769735568	YDR502C	SAM2	10,06639796	7,946116583	0,985761819	1,103650503	Yes	-1,351	-2,316
YDL192W	ARF1	7,965130713	8,387481531	YDL137W	ARF2	8,123696099	8,218296615	0,980481128	1,020586373	Yes	-	-
YHR056C	RSC30	6,065350229	5,523261544	YDR303C	RSC3	5,436667496	5,840916545	1,115637517	0,945615556	Yes	-	-
YGL222C	EDC1	6,113086417	6,815814221	YER035W	EDC2	6,354860064	5,791561666	0,961954528	1,176852568	Yes	-	-
YOR028C	CIN5	3,907204081	5,179594828	YDR259C	YAP6	4,367738666	5,015640928	0,89455995	1,032688524	Yes	1,072	-
YPL077C		3,810042794	4,372365441	YBR197C		5,527229073	4,357905297	0,689322397	1,003318141	Yes	-	-1,364
YLR131C	ACE2	6,651300181	6,394930016	YDR146C	SWI5	7,026673466	5,898001661	0,946578806	1,084253682	Yes	-	-1,326
YML034W	SRC1	6,933104164	6,838177374	YDR458C	HEH2	6,419182376	6,973965572	1,080060319	0,98052927	Yes	-	-
YPL219W	PCL8	5,647286992	4,782302135	YGL134W	PCL10	4,978768529	4,847813755	1,134273859	0,986486358	Yes	-1,059	-
YKR100C	SKG1	6,007998946	6,472182874	YIL158W	AIM20	6,058317801	5,181860892	0,991694253	1,249007453	Yes	-	-1,069
YPL053C	KTR6	7,701760742	8,044956368	YDR483W	KRE2	7,910133934	7,43688267	0,973657438	1,081764595	Yes	-	-
YNL004W	HRB1	8,286183169	7,869342138	YCL011C	GBP2	8,494522125	7,529125044	0,975473728	1,045186803	Yes	-	-1,159
YLR375W	STP3	7,699114295	7,038191578	YDL048C	STP4	6,544170054	7,757817945	1,176484448	0,90723856	Yes	-	1,017
YJL026W	RNR2	8,099180813	8,775074955	YGR180C	RNR4	7,779514541	9,336160598	1,041090774	0,939901886	Yes	-	1,354
YIL006W	YIA6	4,450136718	5,377023271	YEL006W	YEA6	5,404066957	5,281443882	0,823479197	1,018097208	Yes	-	-
YMR279C		3,911571259	4,538306734	YML116W	ATR1	5,469313762	4,43789998	0,715185017	1,022624835	Yes	-	-1,228
YBR037C	SCO1	5,667713898	5,506034023	YBR024W	SCO2	5,36949304	5,760996796	1,055539854	0,955743289	Yes	-	-
YGL056C	SDS23	8,29247574	7,470408611	YBR214W	SDS24	7,561538631	8,657684074	1,096665129	0,862864543	Yes	-1,022	-
YOR092W	ECM3	6,114727997	4,846959629	YNL095C		4,918494777	4,858169287	1,243211241	0,997692617	Yes	-1,463	-
YER089C	PTC2	8,250239254	7,052328229	YBL056W	PTC3	7,601321496	7,972568808	1,085369071	0,884574144	Yes	-1,395	-
YKL203C	TOR2	6,524196971	6,728895785	YJR066W	TOR1	6,486682449	7,048660375	1,005783314	0,9546347	Yes	-	-
YDR516C	EMI2	7,407471039	8,804100139	YCL040W	GLK1	10,13825093	8,616762631	0,730645857	1,021741055	Yes	1,198	-1,717
YPR111W	DBF20	5,407962549	5,426915981	YGR092W	DBF2	6,68035303	5,296589399	0,809532449	1,024605755	Yes	-	-1,580
YML085C	TUB1	8,313725243	8,286903063	YML124C	TUB3	7,626731044	8,490519349	1,09007715	0,976018394	Yes	-	-
YLR048W	RPS0B	9,160461833	8,440595986	YGR214W	RPS0A	9,43739954	8,438269286	0,970655295	1,000275732	Yes	-	-1,186
YPR102C	RPL11A	8,464914472	8,18234138	YGR085C	RPL11B	8,47325135	7,76048263	0,999016095	1,05435986	Yes	-	-
YNL333W	SNZ2	3,30585944	3,152248876	YFL059W	SNZ3	2,777580092	3,178424217	1,190194101	0,99176468	Yes	-	-
YER117W	RPL23B	9,450246868	7,944157167	YBL087C	RPL23A	8,401590098	8,514944656	1,124816464	0,932966389	Yes	-1,697	-
YEL054C	RPL12A	9,003865603	7,726095728	YDR418W	RPL12B	8,756537589	7,762762259	1,028244955	0,995276613	Yes	-1,472	-1,190

C

Acetic acid 200 minutes

Ohnolog 1		LOG2 CPM		Ohnolog 2		LOG2 CPM		RATIO ohnologs			Differential expression	
Gene ID	Gene name	untreated cells at 200 min	treated cells at 200 min	Gene ID	Gene name	untreated cells at 200 min	treated cells at 200 min	Ratio Ohnolog1/Ohnolog2 control	Ratio Ohnolog1/Ohnolog2 treated	Ratio changed	Ohnolog 1 DEGs	Ohnolog 2 DEGs
YBR148W	YSW1	3,713827864	2,965294133	YOL091W	SPO21	3,143905771	3,344725392	1,181278363	0,886558322	Yes	-1,060	-
YNR044W	AGA1	4,747119563	7,04340882	YCR089W	FIG2	4,764157818	6,023939577	0,996423659	1,1692363	Yes	1,983	-
YJR115W		4,296244078	5,190065013	YBL043W	ECM13	5,727370192	4,674773433	0,750125089	1,11022814	Yes	-	-1,367
YKR058W	GLG1	4,659774166	5,382758513	YJL137C	GLG2	4,697519861	3,500737075	0,991964761	1,537607194	Yes	-	-1,501
YJL048C	UBX6	7,689562217	7,638726651	YBR273C	UBX7	6,84526166	7,963223383	1,123340874	0,95925058	Yes	-	-
YOL089C	HAL9	5,539681787	5,375749186	YBR150C	TBS1	4,750855961	5,818588522	1,166038674	0,923892309	Yes	-	-
YMR310C		5,726682795	6,369938385	YGR283C		6,027071567	6,241722112	0,950160079	1,020541811	Yes	-	-
YMR016C	SOK2	7,236028625	6,826589026	YKL043W	PHD1	5,898546477	8,343711612	1,226747751	0,818171737	Yes	-	2,137
YOR338W		6,2518202	5,870962386	YAL034C	FUN19	5,633638935	7,224709166	1,109730367	0,812622661	Yes	-	1,290
YKL027W	TCD2	6,91248803	6,184948683	YHR003C	TCD1	6,309028287	6,58062754	1,095650188	0,93987217	Yes	-1,039	-
YNL194C		4,023671629	4,590175549	YDL222C	FMP45	5,240581561	3,872616825	0,767791052	1,185290401	Yes	-	-1,685
YLR177W		5,627024381	7,198888877	YDR505C	PSP1	6,930331754	7,00976374	0,811941561	1,026980244	Yes	1,262	-
YLR096W	KIN2	6,754382969	7,785300089	YDR122W	KIN1	6,922444889	7,582676789	0,975722173	1,026721869	Yes	-	-
YNR048W		5,015061239	4,712351422	YCR094W	CDC50	4,842369074	5,285952868	1,035662743	0,891485706	Yes	-	-
YPR157W	TDA6	2,619516129	5,738688741	YGR141W	VPS62	5,789728488	4,938218247	0,452441964	1,162097026	Yes	2,797	-1,156
YHR033W		6,927888728	4,758686608	YDR300C	PRO1	6,16868729	6,696811138	1,123073419	0,710589937	Yes	-2,485	-
YKR018C		7,087219075	8,206750268	YJL082W	IML2	8,050900807	7,417844137	0,880301378	1,106352482	Yes	-	-
YOR120W	GCY1	6,648387165	6,719436917	YDR368W	YPR1	6,495690493	7,249253814	1,023507381	0,926914285	Yes	-	-
YDR009W	GAL3	3,01667111	2,771987261	YBR020W	GAL1	2,906176319	4,19062925	1,038020677	0,661472799	Yes	-	-
YPR138C	MEP3	7,148782172	6,511845697	YGR121C	MEP1	7,779875812	5,922927799	0,918881271	1,0994302	Yes	-	-2,164
YLR258W	GSY2	7,656670569	7,646013412	YFR015C	GSY1	5,319135388	7,74921438	1,439457733	0,986682396	Yes	-	2,111
YLR432W	IMD3	8,368469109	7,548305187	YML056C	IMD4	7,831375436	7,887732591	1,068582291	0,956967684	Yes	-1,132	-
YLR180W	SAM1	10,2294222	8,699519271	YDR502C	SAM2	11,02250882	7,963888066	0,928048448	1,092370862	Yes	-1,847	-3,374
YHR056C	RSC30	5,515723336	5,506155899	YDR303C	RSC3	5,406093543	5,724612406	1,02027893	0,961839075	Yes	-	-
YGL222C	EDC1	5,526502439	6,993526955	YER035W	EDC2	5,824765546	5,841986576	0,948793972	1,19711452	Yes	1,167	-
YOR028C	CIN5	3,5990107	5,231410315	YDR259C	YAP6	4,154977145	4,978234548	0,866192659	1,050856536	Yes	1,325	-

Gene ID	Gene name	untreated cells at 200 min	treated cells at 200 min	Gene ID	Gene name	untreated cells at 200 min	treated cells at 200 min	Ratio Ohnolog1/Ohnolog2 control	Ratio Ohnolog1/Ohnolog2 treated	Ratio changed	Ohnolog 1 DEGs	Ohnolog 2 DEGs
YLR131C	ACE2	6,759545931	6,452213469	YDR146C	SWI5	7,31598354	5,949851717	0,923942201	1,084432651	Yes	-	-1,670
YGL021W	ALK1	6,533586045	5,121731084	YBL009W	ALK2	5,394968791	5,659166304	1,211051685	0,905032793	Yes	-1,715	-
YML034W	SRC1	6,754349711	6,831012005	YDR458C	HEH2	6,407615652	7,027720695	1,054112805	0,972009603	Yes	-	-
YPL219W	PCL8	5,243082824	4,880657643	YGL134W	PCL10	4,443798156	4,930693784	1,179865205	0,989852109	Yes	-	-
YKR100C	SKG1	6,085915258	6,45909777	YIL158W	AIM20	6,145944697	5,151266321	0,990232675	1,253885427	Yes	-	-1,301
YPL053C	KTR6	7,347945547	8,068354621	YDR483W	KRE2	7,878139301	7,536256927	0,932700637	1,070605036	Yes	-	-
YNL004W	HRB1	7,949624553	8,025219367	YCL011C	GBP2	8,373204641	7,522676244	0,949412429	1,066803769	Yes	-	-1,158
YGL224C	SDT1	5,31692526	4,821572722	YER037W	PHM8	5,490197096	4,098310838	0,968439778	1,176478045	Yes	-	-1,700
YLR375W	STP3	7,241287162	7,068450705	YDL048C	STP4	6,49267474	8,04458572	1,115301082	0,878659381	Yes	-	1,236
YJL026W	RNR2	8,400335518	8,802600407	YGR180C	RNR4	8,02906419	9,352424569	1,046240922	0,941210522	Yes	-	1,009
YIL006W	YIA6	4,172700549	5,32786571	YEL006W	YEA6	5,37950959	5,267073344	0,775665603	1,011541963	Yes	-	-
YMR279C		3,911560664	4,434086627	YML116W	ATR1	4,81465078	4,336886476	0,812428739	1,022412427	Yes	-	-
YBR037C	SCO1	5,585275647	5,487662996	YBR024W	SCO2	5,360416082	5,813779128	1,041948155	0,943906343	Yes	-	-
YNL116W	DMA2	5,803721262	6,907292653	YHR115C	DMA1	5,834654529	5,437171697	0,994698355	1,270383397	Yes	-	-
YGL056C	SDS23	7,964242415	7,512762287	YBR214W	SDS24	6,985364351	8,821765594	1,140132714	0,85161663	Yes	-	1,524
YOR092W	ECM3	6,066596202	4,865798926	YNL095C		4,576825914	4,891194854	1,325502939	0,994807827	Yes	-1,507	-
YER089C	PTC2	8,17016351	7,164027121	YBL056W	PTC3	7,783940556	8,039321346	1,049617922	0,891123369	Yes	-1,315	-
YDR516C	EMI2	6,845559814	8,998954294	YCL040W	GLK1	9,43279956	8,670499969	0,725718783	1,037881821	Yes	1,838	-1,077
YDR046C	BAP3	8,298699632	7,121652051	YBR068C	BAP2	8,058869567	8,102104853	1,029759765	0,87898789	Yes	-1,482	-
YPR111W	DBF20	5,038805583	5,468386465	YGR092W	DBF2	6,644377104	5,37425606	0,758356352	1,017515058	Yes	-	-1,577
YML085C	TUB1	8,246742492	8,267198441	YML124C	TUB3	7,658662689	8,484662995	1,076786226	0,974369689	Yes	-	-
YLR048W	RPS0B	9,716660508	8,421289914	YGR214W	RPS0A	9,907525498	8,341361346	0,980735352	1,009582197	Yes	-1,608	-1,876
YOR312C	RPL20B	8,96498097	7,535693436	YMR242C	RPL20A	8,909169551	7,989850496	1,006264492	0,943158253	Yes	-1,742	-1,230
YPR102C	RPL11A	8,689578179	8,16120053	YGR085C	RPL11B	8,835060836	7,79521193	0,983533486	1,046950436	Yes	-	-1,349
YER117W	RPL23B	9,675577176	7,919686522	YBL087C	RPL23A	8,782043111	8,392311158	1,101745579	0,943683614	Yes	-2,064	-
YBR084C-A	RPL19A	9,800560586	8,757829903	YBL027W	RPL19B	9,917258328	8,496723585	0,988232863	1,030730236	Yes	-1,349	-1,734
YEL054C	RPL12A	9,326264287	7,672892642	YDR418W	RPL12B	9,086247404	7,777955442	1,026415403	0,986492234	Yes	-1,963	-1,624

Supplementary Table S5: Gene ontology enrichment of WGCNA modules related to programmed cell death.
List of GOs enriched at a FDR less than 0.01 per WGCNA modules identified in treatments and controls. Modules, GO ID, GO Term, p-value and FDR are indicated.

Treatments				
Module	**GO ID**	**GO Term**	**p-Value**	**FDR**
blue	GO:0001775	cell activation	2,57E-21	1,53E-17
blue	GO:0006955	immune response	6,23E-21	3,60E-17
blue	GO:0002376	immune system process	7,90E-17	3,53E-13
blue	GO:0045321	leukocyte activation	7,92E-17	3,53E-13
blue	GO:0002252	immune effector process	1,45E-16	6,29E-13
blue	GO:0002366	leukocyte activation involved in immune response	2,51E-16	1,05E-12
blue	GO:0002263	cell activation involved in immune response	4,42E-16	1,82E-12
blue	GO:0046903	secretion	2,47E-12	7,00E-09
blue	GO:0002275	myeloid cell activation involved in immune response	3,58E-12	9,92E-09
blue	GO:0071944	cell periphery	5,07E-12	1,38E-08
blue	GO:0043299	leukocyte degranulation	5,15E-12	1,39E-08
blue	GO:0032940	secretion by cell	5,42E-12	1,45E-08
blue	GO:0002443	leukocyte mediated immunity	6,54E-12	1,69E-08
blue	GO:0005886	plasma membrane	6,73E-12	1,73E-08
blue	GO:0002274	myeloid leukocyte activation	7,65E-12	1,96E-08
blue	GO:0002444	myeloid leukocyte mediated immunity	1,20E-11	2,97E-08
blue	GO:0050776	regulation of immune response	2,18E-11	5,34E-08
blue	GO:0002757	immune response-activating signal transduction	2,21E-11	5,37E-08
blue	GO:0043312	neutrophil degranulation	2,61E-11	6,29E-08
blue	GO:0002682	regulation of immune system process	2,99E-11	7,16E-08
blue	GO:0002446	neutrophil mediated immunity	3,06E-11	7,28E-08
blue	GO:0002283	neutrophil activation involved in immune response	3,11E-11	7,36E-08
blue	GO:0042119	neutrophil activation	4,39E-11	1,02E-07
blue	GO:0099503	secretory vesicle	7,04E-11	1,61E-07
blue	GO:0036230	granulocyte activation	8,61E-11	1,96E-07
blue	GO:0002764	immune response-regulating signaling pathway	1,26E-10	2,77E-07

Module	GO ID	GO Term	p-Value	FDR
blue	GO:0030141	secretory granule	2,81E-10	5,93E-07
blue	GO:0045055	regulated exocytosis	3,71E-10	7,75E-07
blue	GO:0002253	activation of immune response	5,71E-10	1,17E-06
blue	GO:0050896	response to stimulus	7,67E-10	1,55E-06
blue	GO:0002684	positive regulation of immune system process	1,59E-09	3,09E-06
blue	GO:0002429	immune response-activating cell surface receptor signaling pathway	1,64E-09	3,18E-06
blue	GO:0002250	adaptive immune response	2,14E-09	4,00E-06
blue	GO:0044433	cytoplasmic vesicle part	3,10E-09	5,65E-06
blue	GO:0002768	immune response-regulating cell surface receptor signaling pathway	4,66E-09	8,34E-06
blue	GO:0031410	cytoplasmic vesicle	8,68E-09	1,48E-05
blue	GO:0097708	intracellular vesicle	1,00E-08	1,69E-05
blue	GO:0006887	exocytosis	1,38E-08	2,25E-05
blue	GO:0042110	T cell activation	1,55E-08	2,49E-05
blue	GO:0023052	signaling	2,11E-08	3,38E-05
blue	GO:0050778	positive regulation of immune response	2,57E-08	4,07E-05
blue	GO:0007154	cell communication	4,34E-08	6,74E-05
blue	GO:0019221	cytokine-mediated signaling pathway	4,45E-08	6,87E-05
blue	GO:0050817	coagulation	4,46E-08	6,87E-05
blue	GO:0098657	import into cell	5,02E-08	7,66E-05
blue	GO:0046632	alpha-beta T cell differentiation	5,58E-08	8,48E-05
blue	GO:0043367	CD4-positive, alpha-beta T cell differentiation	8,52E-08	0,000126
blue	GO:0004888	transmembrane signaling receptor activity	8,53E-08	0,000126
blue	GO:0002433	immune response-regulating cell surface receptor signaling pathway involved in phagocytosis	1,01E-07	0,000145
blue	GO:0038094	Fc-gamma receptor signaling pathway	1,01E-07	0,000145
blue	GO:0038096	Fc-gamma receptor signaling pathway involved in phagocytosis	1,01E-07	0,000145
blue	GO:0046631	alpha-beta T cell activation	1,01E-07	0,000145
blue	GO:0007596	blood coagulation	1,26E-07	0,000175
blue	GO:0046649	lymphocyte activation	1,46E-07	0,000202
blue	GO:0007165	signal transduction	1,48E-07	0,000203
blue	GO:0002431	Fc receptor mediated stimulatory signaling pathway	1,48E-07	0,000203
blue	GO:0006897	endocytosis	1,63E-07	0,00022
blue	GO:0007599	hemostasis	1,97E-07	0,000261

Module	GO ID	GO Term	p-Value	FDR
blue	GO:0007166	cell surface receptor signaling pathway	1,98E-07	0,000261
blue	GO:0034097	response to cytokine	2,21E-07	0,00029
blue	GO:0050878	regulation of body fluid levels	2,33E-07	0,000305
blue	GO:0000323	lytic vacuole	2,58E-07	0,000333
blue	GO:0005764	lysosome	2,58E-07	0,000333
blue	GO:0016192	vesicle-mediated transport	2,84E-07	0,000361
blue	GO:0031982	vesicle	3,47E-07	0,000435
blue	GO:0030098	lymphocyte differentiation	3,67E-07	0,000454
blue	GO:0035710	CD4-positive, alpha-beta T cell activation	3,98E-07	0,000491
blue	GO:0006909	phagocytosis	4,31E-07	0,000527
blue	GO:0044459	plasma membrane part	5,00E-07	0,000595
blue	GO:0065008	regulation of biological quality	5,19E-07	0,00061
blue	GO:0098609	cell-cell adhesion	5,91E-07	0,000684
blue	GO:0071345	cellular response to cytokine stimulus	5,99E-07	0,000689
blue	GO:0050865	regulation of cell activation	6,07E-07	0,000695
blue	GO:0002287	alpha-beta T cell activation involved in immune response	6,34E-07	0,000716
blue	GO:0002293	alpha-beta T cell differentiation involved in immune response	6,34E-07	0,000716
blue	GO:0002294	CD4-positive, alpha-beta T cell differentiation involved in immune response	6,34E-07	0,000716
blue	GO:0042093	T-helper cell differentiation	6,34E-07	0,000716
blue	GO:0009605	response to external stimulus	7,25E-07	0,000807
blue	GO:0005773	vacuole	8,49E-07	0,000922
blue	GO:0030217	T cell differentiation	8,55E-07	0,000924
blue	GO:0007264	small GTPase mediated signal transduction	1,22E-06	0,001281
blue	GO:0048584	positive regulation of response to stimulus	1,29E-06	0,001343
blue	GO:0042060	wound healing	1,37E-06	0,001421
blue	GO:0002286	T cell activation involved in immune response	1,64E-06	0,001666
blue	GO:0006954	inflammatory response	1,67E-06	0,001687
blue	GO:0002292	T cell differentiation involved in immune response	1,86E-06	0,001866
blue	GO:0005766	primary lysosome	2,30E-06	0,002263
blue	GO:0042582	azurophil granule	2,30E-06	0,002263
blue	GO:0045619	regulation of lymphocyte differentiation	3,80E-06	0,003598
blue	GO:0035556	intracellular signal transduction	3,88E-06	0,003643

Module	GO ID	GO Term	p-Value	FDR
blue	GO:0002521	leukocyte differentiation	4,13E-06	0,003842
blue	GO:0031983	vesicle lumen	4,50E-06	0,004141
blue	GO:0060205	cytoplasmic vesicle lumen	4,50E-06	0,004141
blue	GO:0016477	cell migration	4,70E-06	0,004289
blue	GO:0034774	secretory granule lumen	4,71E-06	0,004294
blue	GO:0045580	regulation of T cell differentiation	5,10E-06	0,004613
blue	GO:1902531	regulation of intracellular signal transduction	5,15E-06	0,004628
blue	GO:0050867	positive regulation of cell activation	6,30E-06	0,005599
blue	GO:0001816	cytokine production	6,59E-06	0,005821
blue	GO:0010941	**regulation of cell death**	7,91E-06	0,006885
blue	GO:0051716	cellular response to stimulus	8,00E-06	0,006947
blue	GO:0002460	adaptive immune response based on somatic recombination of immune receptors built from immunoglobulin superfamily domains	8,03E-06	0,006961
blue	GO:0002694	regulation of leukocyte activation	8,05E-06	0,006961
blue	GO:0002285	lymphocyte activation involved in immune response	9,27E-06	0,007864
blue	GO:0098805	whole membrane	1,06E-05	0,008833
blue	GO:0043067	**regulation of programmed cell death**	1,14E-05	0,009461
blue	GO:0014070	response to organic cyclic compound	1,19E-05	0,009768
blue	GO:0048870	cell motility	1,19E-05	0,009768
blue	GO:0051674	localization of cell	1,19E-05	0,009768
blue	GO:0009611	response to wounding	1,19E-05	0,009768
blue	GO:0051056	regulation of small GTPase mediated signal transduction	1,20E-05	0,009768
blue	GO:0030667	secretory granule membrane	1,28E-05	0,010361
blue	GO:0019748	secondary metabolic process	1,31E-05	0,010592
blue	GO:0048872	homeostasis of number of cells	1,33E-05	0,010753
blue	GO:0004896	cytokine receptor activity	1,35E-05	0,010851
blue	GO:0031226	intrinsic component of plasma membrane	1,36E-05	0,010879
blue	GO:0012505	endomembrane system	1,36E-05	0,010913
blue	GO:0020037	heme binding	1,38E-05	0,010997
blue	GO:0009617	response to bacterium	1,39E-05	0,011038
blue	GO:0001776	leukocyte homeostasis	1,40E-05	0,011095
blue	GO:0031701	angiotensin receptor binding	1,42E-05	0,011202
blue	GO:0051249	regulation of lymphocyte activation	1,62E-05	0,012624

Module	GO ID	GO Term	p-Value	FDR
blue	GO:0042221	response to chemical	1,70E-05	0,013067
blue	GO:1901700	response to oxygen-containing compound	1,86E-05	0,014247
blue	GO:0007159	leukocyte cell-cell adhesion	1,90E-05	0,014391
blue	GO:0007155	cell adhesion	2,00E-05	0,014954
blue	GO:0043547	positive regulation of GTPase activity	2,11E-05	0,015653
blue	GO:0035578	azurophil granule lumen	2,11E-05	0,015653
blue	GO:0048583	regulation of response to stimulus	2,17E-05	0,016058
blue	GO:0052547	regulation of peptidase activity	2,18E-05	0,016134
blue	GO:0042981	**regulation of apoptotic process**	2,26E-05	0,01657
blue	GO:0050863	regulation of T cell activation	2,26E-05	0,01657
blue	GO:0043370	regulation of CD4-positive, alpha-beta T cell differentiation	2,26E-05	0,01657
blue	GO:0022610	biological adhesion	2,39E-05	0,017396
blue	GO:0008154	actin polymerization or depolymerization	2,44E-05	0,017577
blue	GO:0050790	regulation of catalytic activity	2,48E-05	0,017819
blue	GO:0009607	response to biotic stimulus	2,62E-05	0,018766
blue	GO:0070887	cellular response to chemical stimulus	2,65E-05	0,018959
blue	GO:0043207	response to external biotic stimulus	2,80E-05	0,019637
blue	GO:0051707	response to other organism	2,80E-05	0,019637
blue	GO:0030168	platelet activation	2,89E-05	0,020185
blue	GO:0010466	negative regulation of peptidase activity	2,90E-05	0,020185
blue	GO:0005576	extracellular region	3,10E-05	0,021494
blue	GO:0005887	integral component of plasma membrane	3,23E-05	0,022162
blue	GO:0044425	membrane part	3,55E-05	0,023828
blue	GO:0002313	mature B cell differentiation involved in immune response	3,61E-05	0,024186
blue	GO:0040011	locomotion	3,82E-05	0,025489
blue	GO:0002696	positive regulation of leukocyte activation	3,84E-05	0,025574
blue	GO:0023057	negative regulation of signaling	3,89E-05	0,025807
blue	GO:0051336	regulation of hydrolase activity	3,92E-05	0,025837
blue	GO:0032088	negative regulation of NF-kappaB transcription factor activity	4,01E-05	0,026335
blue	GO:0010646	regulation of cell communication	4,02E-05	0,026335
blue	GO:0051241	negative regulation of multicellular organismal process	4,02E-05	0,026335
blue	GO:0006810	transport	4,28E-05	0,0279

Module	GO ID	GO Term	p-Value	FDR
blue	GO:0051251	positive regulation of lymphocyte activation	4,53E-05	0,029362
blue	GO:0010033	response to organic substance	4,62E-05	0,029921
blue	GO:0010951	negative regulation of endopeptidase activity	5,12E-05	0,032845
blue	GO:0050870	positive regulation of T cell activation	5,12E-05	0,032845
blue	GO:0052548	regulation of endopeptidase activity	5,29E-05	0,033831
blue	GO:0009612	response to mechanical stimulus	5,63E-05	0,035831
blue	GO:1903039	positive regulation of leukocyte cell-cell adhesion	5,63E-05	0,035831
blue	GO:0010648	negative regulation of cell communication	5,73E-05	0,036402
blue	GO:0051345	positive regulation of hydrolase activity	5,74E-05	0,036402
blue	GO:0030029	actin filament-based process	5,84E-05	0,036913
blue	GO:0005200	structural constituent of cytoskeleton	6,00E-05	0,037533
blue	GO:0048534	hematopoietic or lymphoid organ development	6,10E-05	0,037948
blue	GO:0046466	membrane lipid catabolic process	6,22E-05	0,038438
blue	GO:0023051	regulation of signaling	6,34E-05	0,039144
blue	GO:0097237	cellular response to toxic substance	6,48E-05	0,039893
blue	GO:0012506	vesicle membrane	6,74E-05	0,041131
blue	GO:0043087	regulation of GTPase activity	6,82E-05	0,041441
blue	GO:0044421	extracellular region part	6,97E-05	0,042241
blue	GO:0001228	DNA-binding transcription activator activity, RNA polymerase II-specific	7,06E-05	0,042656
blue	GO:0030036	actin cytoskeleton organization	7,22E-05	0,043498
blue	GO:0002315	marginal zone B cell differentiation	7,74E-05	0,046147
blue	GO:0046637	regulation of alpha-beta T cell differentiation	7,89E-05	0,047
blue	GO:0033993	response to lipid	7,98E-05	0,047307
blue	GO:0042493	response to drug	8,25E-05	0,048804
brown	GO:0044782	cilium organization	7,03E-09	1,21E-05
brown	GO:0060271	cilium assembly	3,59E-08	5,64E-05
brown	GO:0005929	cilium	3,60E-08	5,64E-05
brown	GO:0044441	ciliary part	1,12E-07	0,000158
brown	GO:0120031	plasma membrane bounded cell projection assembly	2,73E-07	0,00035
brown	GO:0030031	cell projection assembly	3,12E-07	0,000394
brown	GO:0044450	microtubule organizing center part	3,99E-07	0,000491
brown	GO:0007017	microtubule-based process	5,96E-07	0,000687

Module	GO ID	GO Term	p-Value	FDR
brown	GO:0005814	centriole	2,21E-06	0,002183
brown	GO:0005856	cytoskeleton	3,75E-06	0,003555
brown	GO:0005911	cell-cell junction	4,07E-06	0,003795
brown	GO:0030030	cell projection organization	8,09E-06	0,006985
brown	GO:0070925	organelle assembly	8,60E-06	0,007392
brown	GO:0097711	ciliary basal body-plasma membrane docking	9,64E-06	0,008098
brown	GO:0120036	plasma membrane bounded cell projection organization	1,10E-05	0,009138
brown	GO:0005815	microtubule organizing center	2,22E-05	0,016389
brown	GO:0120025	plasma membrane bounded cell projection	3,28E-05	0,022402
brown	GO:0015630	microtubule cytoskeleton	3,52E-05	0,023672
brown	GO:0140056	organelle localization by membrane tethering	4,76E-05	0,030687
brown	GO:0042995	cell projection	6,05E-05	0,037755
brown	GO:0044085	cellular component biogenesis	6,73E-05	0,041131
cyan	GO:0007049	cell cycle	1,59E-47	7,87E-43
cyan	GO:0022402	cell cycle process	6,70E-47	2,99E-42
cyan	GO:1903047	mitotic cell cycle process	8,22E-42	2,03E-37
cyan	GO:0000278	mitotic cell cycle	1,74E-41	3,87E-37
cyan	GO:0051301	cell division	3,00E-38	5,57E-34
cyan	GO:0007059	chromosome segregation	5,26E-36	7,10E-32
cyan	GO:0000280	nuclear division	8,21E-32	9,89E-28
cyan	GO:0000793	condensed chromosome	1,03E-30	1,12E-26
cyan	GO:0098687	chromosomal region	4,36E-30	4,52E-26
cyan	GO:0005694	chromosome	6,58E-30	6,66E-26
cyan	GO:0098813	nuclear chromosome segregation	8,50E-30	8,41E-26
cyan	GO:0048285	organelle fission	1,03E-29	9,98E-26
cyan	GO:0051276	chromosome organization	2,88E-29	2,73E-25
cyan	GO:0140014	mitotic nuclear division	5,97E-28	5,43E-24
cyan	GO:0044427	chromosomal part	3,46E-26	3,02E-22
cyan	GO:0044770	cell cycle phase transition	5,95E-26	5,10E-22
cyan	GO:0044772	mitotic cell cycle phase transition	1,64E-25	1,35E-21
cyan	GO:0000819	sister chromatid segregation	1,83E-25	1,48E-21
cyan	GO:0000070	mitotic sister chromatid segregation	3,77E-25	2,94E-21

Module	GO ID	GO Term	p-Value	FDR
cyan	GO:0000775	chromosome, centromeric region	3,66E-24	2,63E-20
cyan	GO:0043232	intracellular non-membrane-bounded organelle	1,43E-23	9,67E-20
cyan	GO:0043228	non-membrane-bounded organelle	1,71E-23	1,13E-19
cyan	GO:0000779	condensed chromosome, centromeric region	1,72E-23	1,13E-19
cyan	GO:0000777	condensed chromosome kinetochore	3,60E-22	2,26E-18
cyan	GO:0006260	DNA replication	6,65E-22	4,12E-18
cyan	GO:0051726	regulation of cell cycle	1,15E-21	6,99E-18
cyan	GO:0000776	kinetochore	4,50E-21	2,64E-17
cyan	GO:0010564	regulation of cell cycle process	1,02E-20	5,83E-17
cyan	GO:0015630	microtubule cytoskeleton	1,34E-19	7,02E-16
cyan	GO:0007346	regulation of mitotic cell cycle	5,52E-19	2,79E-15
cyan	GO:0071103	DNA conformation change	4,62E-18	2,24E-14
cyan	GO:0006996	organelle organization	3,80E-17	1,78E-13
cyan	GO:0044430	cytoskeletal part	5,92E-17	2,75E-13
cyan	GO:0006259	DNA metabolic process	7,10E-17	3,23E-13
cyan	GO:0000075	cell cycle checkpoint	9,86E-17	4,35E-13
cyan	GO:0006323	DNA packaging	1,39E-16	6,08E-13
cyan	GO:0005819	spindle	8,00E-16	3,18E-12
cyan	GO:1901990	regulation of mitotic cell cycle phase transition	2,82E-15	1,06E-11
cyan	GO:1901987	regulation of cell cycle phase transition	2,92E-15	1,09E-11
cyan	GO:0000226	microtubule cytoskeleton organization	3,27E-15	1,20E-11
cyan	GO:0007093	mitotic cell cycle checkpoint	4,64E-15	1,69E-11
cyan	GO:0090068	positive regulation of cell cycle process	2,06E-14	7,22E-11
cyan	GO:0006261	DNA-dependent DNA replication	2,88E-14	9,87E-11
cyan	GO:0007088	regulation of mitotic nuclear division	2,88E-14	9,87E-11
cyan	GO:0051983	regulation of chromosome segregation	3,10E-14	1,05E-10
cyan	GO:0005856	cytoskeleton	5,32E-14	1,78E-10
cyan	GO:0045787	positive regulation of cell cycle	5,67E-14	1,89E-10
cyan	GO:0051783	regulation of nuclear division	8,09E-14	2,67E-10
cyan	GO:0045786	negative regulation of cell cycle	1,45E-13	4,71E-10
cyan	GO:0045930	negative regulation of mitotic cell cycle	2,03E-13	6,43E-10
cyan	GO:0016043	cellular component organization	2,13E-13	6,68E-10

Module	GO ID	GO Term	p-Value	FDR
cyan	GO:0007051	spindle organization	2,59E-13	7,97E-10
cyan	GO:0044843	cell cycle G1/S phase transition	3,27E-13	9,96E-10
cyan	GO:0007017	microtubule-based process	3,30E-13	1,00E-09
cyan	GO:0008608	attachment of spindle microtubules to kinetochore	4,22E-13	1,26E-09
cyan	GO:0000082	G1/S transition of mitotic cell cycle	6,85E-13	2,02E-09
cyan	GO:0005634	nucleus	2,80E-12	7,84E-09
cyan	GO:0030496	midbody	3,32E-12	9,24E-09
cyan	GO:0071840	cellular component organization or biogenesis	6,08E-12	1,60E-08
cyan	GO:0031981	nuclear lumen	8,12E-12	2,07E-08
cyan	GO:0005815	microtubule organizing center	8,25E-12	2,09E-08
cyan	GO:0044428	nuclear part	9,36E-12	2,35E-08
cyan	GO:0005654	nucleoplasm	9,80E-12	2,45E-08
cyan	GO:1902850	microtubule cytoskeleton organization involved in mitosis	3,46E-11	8,17E-08
cyan	GO:0051321	meiotic cell cycle	3,92E-11	9,19E-08
cyan	GO:0006974	cellular response to DNA damage stimulus	6,61E-11	1,52E-07
cyan	GO:0050000	chromosome localization	8,96E-11	2,02E-07
cyan	GO:0051303	establishment of chromosome localization	8,96E-11	2,02E-07
cyan	GO:0051310	metaphase plate congression	9,61E-11	2,15E-07
cyan	GO:0030261	chromosome condensation	1,41E-10	3,06E-07
cyan	GO:0044839	cell cycle G2/M phase transition	1,51E-10	3,25E-07
cyan	GO:1901988	negative regulation of cell cycle phase transition	1,63E-10	3,48E-07
cyan	GO:1903046	meiotic cell cycle process	2,54E-10	5,42E-07
cyan	GO:0007010	cytoskeleton organization	2,71E-10	5,75E-07
cyan	GO:0051304	chromosome separation	4,15E-10	8,63E-07
cyan	GO:0000228	nuclear chromosome	4,91E-10	1,01E-06
cyan	GO:0010948	negative regulation of cell cycle process	5,18E-10	1,06E-06
cyan	GO:0140013	meiotic nuclear division	7,08E-10	1,43E-06
cyan	GO:0031974	membrane-enclosed lumen	1,01E-09	2,00E-06
cyan	GO:0043233	organelle lumen	1,01E-09	2,00E-06
cyan	GO:0070013	intracellular organelle lumen	1,01E-09	2,00E-06
cyan	GO:0007052	mitotic spindle organization	1,46E-09	2,86E-06
cyan	GO:1901991	negative regulation of mitotic cell cycle phase transition	1,70E-09	3,28E-06

Module	GO ID	GO Term	p-Value	FDR
cyan	GO:0033045	regulation of sister chromatid segregation	1,91E-09	3,66E-06
cyan	GO:0007091	metaphase/anaphase transition of mitotic cell cycle	1,99E-09	3,74E-06
cyan	GO:0010965	regulation of mitotic sister chromatid separation	1,99E-09	3,74E-06
cyan	GO:0044784	metaphase/anaphase transition of cell cycle	1,99E-09	3,74E-06
cyan	GO:0000940	condensed chromosome outer kinetochore	2,87E-09	5,25E-06
cyan	GO:0042555	MCM complex	2,87E-09	5,25E-06
cyan	GO:0051306	mitotic sister chromatid separation	3,72E-09	6,77E-06
cyan	GO:0000922	spindle pole	4,08E-09	7,39E-06
cyan	GO:0031145	anaphase-promoting complex-dependent catabolic process	4,43E-09	7,95E-06
cyan	GO:0000086	G2/M transition of mitotic cell cycle	4,93E-09	8,78E-06
cyan	GO:1905818	regulation of chromosome separation	5,01E-09	8,90E-06
cyan	GO:0005813	centrosome	5,18E-09	9,15E-06
cyan	GO:0006336	DNA replication-independent nucleosome assembly	6,42E-09	1,12E-05
cyan	GO:0034508	centromere complex assembly	6,42E-09	1,12E-05
cyan	GO:0034724	DNA replication-independent nucleosome organization	6,42E-09	1,12E-05
cyan	GO:0072686	mitotic spindle	6,49E-09	1,13E-05
cyan	GO:0071459	protein localization to chromosome, centromeric region	8,62E-09	1,47E-05
cyan	GO:0051225	spindle assembly	9,38E-09	1,59E-05
cyan	GO:0031570	DNA integrity checkpoint	1,10E-08	1,84E-05
cyan	GO:0006334	nucleosome assembly	1,11E-08	1,85E-05
cyan	GO:1902749	regulation of cell cycle G2/M phase transition	1,12E-08	1,85E-05
cyan	GO:0030071	regulation of mitotic metaphase/anaphase transition	1,25E-08	2,05E-05
cyan	GO:1902099	regulation of metaphase/anaphase transition of cell cycle	1,25E-08	2,05E-05
cyan	GO:0044422	organelle part	1,30E-08	2,12E-05
cyan	GO:0044446	intracellular organelle part	1,32E-08	2,15E-05
cyan	GO:0034501	protein localization to kinetochore	1,42E-08	2,30E-05
cyan	GO:0007080	mitotic metaphase plate congression	2,30E-08	3,68E-05
cyan	GO:0033047	regulation of mitotic sister chromatid segregation	3,20E-08	5,05E-05
cyan	GO:0034080	CENP-A containing nucleosome assembly	3,74E-08	5,82E-05
cyan	GO:0061641	CENP-A containing chromatin organization	3,74E-08	5,82E-05
cyan	GO:0006281	DNA repair	6,92E-08	0,000105
cyan	GO:0000022	mitotic spindle elongation	8,06E-08	0,00012

Module	GO ID	GO Term	p-Value	FDR
cyan	GO:0000003	reproduction	9,02E-08	0,000132
cyan	GO:0022414	reproductive process	9,02E-08	0,000132
cyan	GO:0051052	regulation of DNA metabolic process	9,51E-08	0,000138
cyan	GO:0045839	negative regulation of mitotic nuclear division	1,06E-07	0,000149
cyan	GO:0006275	regulation of DNA replication	1,13E-07	0,000159
cyan	GO:0031055	chromatin remodeling at centromere	1,26E-07	0,000175
cyan	GO:0051383	kinetochore organization	1,47E-07	0,000203
cyan	GO:0031497	chromatin assembly	1,51E-07	0,000206
cyan	GO:0045841	negative regulation of mitotic metaphase/anaphase transition	1,81E-07	0,000241
cyan	GO:1902100	negative regulation of metaphase/anaphase transition of cell cycle	1,81E-07	0,000241
cyan	GO:1905819	negative regulation of chromosome separation	1,81E-07	0,000241
cyan	GO:2000816	negative regulation of mitotic sister chromatid separation	1,81E-07	0,000241
cyan	GO:0051784	negative regulation of nuclear division	1,89E-07	0,000251
cyan	GO:0000077	DNA damage checkpoint	1,95E-07	0,000259
cyan	GO:0034502	protein localization to chromosome	2,51E-07	0,000326
cyan	GO:0044454	nuclear chromosome part	2,71E-07	0,000349
cyan	GO:0000796	condensin complex	2,76E-07	0,000352
cyan	GO:0051231	spindle elongation	2,76E-07	0,000352
cyan	GO:0045931	positive regulation of mitotic cell cycle	2,82E-07	0,000358
cyan	GO:0065004	protein-DNA complex assembly	3,55E-07	0,000444
cyan	GO:0010389	regulation of G2/M transition of mitotic cell cycle	4,25E-07	0,000522
cyan	GO:0000781	chromosome, telomeric region	4,48E-07	0,000546
cyan	GO:0042770	signal transduction in response to DNA damage	4,61E-07	0,000557
cyan	GO:0072395	signal transduction involved in cell cycle checkpoint	4,62E-07	0,000557
cyan	GO:0072401	signal transduction involved in DNA integrity checkpoint	4,62E-07	0,000557
cyan	GO:0072422	signal transduction involved in DNA damage checkpoint	4,62E-07	0,000557
cyan	GO:0034728	nucleosome organization	4,77E-07	0,000572
cyan	GO:0033048	negative regulation of mitotic sister chromatid segregation	4,85E-07	0,000579
cyan	GO:0043486	histone exchange	4,85E-07	0,000579
cyan	GO:0051256	mitotic spindle midzone assembly	5,18E-07	0,00061
cyan	GO:0005622	intracellular	5,26E-07	0,000615
cyan	GO:0044424	intracellular part	5,26E-07	0,000615

Module	GO ID	GO Term	p-Value	FDR
cyan	GO:0015949	nucleobase-containing small molecule interconversion	5,47E-07	0,000636
cyan	GO:0007098	centrosome cycle	5,67E-07	0,000658
cyan	GO:0005874	microtubule	6,26E-07	0,000713
cyan	GO:0033046	negative regulation of sister chromatid segregation	6,54E-07	0,000734
cyan	GO:0051985	negative regulation of chromosome segregation	6,54E-07	0,000734
cyan	GO:0006271	DNA strand elongation involved in DNA replication	7,20E-07	0,000804
cyan	GO:0051302	regulation of cell division	7,49E-07	0,00083
cyan	GO:0032467	positive regulation of cytokinesis	8,02E-07	0,000881
cyan	GO:0005524	ATP binding	8,03E-07	0,000881
cyan	GO:0000910	cytokinesis	8,44E-07	0,000919
cyan	GO:0008283	cell proliferation	8,53E-07	0,000924
cyan	GO:0000794	condensed nuclear chromosome	1,07E-06	0,001142
cyan	GO:0031023	microtubule organizing center organization	1,09E-06	0,00116
cyan	GO:0043226	organelle	1,12E-06	0,001191
cyan	GO:0045132	meiotic chromosome segregation	1,15E-06	0,001213
cyan	GO:0008144	drug binding	1,27E-06	0,001331
cyan	GO:0007076	mitotic chromosome condensation	1,48E-06	0,001532
cyan	GO:0032559	adenyl ribonucleotide binding	1,57E-06	0,001622
cyan	GO:0043142	single-stranded DNA-dependent ATPase activity	1,58E-06	0,00163
cyan	GO:0006270	DNA replication initiation	1,61E-06	0,001641
cyan	GO:0007094	mitotic spindle assembly checkpoint	1,61E-06	0,001641
cyan	GO:0031577	spindle checkpoint	1,61E-06	0,001641
cyan	GO:0071173	spindle assembly checkpoint	1,61E-06	0,001641
cyan	GO:0071174	mitotic spindle checkpoint	1,61E-06	0,001641
cyan	GO:0033044	regulation of chromosome organization	1,80E-06	0,001811
cyan	GO:0030554	adenyl nucleotide binding	1,91E-06	0,001917
cyan	GO:0043229	intracellular organelle	1,94E-06	0,001933
cyan	GO:0044773	mitotic DNA damage checkpoint	1,99E-06	0,001977
cyan	GO:0032465	regulation of cytokinesis	2,38E-06	0,002338
cyan	GO:0070925	organelle assembly	2,42E-06	0,002367
cyan	GO:0006333	chromatin assembly or disassembly	2,56E-06	0,002505
cyan	GO:0071824	protein-DNA complex subunit organization	2,89E-06	0,002807

Module	GO ID	GO Term	p-Value	FDR
cyan	GO:0051640	organelle localization	2,93E-06	0,002838
cyan	GO:0016572	histone phosphorylation	3,02E-06	0,002907
cyan	GO:0044774	mitotic DNA integrity checkpoint	3,07E-06	0,00294
cyan	GO:0072331	signal transduction by p53 class mediator	3,33E-06	0,003178
cyan	GO:0070192	chromosome organization involved in meiotic cell cycle	3,50E-06	0,00332
cyan	GO:0008094	DNA-dependent ATPase activity	3,88E-06	0,003643
cyan	GO:0099513	polymeric cytoskeletal fiber	4,19E-06	0,003893
cyan	GO:0044786	cell cycle DNA replication	4,34E-06	0,004021
cyan	GO:0051233	spindle midzone	5,13E-06	0,004622
cyan	GO:0051988	regulation of attachment of spindle microtubules to kinetochore	5,56E-06	0,00498
cyan	GO:0044464	cell part	5,86E-06	0,005227
cyan	GO:0061640	cytoskeleton-dependent cytokinesis	6,12E-06	0,005454
cyan	GO:0051781	positive regulation of cell division	6,95E-06	0,006128
cyan	GO:1901989	positive regulation of cell cycle phase transition	7,34E-06	0,006425
cyan	GO:0006268	DNA unwinding involved in DNA replication	7,45E-06	0,006492
cyan	GO:0051255	spindle midzone assembly	7,45E-06	0,006492
cyan	GO:2001251	negative regulation of chromosome organization	8,40E-06	0,007238
cyan	GO:0031571	mitotic G1 DNA damage checkpoint	8,67E-06	0,007429
cyan	GO:0044819	mitotic G1/S transition checkpoint	8,67E-06	0,007429
cyan	GO:0005876	spindle microtubule	9,08E-06	0,007732
cyan	GO:0033260	nuclear DNA replication	9,08E-06	0,007732
cyan	GO:0005623	cell	9,14E-06	0,007766
cyan	GO:0045120	pronucleus	9,32E-06	0,00789
cyan	GO:0099080	supramolecular complex	9,48E-06	0,007983
cyan	GO:0099081	supramolecular polymer	9,48E-06	0,007983
cyan	GO:0099512	supramolecular fiber	9,48E-06	0,007983
cyan	GO:0044783	G1 DNA damage checkpoint	1,02E-05	0,008528
cyan	GO:0033043	regulation of organelle organization	1,19E-05	0,009768
cyan	GO:0005515	protein binding	1,21E-05	0,00984
cyan	GO:0033554	cellular response to stress	1,22E-05	0,009896
cyan	GO:0032508	DNA duplex unwinding	1,24E-05	0,010063
cyan	GO:0035639	purine ribonucleoside triphosphate binding	1,39E-05	0,011061

Module	GO ID	GO Term	p-Value	FDR
cyan	GO:0000083	regulation of transcription involved in G1/S transition of mitotic cell cycle	1,40E-05	0,011095
cyan	GO:0007276	gamete generation	1,59E-05	0,012396
cyan	GO:0000281	mitotic cytokinesis	1,63E-05	0,012642
cyan	GO:0005829	cytosol	1,66E-05	0,012842
cyan	GO:0046605	regulation of centrosome cycle	1,91E-05	0,014391
cyan	GO:0090307	mitotic spindle assembly	1,91E-05	0,014391
cyan	GO:0010032	meiotic chromosome condensation	1,95E-05	0,014563
cyan	GO:0031262	Ndc80 complex	1,95E-05	0,014563
cyan	GO:0032133	chromosome passenger complex	1,95E-05	0,014563
cyan	GO:0097149	centralspindlin complex	1,95E-05	0,014563
cyan	GO:0051656	establishment of organelle localization	2,10E-05	0,015653
cyan	GO:0022616	DNA strand elongation	2,25E-05	0,01657
cyan	GO:0032555	purine ribonucleotide binding	2,39E-05	0,017379
cyan	GO:0000784	nuclear chromosome, telomeric region	2,48E-05	0,017819
cyan	GO:0017111	nucleoside-triphosphatase activity	2,66E-05	0,018959
cyan	GO:2000134	negative regulation of G1/S transition of mitotic cell cycle	2,66E-05	0,018959
cyan	GO:0016462	pyrophosphatase activity	2,68E-05	0,019035
cyan	GO:0072431	signal transduction involved in mitotic G1 DNA damage checkpoint	2,68E-05	0,019035
cyan	GO:1902400	intracellular signal transduction involved in G1 DNA damage checkpoint	2,68E-05	0,019035
cyan	GO:0008017	microtubule binding	2,76E-05	0,019511
cyan	GO:0016817	hydrolase activity, acting on acid anhydrides	2,79E-05	0,019637
cyan	GO:0016818	hydrolase activity, acting on acid anhydrides, in phosphorus-containing anhydrides	2,79E-05	0,019637
cyan	GO:0032553	ribonucleotide binding	2,80E-05	0,019637
cyan	GO:0032991	protein-containing complex	2,85E-05	0,019933
cyan	GO:0017076	purine nucleotide binding	2,87E-05	0,020074
cyan	GO:1902807	negative regulation of cell cycle G1/S phase transition	2,99E-05	0,0208
cyan	GO:0072413	signal transduction involved in mitotic cell cycle checkpoint	3,15E-05	0,021721
cyan	GO:1902402	signal transduction involved in mitotic DNA damage checkpoint	3,15E-05	0,021721
cyan	GO:1902403	signal transduction involved in mitotic DNA integrity checkpoint	3,15E-05	0,021721
cyan	GO:0006302	double-strand break repair	3,18E-05	0,021842
cyan	GO:0000307	cyclin-dependent protein kinase holoenzyme complex	3,24E-05	0,022181
cyan	GO:0032392	DNA geometric change	3,37E-05	0,022825

Module	GO ID	GO Term	p-Value	FDR
cyan	GO:0043044	ATP-dependent chromatin remodeling	3,70E-05	0,024741
cyan	GO:0042623	ATPase activity, coupled	4,00E-05	0,026335
cyan	GO:0051347	positive regulation of transferase activity	4,38E-05	0,028552
cyan	GO:0019953	sexual reproduction	4,48E-05	0,029099
cyan	GO:0048609	multicellular organismal reproductive process	5,51E-05	0,035135
cyan	GO:0032504	multicellular organism reproduction	5,79E-05	0,036702
cyan	GO:0016887	ATPase activity	5,85E-05	0,036913
cyan	GO:0007100	mitotic centrosome separation	5,87E-05	0,036913
cyan	GO:0009263	deoxyribonucleotide biosynthetic process	5,87E-05	0,036913
cyan	GO:0090329	regulation of DNA-dependent DNA replication	5,89E-05	0,036974
cyan	GO:0097367	carbohydrate derivative binding	6,08E-05	0,037863
cyan	GO:0007127	meiosis I	6,67E-05	0,040852
cyan	GO:2000045	regulation of G1/S transition of mitotic cell cycle	6,76E-05	0,041131
cyan	GO:0044450	microtubule organizing center part	6,99E-05	0,04231
cyan	GO:0000912	assembly of actomyosin apparatus involved in cytokinesis	7,63E-05	0,045593
cyan	GO:0000915	actomyosin contractile ring assembly	7,63E-05	0,045593
cyan	GO:0000942	condensed nuclear chromosome outer kinetochore	7,63E-05	0,045593
cyan	GO:0072687	meiotic spindle	7,63E-05	0,045593
cyan	GO:0051054	positive regulation of DNA metabolic process	7,71E-05	0,046046
cyan	GO:0006325	chromatin organization	7,97E-05	0,047307
cyan	GO:0061982	meiosis I cell cycle process	8,30E-05	0,049012
grey60	GO:0000323	lytic vacuole	1,15E-10	2,54E-07
grey60	GO:0005764	lysosome	1,15E-10	2,54E-07
grey60	GO:0005773	vacuole	4,78E-10	9,90E-07
grey60	GO:0044437	vacuolar part	1,97E-09	3,74E-06
grey60	GO:0005768	endosome	1,49E-08	2,40E-05
grey60	GO:0071944	cell periphery	8,54E-08	0,000126
grey60	GO:0044440	endosomal part	9,98E-08	0,000145
grey60	GO:0005765	lysosomal membrane	1,02E-07	0,000145
grey60	GO:0098852	lytic vacuole membrane	1,02E-07	0,000145
grey60	GO:0010008	endosome membrane	1,53E-07	0,000208
grey60	GO:0005774	vacuolar membrane	5,11E-07	0,000605

Module	GO ID	GO Term	p-Value	FDR
grey60	GO:0005886	plasma membrane	5,38E-07	0,000628
grey60	GO:0031982	vesicle	1,77E-06	0,001788
grey60	GO:0031410	cytoplasmic vesicle	2,86E-06	0,002783
grey60	GO:0097708	intracellular vesicle	3,01E-06	0,002904
grey60	GO:0007610	behavior	4,36E-06	0,004025
grey60	GO:0043202	lysosomal lumen	9,90E-06	0,008307
grey60	GO:0002376	immune system process	1,02E-05	0,008528
grey60	GO:0044433	cytoplasmic vesicle part	1,32E-05	0,01064
grey60	GO:0060337	type I interferon signaling pathway	1,78E-05	0,013672
grey60	GO:0071357	cellular response to type I interferon	1,78E-05	0,013672
grey60	GO:0002252	immune effector process	2,32E-05	0,016947
grey60	GO:0034340	response to type I interferon	3,05E-05	0,021181
grey60	GO:0050896	response to stimulus	3,25E-05	0,022181
grey60	GO:0098657	import into cell	3,45E-05	0,023352
grey60	GO:0006955	immune response	3,63E-05	0,024345
grey60	GO:1900223	positive regulation of amyloid-beta clearance	3,89E-05	0,025807
grey60	GO:0006897	endocytosis	3,96E-05	0,02607
grey60	GO:0016192	vesicle-mediated transport	4,42E-05	0,028746
grey60	GO:0002708	positive regulation of lymphocyte mediated immunity	5,27E-05	0,033699
grey60	GO:0023052	signaling	6,13E-05	0,03807
grey60	GO:0001912	positive regulation of leukocyte mediated cytotoxicity	6,15E-05	0,038072
grey60	GO:0008289	lipid binding	6,96E-05	0,042233
lightgreen	GO:0002702	positive regulation of production of molecular mediator of immune response	5,81E-06	0,005193
lightgreen	GO:0031981	nuclear lumen	7,34E-06	0,006425
lightgreen	GO:0002440	production of molecular mediator of immune response	1,50E-05	0,011813
lightgreen	GO:0031974	membrane-enclosed lumen	1,91E-05	0,014391
lightgreen	GO:0043233	organelle lumen	1,91E-05	0,014391
lightgreen	GO:0070013	intracellular organelle lumen	1,91E-05	0,014391
lightgreen	GO:0002699	positive regulation of immune effector process	2,31E-05	0,01692
lightgreen	GO:0031860	telomeric 3' overhang formation	3,11E-05	0,02152
lightgreen	GO:0005730	nucleolus	3,45E-05	0,023352
lightgreen	GO:0002700	regulation of production of molecular mediator of immune response	4,19E-05	0,027378

Module	GO ID	GO Term	p-Value	FDR
lightyellow	GO:0022626	cytosolic ribosome	6,64E-56	2,96E-50
lightyellow	GO:0006413	translational initiation	2,22E-55	4,93E-50
lightyellow	GO:0000184	nuclear-transcribed mRNA catabolic process, nonsense-mediated decay	1,49E-54	2,00E-49
lightyellow	GO:0006614	SRP-dependent cotranslational protein targeting to membrane	1,80E-54	2,00E-49
lightyellow	GO:0006613	cotranslational protein targeting to membrane	1,15E-53	1,02E-48
lightyellow	GO:0045047	protein targeting to ER	3,79E-53	2,81E-48
lightyellow	GO:0072599	establishment of protein localization to endoplasmic reticulum	2,12E-52	1,35E-47
lightyellow	GO:0070972	protein localization to endoplasmic reticulum	1,09E-49	6,05E-45
lightyellow	GO:0006612	protein targeting to membrane	1,87E-46	7,57E-42
lightyellow	GO:0019083	viral transcription	8,25E-45	3,06E-40
lightyellow	GO:0019080	viral gene expression	1,41E-44	4,85E-40
lightyellow	GO:0006402	mRNA catabolic process	6,55E-44	2,08E-39
lightyellow	GO:0044391	ribosomal subunit	1,08E-43	3,22E-39
lightyellow	GO:0000956	nuclear-transcribed mRNA catabolic process	1,47E-43	4,10E-39
lightyellow	GO:0006401	RNA catabolic process	2,98E-42	7,82E-38
lightyellow	GO:0044445	cytosolic part	1,24E-41	2,91E-37
lightyellow	GO:0005840	ribosome	3,66E-40	7,76E-36
lightyellow	GO:0006412	translation	6,54E-39	1,32E-34
lightyellow	GO:0043043	peptide biosynthetic process	2,29E-38	4,43E-34
lightyellow	GO:0034655	nucleobase-containing compound catabolic process	2,08E-37	3,70E-33
lightyellow	GO:0046700	heterocycle catabolic process	6,64E-37	1,14E-32
lightyellow	GO:0006518	peptide metabolic process	7,53E-37	1,20E-32
lightyellow	GO:0044270	cellular nitrogen compound catabolic process	7,54E-37	1,20E-32
lightyellow	GO:0019439	aromatic compound catabolic process	9,72E-37	1,49E-32
lightyellow	GO:1901361	organic cyclic compound catabolic process	2,65E-36	3,93E-32
lightyellow	GO:0090150	establishment of protein localization to membrane	4,51E-36	6,49E-32
lightyellow	GO:0003735	structural constituent of ribosome	4,90E-36	6,83E-32
lightyellow	GO:1990904	ribonucleoprotein complex	4,50E-35	5,90E-31
lightyellow	GO:0043604	amide biosynthetic process	4,96E-35	6,31E-31
lightyellow	GO:0006605	protein targeting	1,29E-32	1,60E-28
lightyellow	GO:0043603	cellular amide metabolic process	1,04E-31	1,22E-27
lightyellow	GO:0072594	establishment of protein localization to organelle	4,11E-31	4,69E-27

Module	GO ID	GO Term	p-Value	FDR
lightyellow	GO:0022625	cytosolic large ribosomal subunit	7,95E-31	8,85E-27
lightyellow	GO:0016071	mRNA metabolic process	3,46E-30	3,67E-26
lightyellow	GO:0072657	protein localization to membrane	7,93E-29	7,36E-25
lightyellow	GO:0005198	structural molecule activity	8,52E-28	7,59E-24
lightyellow	GO:0016032	viral process	1,56E-25	1,31E-21
lightyellow	GO:0044265	cellular macromolecule catabolic process	3,63E-25	2,88E-21
lightyellow	GO:0022627	cytosolic small ribosomal subunit	3,92E-25	3,01E-21
lightyellow	GO:0044403	symbiont process	1,12E-24	8,45E-21
lightyellow	GO:0044419	interspecies interaction between organisms	1,64E-24	1,22E-20
lightyellow	GO:0003723	RNA binding	2,42E-24	1,77E-20
lightyellow	GO:0010629	negative regulation of gene expression	4,86E-24	3,44E-20
lightyellow	GO:0009057	macromolecule catabolic process	6,90E-24	4,80E-20
lightyellow	GO:0006886	intracellular protein transport	1,03E-23	7,05E-20
lightyellow	GO:0015934	large ribosomal subunit	1,83E-23	1,18E-19
lightyellow	GO:1901566	organonitrogen compound biosynthetic process	4,73E-23	3,01E-19
lightyellow	GO:0033365	protein localization to organelle	1,41E-21	8,48E-18
lightyellow	GO:0044271	cellular nitrogen compound biosynthetic process	2,07E-20	1,17E-16
lightyellow	GO:0002181	cytoplasmic translation	2,17E-20	1,21E-16
lightyellow	GO:0044248	cellular catabolic process	2,21E-20	1,22E-16
lightyellow	GO:1901575	organic substance catabolic process	2,79E-20	1,52E-16
lightyellow	GO:0010605	negative regulation of macromolecule metabolic process	2,90E-20	1,55E-16
lightyellow	GO:0015935	small ribosomal subunit	6,67E-20	3,54E-16
lightyellow	GO:0034645	cellular macromolecule biosynthetic process	1,46E-19	7,54E-16
lightyellow	GO:0051704	multi-organism process	4,99E-19	2,56E-15
lightyellow	GO:0009892	negative regulation of metabolic process	6,11E-19	3,06E-15
lightyellow	GO:0009059	macromolecule biosynthetic process	1,00E-18	4,96E-15
lightyellow	GO:0009056	catabolic process	1,74E-18	8,51E-15
lightyellow	GO:0032991	protein-containing complex	1,66E-17	7,95E-14
lightyellow	GO:0003676	nucleic acid binding	3,14E-17	1,49E-13
lightyellow	GO:0010467	gene expression	6,91E-17	3,17E-13
lightyellow	GO:0042788	polysomal ribosome	1,56E-16	6,66E-13
lightyellow	GO:0010468	regulation of gene expression	2,33E-16	9,88E-13

Module	GO ID	GO Term	p-Value	FDR
lightyellow	GO:0015031	protein transport	3,55E-16	1,48E-12
lightyellow	GO:0015833	peptide transport	4,63E-16	1,89E-12
lightyellow	GO:0034613	cellular protein localization	6,29E-16	2,55E-12
lightyellow	GO:0042886	amide transport	7,16E-16	2,87E-12
lightyellow	GO:0070727	cellular macromolecule localization	8,51E-16	3,36E-12
lightyellow	GO:0044249	cellular biosynthetic process	1,00E-15	3,91E-12
lightyellow	GO:0045184	establishment of protein localization	1,60E-15	6,19E-12
lightyellow	GO:0046907	intracellular transport	2,67E-15	1,03E-11
lightyellow	GO:0034641	cellular nitrogen compound metabolic process	2,76E-15	1,05E-11
lightyellow	GO:0090304	nucleic acid metabolic process	3,17E-15	1,18E-11
lightyellow	GO:0009058	biosynthetic process	5,09E-15	1,84E-11
lightyellow	GO:0016070	RNA metabolic process	7,92E-15	2,85E-11
lightyellow	GO:0071705	nitrogen compound transport	1,10E-14	3,93E-11
lightyellow	GO:1901576	organic substance biosynthetic process	1,29E-14	4,55E-11
lightyellow	GO:0044267	cellular protein metabolic process	2,11E-14	7,34E-11
lightyellow	GO:0005844	polysome	4,42E-14	1,49E-10
lightyellow	GO:1901363	heterocyclic compound binding	1,03E-13	3,36E-10
lightyellow	GO:0097159	organic cyclic compound binding	1,63E-13	5,26E-10
lightyellow	GO:0022613	ribonucleoprotein complex biogenesis	1,82E-13	5,85E-10
lightyellow	GO:0071702	organic substance transport	1,88E-13	5,98E-10
lightyellow	GO:0019538	protein metabolic process	2,24E-13	6,99E-10
lightyellow	GO:0051649	establishment of localization in cell	2,33E-13	7,22E-10
lightyellow	GO:0006364	rRNA processing	3,70E-13	1,11E-09
lightyellow	GO:0060255	regulation of macromolecule metabolic process	4,59E-13	1,36E-09
lightyellow	GO:0042254	ribosome biogenesis	1,02E-12	3,00E-09
lightyellow	GO:0006139	nucleobase-containing compound metabolic process	1,15E-12	3,36E-09
lightyellow	GO:0043232	intracellular non-membrane-bounded organelle	1,36E-12	3,95E-09
lightyellow	GO:0043228	non-membrane-bounded organelle	1,51E-12	4,33E-09
lightyellow	GO:0016072	rRNA metabolic process	1,73E-12	4,93E-09
lightyellow	GO:0048519	negative regulation of biological process	2,76E-12	7,77E-09
lightyellow	GO:0046483	heterocycle metabolic process	3,91E-12	1,08E-08
lightyellow	GO:0006725	cellular aromatic compound metabolic process	4,27E-12	1,17E-08

Module	GO ID	GO Term	p-Value	FDR
lightyellow	GO:0005924	cell-substrate adherens junction	5,75E-12	1,52E-08
lightyellow	GO:0005925	focal adhesion	5,75E-12	1,52E-08
lightyellow	GO:0044260	cellular macromolecule metabolic process	6,24E-12	1,63E-08
lightyellow	GO:0030055	cell-substrate junction	6,25E-12	1,63E-08
lightyellow	GO:0008104	protein localization	1,13E-11	2,81E-08
lightyellow	GO:0033036	macromolecule localization	1,31E-11	3,23E-08
lightyellow	GO:1901360	organic cyclic compound metabolic process	2,24E-11	5,42E-08
lightyellow	GO:0019222	regulation of metabolic process	4,00E-11	9,34E-08
lightyellow	GO:1901564	organonitrogen compound metabolic process	6,43E-11	1,48E-07
lightyellow	GO:0005912	adherens junction	9,93E-11	2,21E-07
lightyellow	GO:0070161	anchoring junction	1,41E-10	3,06E-07
lightyellow	GO:0051641	cellular localization	2,92E-10	6,15E-07
lightyellow	GO:0005829	cytosol	5,88E-10	1,20E-06
lightyellow	GO:0042274	ribosomal small subunit biogenesis	9,24E-10	1,85E-06
lightyellow	GO:0043170	macromolecule metabolic process	1,51E-09	2,94E-06
lightyellow	GO:0034470	ncRNA processing	2,30E-09	4,26E-06
lightyellow	GO:0006807	nitrogen compound metabolic process	8,53E-09	1,46E-05
lightyellow	GO:0006396	RNA processing	7,45E-08	0,000112
lightyellow	GO:0099572	postsynaptic specialization	1,44E-07	0,0002
lightyellow	GO:0030054	cell junction	1,73E-07	0,000233
lightyellow	GO:0042273	ribosomal large subunit biogenesis	2,28E-07	0,000299
lightyellow	GO:0034660	ncRNA metabolic process	2,50E-07	0,000326
lightyellow	GO:0070062	extracellular exosome	3,17E-07	0,0004
lightyellow	GO:0010608	posttranscriptional regulation of gene expression	3,29E-07	0,000413
lightyellow	GO:0043230	extracellular organelle	3,61E-07	0,000448
lightyellow	GO:1903561	extracellular vesicle	3,61E-07	0,000448
lightyellow	GO:0044238	primary metabolic process	4,52E-07	0,00055
lightyellow	GO:0006810	transport	6,00E-07	0,000689
lightyellow	GO:0014069	postsynaptic density	7,48E-07	0,00083
lightyellow	GO:0032279	asymmetric synapse	8,19E-07	0,000896
lightyellow	GO:0051234	establishment of localization	8,66E-07	0,000934
lightyellow	GO:0071704	organic substance metabolic process	1,14E-06	0,001211

Module	GO ID	GO Term	p-Value	FDR
lightyellow	GO:0098984	neuron to neuron synapse	1,27E-06	0,001329
lightyellow	GO:0044237	cellular metabolic process	1,53E-06	0,001581
lightyellow	GO:0003729	mRNA binding	1,77E-06	0,001788
lightyellow	GO:0045727	positive regulation of translation	2,03E-06	0,00201
lightyellow	GO:0005634	nucleus	2,66E-06	0,002588
lightyellow	GO:0005615	extracellular space	4,58E-06	0,004204
lightyellow	GO:0005654	nucleoplasm	4,60E-06	0,00421
lightyellow	GO:1902255	**positive regulation of intrinsic apoptotic signaling pathway by p53 class mediator**	4,75E-06	0,004317
lightyellow	GO:0098794	postsynapse	6,48E-06	0,005752
lightyellow	GO:0034250	positive regulation of cellular amide metabolic process	7,16E-06	0,006289
lightyellow	GO:0031981	nuclear lumen	1,13E-05	0,009341
lightyellow	GO:0044421	extracellular region part	1,43E-05	0,011332
lightyellow	GO:0001732	formation of cytoplasmic translation initiation complex	1,53E-05	0,011939
lightyellow	GO:0033290	eukaryotic 48S preinitiation complex	1,53E-05	0,011939
lightyellow	GO:0048027	mRNA 5'-UTR binding	1,63E-05	0,012662
lightyellow	GO:0045202	synapse	1,88E-05	0,014284
lightyellow	GO:0098556	cytoplasmic side of rough endoplasmic reticulum membrane	1,88E-05	0,014284
lightyellow	GO:0070993	translation preinitiation complex	2,37E-05	0,017243
lightyellow	GO:0002183	cytoplasmic translational initiation	2,70E-05	0,019129
lightyellow	GO:0008152	metabolic process	2,71E-05	0,01916
lightyellow	GO:0005852	eukaryotic translation initiation factor 3 complex	3,50E-05	0,02363
lightyellow	GO:0050789	regulation of biological process	3,52E-05	0,023672
lightyellow	GO:1990948	ubiquitin ligase inhibitor activity	4,63E-05	0,029944
lightyellow	GO:0008135	translation factor activity, RNA binding	4,99E-05	0,032063
lightyellow	GO:0044428	nuclear part	6,04E-05	0,037718
lightyellow	GO:0043488	regulation of mRNA stability	6,14E-05	0,03807
lightyellow	GO:0043487	regulation of RNA stability	7,95E-05	0,047291
magenta	GO:0042886	amide transport	7,26E-08	0,000109
magenta	GO:0015031	protein transport	8,07E-08	0,00012
magenta	GO:0015833	peptide transport	1,04E-07	0,000147
magenta	GO:0070972	protein localization to endoplasmic reticulum	1,17E-07	0,000163
magenta	GO:0045184	establishment of protein localization	1,57E-07	0,000213

Module	GO ID	GO Term	p-Value	FDR
magenta	GO:0045047	protein targeting to ER	3,24E-07	0,000407
magenta	GO:0072599	establishment of protein localization to endoplasmic reticulum	5,15E-07	0,000608
magenta	GO:0006614	SRP-dependent cotranslational protein targeting to membrane	7,94E-07	0,000875
magenta	GO:0006886	intracellular protein transport	8,41E-07	0,000919
magenta	GO:0006613	cotranslational protein targeting to membrane	1,26E-06	0,001319
magenta	GO:0022626	cytosolic ribosome	1,94E-06	0,001936
magenta	GO:0071705	nitrogen compound transport	3,84E-06	0,003623
magenta	GO:0006612	protein targeting to membrane	4,99E-06	0,004527
magenta	GO:0008104	protein localization	8,71E-06	0,007448
magenta	GO:0071702	organic substance transport	1,29E-05	0,010432
magenta	GO:0000184	nuclear-transcribed mRNA catabolic process, nonsense-mediated decay	1,52E-05	0,011939
magenta	GO:0046907	intracellular transport	1,66E-05	0,012842
magenta	GO:0044445	cytosolic part	3,33E-05	0,022659
magenta	GO:0072594	establishment of protein localization to organelle	3,90E-05	0,025807
magenta	GO:0033036	macromolecule localization	3,91E-05	0,025837
magenta	GO:0090150	establishment of protein localization to membrane	5,86E-05	0,036913
magenta	GO:0072717	cellular response to actinomycin D	7,28E-05	0,043848
midnightblue	GO:0098796	membrane protein complex	2,49E-09	4,60E-06
midnightblue	GO:0022904	respiratory electron transport chain	7,18E-08	0,000108
midnightblue	GO:0022900	electron transport chain	5,06E-07	0,000601
midnightblue	GO:0042775	mitochondrial ATP synthesis coupled electron transport	1,12E-06	0,001192
midnightblue	GO:0042773	ATP synthesis coupled electron transport	1,29E-06	0,001345
midnightblue	GO:0015980	energy derivation by oxidation of organic compounds	3,92E-06	0,003666
midnightblue	GO:0045333	cellular respiration	3,96E-06	0,003702
midnightblue	GO:0006119	oxidative phosphorylation	6,57E-06	0,00582
midnightblue	GO:0005576	extracellular region	1,02E-05	0,008549
midnightblue	GO:0043473	pigmentation	1,86E-05	0,014249
midnightblue	GO:0044421	extracellular region part	2,20E-05	0,01627
midnightblue	GO:0005615	extracellular space	2,90E-05	0,020185
midnightblue	GO:0070469	respiratory chain	3,21E-05	0,022041
midnightblue	GO:0006091	generation of precursor metabolites and energy	3,87E-05	0,025786
midnightblue	GO:0098803	respiratory chain complex	3,88E-05	0,025807

Module	GO ID	GO Term	p-Value	FDR
midnightblue	GO:0003924	GTPase activity	6,75E-05	0,041131
pink	GO:0042611	MHC protein complex	2,25E-09	4,20E-06
pink	GO:0071346	cellular response to interferon-gamma	7,71E-07	0,000853
pink	GO:0060333	interferon-gamma-mediated signaling pathway	8,81E-07	0,000948
pink	GO:0042612	MHC class I protein complex	9,09E-07	0,000976
pink	GO:0002480	antigen processing and presentation of exogenous peptide antigen via MHC class I, TAP-independent	3,07E-06	0,00294
pink	GO:0034341	response to interferon-gamma	3,41E-06	0,003245
pink	GO:0030670	phagocytic vesicle membrane	5,12E-06	0,004622
pink	GO:0005178	integrin binding	1,38E-05	0,010997
pink	GO:0030666	endocytic vesicle membrane	1,62E-05	0,012624
pink	GO:0045649	regulation of macrophage differentiation	1,71E-05	0,01316
pink	GO:0071556	integral component of lumenal side of endoplasmic reticulum membrane	2,42E-05	0,017507
pink	GO:0098553	lumenal side of endoplasmic reticulum membrane	2,42E-05	0,017507
pink	GO:0042605	peptide antigen binding	3,30E-05	0,022466
pink	GO:0045335	phagocytic vesicle	3,35E-05	0,022766
pink	GO:0045087	innate immune response	8,25E-05	0,048804
purple	GO:0000118	histone deacetylase complex	1,46E-05	0,011504
purple	GO:0098800	inner mitochondrial membrane protein complex	1,65E-05	0,012772
purple	GO:0099132	ATP hydrolysis coupled cation transmembrane transport	4,64E-05	0,02997
purple	GO:1902600	proton transmembrane transport	5,95E-05	0,037283
purple	GO:0070491	repressing transcription factor binding	6,18E-05	0,038251
purple	GO:0006119	oxidative phosphorylation	6,72E-05	0,04112
royalblue	GO:0048525	negative regulation of viral process	1,51E-10	3,25E-07
royalblue	GO:0060333	interferon-gamma-mediated signaling pathway	1,06E-09	2,08E-06
royalblue	GO:0034341	response to interferon-gamma	1,85E-09	3,55E-06
royalblue	GO:0006952	defense response	4,18E-09	7,55E-06
royalblue	GO:0071346	cellular response to interferon-gamma	6,96E-09	1,21E-05
royalblue	GO:0045087	innate immune response	7,44E-09	1,28E-05
royalblue	GO:0034097	response to cytokine	1,01E-08	1,70E-05
royalblue	GO:1903901	negative regulation of viral life cycle	1,12E-08	1,85E-05
royalblue	GO:0043901	negative regulation of multi-organism process	2,33E-08	3,71E-05
royalblue	GO:0060337	type I interferon signaling pathway	4,92E-08	7,53E-05

Module	GO ID	GO Term	p-Value	FDR
royalblue	GO:0071357	cellular response to type I interferon	4,92E-08	7,53E-05
royalblue	GO:0034340	response to type I interferon	9,41E-08	0,000137
royalblue	GO:0019221	cytokine-mediated signaling pathway	6,09E-07	0,000696
royalblue	GO:0009615	response to virus	7,06E-07	0,00079
royalblue	GO:0051607	defense response to virus	9,15E-07	0,00098
royalblue	GO:0043900	regulation of multi-organism process	2,08E-06	0,002061
royalblue	GO:0006955	immune response	2,98E-06	0,002879
royalblue	GO:0071345	cellular response to cytokine stimulus	3,09E-06	0,002951
royalblue	GO:0050792	regulation of viral process	3,89E-06	0,003646
royalblue	GO:0045071	negative regulation of viral genome replication	4,59E-06	0,004204
royalblue	GO:1903900	regulation of viral life cycle	5,15E-06	0,004628
royalblue	GO:0043903	regulation of symbiosis, encompassing mutualism through parasitism	7,12E-06	0,006265
royalblue	GO:0009605	response to external stimulus	1,03E-05	0,008567
royalblue	GO:0098542	defense response to other organism	2,11E-05	0,015653
royalblue	GO:0043207	response to external biotic stimulus	2,42E-05	0,017507
royalblue	GO:0051707	response to other organism	2,42E-05	0,017507
royalblue	GO:0071310	cellular response to organic substance	4,24E-05	0,027683
royalblue	GO:0009607	response to biotic stimulus	4,97E-05	0,031966
royalblue	GO:0002376	immune system process	5,92E-05	0,037158
royalblue	GO:0007166	cell surface receptor signaling pathway	6,47E-05	0,039857
royalblue	GO:0003725	double-stranded RNA binding	6,55E-05	0,040231
royalblue	GO:0005576	extracellular region	6,65E-05	0,04079
royalblue	GO:0070887	cellular response to chemical stimulus	7,21E-05	0,043492
royalblue	GO:0007165	signal transduction	7,54E-05	0,04534

Supplementary Table S6: Pathways enrichment results of WGCNA modules related to programmed cell death.
List of pathways (Pathway) enriched for modules identified by WGCNA (Module). Reference source database (Source), p-values (p-value) and q-value (q-value) are also indicated.

Module	Pathway	p-value	q-value
Black	Separation of Sister Chromatids	3,86E-08	2,91E-05
Black	Mitotic Anaphase	1,17E-07	3,25E-05
Black	Mitotic Metaphase and Anaphase	1,29E-07	3,25E-05
Black	Mitotic Spindle Checkpoint	2,39E-06	0,000418144
Black	Cell Cycle	2,77E-06	0,000418144
Black	M Phase	4,36E-06	0,000535287
Black	Metabolism of RNA	4,96E-06	0,000535287
Black	Resolution of Sister Chromatid Cohesion	1,13E-05	0,000970586
Black	Cell Cycle, Mitotic	1,16E-05	0,000970586
Black	Cohesin Loading onto Chromatin	2,99E-05	0,002258879
Black	isoleucine degradation	6,82E-05	0,004689679
Black	pyruvate decarboxylation to acetyl CoA	7,68E-05	0,004838519
Black	Mitotic Prometaphase	9,38E-05	0,005297144
Black	Processing of Capped Intron-Containing Pre-mRNA	9,81E-05	0,005297144
Black	Mitotic Telophase/Cytokinesis	0,000133696	0,006672934
Black	Cell Cycle Checkpoints	0,000141226	0,006672934
Blue	Innate Immune System	2,20E-17	4,09E-14
Blue	Neutrophil degranulation	4,76E-15	3,65E-12
Blue	Immune System	5,88E-15	3,65E-12
Blue	VEGFA-VEGFR2 Signaling Pathway	4,48E-10	2,08E-07
Blue	CLEC7A (Dectin-1) signaling	1,86E-09	6,90E-07
Blue	miR-targeted genes in leukocytes - TarBase	1,45E-08	4,48E-06
Blue	PDGFR-beta signaling pathway	2,55E-08	6,77E-06
Blue	EGFR1	6,04E-08	1,40E-05
Blue	EPO signaling pathway	1,86E-07	3,82E-05
Blue	IL5	2,25E-07	3,82E-05
Blue	C-type lectin receptors (CLRs)	2,26E-07	3,82E-05
Blue	Shigellosis - Homo sapiens (human)	2,65E-07	4,08E-05
Blue	Lysosome - Homo sapiens (human)	2,92E-07	4,08E-05

Module	Pathway	p-value	q-value
Blue	NOD-like receptor signaling pathway - Homo sapiens (human)	3,07E-07	4,08E-05
Blue	JAK STAT MolecularVariation 2	3,79E-07	4,42E-05
Blue	TCR	4,00E-07	4,42E-05
Blue	Apoptosis - Homo sapiens (human)	4,04E-07	4,42E-05
Blue	Osteoclast differentiation - Homo sapiens (human)	4,44E-07	4,58E-05
Blue	TNFalpha	6,61E-07	6,11E-05
Blue	B Cell Receptor Signaling Pathway	6,75E-07	6,11E-05
Blue	RHO GTPases Activate WASPs and WAVEs	6,90E-07	6,11E-05
Blue	hiv-1 nef: negative effector of fas and tnf	7,87E-07	6,66E-05
Blue	Epstein-Barr virus infection - Homo sapiens (human)	8,65E-07	6,99E-05
Blue	T-Cell antigen Receptor (TCR) Signaling Pathway	9,13E-07	7,08E-05
Blue	Hepatitis B - Homo sapiens (human)	1,10E-06	8,22E-05
Blue	RANKL-RANK (Receptor activator of NFKB (ligand)) Signaling Pathway	1,24E-06	8,90E-05
Blue	TNF alpha Signaling Pathway	1,48E-06	0,000101665
Blue	EPHB-mediated forward signaling	3,34E-06	0,00022199
Blue	Signaling by Interleukins	3,71E-06	0,000237708
Blue	Oncogenic MAPK signaling	4,33E-06	0,000268502
Blue	IL4	6,33E-06	0,000369488
Blue	NRF2-ARE regulation	6,36E-06	0,000369488
Blue	NF-kappa B signaling pathway - Homo sapiens (human)	6,80E-06	0,000383476
Blue	C-type lectin receptor signaling pathway - Homo sapiens (human)	7,23E-06	0,000395345
Blue	Death Receptor Signalling	7,71E-06	0,00039933
Blue	Kaposi sarcoma-associated herpesvirus infection - Homo sapiens (human)	7,73E-06	0,00039933
Blue	DDX58/IFIH1-mediated induction of interferon-alpha/beta	9,52E-06	0,000478733
Blue	TCR signaling in naïve CD4+ T cells	1,08E-05	0,000528662
Blue	Toll-Like Receptors Cascades	1,21E-05	0,000528662
Blue	Ferroptosis - Homo sapiens (human)	1,24E-05	0,000528662
Blue	Ferroptosis	1,24E-05	0,000528662
Blue	Apoptosis	1,28E-05	0,000528662
Blue	MyD88 cascade initiated on plasma membrane	1,28E-05	0,000528662
Blue	Toll Like Receptor 10 (TLR10) Cascade	1,28E-05	0,000528662
Blue	Toll Like Receptor 5 (TLR5) Cascade	1,28E-05	0,000528662
Blue	Endocytosis - Homo sapiens (human)	1,34E-05	0,00054379

Module	Pathway	p-value	q-value
Blue	Signaling by BRAF and RAF fusions	1,39E-05	0,000548913
Blue	Cytokine Signaling in Immune system	1,43E-05	0,000548913
Blue	Brain-Derived Neurotrophic Factor (BDNF) signaling pathway	1,47E-05	0,000548913
Blue	TRAF6 mediated induction of NFkB and MAP kinases upon TLR7/8 or 9 activation	1,48E-05	0,000548913
Blue	Platelet activation, signaling and aggregation	1,63E-05	0,000596041
Blue	MyD88 dependent cascade initiated on endosome	1,95E-05	0,000678399
Blue	Toll Like Receptor 7/8 (TLR7/8) Cascade	1,95E-05	0,000678399
Blue	IFN-gamma pathway	1,98E-05	0,000678399
Blue	Interleukin-1 signaling	2,01E-05	0,000678399
Blue	Insulin Signaling	2,18E-05	0,000725392
Blue	Apoptosis Modulation and Signaling	2,24E-05	0,000729389
Blue	IL5-mediated signaling events	2,40E-05	0,000757691
Blue	Atypical NF-kappaB pathway	2,40E-05	0,000757691
Blue	Fas Ligand (FasL) pathway and Stress induction of Heat Shock Proteins (HSP) regulation	2,48E-05	0,000767378
Blue	Role Altered Glycolysation of MUC1 in Tumour Microenvironment	2,54E-05	0,00077314
Blue	Necroptosis - Homo sapiens (human)	2,64E-05	0,00078587
Blue	HIV-1 Nef: Negative effector of Fas and TNF-alpha	2,66E-05	0,00078587
Blue	JAK STAT pathway and regulation	2,74E-05	0,000796903
Blue	Toll Like Receptor 4 (TLR4) Cascade	2,96E-05	0,000847779
Blue	Interleukin-11 Signaling Pathway	3,07E-05	0,000864913
Blue	Toll Like Receptor 9 (TLR9) Cascade	3,32E-05	0,000898962
Blue	Rho GTPase cycle	3,33E-05	0,000898962
Blue	nf-kb signaling pathway	3,38E-05	0,000898962
Blue	TSLP	3,38E-05	0,000898962
Blue	IL-4 Signaling Pathway	3,70E-05	0,000956763
Blue	RAC1 signaling pathway	3,70E-05	0,000956763
Blue	Phytochemical activity on NRF2 transcriptional activation	3,85E-05	0,000979809
Blue	IL6	3,92E-05	0,000984042
Blue	CXCR4-mediated signaling events	4,21E-05	0,001044208
Blue	Pathways in cancer - Homo sapiens (human)	4,34E-05	0,001054824
Blue	Nonalcoholic fatty liver disease	4,37E-05	0,001054824
Blue	Neurotrophin signaling pathway - Homo sapiens (human)	4,42E-05	0,001054824
Blue	Toll Like Receptor 3 (TLR3) Cascade	4,85E-05	0,001086449

Module	Pathway	p-value	q-value
Blue	MyD88:Mal cascade initiated on plasma membrane	4,85E-05	0,001086449
Blue	Toll Like Receptor TLR1:TLR2 Cascade	4,85E-05	0,001086449
Blue	Toll Like Receptor TLR6:TLR2 Cascade	4,85E-05	0,001086449
Blue	Toll Like Receptor 2 (TLR2) Cascade	4,85E-05	0,001086449
Blue	Signaling by moderate kinase activity BRAF mutants	5,41E-05	0,001176632
Blue	Paradoxical activation of RAF signaling by kinase inactive BRAF	5,41E-05	0,001176632
Blue	AGE-RAGE pathway	5,44E-05	0,001176632
Blue	TNF signaling pathway - Homo sapiens (human)	5,90E-05	0,001261696
Blue	Canonical NF-kappaB pathway	6,56E-05	0,001387534
Blue	Platelet activation - Homo sapiens (human)	6,78E-05	0,001416454
Blue	Toll-like Receptor Signaling	7,30E-05	0,001509168
Blue	TRIF(TICAM1)-mediated TLR4 signaling	7,82E-05	0,001581536
Blue	MyD88-independent TLR4 cascade	7,82E-05	0,001581536
Blue	Non-alcoholic fatty liver disease (NAFLD) - Homo sapiens (human)	7,93E-05	0,001585208
Blue	Adipocytokine signaling pathway - Homo sapiens (human)	8,55E-05	0,001692763
Blue	TAK1 activates NFkB by phosphorylation and activation of IKKs complex	9,34E-05	0,001808869
Blue	rho cell motility signaling pathway	9,34E-05	0,001808869
Blue	Photodynamic therapy-induced AP-1 survival signaling,	9,83E-05	0,001884475
Blue	Fluid shear stress and atherosclerosis - Homo sapiens (human)	9,93E-05	0,001884575
Blue	BCR	0,000112262	0,00210917
Blue	IL3	0,000117131	0,002154876
Blue	Oxidative Stress	0,000118171	0,002154876
Blue	Resistin as a regulator of inflammation	0,000118171	0,002154876
Blue	ErbB1 downstream signaling	0,000136954	0,002473155
Blue	tnfr2 signaling pathway	0,000141453	0,002505739
Blue	how does salmonella hijack a cell	0,000141453	0,002505739
Blue	Th17 cell differentiation - Homo sapiens (human)	0,000152465	0,002675331
Blue	TRAF6 mediated NF-kB activation	0,000155554	0,002704028
Blue	LPA receptor mediated events	0,000161714	0,002785081
Blue	keratinocyte differentiation	0,000164107	0,002800359
Blue	Bacterial invasion of epithelial cells - Homo sapiens (human)	0,000171547	0,00287457
Blue	EPH-Ephrin signaling	0,000171547	0,00287457
Blue	Apoptosis Modulation by HSP70	0,000177123	0,002941499

Module	Pathway	p-value	q-value
Blue	Tacrolimus/Cyclosporine Pathway, Pharmacodynamics	0,000182414	0,003002563
Blue	FAS (CD95) signaling pathway	0,000184201	0,003005388
Blue	RAGE	0,000218566	0,003506253
Blue	IL2	0,00022244	0,003506253
Blue	Leptin signaling pathway	0,00022244	0,003506253
Blue	Chronic myeloid leukemia - Homo sapiens (human)	0,00022244	0,003506253
Blue	Gene and protein expression by JAK-STAT signaling after Interleukin-12 stimulation	0,000227112	0,00351412
Blue	Signaling by RAS mutants	0,000227112	0,00351412
Blue	AGE-RAGE signaling pathway in diabetic complications - Homo sapiens (human)	0,000228607	0,00351412
Blue	Membrane Trafficking	0,00024121	0,003677466
Blue	Interleukin-1 family signaling	0,000252369	0,003816316
Blue	TNF receptor signaling pathway	0,000260474	0,003907107
Blue	MAPK Signaling Pathway	0,000272518	0,004055068
Blue	Glutaminolysis and Cancer	0,000277881	0,004102046
Blue	Toxoplasmosis - Homo sapiens (human)	0,000281523	0,004123093
Blue	BH3-only proteins associate with and inactivate anti-apoptotic BCL-2 members	0,000300823	0,004371339
Blue	Chemokine signaling pathway	0,000306417	0,004384846
Blue	Nucleotide-binding domain, leucine rich repeat containing receptor (NLR) signaling pathways	0,000308825	0,004384846
Blue	Thymic Stromal LymphoPoietin (TSLP) Signaling Pathway	0,000308825	0,004384846
Blue	Chagas disease (American trypanosomiasis) - Homo sapiens (human)	0,000313892	0,004423026
Blue	BCR signaling pathway	0,000324803	0,004452867
Blue	Epithelial cell signaling in Helicobacter pylori infection - Homo sapiens (human)	0,000324803	0,004452867
Blue	stress induction of hsp regulation	0,0003303	0,004452867
Blue	Spry regulation of FGF signaling	0,0003303	0,004452867
Blue	chaperones modulate interferon signaling pathway	0,0003303	0,004452867
Blue	Signaling by Rho GTPases	0,000332599	0,004452867
Blue	G13 Signaling Pathway	0,000337556	0,004452867
Blue	Intracellular Signalling Through Adenosine Receptor A2b and Adenosine	0,000337556	0,004452867
Blue	Intracellular Signalling Through Adenosine Receptor A2a and Adenosine	0,000337556	0,004452867
Blue	MAPK signaling pathway - Homo sapiens (human)	0,000373684	0,004894728
Blue	Th1 and Th2 cell differentiation - Homo sapiens (human)	0,000382144	0,004970551
Blue	NRF2 pathway	0,000397102	0,005129238
Blue	Ghrelin	0,000407273	0,005206752

Module	Pathway	p-value	q-value
Blue	Signaling events mediated by Hepatocyte Growth Factor Receptor (c-Met)	0,000408702	0,005206752
Blue	IL-3 Signaling Pathway	0,000427881	0,005383161
Blue	The human immune response to tuberculosis	0,000431232	0,005383161
Blue	Vitamin D in inflammatory diseases	0,000431232	0,005383161
Blue	Measles - Homo sapiens (human)	0,000465839	0,005724119
Blue	JAK-STAT	0,000468938	0,005724119
Blue	Quercetin and Nf-kB- AP-1 Induced Cell Apoptosis	0,000476223	0,005724119
Blue	GRB2:SOS provides linkage to MAPK signaling for Integrins	0,000476223	0,005724119
Blue	Interleukin-4 and 13 signaling	0,000476223	0,005724119
Blue	CDC42 signaling events	0,00047701	0,005724119
Blue	Integrated Lung Cancer Pathway	0,000488252	0,005821465
Blue	cd40l signaling pathway	0,000521197	0,006097027
Blue	MET activates RAP1 and RAC1	0,000521197	0,006097027
Blue	Supression of HMGB1 mediated inflammation by THBD	0,000521197	0,006097027
Blue	RANKL	0,000560262	0,006472589
Blue	RIP-mediated NFkB activation via ZBP1	0,000560262	0,006472589
Blue	VEGF	0,000568205	0,006523836
Blue	Nucleotide-binding Oligomerization Domain (NOD) pathway	0,0005818	0,006604437
Blue	Cytosolic sensors of pathogen-associated DNA	0,000582327	0,006604437
Blue	Chemokine signaling pathway - Homo sapiens (human)	0,000608396	0,006858282
Blue	Salmonella infection - Homo sapiens (human)	0,000639939	0,007170405
Blue	MAP3K8 (TPL2)-dependent MAPK1/3 activation	0,000665838	0,007285054
Blue	Omega-3 fatty acid metabolism	0,000665838	0,007285054
Blue	bone remodeling	0,000665838	0,007285054
Blue	p75NTR signals via NF-kB	0,000665838	0,007285054
Blue	JAK-STAT signaling pathway - Homo sapiens (human)	0,000672611	0,007316125
Blue	DNA Damage Response (only ATM dependent)	0,000684936	0,007406867
Blue	JAK STAT MolecularVariation 1	0,000709364	0,007626691
Blue	Human T-cell leukemia virus 1 infection - Homo sapiens (human)	0,000727825	0,007742227
Blue	Diseases of signal transduction	0,000728435	0,007742227
Blue	ceramide signaling pathway	0,000756721	0,007907311
Blue	Trk receptor signaling mediated by the MAPK pathway	0,000756721	0,007907311
Blue	NOD1/2 Signaling Pathway	0,000756721	0,007907311

Module	Pathway	p-value	q-value
Blue	Apoptosis-related network due to altered Notch3 in ovarian cancer	0,000779652	0,008101416
Blue	IL-1 NFkB	0,000797914	0,008245116
Blue	Leukocyte transendothelial migration - Homo sapiens (human)	0,000821262	0,008439491
Blue	IL-13 signaling	0,000836175	0,00854552
Blue	TCR signaling in naïve CD8+ T cells	0,000896985	0,00895238
Blue	Interferon type I signaling pathways	0,000896985	0,00895238
Blue	MAP kinase activation	0,000903772	0,00895238
Blue	Interleukin-17 signaling	0,000903772	0,00895238
Blue	role of pi3k subunit p85 in regulation of actin organization and cell migration	0,000906753	0,00895238
Blue	y branching of actin filaments	0,000906753	0,00895238
Blue	Signaling by high-kinase activity BRAF mutants	0,00091449	0,00895238
Blue	CD40/CD40L signaling	0,00091449	0,00895238
Blue	Structural Pathway of Interleukin 1 (IL-1)	0,000952235	0,009273069
Blue	Vesicle-mediated transport	0,000965678	0,009316374
Blue	Signaling by Receptor Tyrosine Kinases	0,000966699	0,009316374
Blue	Human cytomegalovirus infection - Homo sapiens (human)	0,000983068	0,009425292
Blue	miR-targeted genes in lymphocytes - TarBase	0,001020689	0,009687953
Blue	Beta-agonist/Beta-blocker Pathway, Pharmacodynamics	0,001020881	0,009687953
Blue	IL-1 signaling pathway	0,001028261	0,009708459
Blue	Nuclear Receptors Meta-Pathway	0,001048979	0,009854048
Brown	Cilium Assembly	5,48E-13	8,22E-10
Brown	Organelle biogenesis and maintenance	3,39E-11	2,54E-08
Brown	Anchoring of the basal body to the plasma membrane	2,57E-10	1,28E-07
Brown	Intra-Golgi and retrograde Golgi-to-ER traffic	4,84E-09	1,82E-06
Brown	Metabolism of proteins	1,30E-08	3,90E-06
Brown	Membrane Trafficking	6,61E-08	1,65E-05
Brown	Vesicle-mediated transport	2,36E-07	5,06E-05
Brown	Loss of Nlp from mitotic centrosomes	3,35E-07	5,59E-05
Brown	Loss of proteins required for interphase microtubule organization from the centrosome	3,35E-07	5,59E-05
Brown	Recruitment of NuMA to mitotic centrosomes	3,83E-07	5,74E-05
Brown	Recruitment of mitotic centrosome proteins and complexes	4,59E-07	5,74E-05
Brown	Centrosome maturation	4,59E-07	5,74E-05
Brown	AURKA Activation by TPX2	6,03E-07	6,96E-05

Module	Pathway	p-value	q-value
Brown	Retrograde transport at the Trans-Golgi-Network	1,31E-06	0,000140203
Brown	Regulation of PLK1 Activity at G2/M Transition	1,50E-06	0,000150298
Brown	Neddylation	2,49E-06	0,000233385
Brown	G2/M Transition	3,42E-06	0,000291195
Brown	Mitotic Prometaphase	3,49E-06	0,000291195
Brown	Mitotic G2-G2/M phases	4,30E-06	0,000339187
Brown	Post-translational protein modification	8,49E-06	0,000593876
Brown	rRNA modification in the nucleus and cytosol	8,71E-06	0,000593876
Brown	rRNA processing in the nucleus and cytosol	8,71E-06	0,000593876
Brown	TGF-beta super family signaling pathway canonical	1,55E-05	0,001012912
Brown	TLR JNK	1,79E-05	0,001031539
Brown	Signaling events mediated by focal adhesion kinase	1,79E-05	0,001031539
Brown	IL-1 JNK	1,79E-05	0,001031539
Brown	rRNA processing	2,50E-05	0,001358378
Brown	Proteasome - Homo sapiens (human)	2,54E-05	0,001358378
Brown	IL-1 p38	3,45E-05	0,001761846
Brown	Ciliary landscape	3,52E-05	0,001761846
Brown	Asparagine N-linked glycosylation	3,86E-05	0,001868761
Brown	TNF	4,04E-05	0,001892423
Brown	ER to Golgi Anterograde Transport	4,50E-05	0,002045422
Brown	S Phase	5,18E-05	0,002286362
Brown	Protein processing in endoplasmic reticulum - Homo sapiens (human)	5,59E-05	0,002397687
Brown	Transport to the Golgi and subsequent modification	7,23E-05	0,003011508
Brown	TLR p38	0,000107115	0,004342501
Brown	IL-1 NFkB	0,000124152	0,004775085
Brown	Proteasome Degradation	0,000124152	0,004775085
Brown	DroToll-like	0,000143443	0,005379123
Brown	Notch	0,000185771	0,006796492
Brown	UCH proteinases	0,000194507	0,006946694
Brown	TLR NFkB	0,000248136	0,008655922
Cyan	Cell Cycle	1,46E-62	8,05E-60
Cyan	Cell Cycle, Mitotic	1,15E-58	3,18E-56
Cyan	Cell Cycle Checkpoints	7,97E-47	1,46E-44

Module	Pathway	p-value	q-value
Cyan	Mitotic Prometaphase	6,48E-36	8,93E-34
Cyan	Resolution of Sister Chromatid Cohesion	4,63E-33	5,10E-31
Cyan	M Phase	2,20E-32	2,02E-30
Cyan	Retinoblastoma Gene in Cancer	1,02E-29	8,03E-28
Cyan	Mitotic Metaphase and Anaphase	2,41E-29	1,66E-27
Cyan	Separation of Sister Chromatids	3,28E-29	2,01E-27
Cyan	Amplification of signal from unattached kinetochores via a MAD2 inhibitory signal	1,04E-28	5,22E-27
Cyan	Amplification of signal from the kinetochores	1,04E-28	5,22E-27
Cyan	Mitotic Spindle Checkpoint	3,73E-28	1,71E-26
Cyan	Mitotic Anaphase	4,73E-28	2,00E-26
Cyan	RHO GTPases Activate Formins	1,63E-25	6,42E-24
Cyan	DNA Replication	1,83E-20	6,71E-19
Cyan	Cell cycle - Homo sapiens (human)	4,50E-20	1,55E-18
Cyan	PLK1 signaling events	1,86E-19	6,02E-18
Cyan	DNA strand elongation	1,53E-18	4,69E-17
Cyan	Aurora B signaling	2,34E-18	6,77E-17
Cyan	Synthesis of DNA	3,52E-18	9,70E-17
Cyan	S Phase	4,40E-18	1,15E-16
Cyan	RHO GTPase Effectors	5,50E-18	1,38E-16
Cyan	G1/S Transition	5,93E-18	1,41E-16
Cyan	G2/M Checkpoints	6,13E-18	1,41E-16
Cyan	Mitotic G1-G1/S phases	6,60E-18	1,45E-16
Cyan	Cell Cycle	7,34E-18	1,56E-16
Cyan	Activation of ATR in response to replication stress	1,87E-17	3,82E-16
Cyan	Signaling by Rho GTPases	4,02E-17	7,91E-16
Cyan	APC/C-mediated degradation of cell cycle proteins	6,86E-17	1,26E-15
Cyan	Regulation of mitotic cell cycle	6,86E-17	1,26E-15
Cyan	Unwinding of DNA	2,60E-15	4,62E-14
Cyan	DNA Replication	5,82E-15	1,00E-13
Cyan	Mitotic G1-G1-S phases	2,58E-14	4,31E-13
Cyan	ATR signaling pathway	1,26E-12	2,05E-11
Cyan	APC/C:Cdc20 mediated degradation of mitotic proteins	3,74E-12	5,88E-11
Cyan	Activation of APC/C and APC/C:Cdc20 mediated degradation of mitotic proteins	5,45E-12	8,35E-11

Module	Pathway	p-value	q-value
Cyan	Activation of the pre-replicative complex	1,11E-11	1,66E-10
Cyan	Regulation of APC/C activators between G1/S and early anaphase	2,15E-11	3,12E-10
Cyan	DNA replication - Homo sapiens (human)	2,95E-11	4,17E-10
Cyan	DNA Replication Pre-Initiation	3,99E-11	5,37E-10
Cyan	M/G1 Transition	3,99E-11	5,37E-10
Cyan	G1 to S cell cycle control	4,54E-11	5,95E-10
Cyan	Condensation of Prometaphase Chromosomes	5,47E-11	7,00E-10
Cyan	Gastric Cancer Network 1	6,78E-11	8,49E-10
Cyan	FOXM1 transcription factor network	1,59E-10	1,95E-09
Cyan	DNA Repair	2,93E-10	3,51E-09
Cyan	E2F transcription factor network	3,17E-10	3,72E-09
Cyan	Switching of origins to a post-replicative state	3,33E-10	3,83E-09
Cyan	Regulation of sister chromatid separation at the metaphase-anaphase transition	4,29E-10	4,83E-09
Cyan	Mitotic G2-G2/M phases	5,72E-10	6,30E-09
Cyan	G0 and Early G1	8,43E-10	9,11E-09
Cyan	DNA Double-Strand Break Repair	8,83E-10	9,36E-09
Cyan	Transcriptional Regulation by TP53	1,03E-09	1,07E-08
Cyan	Orc1 removal from chromatin	1,20E-09	1,23E-08
Cyan	DNA Damage Response	1,58E-09	1,58E-08
Cyan	APC:Cdc20 mediated degradation of cell cycle proteins prior to satisfation of the cell cycle checkpoint	2,34E-09	2,30E-08
Cyan	miRNA Regulation of DNA Damage Response	2,45E-09	2,37E-08
Cyan	Chromosome Maintenance	3,05E-09	2,90E-08
Cyan	Regulation of TP53 Activity through Phosphorylation	4,10E-09	3,83E-08
Cyan	G2/M Transition	4,50E-09	4,13E-08
Cyan	Kinesins	4,65E-09	4,20E-08
Cyan	Assembly of the pre-replicative complex	4,88E-09	4,34E-08
Cyan	Fanconi anemia pathway	8,78E-09	7,68E-08
Cyan	TP53 Regulates Transcription of Cell Cycle Genes	2,29E-08	1,97E-07
Cyan	Homology Directed Repair	4,77E-08	4,04E-07
Cyan	Cdc20:Phospho-APC/C mediated degradation of Cyclin A	5,17E-08	4,31E-07
Cyan	Activation of E2F1 target genes at G1/S	6,12E-08	4,96E-07
Cyan	G1/S-Specific Transcription	6,12E-08	4,96E-07
Cyan	Processing of DNA double-strand break ends	8,12E-08	6,49E-07

Module	Pathway	p-value	q-value
Cyan	cdk regulation of dna replication	9,08E-08	7,03E-07
Cyan	Deposition of new CENPA-containing nucleosomes at the centromere	9,19E-08	7,03E-07
Cyan	Nucleosome assembly	9,19E-08	7,03E-07
Cyan	Oocyte meiosis - Homo sapiens (human)	1,19E-07	9,00E-07
Cyan	Aurora A signaling	1,46E-07	1,09E-06
Cyan	role of ran in mitotic spindle regulation	1,84E-07	1,35E-06
Cyan	HDR through Homologous Recombination (HR) or Single Strand Annealing (SSA)	2,37E-07	1,72E-06
Cyan	Interconversion of nucleotide di- and triphosphates	2,89E-07	2,05E-06
Cyan	Regulation of TP53 Activity	2,90E-07	2,05E-06
Cyan	Phosphorylation of Emi1	4,74E-07	3,30E-06
Cyan	p53 signaling pathway - Homo sapiens (human)	5,02E-07	3,46E-06
Cyan	Presynaptic phase of homologous DNA pairing and strand exchange	7,80E-07	5,31E-06
Cyan	Cyclin A/B1/B2 associated events during G2/M transition	8,01E-07	5,31E-06
Cyan	APC-Cdc20 mediated degradation of Nek2A	8,01E-07	5,31E-06
Cyan	Homologous DNA Pairing and Strand Exchange	1,32E-06	8,68E-06
Cyan	COPI-dependent Golgi-to-ER retrograde traffic	1,54E-06	9,98E-06
Cyan	BARD1 signaling events	2,05E-06	1,32E-05
Cyan	Recognition of DNA damage by PCNA-containing replication complex	3,11E-06	1,97E-05
Cyan	TP53 Regulates Transcription of Genes Involved in G2 Cell Cycle Arrest	3,16E-06	1,98E-05
Cyan	HDR through Homologous Recombination (HRR)	3,52E-06	2,18E-05
Cyan	Gastric Cancer Network 2	3,79E-06	2,32E-05
Cyan	DNA Damage Bypass	3,89E-06	2,36E-05
Cyan	G2/M DNA damage checkpoint	5,31E-06	3,18E-05
Cyan	Lagging Strand Synthesis	5,60E-06	3,25E-05
Cyan	Inhibition of the proteolytic activity of APC/C required for the onset of anaphase by mitotic spindle checkpoint components	5,60E-06	3,25E-05
Cyan	Inactivation of APC/C via direct inhibition of the APC/C complex	5,60E-06	3,25E-05
Cyan	cell cycle: g2/m checkpoint	7,27E-06	4,17E-05
Cyan	Human T-cell leukemia virus 1 infection - Homo sapiens (human)	8,55E-06	4,86E-05
Cyan	HDR through Single Strand Annealing (SSA)	9,19E-06	5,16E-05
Cyan	superpathway of pyrimidine deoxyribonucleotides de novo biosynthesis	9,31E-06	5,18E-05
Cyan	Transcription of E2F targets under negative control by p107 (RBL1) and p130 (RBL2) in complex with HDAC1	9,88E-06	5,39E-05
Cyan	The role of GTSE1 in G2/M progression after G2 checkpoint	9,88E-06	5,39E-05
Cyan	p73 transcription factor network	1,09E-05	5,91E-05

Module	Pathway	p-value	q-value
Cyan	Factors involved in megakaryocyte development and platelet production	1,11E-05	5,93E-05
Cyan	cyclins and cell cycle regulation	1,18E-05	6,23E-05
Cyan	Telomere C-strand (Lagging Strand) Synthesis	1,47E-05	7,71E-05
Cyan	rb tumor suppressor/checkpoint signaling in response to dna damage	2,10E-05	0,000106935
Cyan	Gemcitabine Action Pathway	2,10E-05	0,000106935
Cyan	Gemcitabine Metabolism Pathway	2,10E-05	0,000106935
Cyan	APC/C:Cdh1 mediated degradation of Cdc20 and other APC/C:Cdh1 targeted proteins in late mitosis/early G1	2,23E-05	0,00011194
Cyan	Regulation of PLK1 Activity at G2/M Transition	2,23E-05	0,00011194
Cyan	G2/M DNA replication checkpoint	2,38E-05	0,000116012
Cyan	G2 Phase	2,38E-05	0,000116012
Cyan	Mitotic G2-G2-M phases	2,38E-05	0,000116012
Cyan	Golgi-to-ER retrograde transport	2,70E-05	0,000130696
Cyan	TP53 Regulates Transcription of DNA Repair Genes	2,90E-05	0,00013444
Cyan	Polymerase switching on the C-strand of the telomere	2,90E-05	0,00013444
Cyan	Polymerase switching	2,90E-05	0,00013444
Cyan	Leading Strand Synthesis	2,90E-05	0,00013444
Cyan	TP53 Regulates Transcription of Genes Involved in G1 Cell Cycle Arrest	2,90E-05	0,00013444
Cyan	ATM Signaling Network in Development and Disease	3,35E-05	0,000153672
Cyan	estrogen responsive protein efp controls cell cycle and breast tumors growth	3,92E-05	0,000178399
Cyan	Extension of Telomeres	4,62E-05	0,00020844
Cyan	AURKA Activation by TPX2	5,14E-05	0,000224242
Cyan	Polo-like kinase mediated events	5,17E-05	0,000224242
Cyan	Transcription of E2F targets under negative control by DREAM complex	5,17E-05	0,000224242
Cyan	Translesion synthesis by REV1	5,17E-05	0,000224242
Cyan	pyrimidine deoxyribonucleotides de novo biosynthesis	5,17E-05	0,000224242
Cyan	Progesterone-mediated oocyte maturation - Homo sapiens (human)	5,71E-05	0,000245662
Cyan	Cellular senescence - Homo sapiens (human)	5,92E-05	0,000252876
Cyan	Termination of translesion DNA synthesis	6,38E-05	0,000270443
Cyan	Translesion synthesis by POLK	6,69E-05	0,000279165
Cyan	Translesion synthesis by POLI	6,69E-05	0,000279165
Cyan	Activation of NIMA Kinases NEK9, NEK6, NEK7	8,16E-05	0,000338152
Cyan	regulation of cell cycle progression by plk3	8,51E-05	0,000349851
Cyan	Nuclear Pore Complex (NPC) Disassembly	8,63E-05	0,000352072

Module	Pathway	p-value	q-value
Cyan	Transcriptional Regulation by E2F6	9,95E-05	0,000403302
Cyan	Translesion Synthesis by POLH	0,000106637	0,000428885
Cyan	brca1 dependent ub ligase activity	0,000129298	0,000516256
Cyan	PCNA-Dependent Long Patch Base Excision Repair	0,000161219	0,000639078
Cyan	Translesion synthesis by Y family DNA polymerases bypasses lesions on DNA template	0,000169007	0,000665165
Cyan	E2F-enabled inhibition of pre-replication complex formation	0,000192021	0,000750379
Cyan	E2F mediated regulation of DNA replication	0,000194977	0,000756566
Cyan	Intra-Golgi and retrograde Golgi-to-ER traffic	0,000216908	0,000835777
Cyan	APC/C:Cdc20 mediated degradation of Cyclin B	0,000233548	0,000852218
Cyan	Pyrimidine Metabolism	0,000233548	0,000852218
Cyan	UMP Synthase Deiciency (Orotic Aciduria)	0,000233548	0,000852218
Cyan	MNGIE (Mitochondrial Neurogastrointestinal Encephalopathy)	0,000233548	0,000852218
Cyan	Beta Ureidopropionase Deficiency	0,000233548	0,000852218
Cyan	Dihydropyrimidinase Deficiency	0,000233548	0,000852218
Cyan	Mismatch repair - Homo sapiens (human)	0,000233548	0,000852218
Cyan	G1/S DNA Damage Checkpoints	0,000233548	0,000852218
Cyan	Transcriptional Regulation by E2F6	0,000271592	0,00098452
Cyan	Resolution of AP sites via the multiple-nucleotide patch replacement pathway	0,000277318	0,000998707
Cyan	Gap-filling DNA repair synthesis and ligation in GG-NER	0,000326678	0,00116883
Cyan	CDK-mediated phosphorylation and removal of Cdc6	0,000443769	0,001577527
Cyan	Phosphorylation of proteins involved in the G2/M transition by Cyclin A:Cdc2 complexes	0,00054007	0,001907556
Cyan	Metabolism of nucleotides	0,000546731	0,00191878
Cyan	Pyrimidine nucleotides nucleosides metabolism	0,000605075	0,002096834
Cyan	Nuclear Envelope Breakdown	0,000605075	0,002096834
Cyan	Gene expression (Transcription)	0,000616236	0,002122162
Cyan	Chk1/Chk2(Cds1) mediated inactivation of Cyclin B:Cdk1 complex	0,000628228	0,00213675
Cyan	p53 signaling pathway	0,000628228	0,00213675
Cyan	Mitotic Prophase	0,000716776	0,002422968
Cyan	Fanconi anemia pathway - Homo sapiens (human)	0,00078848	0,002643611
Cyan	Golgi Cisternae Pericentriolar Stack Reorganization	0,000791644	0,002643611
Cyan	Rev-mediated nuclear export of HIV RNA	0,000971427	0,003205126
Cyan	Transport of the SLBP independent Mature mRNA	0,000971427	0,003205126
Cyan	tRNA processing in the nucleus	0,001010481	0,003314137

Module	Pathway	p-value	q-value
Cyan	Phosphorylation of proteins involved in G1/S transition by active Cyclin E:Cdk2 complexes	0,001070528	0,003490302
Cyan	Transport of the SLBP Dependant Mature mRNA	0,001089449	0,003524714
Cyan	p53 pathway	0,001093877	0,003524714
Cyan	Validated targets of C-MYC transcriptional activation	0,001143252	0,003662393
Cyan	pyrimidine deoxyribonucleotides biosynthesis from CTP	0,001193932	0,00380264
Cyan	Resolution of Abasic Sites (AP sites)	0,001503427	0,00468016
Cyan	Base Excision Repair	0,001503427	0,00468016
Cyan	SUMOylation of DNA replication proteins	0,001503427	0,00468016
Cyan	Interactions of Rev with host cellular proteins	0,001503427	0,00468016
Cyan	SCF(Skp2)-mediated degradation of p27/p21	0,001705516	0,005279435
Cyan	Aurora C signaling	0,001768352	0,005443364
Cyan	Phosphorylation of the APC/C	0,002005306	0,006103342
Cyan	Fanconi Anemia Pathway	0,002015986	0,006103342
Cyan	Transport of Mature mRNA Derived from an Intronless Transcript	0,002015986	0,006103342
Cyan	Dual Incision in GG-NER	0,002210662	0,006619972
Cyan	Transport of Mature mRNAs Derived from Intronless Transcripts	0,002210662	0,006619972
Cyan	Nonhomologous End-Joining (NHEJ)	0,002381627	0,00701752
Cyan	Loss of Nlp from mitotic centrosomes	0,002381627	0,00701752
Cyan	Loss of proteins required for interphase microtubule organization from the centrosome	0,002381627	0,00701752
Cyan	Ciliary landscape	0,002438788	0,007147725
Cyan	p53-Dependent G1 DNA Damage Response	0,002698356	0,007823769
Cyan	p53-Dependent G1/S DNA damage checkpoint	0,002698356	0,007823769
Cyan	tRNA processing	0,00271205	0,007823769
Cyan	role of brca1 brca2 and atr in cancer susceptibility	0,003093626	0,008832063
Cyan	APC/C:Cdc20 mediated degradation of Securin	0,003093626	0,008832063
Cyan	Nucleotide excision repair - Homo sapiens (human)	0,003380765	0,00960207
Cyan	Hepatitis B - Homo sapiens (human)	0,003404775	0,009620671
Green	Metabolism of RNA	4,25E-06	0,004091687
Green	DNA Repair	1,49E-05	0,007161394
Greenyellow	Metabolism of RNA	3,30E-11	1,70E-08
Greenyellow	tRNA processing	8,72E-09	2,25E-06
Greenyellow	Late Phase of HIV Life Cycle	3,79E-07	6,51E-05
Greenyellow	HIV Life Cycle	1,05E-06	0,000130665

Module	Pathway	p-value	q-value
Greenyellow	Aminosugars metabolism	1,27E-06	0,000130665
Greenyellow	Influenza Life Cycle	1,72E-06	0,000147487
Greenyellow	tRNA processing in the nucleus	3,03E-06	0,000223188
Greenyellow	Cellular response to heat stress	3,80E-06	0,000244519
Greenyellow	Influenza Viral RNA Transcription and Replication	5,42E-06	0,000259579
Greenyellow	NEP/NS2 Interacts with the Cellular Export Machinery	6,51E-06	0,000259579
Greenyellow	Transport of Ribonucleoproteins into the Host Nucleus	6,51E-06	0,000259579
Greenyellow	Regulation of Glucokinase by Glucokinase Regulatory Protein	6,51E-06	0,000259579
Greenyellow	Influenza Infection	6,55E-06	0,000259579
Greenyellow	Cell Cycle, Mitotic	7,87E-06	0,000273493
Greenyellow	Export of Viral Ribonucleoproteins from Nucleus	7,97E-06	0,000273493
Greenyellow	Vpr-mediated nuclear import of PICs	9,67E-06	0,000300482
Greenyellow	Cell Cycle	1,02E-05	0,000300482
Greenyellow	Infectious disease	1,16E-05	0,000300482
Greenyellow	Rev-mediated nuclear export of HIV RNA	1,17E-05	0,000300482
Greenyellow	Transport of the SLBP independent Mature mRNA	1,17E-05	0,000300482
Greenyellow	Nuclear import of Rev protein	1,40E-05	0,000301715
Greenyellow	Transport of the SLBP Dependant Mature mRNA	1,40E-05	0,000301715
Greenyellow	Nuclear Pore Complex (NPC) Disassembly	1,40E-05	0,000301715
Greenyellow	HIV Infection	1,42E-05	0,000301715
Greenyellow	Nuclear Envelope Breakdown	1,49E-05	0,000301715
Greenyellow	Phosphatidylinositol phosphate metabolism	1,66E-05	0,000301715
Greenyellow	Interactions of Vpr with host cellular proteins	1,67E-05	0,000301715
Greenyellow	snRNP Assembly	1,70E-05	0,000301715
Greenyellow	Metabolism of non-coding RNA	1,70E-05	0,000301715
Greenyellow	RNA transport - Homo sapiens (human)	1,83E-05	0,000314937
Greenyellow	Transport of Mature mRNA derived from an Intron-Containing Transcript	1,99E-05	0,000329779
Greenyellow	SUMOylation of DNA replication proteins	2,32E-05	0,000362519
Greenyellow	Interactions of Rev with host cellular proteins	2,32E-05	0,000362519
Greenyellow	Processing of Capped Intron-Containing Pre-mRNA	2,99E-05	0,0004527
Greenyellow	rRNA modification in the nucleus and cytosol	3,52E-05	0,000503915
Greenyellow	rRNA processing in the nucleus and cytosol	3,52E-05	0,000503915
Greenyellow	Transport of Mature mRNA Derived from an Intronless Transcript	3,69E-05	0,000513052

Module	Pathway	p-value	q-value
Greenyellow	Regulation of HSF1-mediated heat shock response	4,26E-05	0,000562688
Greenyellow	Transport of Mature mRNAs Derived from Intronless Transcripts	4,26E-05	0,000562688
Greenyellow	Lysine metabolism	4,40E-05	0,000567096
Greenyellow	Transport of Mature Transcript to Cytoplasm	4,66E-05	0,000585063
Greenyellow	Viral Messenger RNA Synthesis	4,91E-05	0,000601568
Greenyellow	Vitamin D3 (cholecalciferol) metabolism	5,89E-05	0,000705919
Greenyellow	Basal transcription factors - Homo sapiens (human)	6,43E-05	0,000752543
Greenyellow	rRNA processing	6,71E-05	0,000768433
Greenyellow	Mitochondrial translation termination	7,74E-05	0,000830789
Greenyellow	Mitochondrial translation elongation	7,74E-05	0,000830789
Greenyellow	Mitochondrial translation initiation	7,74E-05	0,000830789
Greenyellow	RNA Polymerase II Promoter Escape	8,31E-05	0,000853175
Greenyellow	SUMOylation of RNA binding proteins	8,31E-05	0,000853175
Greenyellow	Pentose phosphate pathway	8,45E-05	0,000853175
Greenyellow	RNA Polymerase II Transcription Pre-Initiation And Promoter Opening	9,40E-05	0,000864446
Greenyellow	RNA Polymerase II Transcription Initiation	9,40E-05	0,000864446
Greenyellow	RNA Polymerase II Transcription Initiation And Promoter Clearance	9,40E-05	0,000864446
Greenyellow	HIV Transcription Initiation	9,40E-05	0,000864446
Greenyellow	RNA Polymerase II HIV Promoter Escape	9,40E-05	0,000864446
Greenyellow	M Phase	0,000101112	0,000913554
Greenyellow	Glycosphingolipid metabolism	0,000109049	0,00096828
Greenyellow	Vitamin B5 - CoA biosynthesis from pantothenate	0,0001178	0,001009333
Greenyellow	Prostaglandin formation from dihomo gama-linoleic acid	0,0001178	0,001009333
Greenyellow	Glycolysis	0,000119552	0,001009333
Greenyellow	Mitochondrial translation	0,000123623	0,001026871
Greenyellow	Transcription of the HIV genome	0,000185118	0,001513267
Greenyellow	Mitotic Prometaphase	0,000191005	0,001536996
Greenyellow	Methionine and cysteine metabolism	0,000236701	0,001875398
Greenyellow	Selenoamino acid metabolism	0,000245036	0,001912024
Greenyellow	Squalene and cholesterol biosynthesis	0,000279693	0,002149882
Greenyellow	RNA Polymerase II Pre-transcription Events	0,000432566	0,003276052
Greenyellow	Eukaryotic Transcription Initiation	0,000456701	0,003408711
Greenyellow	Mitotic Prophase	0,000465164	0,003422281

Module	Pathway	p-value	q-value
Greenyellow	Disease	0,000484098	0,003511414
Greenyellow	Putative anti-Inflammatory metabolites formation from EPA	0,000511788	0,003660704
Greenyellow	Glucose metabolism	0,000570185	0,003925843
Greenyellow	Vitamin E metabolism	0,000571725	0,003925843
Greenyellow	De novo fatty acid biosynthesis	0,000571725	0,003925843
Greenyellow	Gene expression (Transcription)	0,000782644	0,005303444
Greenyellow	Amplification of signal from unattached kinetochores via a MAD2 inhibitory signal	0,000839639	0,005502263
Greenyellow	Amplification of signal from the kinetochores	0,000839639	0,005502263
Greenyellow	SUMOylation of chromatin organization proteins	0,000847817	0,005502263
Greenyellow	Purine metabolism	0,000855964	0,005502263
Greenyellow	Vitamin B3 (nicotinate and nicotinamide) metabolism	0,000865405	0,005502263
Greenyellow	Processing of SMDT1	0,001009021	0,006337142
Greenyellow	RNA Polymerase I Promoter Escape	0,001232984	0,00765044
Greenyellow	SUMOylation of DNA damage response and repair proteins	0,001306606	0,00801074
Greenyellow	RNA Polymerase I Transcription Termination	0,001398196	0,008466576
Greenyellow	Pyrimidine metabolism	0,001413836	0,008466576
Greenyellow	Transcription from mitochondrial promoters	0,001479904	0,008760348
Greenyellow	G2/M Transition	0,001552988	0,00908851
Greenyellow	Mitotic G2-G2/M phases	0,001702789	0,009853215
Grey60	Lysosome - Homo sapiens (human)	2,68E-09	1,16E-06
Grey60	Interferon alpha-beta signaling	3,80E-08	8,20E-06
Grey60	Interferon alpha/beta signaling	5,31E-06	0,00076294
Grey60	Immune System	7,12E-06	0,000767688
Grey60	Innate Immune System	1,01E-05	0,000870491
Lightcyan	Oxidative phosphorylation - Homo sapiens (human)	6,18E-06	0,002961062
Lightgreen	Cell Cycle	1,66E-08	8,94E-06
Lightgreen	Homologous recombination - Homo sapiens (human)	1,43E-06	0,000384677
Lightgreen	Resolution of D-loop Structures through Holliday Junction Intermediates	9,44E-06	0,001317535
Lightgreen	Metabolism of RNA	1,18E-05	0,001317535
Lightgreen	Resolution of D-Loop Structures	1,27E-05	0,001317535
Lightgreen	DNA Double-Strand Break Repair	1,62E-05	0,001317535
Lightgreen	Cell Cycle, Mitotic	1,92E-05	0,001317535
Lightgreen	Presynaptic phase of homologous DNA pairing and strand exchange	2,20E-05	0,001317535

Module	Pathway	p-value	q-value
Lightgreen	HDR through Homologous Recombination (HR) or Single Strand Annealing (SSA)	2,22E-05	0,001317535
Lightgreen	HDR through Homologous Recombination (HRR)	2,86E-05	0,001317535
Lightgreen	Regulation of Telomerase	2,86E-05	0,001317535
Lightgreen	Homology Directed Repair	3,05E-05	0,001317535
Lightgreen	Homologous DNA Pairing and Strand Exchange	3,18E-05	0,001317535
Lightgreen	M Phase	4,18E-05	0,001609252
Lightgreen	Fanconi anemia pathway	4,98E-05	0,001789149
Lightgreen	Resolution of D-loop Structures through Synthesis-Dependent Strand Annealing (SDSA)	8,56E-05	0,002881966
Lightgreen	IRF3-mediated induction of type I IFN	0,000178274	0,005323243
Lightgreen	Homologous recombination	0,000178274	0,005323243
Lightgreen	G2/M DNA damage checkpoint	0,000187647	0,005323243
Lightgreen	Cellular responses to stress	0,000211215	0,005450436
Lightgreen	ATM pathway	0,000215586	0,005450436
Lightgreen	Processing of DNA double-strand break ends	0,000222467	0,005450436
Lightgreen	Processing of Capped Intron-Containing Pre-mRNA	0,000265903	0,006062012
Lightgreen	Gene expression (Transcription)	0,000269923	0,006062012
Lightgreen	Human Thyroid Stimulating Hormone (TSH) signaling pathway	0,000282263	0,006085596
Lightgreen	HDR through Single Strand Annealing (SSA)	0,000300845	0,006236746
Lightgreen	STING mediated induction of host immune responses	0,000342403	0,006460612
Lightgreen	Interactome of polycomb repressive complex 2 (PRC2)	0,000342403	0,006460612
Lightgreen	Nonhomologous End-Joining (NHEJ)	0,000347603	0,006460612
Lightgreen	Breast cancer pathway	0,000417395	0,0073685
Lightgreen	AURKA Activation by TPX2	0,000423791	0,0073685
Lightgreen	Transport of Mature mRNA derived from an Intron-Containing Transcript	0,000451791	0,007609857
Lightgreen	DNA Repair	0,000481628	0,007866584
Lightgreen	Cellular senescence - Homo sapiens (human)	0,000505796	0,007884048
Lightgreen	Pancreatic cancer - Homo sapiens (human)	0,000511951	0,007884048
Lightgreen	Leptin signaling pathway	0,000544198	0,008147855
Lightgreen	EGF-EGFR Signaling Pathway	0,000565616	0,008239655
Lightgreen	G2/M Checkpoints	0,000631698	0,008960132
Lightgreen	p73 transcription factor network	0,000650137	0,00898523
Lightgreen	ATM Signaling Network in Development and Disease	0,000699434	0,009424879
Lightyellow	L13a-mediated translational silencing of Ceruloplasmin expression	2,21E-74	8,31E-72

Module	Pathway	p-value	q-value
Lightyellow	Cap-dependent Translation Initiation	1,35E-72	1,69E-70
Lightyellow	Eukaryotic Translation Initiation	1,35E-72	1,69E-70
Lightyellow	GTP hydrolysis and joining of the 60S ribosomal subunit	4,98E-72	4,68E-70
Lightyellow	Formation of a pool of free 40S subunits	2,45E-70	1,84E-68
Lightyellow	Eukaryotic Translation Elongation	5,10E-68	3,19E-66
Lightyellow	Peptide chain elongation	3,83E-67	1,80E-65
Lightyellow	Cytoplasmic Ribosomal Proteins	3,84E-67	1,80E-65
Lightyellow	Nonsense Mediated Decay (NMD) independent of the Exon Junction Complex (EJC)	7,04E-66	2,94E-64
Lightyellow	Nonsense Mediated Decay (NMD) enhanced by the Exon Junction Complex (EJC)	3,24E-65	1,11E-63
Lightyellow	Nonsense-Mediated Decay (NMD)	3,24E-65	1,11E-63
Lightyellow	Eukaryotic Translation Termination	3,05E-64	8,83E-63
Lightyellow	Selenocysteine synthesis	3,05E-64	8,83E-63
Lightyellow	Ribosome - Homo sapiens (human)	7,37E-62	1,98E-60
Lightyellow	SRP-dependent cotranslational protein targeting to membrane	6,14E-60	1,54E-58
Lightyellow	Selenoamino acid metabolism	7,96E-59	1,87E-57
Lightyellow	Translation	1,65E-57	3,64E-56
Lightyellow	Metabolism of amino acids and derivatives	1,75E-41	3,66E-40
Lightyellow	Metabolism of RNA	1,52E-40	3,01E-39
Lightyellow	Translation initiation complex formation	1,01E-37	1,90E-36
Lightyellow	Activation of the mRNA upon binding of the cap-binding complex and eIFs, and subsequent binding to 43S	1,69E-37	3,03E-36
Lightyellow	Ribosomal scanning and start codon recognition	9,63E-36	1,65E-34
Lightyellow	Formation of the ternary complex, and subsequently, the 43S complex	2,48E-35	4,05E-34
Lightyellow	Metabolism of proteins	4,15E-22	6,50E-21
Lightyellow	Metabolism	5,10E-13	7,67E-12
Lightyellow	Translation Factors	1,37E-08	1,98E-07
Lightyellow	RNA transport - Homo sapiens (human)	4,00E-07	5,57E-06
Lightyellow	Cellular response to heat stress	3,08E-05	0,000413499
Lightyellow	Cellular responses to stress	6,06E-05	0,000785359
Lightyellow	Cellular responses to external stimuli	8,51E-05	0,001066675
Lightyellow	rRNA modification in the nucleus and cytosol	0,000172891	0,002031465
Lightyellow	rRNA processing in the nucleus and cytosol	0,000172891	0,002031465
Lightyellow	rRNA processing	0,000275561	0,003139728
Lightyellow	Autodegradation of Cdh1 by Cdh1:APC/C	0,000849284	0,009392079

Module	Pathway	p-value	q-value
Magenta	SRP-dependent cotranslational protein targeting to membrane	1,08E-11	6,92E-09
Magenta	Cytoplasmic Ribosomal Proteins	1,34E-11	6,92E-09
Magenta	Peptide chain elongation	4,93E-11	1,53E-08
Magenta	Eukaryotic Translation Termination	7,76E-11	1,53E-08
Magenta	Selenocysteine synthesis	7,76E-11	1,53E-08
Magenta	Eukaryotic Translation Elongation	1,04E-10	1,53E-08
Magenta	Nonsense Mediated Decay (NMD) independent of the Exon Junction Complex (EJC)	1,04E-10	1,53E-08
Magenta	Cap-dependent Translation Initiation	3,07E-10	3,26E-08
Magenta	Eukaryotic Translation Initiation	3,07E-10	3,26E-08
Magenta	Formation of a pool of free 40S subunits	3,16E-10	3,26E-08
Magenta	Nonsense Mediated Decay (NMD) enhanced by the Exon Junction Complex (EJC)	5,32E-10	4,57E-08
Magenta	Nonsense-Mediated Decay (NMD)	5,32E-10	4,57E-08
Magenta	L13a-mediated translational silencing of Ceruloplasmin expression	1,11E-09	8,83E-08
Magenta	GTP hydrolysis and joining of the 60S ribosomal subunit	1,25E-09	9,23E-08
Magenta	Selenoamino acid metabolism	2,24E-09	1,53E-07
Magenta	Asparagine N-linked glycosylation	1,11E-08	7,16E-07
Magenta	Ribosome - Homo sapiens (human)	3,63E-08	2,20E-06
Magenta	Protein processing in endoplasmic reticulum - Homo sapiens (human)	9,97E-08	5,71E-06
Magenta	Cellular responses to external stimuli	3,47E-07	1,88E-05
Magenta	ER to Golgi Anterograde Transport	4,43E-07	2,28E-05
Magenta	Translation	7,07E-07	3,47E-05
Magenta	Metabolism of amino acids and derivatives	3,02E-06	0,000141341
Magenta	Transport to the Golgi and subsequent modification	4,47E-06	0,000200261
Magenta	Metabolism of proteins	7,66E-06	0,000328785
Magenta	Signaling Pathways in Glioblastoma	9,21E-06	0,000364692
Magenta	COPI-mediated anterograde transport	9,21E-06	0,000364692
Magenta	Vesicle-mediated transport	1,27E-05	0,000485301
Magenta	Cellular responses to stress	1,61E-05	0,00059101
Magenta	Class I PI3K signaling events mediated by Akt	2,12E-05	0,000753671
Magenta	Prostate cancer - Homo sapiens (human)	3,28E-05	0,001124524
Magenta	Membrane Trafficking	3,68E-05	0,001222506
Magenta	Constitutive Signaling by AKT1 E17K in Cancer	4,88E-05	0,001571571
Magenta	Autophagy - animal - Homo sapiens (human)	5,33E-05	0,001662907

Module	Pathway	p-value	q-value
Magenta	AKT phosphorylates targets in the cytosol	6,49E-05	0,001967295
Magenta	Cellular Senescence	6,73E-05	0,001981538
Magenta	Metabolism	7,61E-05	0,002176789
Magenta	DNA Damage/Telomere Stress Induced Senescence	8,67E-05	0,002369141
Magenta	Sorafenib Metabolism Pathway	8,74E-05	0,002369141
Magenta	Metabolism of RNA	9,50E-05	0,00250987
Magenta	Longevity regulating pathway - Homo sapiens (human)	0,000113051	0,002889747
Magenta	Morphine Metabolism Pathway	0,000115029	0,002889747
Magenta	Sterol Regulatory Element-Binding Proteins (SREBP) signalling	0,000129639	0,003105312
Magenta	AMP-activated Protein Kinase (AMPK) Signaling	0,000129639	0,003105312
Magenta	COPII-mediated vesicle transport	0,000142269	0,003253754
Magenta	ErbB Signaling Pathway	0,000142796	0,003253754
Magenta	4-hydroxytamoxifen, Dexamethasone, and Retinoic Acids Regulation of p27 Expression	0,000148472	0,003253754
Magenta	Formation of Senescence-Associated Heterochromatin Foci (SAHF)	0,000148472	0,003253754
Magenta	Ibuprofen Action Pathway	0,000168855	0,00358445
Magenta	Glioma - Homo sapiens (human)	0,000170522	0,00358445
Magenta	Etoposide Action Pathway	0,000235574	0,004757674
Magenta	Etoposide Metabolism Pathway	0,000235574	0,004757674
Magenta	Chronic myeloid leukemia - Homo sapiens (human)	0,000261375	0,005177238
Magenta	Formation of the ternary complex, and subsequently, the 43S complex	0,000317635	0,006172914
Magenta	Macroautophagy	0,000350151	0,006404092
Magenta	Caloric restriction and aging	0,000352259	0,006404092
Magenta	p53-Dependent G1 DNA Damage Response	0,000354401	0,006404092
Magenta	p53-Dependent G1/S DNA damage checkpoint	0,000354401	0,006404092
Magenta	p53 pathway	0,000385215	0,00675733
Magenta	Oncostatin_M	0,00038707	0,00675733
Magenta	CD28 dependent PI3K/Akt signaling	0,000427556	0,007219394
Magenta	hypoxia and p53 in the cardiovascular system	0,000427556	0,007219394
Magenta	IL11	0,00051088	0,007972818
Magenta	G1/S DNA Damage Checkpoints	0,00051088	0,007972818
Magenta	Ibuprofen Metabolism Pathway	0,00051088	0,007972818
Magenta	Irinotecan Action Pathway	0,00051088	0,007972818
Magenta	Irinotecan Metabolism Pathway	0,00051088	0,007972818

Module	Pathway	p-value	q-value
Magenta	Translation initiation complex formation	0,000603692	0,00914416
Magenta	Ribosomal scanning and start codon recognition	0,000603692	0,00914416
Magenta	Activation of the mRNA upon binding of the cap-binding complex and eIFs, and subsequent binding to 43S	0,000657054	0,009808194
Midnightblue	Respiratory electron transport	1,05E-11	5,91E-09
Midnightblue	Respiratory electron transport, ATP synthesis by chemiosmotic coupling, and heat production by uncoupling proteins,	1,43E-11	5,91E-09
Midnightblue	Huntington disease - Homo sapiens (human)	1,14E-10	2,38E-08
Midnightblue	Parkinson disease - Homo sapiens (human)	1,15E-10	2,38E-08
Midnightblue	The citric acid (TCA) cycle and respiratory electron transport	2,01E-10	3,09E-08
Midnightblue	Electron Transport Chain (OXPHOS system in mitochondria)	2,25E-10	3,09E-08
Midnightblue	Oxidative phosphorylation - Homo sapiens (human)	5,53E-09	6,51E-07
Midnightblue	Non-alcoholic fatty liver disease (NAFLD) - Homo sapiens (human)	2,20E-08	2,27E-06
Midnightblue	Nonalcoholic fatty liver disease	3,54E-08	3,24E-06
Midnightblue	Alzheimer disease - Homo sapiens (human)	1,13E-07	9,35E-06
Midnightblue	Membrane Trafficking	3,32E-07	2,49E-05
Midnightblue	Thermogenesis - Homo sapiens (human)	5,36E-07	3,48E-05
Midnightblue	Oxidative phosphorylation	5,48E-07	3,48E-05
Midnightblue	TP53 Regulates Metabolic Genes	7,52E-07	4,42E-05
Midnightblue	Vesicle-mediated transport	1,00E-06	5,50E-05
Midnightblue	Complex I biogenesis	3,54E-06	0,000182161
Midnightblue	Retrograde endocannabinoid signaling - Homo sapiens (human)	9,99E-06	0,000484081
Midnightblue	Translocation of GLUT4 to the plasma membrane	3,36E-05	0,001537502
Midnightblue	Human immunodeficiency virus 1 infection - Homo sapiens (human)	4,10E-05	0,001777196
Midnightblue	Kaposi sarcoma-associated herpesvirus infection - Homo sapiens (human)	7,15E-05	0,002943987
Midnightblue	RAB GEFs exchange GTP for GDP on RABs	9,89E-05	0,003882386
Midnightblue	Rab regulation of trafficking	0,000122459	0,004586657
Midnightblue	RAF-independent MAPK1/3 activation	0,000139338	0,004964727
Midnightblue	Intrinsic Pathway for Apoptosis	0,000144604	0,004964727
Midnightblue	Fas	0,000165675	0,005460653
Midnightblue	HIF-1 signaling pathway - Homo sapiens (human)	0,000179116	0,005676603
Midnightblue	Infectious disease	0,000192908	0,005887273
Midnightblue	Ciliary landscape	0,000218123	0,006419056
Midnightblue	Hedgehog signaling events mediated by Gli proteins	0,000245306	0,006970086
Midnightblue	ErbB1 downstream signaling	0,000257085	0,007061281

Module	Pathway	p-value	q-value
Midnightblue	Hepatitis B - Homo sapiens (human)	0,000306852	0,00792378
Midnightblue	EGF	0,00030772	0,00792378
Midnightblue	Insulin-mediated glucose transport	0,000353694	0,008831629
Pink	Interferon gamma signaling	3,61E-08	2,79E-05
Pink	Antigen processing and presentation - Homo sapiens (human)	1,69E-07	6,53E-05
Pink	Antigen Presentation: Folding, assembly and peptide loading of class I MHC	2,75E-07	7,10E-05
Pink	Epstein-Barr virus infection - Homo sapiens (human)	4,36E-07	8,43E-05
Pink	Endosomal/Vacuolar pathway	3,22E-06	0,000498818
Pink	Respiratory electron transport	4,20E-06	0,000542083
Pink	Respiratory electron transport, ATP synthesis by chemiosmotic coupling, and heat production by uncoupling proteins,	5,46E-06	0,000603187
Pink	The citric acid (TCA) cycle and respiratory electron transport	8,20E-06	0,000793275
Pink	Oxidative phosphorylation - Homo sapiens (human)	1,22E-05	0,001051456
Pink	Interferon Signaling	1,45E-05	0,001120554
Pink	Toll Like Receptor 3 (TLR3) Cascade	2,06E-05	0,001447311
Pink	Parkinson disease - Homo sapiens (human)	2,37E-05	0,001529824
Pink	TRIF(TICAM1)-mediated TLR4 signaling	2,93E-05	0,001621591
Pink	MyD88-independent TLR4 cascade	2,93E-05	0,001621591
Pink	Electron Transport Chain (OXPHOS system in mitochondria)	3,48E-05	0,001795537
Pink	Human cytomegalovirus infection - Homo sapiens (human)	3,75E-05	0,001812997
Pink	TICAM1, RIP1-mediated IKK complex recruitment	4,48E-05	0,001929166
Pink	Antigen processing-Cross presentation	4,49E-05	0,001929166
Pink	antigen processing and presentation	6,42E-05	0,002485398
Pink	NF-kB activation through FADD/RIP-1 pathway mediated by caspase-8 and -10	6,42E-05	0,002485398
Pink	Human immunodeficiency virus 1 infection - Homo sapiens (human)	7,52E-05	0,002648844
Pink	hiv-1 nef: negative effector of fas and tnf	7,53E-05	0,002648844
Pink	IKK complex recruitment mediated by RIP1	0,000109607	0,003688517
Pink	TLR3-mediated TICAM1-dependent programmed cell death	0,000144501	0,00448597
Pink	Alzheimer disease - Homo sapiens (human)	0,000144896	0,00448597
Pink	Thermogenesis - Homo sapiens (human)	0,000178987	0,005328319
Pink	Toll Like Receptor 4 (TLR4) Cascade	0,000204213	0,005540223
Pink	Class I MHC mediated antigen processing & presentation	0,000212181	0,005540223
Pink	ID signaling pathway	0,000221895	0,005540223
Pink	RIPK1-mediated regulated necrosis	0,000221895	0,005540223

Module	Pathway	p-value	q-value
Pink	Regulated Necrosis	0,000221895	0,005540223
Pink	Toll-Like Receptors Cascades	0,000234214	0,005665044
Pink	Interferon gamma signaling	0,000249196	0,005844774
Pink	tnfr1 signaling pathway	0,000285702	0,006390099
Pink	Cytokine Signaling in Immune system	0,000288958	0,006390099
Pink	Herpes simplex infection - Homo sapiens (human)	0,000301379	0,00647964
Pink	Endocytosis - Homo sapiens (human)	0,000343651	0,007188799
Purple	Oxidative phosphorylation - Homo sapiens (human)	4,13E-12	3,12E-09
Purple	Huntington disease - Homo sapiens (human)	3,83E-11	1,45E-08
Purple	Parkinson disease - Homo sapiens (human)	1,22E-10	3,07E-08
Purple	Respiratory electron transport, ATP synthesis by chemiosmotic coupling, and heat production by uncoupling proteins,	1,20E-09	2,27E-07
Purple	Alzheimer disease - Homo sapiens (human)	2,27E-09	3,43E-07
Purple	Electron Transport Chain (OXPHOS system in mitochondria)	1,04E-08	1,31E-06
Purple	Oxidative phosphorylation	4,26E-08	4,60E-06
Purple	The citric acid (TCA) cycle and respiratory electron transport	1,29E-07	1,22E-05
Purple	Thermogenesis - Homo sapiens (human)	1,77E-07	1,49E-05
Purple	PTEN Regulation	3,26E-06	0,000246677
Purple	Respiratory electron transport	4,73E-06	0,000325389
Purple	Non-alcoholic fatty liver disease (NAFLD) - Homo sapiens (human)	5,21E-06	0,000328432
Purple	Cristae formation	7,54E-06	0,000381166
Purple	Formation of ATP by chemiosmotic coupling	7,54E-06	0,000381166
Purple	Nonalcoholic fatty liver disease	7,83E-06	0,000381166
Purple	Processing of Capped Intron-Containing Pre-mRNA	8,07E-06	0,000381166
Purple	Complex I biogenesis	2,72E-05	0,001207911
Purple	Regulation of PTEN gene transcription	5,98E-05	0,002513076
Purple	Metabolism	6,73E-05	0,002676851
Purple	Mitochondrial biogenesis	0,000144705	0,005309518
Purple	Initiation of transcription and translation elongation at the HIV-1 LTR	0,000147487	0,005309518
Purple	PIP3 activates AKT signaling	0,00018508	0,006360027
Purple	mRNA Splicing	0,000216619	0,007120163
Purple	Mitochondrial Electron Transport Chain	0,000260885	0,008217873
Red	mRNA Processing	5,07E-10	5,00E-07
Red	mRNA Splicing - Major Pathway	5,27E-09	2,59E-06

Module	Pathway	p-value	q-value
Red	mRNA Splicing	1,16E-08	3,82E-06
Red	Spliceosome - Homo sapiens (human)	5,30E-08	1,30E-05
Red	miR-targeted genes in lymphocytes - TarBase	1,13E-07	2,13E-05
Red	miR-targeted genes in muscle cell - TarBase	1,30E-07	2,13E-05
Red	Processing of Capped Intron-Containing Pre-mRNA	9,20E-07	0,000129526
Red	Metabolism of RNA	1,99E-06	0,000245419
Red	NS1 Mediated Effects on Host Pathways	7,80E-05	0,008533368
Red	Metabolism of proteins	8,97E-05	0,008832175
Royalblue	Interferon Signaling	3,39E-14	7,55E-12
Royalblue	Interferon alpha/beta signaling	3,97E-10	4,42E-08
Royalblue	Interferon gamma signaling	5,76E-09	4,28E-07
Royalblue	Cytokine Signaling in Immune system	1,55E-08	8,65E-07
Royalblue	The human immune response to tuberculosis	1,92E-07	8,58E-06
Royalblue	Immune System	6,27E-06	0,000233122
Royalblue	Interferon alpha-beta signaling	7,47E-06	0,000237816
Royalblue	Herpes simplex infection - Homo sapiens (human)	1,80E-05	0,00050145
Royalblue	ISG15 antiviral mechanism	3,28E-05	0,000730724
Royalblue	Antiviral mechanism by IFN-stimulated genes	3,28E-05	0,000730724
Royalblue	Hepatitis C - Homo sapiens (human)	4,70E-05	0,000953054
Royalblue	Type II interferon signaling (IFNG)	7,64E-05	0,001420122
Royalblue	Ebola Virus Pathway on Host	0,000149292	0,002560924
Royalblue	Other glycan degradation - Homo sapiens (human)	0,000173347	0,002761169
Royalblue	Amino sugar and nucleotide sugar metabolism - Homo sapiens (human)	0,000213838	0,003179062
Royalblue	Epstein-Barr virus infection - Homo sapiens (human)	0,000231348	0,003224412
Royalblue	Validated transcriptional targets of TAp63 isoforms	0,000362737	0,004758253
Tan	Respiratory electron transport	7,75E-06	0,002426657
Tan	Gene expression (Transcription)	8,76E-06	0,002426657
Tan	Transcriptional Regulation by TP53	1,05E-05	0,002426657
Tan	TP53 Regulates Metabolic Genes	1,97E-05	0,003426641
Tan	RNA Polymerase II Transcription	3,28E-05	0,004558878
Tan	Respiratory electron transport, ATP synthesis by chemiosmotic coupling, and heat production by uncoupling proteins,	4,12E-05	0,004775329
Tan	Generic Transcription Pathway	5,46E-05	0,005428784
Tan	Cell Cycle	6,67E-05	0,005804572

Module	Pathway	p-value	q-value
Tan	Processing of Capped Intron-Containing Pre-mRNA	9,65E-05	0,006984627
Tan	Metabolism of RNA	0,000100354	0,006984627
Tan	The citric acid (TCA) cycle and respiratory electron transport	0,000114332	0,007234124
Tan	Cell Cycle Checkpoints	0,000131531	0,007628804
Tan	mRNA Splicing - Major Pathway	0,000144616	0,007742495
Tan	G2/M Checkpoints	0,000200005	0,009216473
Tan	mRNA Splicing	0,000207051	0,009216473
Tan	SUMO E3 ligases SUMOylate target proteins	0,000211873	0,009216473
Torquoise	Gene expression (Transcription)	2,55E-10	4,66E-07
Torquoise	RNA Polymerase II Transcription	3,16E-09	2,88E-06
Torquoise	Metabolism of proteins	1,76E-08	1,07E-05
Torquoise	Cholesterol Biosynthesis Pathway	6,78E-08	3,10E-05
Torquoise	Generic Transcription Pathway	9,61E-08	3,51E-05
Torquoise	Post-translational protein modification	3,32E-07	0,00010115
Torquoise	Neddylation	1,05E-06	0,000226023
Torquoise	superpathway of cholesterol biosynthesis	1,65E-06	0,000226023
Torquoise	Cholesterol biosynthesis	1,65E-06	0,000226023
Torquoise	Activation of gene expression by SREBF (SREBP)	1,69E-06	0,000226023
Torquoise	Regulation of cholesterol biosynthesis by SREBP (SREBF)	2,02E-06	0,000226023
Torquoise	Macroautophagy	2,22E-06	0,000226023
Torquoise	Activation of gene expression by SREBF (SREBP)	2,53E-06	0,000226023
Torquoise	Alendronate Action Pathway	4,45E-06	0,000226023
Torquoise	Risedronate Action Pathway	4,45E-06	0,000226023
Torquoise	Pamidronate Action Pathway	4,45E-06	0,000226023
Torquoise	Zoledronate Action Pathway	4,45E-06	0,000226023
Torquoise	Ibandronate Action Pathway	4,45E-06	0,000226023
Torquoise	Pravastatin Action Pathway	4,45E-06	0,000226023
Torquoise	Atorvastatin Action Pathway	4,45E-06	0,000226023
Torquoise	Rosuvastatin Action Pathway	4,45E-06	0,000226023
Torquoise	Lovastatin Action Pathway	4,45E-06	0,000226023
Torquoise	Cerivastatin Action Pathway	4,45E-06	0,000226023
Torquoise	Fluvastatin Action Pathway	4,45E-06	0,000226023
Torquoise	Simvastatin Action Pathway	4,45E-06	0,000226023

Module	Pathway	p-value	q-value
Torquoise	Hyper-IgD syndrome	4,45E-06	0,000226023
Torquoise	Cholesteryl ester storage disease	4,45E-06	0,000226023
Torquoise	Lysosomal Acid Lipase Deficiency (Wolman Disease)	4,45E-06	0,000226023
Torquoise	Mevalonic aciduria	4,45E-06	0,000226023
Torquoise	Wolman disease	4,45E-06	0,000226023
Torquoise	Smith-Lemli-Opitz Syndrome (SLOS)	4,45E-06	0,000226023
Torquoise	Chondrodysplasia Punctata II, X Linked Dominant (CDPX2)	4,45E-06	0,000226023
Torquoise	CHILD Syndrome	4,45E-06	0,000226023
Torquoise	Desmosterolosis	4,45E-06	0,000226023
Torquoise	Hypercholesterolemia	4,45E-06	0,000226023
Torquoise	Steroid Biosynthesis	4,45E-06	0,000226023
Torquoise	Cholesterol biosynthesis, regulation and transport	5,16E-06	0,000254708
Torquoise	Chromatin modifying enzymes	5,75E-06	0,000269233
Torquoise	Chromatin organization	5,75E-06	0,000269233
Torquoise	Transcriptional Regulation by TP53	7,23E-06	0,000330188
Torquoise	Steroids metabolism	3,19E-05	0,001406678
Torquoise	Antigen processing: Ubiquitination & Proteasome degradation	3,23E-05	0,001406678
Torquoise	Membrane Trafficking	6,82E-05	0,002898988
Torquoise	Autophagy - animal - Homo sapiens (human)	7,05E-05	0,002929124
Torquoise	Sterol Regulatory Element-Binding Proteins (SREBP) signalling	9,52E-05	0,00386536
Torquoise	Metabolism of RNA	0,000106957	0,004248069
Torquoise	Translation	0,000144825	0,00562967
Torquoise	Golgi-to-ER retrograde transport	0,000157281	0,005986496
Torquoise	Intra-Golgi and retrograde Golgi-to-ER traffic	0,000165714	0,006178763
Torquoise	p53 signaling pathway - Homo sapiens (human)	0,000181306	0,00662491
Torquoise	Ubiquitin mediated proteolysis - Homo sapiens (human)	0,00019058	0,006807292
Torquoise	Cellular responses to external stimuli	0,000193749	0,006807292
Torquoise	Class I MHC mediated antigen processing & presentation	0,000225001	0,007756149
Torquoise	Metabolic reprogramming in colon cancer	0,000271639	0,009190465
Yellow	Metabolism of proteins	1,44E-06	0,000920282
Yellow	Gene expression (Transcription)	1,51E-06	0,000920282
Yellow	Post-translational protein modification	7,78E-06	0,003157303
Yellow	Membrane Trafficking	1,75E-05	0,005317198

Module	Pathway	p-value	q-value
Yellow	RNA Polymerase II Transcription	2,57E-05	0,005667094
Yellow	Asparagine N-linked glycosylation	2,79E-05	0,005667094
Yellow	Vesicle-mediated transport	3,70E-05	0,0058206
Yellow	Regulation of TP53 Activity	3,82E-05	0,0058206

Supplementary Table S7: List of the 149 genes and their expression trends in 9 apoptotic treatments and in 15 NutriGenomeDB experiments inducing apoptosis.
The gene number (Gene Number), the gene symbol (Symbol), the log2FC in the apoptotic treatments and in nutrigenomic treatments (NutriGenomeDB treatments) are reported.

		log2 FC Apoptotic RNA-seq									NutriGenomeDB	
Gene Number	**Symbol**	**GSC10 NCD38 24h**	**MCF7 TMX 48 h**	**MDA-MB231 Vitamin C 72h**	**ME1 Al-10-49 6h**	**Hela Ethanol 3h**	**MA9 PAM 3h**	**MA9 PAM 24h**	**hNCC Zika Virus 65h**	**hPN Zika Virus 65h**	**log2 FC**	**Treatment**
1	ABCC5	0,00	-1,79	0,00	0,00	0,00	0,00	0,00	0,00	0,00	-1,6	MCF7 Narciclasine 10uM 12h
2	ARRDC3	0,00	1,45	0,00	2,03	1,02	0,00	1,24	0,00	0,00	4	SW620 Rosemary 100ug 48h
2	ARRDC3	0,00	1,45	0,00	2,03	1,02	0,00	1,24	0,00	0,00	2,6	SW620 Rosemary 60ug 48h
2	ARRDC3	0,00	1,45	0,00	2,03	1,02	0,00	1,24	0,00	0,00	1,9	SK-MEL-3 TrichostatinA
2	ARRDC3	0,00	1,45	0,00	2,03	1,02	0,00	1,24	0,00	0,00	1,8	MDA WithaferinA 72h
2	ARRDC3	0,00	1,45	0,00	2,03	1,02	0,00	1,24	0,00	0,00	1,7	HT29 RosemaryExtract 24h
2	ARRDC3	0,00	1,45	0,00	2,03	1,02	0,00	1,24	0,00	0,00	1,5	T47D Indole3carbinol 24h
3	ASB6	0,00	1,26	0,00	0,00	0,00	0,00	0,00	0,00	0,00	2,7	MCF7 Indole3carbinol 24h
3	ASB6	0,00	1,26	0,00	0,00	0,00	0,00	0,00	0,00	0,00	2,2	ZR75 Indole3carbinol 24h
3	ASB6	0,00	1,26	0,00	0,00	0,00	0,00	0,00	0,00	0,00	1,5	T47D Indole3carbinol 24h
4	BACH1	0,00	0,00	0,00	0,00	0,00	0,00	1,36	0,00	0,00	1,7	MCF10A Sulforaphane 15uM 24h
4	BACH1	0,00	0,00	0,00	0,00	0,00	0,00	1,36	0,00	0,00	1,5	SW620 Rosemary 60ug 48h
5	BAHCC1	0,00	-2,11	0,00	-1,21	0,00	0,00	0,00	-1,23	0,00	-2	SW620 Rosemary 30ug 48h
5	BAHCC1	0,00	-2,11	0,00	-1,21	0,00	0,00	0,00	-1,23	0,00	-2,1	SW620 Rosemary 60ug 48h
5	BAHCC1	0,00	-2,11	0,00	-1,21	0,00	0,00	0,00	-1,23	0,00	-3	SW620 Rosemary 100ug 48h
6	BAIAP2	0,00	0,00	0,00	0,00	0,00	0,00	0,00	0,00	1,08	1,5	A498 EnglerinA 8h
7	BRI3	0,00	0,00	0,00	0,00	1,81	0,00	0,00	0,00	0,00	1,7	T47D Indole3carbinol 24h
8	BTBD2	0,00	-1,06	0,00	0,00	0,00	0,00	0,00	0,00	0,00	-1,6	MDA WithaferinA 72h
8	BTBD2	0,00	-1,06	0,00	0,00	0,00	0,00	0,00	0,00	0,00	-2,4	SW620 Rosemary 60ug 48h
8	BTBD2	0,00	-1,06	0,00	0,00	0,00	0,00	0,00	0,00	0,00	-3,4	SW620 Rosemary 100ug 48h

Gene Number	Symbol	GSC10 NCD38 24h	MCF7 TMX 48 h	MDA-MB231 Vitamin C 72h	ME1 Al-10-49 6h	Hela Ethanol 3h	MA9 PAM 3h	MA9 PAM 24h	hNCC Zika Virus 65h	hPN Zika Virus 65h	log2 FC	Treatment
9	BUD31	0,00	1,18	0,00	1,32	0,00	0,00	0,00	1,01	0,00	2	MDA WithaferinA 72h
10	C1ORF109	0,00	1,81	0,00	0,00	0,00	0,00	0,00	0,00	0,00	1,9	T47D Indole3carbinol 24h
10	C1ORF109	0,00	1,81	0,00	0,00	0,00	0,00	0,00	0,00	0,00	1,5	MCF7 Indole3carbinol 24h
11	C2ORF42	0,00	1,17	0,00	0,00	0,00	0,00	0,00	0,00	0,00	1,8	MDA WithaferinA 72h
12	C6orf62	0,00	0,00	0,00	0,00	0,00	0,00	1,06	0,00	0,00	1,6	Ishikawa Genistein 10uM 24h
13	CABLES2	0,00	0,00	0,00	-1,01	0,00	0,00	0,00	0,00	0,00	-1,8	SW620 Rosemary 60ug 48h
13	CABLES2	0,00	0,00	0,00	-1,01	0,00	0,00	0,00	0,00	0,00	-2,7	SW620 Rosemary 100ug 48h
14	CARHSP1	0,00	0,00	0,00	0,00	0,00	0,00	-1,10	0,00	0,00	-1,9	MCF7 Narciclasine 10uM 12h
15	CBLL1	0,00	1,04	0,00	0,00	0,00	0,00	0,00	0,00	0,00	1,7	T47D Indole3carbinol 24h
16	CBX5	0,00	-2,23	0,00	0,00	0,00	0,00	-1,03	-1,39	0,00	-1,5	MCF7 Hydroxyalantolactone 10uM 12h
16	CBX5	0,00	-2,23	0,00	0,00	0,00	0,00	-1,03	-1,39	0,00	-2	MCF7 BruceineD 10uM 12h
16	CBX5	0,00	-2,23	0,00	0,00	0,00	0,00	-1,03	-1,39	0,00	-2,6	MCF7 JaponiconeA 10uM 12h
16	CBX5	0,00	-2,23	0,00	0,00	0,00	0,00	-1,03	-1,39	0,00	-2,8	MCF7 Narciclasine 10uM 12h
16	CBX5	0,00	-2,23	0,00	0,00	0,00	0,00	-1,03	-1,39	0,00	-3,1	SW620 Rosemary 100ug 48h
17	CCNT1	1,26	1,21	0,00	0,00	0,00	0,00	0,00	0,00	0,00	1,8	T47D Indole3carbinol 24h
18	CD47	0,00	-1,29	0,00	0,00	0,00	0,00	0,00	0,00	0,00	-1,6	MCF7 Indole3carbinol 24h
18	CD47	0,00	-1,29	0,00	0,00	0,00	0,00	0,00	0,00	0,00	-1,8	T47D Indole3carbinol 24h
18	CD47	0,00	-1,29	0,00	0,00	0,00	0,00	0,00	0,00	0,00	-1,9	ZR75 Indole3carbinol 24h
18	CD47	0,00	-1,29	0,00	0,00	0,00	0,00	0,00	0,00	0,00	-2,1	MDA WithaferinA 72h
19	CD55	0,00	0,00	0,00	0,00	0,00	1,03	0,00	0,00	0,00	9,7	SW620 Rosemary 100ug 48h
19	CD55	0,00	0,00	0,00	0,00	0,00	1,03	0,00	0,00	0,00	7,1	SW620 Rosemary 60ug 48h
19	CD55	0,00	0,00	0,00	0,00	0,00	1,03	0,00	0,00	0,00	2,2	MDA MB157 Indole3carbinol 24h
19	CD55	0,00	0,00	0,00	0,00	0,00	1,03	0,00	0,00	0,00	2	MCF7 Resveratrol 150mM 48h
19	CD55	0,00	0,00	0,00	0,00	0,00	1,03	0,00	0,00	0,00	1,7	MCF7 Resveratrol 250mM 48h
20	CENPB	0,00	0,00	0,00	-1,31	0,00	0,00	0,00	0,00	0,00	-1,5	MDA WithaferinA 72h
20	CENPB	0,00	0,00	0,00	-1,31	0,00	0,00	0,00	0,00	0,00	-1,5	MCF7 Indole3carbinol 24h

Gene Number	Symbol	GSC10 NCD38 24h	MCF7 TMX 48 h	MDA-MB231 Vitamin C 72h	ME1 Al-10-49 6h	Hela Ethanol 3h	MA9 PAM 3h	MA9 PAM 24h	hNCC Zika Virus 65h	hPN Zika Virus 65h	log2 FC	Treatment
21	CHD1L	0,00	0,00	0,00	0,00	0,00	0,00	-1,16	0,00	0,00	-1,5	T47D Indole3carbinol 24h
22	COA7	0,00	0,00	0,00	-1,06	0,00	0,00	0,00	0,00	0,00	-1,5	MCF7 Resveratrol 250mM 48h
23	COG3	1,45	2,06	0,00	0,00	0,00	0,00	0,00	0,00	0,00	1,8	Ishikawa Genistein 10uM 24h
24	COQ4	0,00	0,00	0,00	0,00	0,00	0,00	-1,27	0,00	0,00	-1,8	A498 EnglerinA 3h
25	CRY2	0,00	1,09	0,00	0,00	0,00	0,00	0,00	1,06	1,28	2	ZR75 Indole3carbinol 24h
25	CRY2	0,00	1,09	0,00	0,00	0,00	0,00	0,00	1,06	1,28	1,7	MCF7 Narciclasine 10uM 12h
26	CSGALNACT2	0,00	1,74	0,00	1,39	0,00	0,00	0,00	0,00	0,00	2,5	T47D Indole3carbinol 24h
26	CSGALNACT2	0,00	1,74	0,00	1,39	0,00	0,00	0,00	0,00	0,00	1,7	HT29 RosemaryExtract 24h
27	CTDSP1	0,00	-2,35	0,00	0,00	0,00	0,00	0,00	0,00	0,00	-1,9	MCF7 Indole3carbinol 24h
28	DDX49	0,00	1,67	0,00	0,00	0,00	0,00	0,00	0,00	0,00	1,5	MCF7 Indole3carbinol 24h
29	DDX51	1,17	0,00	0,00	0,00	0,00	0,00	0,00	0,00	0,00	3,3	MCF7 Indole3carbinol 24h
30	DENND4A	0,00	0,00	0,00	0,00	0,00	0,00	0,00	0,00	1,06	1,6	MCF7 Narciclasine 10uM 12h
31	DGAT1	0,00	0,00	0,00	0,00	0,00	0,00	0,00	1,68	1,06	2,1	MCF7 Indole3carbinol 24h
31	DGAT1	0,00	0,00	0,00	0,00	0,00	0,00	0,00	1,68	1,06	1,9	ZR75 Indole3carbinol 24h
31	DGAT1	0,00	0,00	0,00	0,00	0,00	0,00	0,00	1,68	1,06	1,6	T47D Indole3carbinol 24h
32	DIAPH2	0,00	-1,21	0,00	0,00	0,00	0,00	0,00	0,00	0,00	-2,6	MCF7 NitidineChloride 10uM 12h
32	DIAPH2	0,00	-1,21	0,00	0,00	0,00	0,00	0,00	0,00	0,00	-2,7	MCF7 Indole3carbinol 24h
32	DIAPH2	0,00	-1,21	0,00	0,00	0,00	0,00	0,00	0,00	0,00	-3,7	ZR75 Indole3carbinol 24h
32	DIAPH2	0,00	-1,21	0,00	0,00	0,00	0,00	0,00	0,00	0,00	-3,9	MDA MB231 Indole3carbinol 24h
32	DIAPH2	0,00	-1,21	0,00	0,00	0,00	0,00	0,00	0,00	0,00	-4,5	MDA MB436 Indole3carbinol 24h
33	DMXL2	0,00	0,00	0,00	0,00	0,00	0,00	2,68	0,00	0,00	1,6	MCF7 BruceineD 10uM 12h
33	DMXL2	0,00	0,00	0,00	0,00	0,00	0,00	2,68	0,00	0,00	1,6	MCF7 Narciclasine 10uM 12h
34	DNAJB2	0,00	1,75	0,00	1,30	0,00	0,00	0,00	0,00	1,09	2,2	MCF7 JaponiconeA 10uM 12h
34	DNAJB2	0,00	1,75	0,00	1,30	0,00	0,00	0,00	0,00	1,09	1,9	MCF10A Sulforaphane 15uM 24h
34	DNAJB2	0,00	1,75	0,00	1,30	0,00	0,00	0,00	0,00	1,09	1,9	SW620 Rosemary 100ug 48h
34	DNAJB2	0,00	1,75	0,00	1,30	0,00	0,00	0,00	0,00	1,09	1,7	MDA WithaferinA 72h

Gene Number	Symbol	GSC10 NCD38 24h	MCF7 TMX 48 h	MDA-MB231 Vitamin C 72h	ME1 Al-10-49 6h	Hela Ethanol 3h	MA9 PAM 3h	MA9 PAM 24h	hNCC Zika Virus 65h	hPN Zika Virus 65h	log2 FC	Treatment
34	DNAJB2	0,00	1,75	0,00	1,30	0,00	0,00	0,00	0,00	1,09	1,6	MCF7 WithaferinA 72h
35	EIF5	0,00	2,06	0,00	0,00	0,00	0,00	0,00	0,00	0,00	1,9	T47D Indole3carbinol 24h
36	ENTPD7	0,00	0,00	0,00	0,00	0,00	0,00	-1,01	0,00	0,00	-2,3	MCF7 Indole3carbinol 24h
37	ERGIC1	0,00	-1,24	0,00	0,00	0,00	0,00	0,00	0,00	0,00	-1,7	T47D Indole3carbinol 24h
38	ERICH1	0,00	-1,32	0,00	0,00	0,00	0,00	0,00	0,00	0,00	-2,1	T47D Indole3carbinol 24h
39	FAM234B	0,00	-1,15	0,00	0,00	0,00	0,00	0,00	0,00	0,00	-1,5	MCF7 Resveratrol 250mM 48h
40	FAM53C	0,00	0,00	0,00	1,52	0,00	0,00	0,00	0,00	0,00	2	MDA WithaferinA 72h
40	FAM53C	0,00	0,00	0,00	1,52	0,00	0,00	0,00	0,00	0,00	1,5	A498 EnglerinA 3h
41	FCHSD2	0,00	-1,03	0,00	0,00	0,00	0,00	0,00	0,00	0,00	-1,8	MDA MB436 Indole3carbinol 24h
41	FCHSD2	0,00	-1,03	0,00	0,00	0,00	0,00	0,00	0,00	0,00	-2	MCF7 NitidineChloride 10uM 12h
41	FCHSD2	0,00	-1,03	0,00	0,00	0,00	0,00	0,00	0,00	0,00	-3	ZR75 Indole3carbinol 24h
41	FCHSD2	0,00	-1,03	0,00	0,00	0,00	0,00	0,00	0,00	0,00	-3,3	T47D Indole3carbinol 24h
41	FCHSD2	0,00	-1,03	0,00	0,00	0,00	0,00	0,00	0,00	0,00	-3,5	MCF7 Indole3carbinol 24h
42	FLOT2	0,00	-1,04	0,00	0,00	0,00	0,00	0,00	0,00	0,00	-1,6	MDA WithaferinA 72h
42	FLOT2	0,00	-1,04	0,00	0,00	0,00	0,00	0,00	0,00	0,00	-2,5	SW620 Rosemary 100ug 48h
43	GCC1	1,05	1,15	0,00	1,03	0,00	0,00	0,00	0,00	0,00	1,5	ZR75 Indole3carbinol 24h
44	HERC3	0,00	-2,04	0,00	0,00	0,00	0,00	0,00	0,00	0,00	-3,9	SW620 Rosemary 100ug 48h
45	HIVEP1	0,00	0,00	0,00	1,31	0,00	1,36	3,10	0,00	0,00	1,9	MCF7 Narciclasine 10uM 12h
46	HLA-B	0,00	0,00	0,00	0,00	0,00	0,00	0,00	2,26	0,00	3,2	MCF7 Indole3carbinol 24h
46	HLA-B	0,00	0,00	0,00	0,00	0,00	0,00	0,00	2,26	0,00	1,8	MCF7 Narciclasine 10uM 12h
47	HLA-E	0,00	0,00	0,00	0,00	0,00	0,00	1,32	1,75	0,00	1,6	T47D Indole3carbinol 24h
48	HPS5	0,00	1,05	0,00	0,00	0,00	0,00	0,00	0,00	0,00	2,1	MDA WithaferinA 72h
49	IFNGR1	0,00	1,73	0,00	0,00	0,00	0,00	1,73	0,00	0,00	1,8	ZR75 Indole3carbinol 24h
49	IFNGR1	0,00	1,73	0,00	0,00	0,00	0,00	1,73	0,00	0,00	1,6	MCF7 Narciclasine 10uM 12h
50	IFNGR2	0,00	0,00	0,00	0,00	0,00	0,00	1,92	0,00	0,00	1,6	MCF7 Narciclasine 10uM 12h
51	IFT122	0,00	-1,08	0,00	0,00	0,00	0,00	0,00	0,00	0,00	-1,7	T47D Indole3carbinol 24h

Gene Number	Symbol	GSC10 NCD38 24h	MCF7 TMX 48 h	MDA-MB231 Vitamin C 72h	ME1 Al-10-49 6h	Hela Ethanol 3h	MA9 PAM 3h	MA9 PAM 24h	hNCC Zika Virus 65h	hPN Zika Virus 65h	log2 FC	Treatment
52	IFT172	0,00	0,00	0,00	0,00	0,00	0,00	-1,09	0,00	0,00	-2	T47D Indole3carbinol 24h
53	ILKAP	0,00	1,00	0,00	0,00	0,00	0,00	0,00	0,00	0,00	1,6	MCF7 Narciclasine 10uM 12h
54	INPP5A	0,00	0,00	0,00	0,00	0,00	0,00	-1,27	0,00	0,00	-1,7	MDA MB436 Indole3carbinol 24h
54	INPP5A	0,00	0,00	0,00	0,00	0,00	0,00	-1,27	0,00	0,00	-1,8	ZR75 Indole3carbinol 24h
54	INPP5A	0,00	0,00	0,00	0,00	0,00	0,00	-1,27	0,00	0,00	-3,4	T47D Indole3carbinol 24h
55	INTS3	0,00	-1,26	0,00	0,00	0,00	0,00	0,00	0,00	0,00	-1,8	MCF7 Indole3carbinol 24h
56	JARID2	0,00	-1,04	0,00	0,00	0,00	0,00	0,00	0,00	0,00	-2,2	MDA MB436 Indole3carbinol 24h
56	JARID2	0,00	-1,04	0,00	0,00	0,00	0,00	0,00	0,00	0,00	-2,3	MCF7 NitidineChloride 10uM 12h
56	JARID2	0,00	-1,04	0,00	0,00	0,00	0,00	0,00	0,00	0,00	-3,2	ZR75 Indole3carbinol 24h
56	JARID2	0,00	-1,04	0,00	0,00	0,00	0,00	0,00	0,00	0,00	-4,7	T47D Indole3carbinol 24h
56	JARID2	0,00	-1,04	0,00	0,00	0,00	0,00	0,00	0,00	0,00	-6	MCF7 Indole3carbinol 24h
57	KLHL28	1,41	1,43	0,00	0,00	0,00	0,00	1,15	0,00	0,00	4,2	MCF7 Indole3carbinol 24h
57	KLHL28	1,41	1,43	0,00	0,00	0,00	0,00	1,15	0,00	0,00	1,7	T47D Indole3carbinol 24h
57	KLHL28	1,41	1,43	0,00	0,00	0,00	0,00	1,15	0,00	0,00	1,7	ZR75 Indole3carbinol 24h
58	LIN52	0,00	1,36	0,00	0,00	0,00	0,00	0,00	0,00	0,00	3,6	MCF7 Indole3carbinol 24h
59	LNX2	0,00	1,42	0,00	0,00	0,00	0,00	0,00	0,00	0,00	1,5	T47D Indole3carbinol 24h
60	LRRK1	0,00	-1,46	0,00	0,00	0,00	0,00	0,00	0,00	0,00	-1,5	MDA MB436 Indole3carbinol 24h
61	LZTS2	0,00	-1,50	0,00	-1,32	0,00	0,00	-1,25	0,00	0,00	-3	MCF7 Indole3carbinol 24h
62	MAFG	1,45	1,16	0,00	0,00	0,00	1,08	0,00	0,00	0,00	4,2	T47D Indole3carbinol 24h
62	MAFG	1,45	1,16	0,00	0,00	0,00	1,08	0,00	0,00	0,00	3,6	ZR75 Indole3carbinol 24h
62	MAFG	1,45	1,16	0,00	0,00	0,00	1,08	0,00	0,00	0,00	3,2	MCF7 Indole3carbinol 24h
62	MAFG	1,45	1,16	0,00	0,00	0,00	1,08	0,00	0,00	0,00	2,4	MCF7 JaponiconeA 10uM 12h
62	MAFG	1,45	1,16	0,00	0,00	0,00	1,08	0,00	0,00	0,00	1,7	MDA WithaferinA 72h
62	MAFG	1,45	1,16	0,00	0,00	0,00	1,08	0,00	0,00	0,00	1,7	MCF7 Hydroxyalantolactone 10uM 12h
62	MAFG	1,45	1,16	0,00	0,00	0,00	1,08	0,00	0,00	0,00	1,5	MCF7 Narciclasine 10uM 12h
63	MAN1B1	0,00	-1,11	0,00	0,00	0,00	0,00	0,00	0,00	0,00	-1,5	A498 EnglerinA 3h

Gene Number	Symbol	GSC10 NCD38 24h	MCF7 TMX 48 h	MDA-MB231 Vitamin C 72h	ME1 Al-10-49 6h	Hela Ethanol 3h	MA9 PAM 3h	MA9 PAM 24h	hNCC Zika Virus 65h	hPN Zika Virus 65h	log2 FC	Treatment
63	MAN1B1	0,00	-1,11	0,00	0,00	0,00	0,00	0,00	0,00	0,00	-2,1	MDA WithaferinA 72h
64	MAPRE2	0,00	1,35	0,00	0,00	0,00	0,00	0,00	0,00	0,00	1,6	MCF7 Narciclasine 10uM 12h
65	MARVELD1	0,00	0,00	0,00	-2,02	0,00	0,00	0,00	0,00	0,00	-1,6	SK-MEL-3 TrichostatinA
66	MBNL1	0,00	0,00	0,00	0,00	-1,07	0,00	0,00	0,00	0,00	-1,6	MCF7 JaponiconeA 10uM 12h
66	MBNL1	0,00	0,00	0,00	0,00	-1,07	0,00	0,00	0,00	0,00	-1,9	ZR75 Indole3carbinol 24h
66	MBNL1	0,00	0,00	0,00	0,00	-1,07	0,00	0,00	0,00	0,00	-2,2	T47D Indole3carbinol 24h
67	MCTP1	0,00	0,00	0,00	1,34	0,00	1,74	1,81	0,00	0,00	1,6	HT29 RosemaryExtract 24h
68	MED13L	0,00	-1,51	0,00	0,00	0,00	0,00	0,00	0,00	0,00	-2,5	MCF7 NitidineChloride 10uM 12h
68	MED13L	0,00	-1,51	0,00	0,00	0,00	0,00	0,00	0,00	0,00	-3,4	MCF7 Indole3carbinol 24h
68	MED13L	0,00	-1,51	0,00	0,00	0,00	0,00	0,00	0,00	0,00	-4,1	T47D Indole3carbinol 24h
69	MED26	0,00	1,21	0,00	0,00	0,00	0,00	0,00	0,00	0,00	1,8	T47D Indole3carbinol 24h
69	MED26	0,00	1,21	0,00	0,00	0,00	0,00	0,00	0,00	0,00	1,5	MDA WithaferinA 72h
70	MIB2	1,25	0,00	0,00	0,00	0,00	0,00	0,00	0,00	0,00	1,9	ZR75 Indole3carbinol 24h
70	MIB2	1,25	0,00	0,00	0,00	0,00	0,00	0,00	0,00	0,00	1,5	MCF7 Indole3carbinol 24h
71	MID1IP1	0,00	1,64	0,00	0,00	0,00	0,00	0,00	0,00	0,00	1,5	T47D Indole3carbinol 24h
72	MLEC	0,00	0,00	0,00	-1,08	0,00	0,00	0,00	0,00	0,00	-1,5	MCF7 BruceineD 10uM 12h
72	MLEC	0,00	0,00	0,00	-1,08	0,00	0,00	0,00	0,00	0,00	-1,6	MCF7 Narciclasine 10uM 12h
73	MPV17L2	0,00	3,27	0,00	0,00	0,00	0,00	0,00	0,00	0,00	2,1	MCF7 Indole3carbinol 24h
73	MPV17L2	0,00	3,27	0,00	0,00	0,00	0,00	0,00	0,00	0,00	1,6	T47D Indole3carbinol 24h
73	MPV17L2	0,00	3,27	0,00	0,00	0,00	0,00	0,00	0,00	0,00	1,6	ZR75 Indole3carbinol 24h
74	MTF1	0,00	1,14	0,00	0,00	0,00	1,34	1,60	0,00	0,00	1,6	T47D Indole3carbinol 24h
75	MTHFD1L	0,00	0,00	0,00	0,00	0,00	0,00	-1,55	0,00	0,00	-1,7	MDA MB436 Indole3carbinol 24h
75	MTHFD1L	0,00	0,00	0,00	0,00	0,00	0,00	-1,55	0,00	0,00	-2,7	T47D Indole3carbinol 24h
75	MTHFD1L	0,00	0,00	0,00	0,00	0,00	0,00	-1,55	0,00	0,00	-2,7	ZR75 Indole3carbinol 24h
76	MYCBP	0,00	0,00	0,00	-1,33	0,00	0,00	0,00	0,00	0,00	-2	MDA MB436 Indole3carbinol 24h
77	MZT2A	0,00	0,00	0,00	0,00	0,00	0,00	-1,93	0,00	0,00	-1,9	A498 EnglerinA 3h

Gene Number	Symbol	GSC10 NCD38 24h	MCF7 TMX 48 h	MDA-MB231 Vitamin C 72h	ME1 Al-10-49 6h	Hela Ethanol 3h	MA9 PAM 3h	MA9 PAM 24h	hNCC Zika Virus 65h	hPN Zika Virus 65h	log2 FC	Treatment
78	NAA40	0,00	-1,30	0,00	0,00	0,00	-1,21	-1,14	0,00	0,00	-1,8	MCF7 JaponiconeA 10uM 12h
79	NAT10	0,00	0,00	0,00	0,00	0,00	0,00	-1,07	0,00	0,00	-2,2	MCF7 Indole3carbinol 24h
80	NEU1	0,00	0,00	0,00	0,00	0,00	0,00	1,04	1,20	1,21	2,6	MCF7 Resveratrol 250mM 48h
80	NEU1	0,00	0,00	0,00	0,00	0,00	0,00	1,04	1,20	1,21	2,5	MCF7 Resveratrol 150mM 48h
80	NEU1	0,00	0,00	0,00	0,00	0,00	0,00	1,04	1,20	1,21	2,2	MDA WithaferinA 72h
80	NEU1	0,00	0,00	0,00	0,00	0,00	0,00	1,04	1,20	1,21	2,1	ZR75 Indole3carbinol 24h
80	NEU1	0,00	0,00	0,00	0,00	0,00	0,00	1,04	1,20	1,21	1,9	T47D Indole3carbinol 24h
80	NEU1	0,00	0,00	0,00	0,00	0,00	0,00	1,04	1,20	1,21	1,5	MCF7 WithaferinA 72h
81	NKIRAS2	0,00	1,23	0,00	0,00	0,00	0,00	0,00	0,00	0,00	1,6	T47D Indole3carbinol 24h
82	OSGIN2	0,00	1,05	0,00	0,00	0,00	1,49	0,00	0,00	0,00	1,5	MDA WithaferinA 72h
82	OSGIN2	0,00	1,05	0,00	0,00	0,00	1,49	0,00	0,00	0,00	1,5	T47D Indole3carbinol 24h
83	PAQR4	0,00	-1,49	0,00	-2,31	0,00	0,00	0,00	0,00	0,00	-1,8	MDA WithaferinA 72h
83	PAQR4	0,00	-1,49	0,00	-2,31	0,00	0,00	0,00	0,00	0,00	-1,9	LNCaP eusynstyelamideB 5uM 24h
83	PAQR4	0,00	-1,49	0,00	-2,31	0,00	0,00	0,00	0,00	0,00	-3,1	SW620 Rosemary 100ug 48h
84	PC	0,00	0,00	0,00	-1,32	0,00	0,00	0,00	0,00	0,00	-1,7	ZR75 Indole3carbinol 24h
85	PCF11	0,00	-1,29	0,00	0,00	0,00	0,00	0,00	0,00	0,00	-1,8	T47D Indole3carbinol 24h
85	PCF11	0,00	-1,29	0,00	0,00	0,00	0,00	0,00	0,00	0,00	-1,8	MCF7 JaponiconeA 10uM 12h
85	PCF11	0,00	-1,29	0,00	0,00	0,00	0,00	0,00	0,00	0,00	-2	Ishikawa Genistein 10uM 24h
85	PCF11	0,00	-1,29	0,00	0,00	0,00	0,00	0,00	0,00	0,00	-2,5	Ishikawa Genistein 10uM 8h
86	PCYT2	0,00	1,04	0,00	0,00	0,00	0,00	0,00	0,00	0,00	1,5	MCF7 JaponiconeA 10uM 12h
87	PDE4A	0,00	0,00	0,00	0,00	0,00	0,00	1,50	0,00	0,00	1,6	MCF7 JaponiconeA 10uM 12h
88	PI4K2A	0,00	0,00	0,00	0,00	0,00	0,00	1,58	0,00	0,00	1,5	ZR75 Indole3carbinol 24h
89	PIAS2	0,00	-1,34	0,00	0,00	0,00	0,00	0,00	0,00	0,00	-1,5	MCF7 Indole3carbinol 24h
90	PLCXD1	0,00	-1,83	0,00	-1,04	0,00	-1,26	-1,52	0,00	0,00	-1,6	MCF7 Resveratrol 150mM 48h
90	PLCXD1	0,00	-1,83	0,00	-1,04	0,00	-1,26	-1,52	0,00	0,00	-1,6	MCF7 Resveratrol 250mM 48h
91	PLPP5	1,59	1,86	0,00	0,00	0,00	0,00	0,00	0,00	0,00	1,8	Ishikawa Genistein 10uM 24h

Gene Number	Symbol	GSC10 NCD38 24h	MCF7 TMX 48 h	MDA-MB231 Vitamin C 72h	ME1 Al-10-49 6h	Hela Ethanol 3h	MA9 PAM 3h	MA9 PAM 24h	hNCC Zika Virus 65h	hPN Zika Virus 65h	log2 FC	Treatment
92	PLTP	0,00	0,00	0,00	0,00	0,00	0,00	2,20	0,00	0,00	2,3	SW620 Rosemary 60ug 48h
93	POFUT2	1,44	1,12	0,00	0,00	0,00	0,00	0,00	0,00	0,00	1,8	MCF7 Narciclasine 10uM 12h
94	POMGNT1	0,00	0,00	0,00	-1,09	0,00	0,00	0,00	0,00	0,00	-1,6	MCF7 BruceineD 10uM 12h
95	POU2F1	0,00	0,00	0,00	0,00	0,00	0,00	0,00	-1,07	0,00	-1,8	ZR75 Indole3carbinol 24h
95	POU2F1	0,00	0,00	0,00	0,00	0,00	0,00	0,00	-1,07	0,00	-2,2	MCF7 Indole3carbinol 24h
95	POU2F1	0,00	0,00	0,00	0,00	0,00	0,00	0,00	-1,07	0,00	-2,2	T47D Indole3carbinol 24h
95	POU2F1	0,00	0,00	0,00	0,00	0,00	0,00	0,00	-1,07	0,00	-2,4	MDA MB436 Indole3carbinol 24h
96	PPIB	0,00	1,49	0,00	0,00	0,00	0,00	0,00	0,00	0,00	3,2	MCF7 Indole3carbinol 24h
96	PPIB	0,00	1,49	0,00	0,00	0,00	0,00	0,00	0,00	0,00	2,1	T47D Indole3carbinol 24h
97	PPRC1	0,00	0,00	0,00	-1,86	0,00	0,00	0,00	0,00	0,00	-1,5	MCF7 JaponiconeA 10uM 12h
97	PPRC1	0,00	0,00	0,00	-1,86	0,00	0,00	0,00	0,00	0,00	-2,1	MCF7 Indole3carbinol 24h
98	PPTC7	0,00	1,94	0,00	0,00	0,00	0,00	0,00	0,00	0,00	1,7	T47D Indole3carbinol 24h
99	PRKX	0,00	-1,55	0,00	0,00	0,00	0,00	0,00	0,00	0,00	-1,6	MDA MB436 Indole3carbinol 24h
99	PRKX	0,00	-1,55	0,00	0,00	0,00	0,00	0,00	0,00	0,00	-2	MCF7 BruceineD 10uM 12h
99	PRKX	0,00	-1,55	0,00	0,00	0,00	0,00	0,00	0,00	0,00	-2,2	MCF7 Narciclasine 10uM 12h
100	PSD4	-1,28	-2,44	0,00	0,00	0,00	0,00	0,00	0,00	0,00	-2,4	MCF7 Indole3carbinol 24h
101	PSMD13	0,00	1,03	0,00	0,00	0,00	0,00	0,00	0,00	0,00	1,7	MCF7 Indole3carbinol 24h
102	PVR	0,00	0,00	0,00	0,00	0,00	0,00	1,07	0,00	1,07	1,9	MCF7 Indole3carbinol 24h
102	PVR	0,00	0,00	0,00	0,00	0,00	0,00	1,07	0,00	1,07	1,6	T47D Indole3carbinol 24h
103	RAB31	0,00	-1,82	0,00	0,00	0,00	0,00	0,00	0,00	0,00	-1,5	MDA WithaferinA 72h
103	RAB31	0,00	-1,82	0,00	0,00	0,00	0,00	0,00	0,00	0,00	-1,5	MCF7 JaponiconeA 10uM 12h
103	RAB31	0,00	-1,82	0,00	0,00	0,00	0,00	0,00	0,00	0,00	-1,7	MCF7 Hydroxyalantolactone 10uM 12h
103	RAB31	0,00	-1,82	0,00	0,00	0,00	0,00	0,00	0,00	0,00	-2,3	MCF7 NitidineChloride 10uM 12h
103	RAB31	0,00	-1,82	0,00	0,00	0,00	0,00	0,00	0,00	0,00	-2,6	MCF7 Narciclasine 10uM 12h
103	RAB31	0,00	-1,82	0,00	0,00	0,00	0,00	0,00	0,00	0,00	-2,8	MCF7 BruceineD 10uM 12h
104	RAB8B	0,00	0,00	0,00	0,00	0,00	0,00	1,61	0,00	0,00	1,8	MCF7 JaponiconeA 10uM 12h

Gene Number	Symbol	GSC10 NCD38 24h	MCF7 TMX 48 h	MDA-MB231 Vitamin C 72h	ME1 Al-10-49 6h	Hela Ethanol 3h	MA9 PAM 3h	MA9 PAM 24h	hNCC Zika Virus 65h	hPN Zika Virus 65h	log2 FC	Treatment
105	RAI1	0,00	-1,05	0,00	0,00	0,00	0,00	0,00	0,00	0,00	-2,8	MCF7 Indole3carbinol 24h
106	RBL2	0,00	-1,10	0,00	0,00	0,00	0,00	0,00	0,00	0,00	-1,5	MCF7 Britanin 10uM 12h
106	RBL2	0,00	-1,10	0,00	0,00	0,00	0,00	0,00	0,00	0,00	-2,1	MCF7 JaponiconeA 10uM 12h
107	RCHY1	0,00	1,22	0,00	0,00	0,00	0,00	0,00	0,00	0,00	1,5	MCF7 BruceineD 10uM 12h
108	RHBDD2	0,00	1,37	0,00	0,00	0,00	0,00	0,00	0,00	0,00	2,2	T47D Indole3carbinol 24h
108	RHBDD2	0,00	1,37	0,00	0,00	0,00	0,00	0,00	0,00	0,00	1,8	MDA WithaferinA 72h
108	RHBDD2	0,00	1,37	0,00	0,00	0,00	0,00	0,00	0,00	0,00	1,5	ZR75 Indole3carbinol 24h
109	RNASEH1	0,00	1,36	0,00	0,00	0,00	0,00	0,00	0,00	0,00	2	T47D Indole3carbinol 24h
110	RNF25	0,00	2,15	0,00	0,00	0,00	0,00	0,00	0,00	0,00	2,3	T47D Indole3carbinol 24h
110	RNF25	0,00	2,15	0,00	0,00	0,00	0,00	0,00	0,00	0,00	2	MCF7 BruceineD 10uM 12h
110	RNF25	0,00	2,15	0,00	0,00	0,00	0,00	0,00	0,00	0,00	1,7	ZR75 Indole3carbinol 24h
111	RNMT	1,44	0,00	0,00	0,00	0,00	0,00	0,00	0,00	0,00	2,3	MDA WithaferinA 72h
112	RPS6KA5	0,00	-1,18	0,00	0,00	0,00	0,00	0,00	0,00	0,00	-1,5	MDA MB157 Indole3carbinol 24h
112	RPS6KA5	0,00	-1,18	0,00	0,00	0,00	0,00	0,00	0,00	0,00	-1,8	ZR75 Indole3carbinol 24h
112	RPS6KA5	0,00	-1,18	0,00	0,00	0,00	0,00	0,00	0,00	0,00	-2	MCF7 Indole3carbinol 24h
112	RPS6KA5	0,00	-1,18	0,00	0,00	0,00	0,00	0,00	0,00	0,00	-3,2	T47D Indole3carbinol 24h
113	SDCBP	0,00	0,00	0,00	1,10	0,00	0,00	1,52	0,00	0,00	3,2	SW620 Rosemary 100ug 48h
113	SDCBP	0,00	0,00	0,00	1,10	0,00	0,00	1,52	0,00	0,00	2,2	T47D Indole3carbinol 24h
113	SDCBP	0,00	0,00	0,00	1,10	0,00	0,00	1,52	0,00	0,00	1,5	ZR75 Indole3carbinol 24h
114	SFXN3	0,00	-2,29	0,00	0,00	0,00	0,00	0,00	0,00	0,00	-1,8	MCF7 Hydroxyalantolactone 10uM 12h
115	SGSM2	0,00	-1,02	0,00	0,00	0,00	0,00	0,00	0,00	0,00	-2,7	MDA WithaferinA 72h
116	SH3BGRL	0,00	-1,25	0,00	0,00	0,00	0,00	0,00	0,00	0,00	-1,5	MCF7 Narciclasine 10uM 12h
116	SH3BGRL	0,00	-1,25	0,00	0,00	0,00	0,00	0,00	0,00	0,00	-1,6	MDA MB157 Indole3carbinol 24h
116	SH3BGRL	0,00	-1,25	0,00	0,00	0,00	0,00	0,00	0,00	0,00	-1,8	SW620 Rosemary 60ug 48h
116	SH3BGRL	0,00	-1,25	0,00	0,00	0,00	0,00	0,00	0,00	0,00	-1,9	MDA WithaferinA 72h
116	SH3BGRL	0,00	-1,25	0,00	0,00	0,00	0,00	0,00	0,00	0,00	-3,3	SW620 Rosemary 100ug 48h

Gene Number	Symbol	GSC10 NCD38 24h	MCF7 TMX 48 h	MDA-MB231 Vitamin C 72h	ME1 Al-10-49 6h	Hela Ethanol 3h	MA9 PAM 3h	MA9 PAM 24h	hNCC Zika Virus 65h	hPN Zika Virus 65h	log2 FC	Treatment
117	SH3D19	0,00	0,00	0,00	0,00	0,00	0,00	-1,21	0,00	0,00	-1,6	ZR75 Indole3carbinol 24h
117	SH3D19	0,00	0,00	0,00	0,00	0,00	0,00	-1,21	0,00	0,00	-2,4	T47D Indole3carbinol 24h
117	SH3D19	0,00	0,00	0,00	0,00	0,00	0,00	-1,21	0,00	0,00	-2,7	MCF7 Indole3carbinol 24h
118	SIPA1	-1,03	0,00	0,00	0,00	0,00	0,00	0,00	0,00	0,00	-1,5	MDA WithaferinA 72h
118	SIPA1	-1,03	0,00	0,00	0,00	0,00	0,00	0,00	0,00	0,00	-2,5	T47D Indole3carbinol 24h
119	SIRT7	1,14	0,00	0,00	0,00	0,00	0,00	0,00	0,00	0,00	1,5	T47D Indole3carbinol 24h
120	SLC25A19	0,00	0,00	0,00	-1,75	0,00	0,00	0,00	0,00	0,00	-1,9	LNCaP eusynstyelamideB 5uM 24h
121	SLC30A1	0,00	3,80	0,00	1,68	0,00	0,00	1,97	0,00	0,00	2,6	SW620 Rosemary 60ug 48h
121	SLC30A1	0,00	3,80	0,00	1,68	0,00	0,00	1,97	0,00	0,00	2	T47D Indole3carbinol 24h
121	SLC30A1	0,00	3,80	0,00	1,68	0,00	0,00	1,97	0,00	0,00	1,9	HT29 RosemaryExtract 24h
121	SLC30A1	0,00	3,80	0,00	1,68	0,00	0,00	1,97	0,00	0,00	1,9	Ishikawa Genistein 10uM 24h
121	SLC30A1	0,00	3,80	0,00	1,68	0,00	0,00	1,97	0,00	0,00	1,7	MDA MB436 Indole3carbinol 24h
122	SLC44A1	0,00	-1,13	0,00	0,00	0,00	0,00	0,00	0,00	0,00	-1,8	MDA WithaferinA 72h
122	SLC44A1	0,00	-1,13	0,00	0,00	0,00	0,00	0,00	0,00	0,00	-1,9	T47D Indole3carbinol 24h
123	SLC8B1	0,00	1,03	0,00	0,00	0,00	0,00	0,00	0,00	0,00	1,5	MCF7 JaponiconeA 10uM 12h
124	SPATA5L1	0,00	1,48	0,00	0,00	0,00	0,00	0,00	0,00	0,00	1,5	MCF7 Narciclasine 10uM 12h
125	STIP1	0,00	2,19	0,00	0,00	0,00	0,00	0,00	0,00	0,00	1,5	MCF7 JaponiconeA 10uM 12h
126	SWAP70	0,00	0,00	0,00	0,00	0,00	1,32	1,52	0,00	0,00	1,7	MCF7 JaponiconeA 10uM 12h
126	SWAP70	0,00	0,00	0,00	0,00	0,00	1,32	1,52	0,00	0,00	1,5	MCF7 Narciclasine 10uM 12h
127	SYF2	0,00	0,00	0,00	0,00	0,00	0,00	0,00	1,08	0,00	3,9	SW620 Rosemary 100ug 48h
128	SYNJ1	0,00	0,00	0,00	0,00	0,00	0,00	1,16	0,00	0,00	1,7	MCF7 Narciclasine 10uM 12h
129	TBC1D1	-1,07	0,00	0,00	0,00	0,00	0,00	0,00	0,00	0,00	-1,5	SW620 Rosemary 60ug 48h
129	TBC1D1	-1,07	0,00	0,00	0,00	0,00	0,00	0,00	0,00	0,00	-2,4	SW620 Rosemary 100ug 48h
130	TM2D2	0,00	1,42	0,00	0,00	0,00	0,00	0,00	0,00	0,00	2,7	T47D Indole3carbinol 24h
130	TM2D2	0,00	1,42	0,00	0,00	0,00	0,00	0,00	0,00	0,00	1,8	ZR75 Indole3carbinol 24h
130	TM2D2	0,00	1,42	0,00	0,00	0,00	0,00	0,00	0,00	0,00	1,5	MCF7 Indole3carbinol 24h

Gene Number	Symbol	GSC10 NCD38 24h	MCF7 TMX 48 h	MDA-MB231 Vitamin C 72h	ME1 Al-10-49 6h	Hela Ethanol 3h	MA9 PAM 3h	MA9 PAM 24h	hNCC Zika Virus 65h	hPN Zika Virus 65h	log2 FC	Treatment
131	TMCO3	0,00	1,38	0,00	0,00	0,00	0,00	0,00	0,00	0,00	1,5	MCF7 JaponiconeA 10uM 12h
132	TMCO6	0,00	-1,06	0,00	0,00	0,00	0,00	0,00	0,00	0,00	-1,5	MCF7 JaponiconeA 10uM 12h
133	TMEM170A	0,00	1,13	0,00	0,00	0,00	0,00	0,00	0,00	0,00	1,5	T47D Indole3carbinol 24h
134	TMEM63A	0,00	-1,22	0,00	0,00	0,00	0,00	0,00	0,00	0,00	-2,9	SW620 Rosemary 100ug 48h
135	TOM1	0,00	0,00	0,00	1,34	0,00	0,00	1,84	0,00	0,00	1,7	MCF10A Sulforaphane 15uM 24h
136	TPRA1	0,00	0,00	0,00	0,00	0,00	1,07	0,00	0,00	0,00	3	MCF7 Narciclasine 10uM 12h
137	TRAPPC9	0,00	-1,15	0,00	0,00	0,00	0,00	0,00	0,00	0,00	-2,4	MDA MB231 Indole3carbinol 24h
137	TRAPPC9	0,00	-1,15	0,00	0,00	0,00	0,00	0,00	0,00	0,00	-2,6	MDA MB157 Indole3carbinol 24h
137	TRAPPC9	0,00	-1,15	0,00	0,00	0,00	0,00	0,00	0,00	0,00	-2,6	SW620 Rosemary 100ug 48h
137	TRAPPC9	0,00	-1,15	0,00	0,00	0,00	0,00	0,00	0,00	0,00	-3,9	T47D Indole3carbinol 24h
137	TRAPPC9	0,00	-1,15	0,00	0,00	0,00	0,00	0,00	0,00	0,00	-4,2	ZR75 Indole3carbinol 24h
137	TRAPPC9	0,00	-1,15	0,00	0,00	0,00	0,00	0,00	0,00	0,00	-4,5	MDA MB436 Indole3carbinol 24h
138	WDFY2	0,00	0,00	0,00	0,00	0,00	0,00	-1,08	0,00	0,00	-1,5	MDA MB436 Indole3carbinol 24h
138	WDFY2	0,00	0,00	0,00	0,00	0,00	0,00	-1,08	0,00	0,00	-2	T47D Indole3carbinol 24h
139	WDR34	0,00	-1,11	0,00	-1,21	0,00	0,00	-1,85	0,00	0,00	-1,5	LNCaP eusynstyelamideB 5uM 24h
140	YAF2	0,00	0,00	0,00	1,25	0,00	0,00	0,00	0,00	0,00	2,2	MCF7 Narciclasine 10uM 12h
140	YAF2	0,00	0,00	0,00	1,25	0,00	0,00	0,00	0,00	0,00	1,9	MCF7 BruceineD 10uM 12h
140	YAF2	0,00	0,00	0,00	1,25	0,00	0,00	0,00	0,00	0,00	1,6	MCF7 Hydroxyalantolactone 10uM 12h
141	ZBTB10	0,00	1,16	0,00	0,00	1,09	0,00	1,36	0,00	0,00	2,4	MCF7 Narciclasine 10uM 12h
142	ZBTB7B	0,00	0,00	0,00	0,00	0,00	0,00	0,00	0,00	1,68	1,8	SW620 Rosemary 60ug 48h
143	ZC3H4	0,00	-2,43	0,00	0,00	0,00	0,00	0,00	0,00	0,00	-1,8	Ishikawa Genistein 10uM 24h
143	ZC3H4	0,00	-2,43	0,00	0,00	0,00	0,00	0,00	0,00	0,00	-2,2	MCF7 Indole3carbinol 24h
143	ZC3H4	0,00	-2,43	0,00	0,00	0,00	0,00	0,00	0,00	0,00	-2,5	Ishikawa Genistein 10uM 8h
144	ZNF140	1,23	0,00	0,00	0,00	0,00	0,00	0,00	0,00	0,00	1,7	MCF7 Narciclasine 10uM 12h
145	ZNF213	0,00	1,50	0,00	0,00	0,00	0,00	0,00	0,00	0,00	1,6	T47D Indole3carbinol 24h
146	ZNF3	0,00	1,02	0,00	0,00	0,00	0,00	0,00	0,00	0,00	2,2	Fibroblast Genistein 100uM 48h

Gene Number	Symbol	GSC10 NCD38 24h	MCF7 TMX 48 h	MDA-MB231 Vitamin C 72h	ME1 Al-10-49 6h	Hela Ethanol 3h	MA9 PAM 3h	MA9 PAM 24h	hNCC Zika Virus 65h	hPN Zika Virus 65h	log2 FC	Treatment
147	ZNF33A	0,00	0,00	0,00	0,00	0,00	0,00	0,00	-1,23	0,00	-1,7	T47D Indole3carbinol 24h
148	ZNF518A	0,00	0,00	0,00	0,00	0,00	0,00	0,00	-1,21	0,00	-2,6	MCF7 Indole3carbinol 24h
149	ZNF574	0,00	1,02	0,00	0,00	0,00	0,00	0,00	0,00	0,00	2,4	T47D Indole3carbinol 24h
149	ZNF574	0,00	1,02	0,00	0,00	0,00	0,00	0,00	0,00	0,00	2,2	ZR75 Indole3carbinol 24h
149	ZNF574	0,00	1,02	0,00	0,00	0,00	0,00	0,00	0,00	0,00	1,6	MDA MB436 Indole3carbinol 24h

Supplementary Table S8: List of the 44 genes showing the same expression trend in bulk RNA-seq and scRNA-seq data from tissues and cells from COVID-19 infected patients.
The tissue (Tissue), the cell types, (Cell type), the gene symbol (Gene symbol), the gene expression level (log2FC), the p-value (p-value) and the expression trend in bulk RNA-seq (Up or Down) are reported.

Tissue	Cell Type	Gene Symbol	log2FC	p-value	Expression trend in bulk RNAseq
Intestine	Stem cells	RSL24D1	-0,735	6E-21	Down
Blood	CD4+ T cells	RPS3A	-0,887	0E+00	Down
Blood	CD8+ T cells	RPS3A	-0,804	0E+00	Down
Blood	Conventional dendritic cells 1	RPS3A	-0,599	1E-11	Down
Blood	Natural killer cells	RPS3A	-0,512	3E-116	Down
Blood	NC Monocytes	RPS3A	-0,557	7E-41	Down
Brain	CD8+ T cells	RPL31	-2,045	3E-03	Down
Brain	Naive B cells	RPL31	-2,016	0E+00	Down
Blood	Platelets	RPS24	-0,623	2E-21	Down
Intestine	Cycling transient amplifying cells	MX1	0,793	1E-06	Up
Intestine	Enterocyte 1 cells	CYP1A1	0,998	1E-24	Up
Intestine	Enterocyte 2 cells	MX2	3,789	2E-66	Up
Intestine	Enterocyte 2 cells	MX1	3,963	5E-57	Up
Intestine	Enterocyte 2 cells	XAF1	2,969	3E-56	Up
Intestine	Enterocyte 2 cells	OASL	2,083	2E-51	Up
Intestine	Enterocyte 2 cells	DDX58	2,349	7E-48	Up
Intestine	Enterocyte 2 cells	USP18	1,719	4E-46	Up
Intestine	Enterocyte 2 cells	HERC5	2,526	4E-45	Up
Intestine	Enterocyte 2 cells	EPSTI1	2,356	9E-44	Up
Intestine	Enterocyte 2 cells	OAS3	1,884	5E-43	Up
Intestine	Enterocyte 2 cells	IFIT2	3,352	9E-43	Up

Tissue	Cell Type	Gene Symbol	log2FC	p-value	Expression trend in bulk RNAseq
Intestine	Enterocyte 2 cells	OAS2	2,050	1E-36	Up
Intestine	Enterocyte 2 cells	HELZ2	1,232	4E-35	Up
Intestine	Enterocyte 2 cells	CMPK2	1,602	1E-32	Up
Intestine	Enterocyte 2 cells	IFI44	1,556	1E-29	Up
Intestine	Enterocyte 2 cells	DDX60	1,272	1E-26	Up
Intestine	Enterocyte 2 cells	IFIH1	1,544	1E-25	Up
Intestine	Enterocyte 2 cells	IFITM3	1,715	1E-25	Up
Intestine	Enterocyte 2 cells	DDX60L	1,382	2E-25	Up
Intestine	Enterocyte 2 cells	IRF1	1,734	4E-24	Up
Intestine	Enterocyte 2 cells	CXCL11	2,077	1E-21	Up
Intestine	Enterocyte 2 cells	TRIM22	1,223	6E-19	Up
Intestine	Enterocyte 2 cells	PARP14	1,146	2E-16	Up
Intestine	Enterocyte 2 cells	GBP4	1,117	2E-14	Up
Intestine	Enterocyte 2 cells	BST2	1,281	5E-13	Up
Intestine	Enterocyte 2 cells	SAMD9L	1,030	5E-11	Up
Intestine	Enterocyte 2 cells	SAMD9	1,266	9E-10	Up
Intestine	Secretory transient amplifying cells	MX2	2,532	5E-07	Up
Intestine	Secretory transient amplifying cells	IFIT2	1,922	1E-06	Up
Intestine	Secretory transient amplifying cells	BST2	5,184	2E-06	Up
Intestine	Secretory transient amplifying cells	IFI44	2,176	2E-05	Up
Intestine	Secretory transient amplifying cells	MX1	3,005	3E-05	Up
Intestine	Secretory transient amplifying cells	OAS2	2,996	7E-05	Up
Intestine	Secretory transient amplifying cells	OAS3	2,698	1E-04	Up
Intestine	Secretory transient amplifying cells	DDX58	2,250	1E-04	Up
Intestine	Stem cells	MX1	0,678	3E-14	Up
Intestine	Transient amplifying cells	MX1	0,783	1E-26	Up

Tissue	Cell Type	Gene Symbol	log2FC	p-value	Expression trend in bulk RNAseq
Intestine	Transient amplifying cells	MX2	0,556	9E-16	Up
Intestine	Transient amplifying cells	XAF1	0,813	4E-15	Up
Blood	CD1C CD141 dendritic cells	IFITM3	2,968	4E-46	Up
Blood	CD1C CD141 dendritic cells	PLAUR	2,097	6E-41	Up
Blood	CD1C CD141 dendritic cells	IFI27	2,785	2E-38	Up
Blood	Conventional dendritic cells	PLAUR	2,391	2E-110	Up
Blood	Conventional dendritic cells	CXCL3	2,603	5E-98	Up
Blood	Conventional dendritic cells	IFITM3	1,956	7E-72	Up
Blood	Erythrocytes	IFI27	6,148	4E-286	Up
Blood	Megakaryocyte progenitor cells	IFITM3	3,724	2E-99	Up
Blood	Natural killer cells	OASL	1,132	3E-88	Up
Blood	Natural killer cells	IFIT2	0,814	1E-28	Up
Blood	T cells	CSRNP1	0,660	4E-202	Up
Blood	B cells	IFITM3	7,961	2E-11	Up
Blood	B cells	IFI27	9,578	5E-07	Up
Blood	CD4+ T cells	XAF1	0,994	1E-284	Up
Blood	CD4+ T cells	MX1	0,837	1E-210	Up
Blood	CD4+ T cells	IFITM1	1,006	1E-126	Up
Blood	CD8+ T cells	XAF1	1,355	3E-288	Up
Blood	CD8+ T cells	MX1	1,092	2E-233	Up
Blood	CD8+ T cells	IFITM1	1,331	2E-83	Up
Blood	Conventional dendritic cells 1	MX1	2,250	2E-14	Up
Blood	Conventional dendritic cells 1	EPSTI1	1,596	2E-14	Up
Blood	Conventional dendritic cells 1	IFI27	2,124	4E-07	Up
Blood	Conventional dendritic cells 1	IFITM3	1,595	7E-06	Up
Blood	Conventional dendritic cells 2	XAF1	1,639	1E-305	Up

Tissue	Cell Type	Gene Symbol	log2FC	p-value	Expression trend in bulk RNAseq
Blood	Conventional dendritic cells 2	IFITM3	1,985	2E-178	Up
Blood	Conventional dendritic cells 2	IFI27	2,889	1E-142	Up
Blood	Eosinophil	IFI44	0,631	5E-38	Up
Blood	Monocytes	IFI27	8,510	0E+00	Up
Blood	Monocytes	IFITM3	4,484	0E+00	Up
Blood	Natural killer cells	XAF1	1,423	4E-296	Up
Blood	Natural killer cells	IFITM1	1,740	3E-178	Up
Blood	NC Monocytes	IFI27	12,958	0E+00	Up
Blood	NC Monocytes	IFITM3	9,729	0E+00	Up
Blood	Plasmablasts	IFI27	4,974	1E-17	Up
Blood	Plasmacytoid dendritic cells	MX1	3,823	8E-263	Up
Blood	Plasmacytoid dendritic cells	XAF1	1,892	8E-245	Up
Blood	Plasmacytoid dendritic cells	IFI27	8,394	4E-182	Up
Blood	Plasmacytoid dendritic cells	IRF7	2,953	2E-28	Up
Blood	Platelets	IFI27	9,229	1E-241	Up
Pancreas	Acinar cells	MX1	0,849	4E-77	Up
Pancreas	Acinar cells	IFITM3	0,859	1E-64	Up
Pancreas	Alpha cells	MX1	0,595	3E-94	Up
Pancreas	Delta cells	MX1	0,666	1E-29	Up
Pancreas	Duct cells	IFITM3	1,029	1E-85	Up
Pancreas	Duct cells	TNFSF10	0,941	2E-49	Up
Pancreas	Immune cells	CXCL3	4,657	2E-04	Up
Pancreas	PP cells	MX1	0,720	5E-89	Up
Lung	Macrophage	CXCL11	3,470	0E+00	Up
Lung	Macrophage	IDO1	2,966	0E+00	Up
Lung	Macrophage	IFI27	3,024	0E+00	Up

Tissue	Cell Type	Gene Symbol	log2FC	p-value	Expression trend in bulk RNAseq
Lung	Macrophage	IFIT2	2,944	0E+00	Up
Lung	Macrophage	IFITM3	3,453	0E+00	Up
Lung	Macrophage	TNFSF10	2,884	0E+00	Up
Lung	Myeloid dendritic cells	IDO1	4,583	2E-20	Up
Lung	Myeloid dendritic cells	NR4A3	4,356	2E-19	Up
Lung	Natural killer & T cells	TNFSF10	1,494	8E-182	Up
Lung	Natural killer & T cells	IFITM1	2,052	1E-114	Up
Lung	T cells	IFIT2	3,233	3E-48	Up
Lung	T cells	TNFSF10	1,773	2E-34	Up
Lung	T cells	IFITM3	2,029	3E-34	Up
Lung	T cells	OAS1	0,975	9E-27	Up
Lung	T cells	MX1	1,098	1E-22	Up
Blood	CD4+ T cells	IFITM1	0,946	0E+00	Up
Blood	CD4+ T cells	MX1	0,581	2E-276	Up
Blood	Monocytes+cDCs	IFI27	12,279	0E+00	Up
Blood	Monocytes+cDCs	IFITM3	8,059	0E+00	Up
Blood	Monocytes	IFI27	5,202	2E-85	Up
Blood	Natural killer cells	IFITM1	0,801	5E-128	Up
Brain	Granulocytes	IFI27	5,976	2E-05	Up
Blood	Monocytes	PLAUR	4,036	2E-42	Up
Blood	Natural killer T cells	IFIT2	6,704	2E-92	Up
Blood	Natural killer T cells	OASL	2,658	1E-35	Up
Blood	Natural killer T cells	NFKBIZ	1,295	3E-28	Up
Blood	Natural killer T cells	TNF	1,691	9E-23	Up
Blood	T,B cells	IFIT2	1,303	1E-02	Up
Airway	Basal cells	IFI27	2,159	0E+00	Up

Tissue	Cell Type	Gene Symbol	log2FC	p-value	Expression trend in bulk RNAseq
Airway	Basal cells	IFITM3	1,815	0E+00	Up
Airway	Basal cells(proliferating)	IFI27	1,711	4E-18	Up
Airway	Ciliated cells	IFI27	3,855	0E+00	Up
Airway	Ciliated cells	IFITM3	1,006	0E+00	Up
Airway	Ciliated cells	MX1	1,447	0E+00	Up
Airway	Ciliated cells	MX2	1,035	0E+00	Up
Airway	Ciliated cells	OAS2	1,073	0E+00	Up
Airway	Ciliated cells	XAF1	0,955	0E+00	Up
Airway	Ciliated cells	IFIT2	1,557	2E-188	Up
Airway	Club cells	IFITM3	1,909	6E-198	Up
Airway	Club cells	IFI27	3,560	7E-198	Up
Airway	Club cells	TNFSF10	1,539	6E-180	Up
Airway	Club cells	BST2	1,532	3E-142	Up
Airway	Club cells	MX1	1,944	6E-126	Up
Airway	Club cells	MX2	1,484	8E-123	Up
Airway	Club cells	IFIT2	1,917	2E-70	Up
Airway	Neuroendocrine cells	IFI27	8,106	5E-40	Up
Airway	Alveolar pneumocytes	ICAM1	1,578	4E-82	Up
Airway	Smooth muscle cells	NR4A3	0,582	4E-03	Up
Lung	Ciliated cells	CXCL3	0,585	2E-36	Up
Lymph node	Fibroblasts	IFITM3	0,814	2E-05	Up

Supplementary Table S9: List of the 13 genes showing the same expression trend in bulk RNA-seq, scRNA-seq data from tissues and cells from COVID-19 infected patients, and showing an opposite trend in nutrigenomics treatment.
the gene symbol (Gene symbol), the gene expression level (log2FC), the FDR (FDR), the nutrigenomics treatment (Nutrigenomics treatment) the expression trend in bulk RNA-seq (Up or Down) and in scRNA-seq (Up or Down) are reported.

Gene Symbol	log2FC	FDR	Nutrigenomics treatment	Expression trend in scRNAseq	Expression trend in bulk RNAseq
IFIT2	-2,7	0	Resveratrol	Up	Up
IFI27	-2,7	0	Japonicone A	Up	Up
DDX60	-2,8	0	Resveratrol	Up	Up
MX2	-2,8	0	Resveratrol	Up	Up
SAMD9	-2,8	0	Resveratrol	Up	Up
XAF1	-3,1	0	Resveratrol	Up	Up
HERC5	-3,2	0	Indole-3-carbinol	Up	Up
OAS2	-3,7	0	Resveratrol	Up	Up
IFIH1	-2,5	0,001	Britanin	Up	Up
OAS3	-2,7	0,001	Withaferin A	Up	Up
IFI27	-2,8	0,001	Hydroxyalantolactone	Up	Up
IFIH1	-2,5	0,002	Rosemary	Up	Up
BST2	-2,8	0,002	Rosemary	Up	Up
IFI27	-2,9	0,002	Ursodeoxycholic acid	Up	Up
OAS3	-3,5	0,002	Rosemary	Up	Up
TNFSF10	-3,8	0,002	Rosemary	Up	Up
IFI27	-2,9	0,004	Ginsenoside RB3	Up	Up
IFI27	-3	0,004	Borneol	Up	Up
IFI27	-2,7	0,005	Hyodeoxycholic acid	Up	Up
IFI27	-2,8	0,005	Cholic acid	Up	Up
IFI27	-2,9	0,005	Muscone	Up	Up

Gene Symbol	log2FC	FDR	Nutrigenomics treatment	Expression trend in scRNAseq	Expression trend in bulk RNAseq
IFI27	-3	0,005	Cinnamic acid	Up	Up
IFITM1	-2,7	0,006	Withaferin A	Up	Up
BST2	-2,7	0,006	Rosemary	Up	Up
IFI27	-2,7	0,006	Benzyl Benzoate	Up	Up
IFI27	-2,7	0,006	Cinnamaldehyde	Up	Up
IFI27	-3	0,006	Isoborneol	Up	Up
TNFSF10	-2,5	0,007	Rosemary	Up	Up
IFI27	-2,7	0,008	Ginsenoside RE	Up	Up
IFI27	-3,1	0,008	Ginsenoside B2	Up	Up
IFI27	-2,6	0,009	Deoxycholic acid	Up	Up
IFI27	-2,7	0,013	Salvianic Acid A	Up	Up
IFI27	-2,6	0,014	Ginsenoside RC	Up	Up
IFI27	-2,9	0,018	Protocatechuic Aldehyde	Up	Up
IFI27	-3	0,018	BacopasideI	Up	Up
IFI27	-2,8	0,025	Ginsenoside RD	Up	Up